

DISSERTATION

REDESIGNING ORGANIC CATALYSTS AND POLYMERS FOR RECYCLING TOWARDS
SUSTAINABLE CATALYSIS AND MATERIALS

Submitted by

Robin Marcelle Cywar

Department of Chemistry

In partial fulfillment of the requirements

For the Degree of Doctor of Philosophy

Colorado State University

Fort Collins, Colorado

Fall 2021

Doctoral Committee:

Advisor: Eugene Y.-X. Chen

Co-Advisor: Gregg T. Beckham

Melissa M. Reynolds

Thomas Borch

Christie A.M. Peebles

Copyright by Robin Cywar 2021
All Rights Reserved

ABSTRACT

REDESIGNING ORGANIC CATALYSTS AND POLYMERS FOR RECYCLING TOWARDS SUSTAINABLE CATALYSIS AND MATERIALS

This dissertation describes the development of catalysts and polymers designed for a sustainable, circular materials economy in which end-of-life is considered during the design stage through properties of inherent recyclability. Products that are recyclable-by-design contrast with those of the current, linear economy, which has led to global environmental crises: greenhouse gas emissions due to finite fossil fuel consumption, contributing to climate change, and tremendous accumulations of plastic waste in landfills and the environment. A major challenge associated with the development of circular lifecycle products, including both catalysts and polymers (plastics, in particular), is achieving performance properties competitive with those of their incumbents, which this work aimed to address. A critical literature review provides an overview of materials derived from renewable, biomass feedstocks (referred to as bio-based polymers) which exhibit performance-advantaged properties relative to petroleum-based polymers. Bio-based chemicals and materials are considered to have a circular carbon lifecycle (carbon-neutral), but those with a circular lifecycle (i.e., recyclable or biodegradable) are given special emphasis.

To increase the circularity of all aspects of production of bio-based chemicals and polymers, a polymer-supported organocatalyst has been explored for the coupling of biomass-based

furaldehyde platform chemicals; these products can be used for bio-fuels or polymers after further transformations. The developed thermally activated *N*-heterocyclic carbene (NHC) organocatalyst can be recycled for furfural coupling in excellent yield simply by controlling the temperature, demonstrating promising features for improved circularity in catalyzed chemical processes and ultimately, waste reduction. The discovery of acid-base interactions between the catalyst and hydroxylated substrates has enhanced the understanding of NHC catalysis and contributed to improved design principles for these catalysts.

To address plastic waste accumulation by designing for recyclability, polyester and polyamide materials with full chemical recyclability to monomers have been demonstrated from lactone and lactam monomers, respectively. In each case, study of polymerization activity through chemical catalysis revealed fundamental information about the thermodynamic (de)polymerizability of the novel systems, including selectivity considerations, and enabled synthesis of robust structural models for thermomechanical characterization. Overall, understanding the resultant structure-property relationships informs further development of materials with full chemical recyclability and attractive materials properties, including copolymer formulations and design of new monomers to explore for addressing tradeoffs between (de)polymerization activity and material properties.

ACKNOWLEDGEMENTS

Chapter 2. This dissertation chapter contains the manuscript of a full review article published in Nature Review Materials [Cywar, R. M.; Rorrer, N. A.; Hoyt, C. B.; Beckham, G. T.; Chen, E. Y. -X. Nat. Rev. Mater., 2021]. This work was authored in part by the National Renewable Energy Laboratory, operated by Alliance for Sustainable Energy, LLC, for the US Department of Energy (DOE) under Contract No. DE-AC36-08GO28308. Funding was provided by the US DOE, Office of Energy Efficiency and Renewable Energy Bioenergy Technologies Office and the US National Science Foundation (NSF-1955482). The views expressed in the article do not necessarily represent the views of the DOE or the US Government.

Chapter 3. This work was supported by the US Department of Energy Office of Basic Energy Sciences, grant DE-FG02-10ER16193. This dissertation chapter contains the manuscript of a full paper published in ACS Sustainable Chemistry & Engineering [Cywar, R. M.; Wang, L.; Chen, E. Y. -X. ACS Sustainable Chem. Eng. 2019, 7, 1980-1988].

Chapter 4. This work was supported by the United States National Science Foundation, grant CHE-1664915. This dissertation chapter contains the manuscript of a full paper published in Polymer Chemistry [Cywar, R. M.; Zhu, J. -B.; Chen, E. Y. -X. Polym. Chem. 2019, 10, 3097-3106].

Chapter 5. This work was supported by the U.S. Department of Energy, Office of Energy Efficiency and Renewable Energy, Advanced Manufacturing Office (AMO) and Bioenergy Technologies Office (BETO). This work was performed as part of the BOTTLE™ Consortium, which includes the members from Colorado State University, and funded under contract no. DE-AC36-08GO28308 with the National Renewable Energy Laboratory, operated by Alliance for Sustainable Energy.

DEDICATION

To all those who learn science
For the benefit of mankind and the environment.

To Doug Cywar, Ph.D.
*Thank you for the extraordinary head start in life and science.
Every math problem, dining room table experiment,
take-your-daughter-to-work-day, lead me here.*

TABLE OF CONTENTS

ABSTRACT.....	ii
ACKNOWLEDGEMENTS.....	iv
DEDICATION.....	vi
Chapter 1 Introduction.....	1
Chapter 2 Bio-Based Polymers with Performance-Advantaged Properties	
2.1. Synopsis.....	7
2.2. Introduction.....	8
2.3. Sourcing Bio-Feedstocks.....	10
2.4. Polymer Properties	13
2.5. C-O Linked Polymers.....	17
2.6. C-N Linked Polymers.....	33
2.7. Outlook.....	47
References.....	51
Chapter 3 Thermally Regulated Recyclable Carbene Catalysts for Upgrading of Biomass Furaldehydes	
3.1. Synopsis.....	79
3.2. Introduction.....	80
3.3. Results and Discussion.....	83
3.4. Conclusions.....	96
References.....	98
Chapter 4 Selective or Living Organopolymerization of a Six-Five Bicyclic Lactone to Produce Fully Recyclable Polyesters	
4.1. Synopsis.....	106
4.2. Introduction.....	107
4.3. Results and Discussion.....	110
4.4. Conclusions.....	132

References.....	133
Chapter 5	Redesigned Hybrid Nylons for Optical Clarity and Chemical Recyclability
5.1.	Synopsis.....139
5.2.	Introduction.....140
5.3.	Results.....143
5.4.	Discussion.....160
References.....	166
Chapter 6	Conclusions and Outlook
6.1.	Conclusions and Outlook176
References.....	182
Appendix A – Experimental Details and Supporting Information for Chapter 3	
A.1.	Materials, Reagents, and Methods.....187
A.2.	Additional Figures and Tables.....191
References.....	208
Appendix B – Experimental Details and Supporting Information for Chapter 4	
B.1.	Materials, Reagents, and Methods.....209
B.2.	Additional Figures and Tables.....215
References.....	230
Appendix C – Experimental Details and Supporting Information for Chapter 5	
C.1.	Materials, Reagents, and Methods.....231
C.2.	Additional Figures and Tables.....242
C.3.	DFT Cartesian Coordinates.....296
References.....	303

Chapter 1

Introduction

The purpose of this dissertation work is to define structure—activity/property relationships of new catalysts and polymers designed for recyclability towards a circular materials economy (Fig 1.1). A central challenge to new materials designed for circular lifecycles, which this work aimed to address, is to overcome tradeoffs between polymerizability and depolymerizability as well as between performance and recyclability, achieving balanced performance properties that are competitive with those of the incumbent non-recyclable or hard-to-recycle materials.

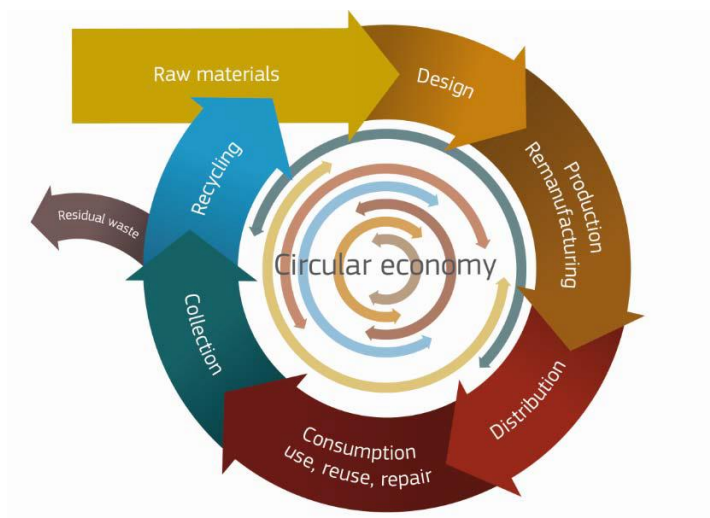


Figure 1.1. Conceptual diagram illustrating the main phases of a circular economy model (Source: European Commission, 2014).

Chemicals and polymers derived from renewable, plant-based feedstocks offer an opportunity to depart from the unsustainable use of finite, fossil fuel feedstocks. Such bio-based products are considered to have a circular carbon, or carbon-neutral, lifecycle because the carbon sequestered during plant growth is retained within the material until combustion or degradation in a circular

fashion. Achieving enhanced properties relative to petroleum incumbents, or performance-advantages, is essential to the realization of bio-based products in the marketplace. Successes are highlighted in the discussion and critical review of bio-based polymers with performance-advantaged properties, with emphasis on materials also designed for circularity by chemical recycling or biodegradation.

Catalysis is the essential tool to transform bio-feedstocks to renewable chemicals, liquid fuels, and polymeric materials. molecular catalysts require separation from a homogeneous reaction mixture, whereas heterogenous catalysts offer straightforward separation and easy recovery by simple filtration. Maintaining high performance of the heterogeneous catalyst with continued use will increase the circularity and sustainability of the catalyzed chemical process. Thus, a heterogeneous adaptation of a molecular catalyst must demonstrate reactivity on-par with its analog over multiple cycles of use. Furthermore, many catalysts require chemical activation/deactivation from a pre-catalyst form, including *N*-heterocyclic carbene (NHC) organocatalysts employed in biomass upgrading, contributing to additional resource use, separations, and waste generation; however, these issues can be circumvented by designing catalysts to be thermally activatable. These design challenges are explored by the investigation of a polymer-supported NHC catalyst designed for recyclability through a polymer support and thermal (de)activation devoid of need for stoichiometric chemicals for each catalyst deactivation and reactivation cycle.

Industrial polymer production requires significant use of finite fossil-fuel feedstocks, resulting in greenhouse gas emissions, while limited recycling of the plastic products has resulted in massive waste accumulations in landfills and the environment. Discarding plastic waste is also considered to be a substantial loss to the global economy. To combat these issues, polymers must be re-designed for effective recycling. While mechanical recycling typically results in poor quality

polymer (i.e., down-cycling), chemical recycling back to constituent monomers offers an opportunity to regenerate virgin-quality polymers. Re-designing polymers for complete chemical recyclability requires a thorough understanding of fundamental thermodynamics governing (de)polymerization processes as well as the resulting structure-property relationships of novel materials – study of which relies on robust catalytic methods for polymer synthesis and deconstruction. Achieving balance between (de)polymerization activity and performance properties is essential to the successful deployment of sustainable polymers, as exemplified in the fundamental investigations of re-designed polyester and polyamide (nylon) materials.

A critical literature review, followed by results of fundamental investigations are presented and discussed in detail in the following chapters:

- 2) Bio-Based Polymers with Performance-Advantaged Properties
- 3) Thermally Regulated Recyclable Carbene Catalysts for Upgrading of Biomass Furaldehydes
- 4) Selective or Living Organopolymerization of a Six-Five Bicyclic Lactone to Produce Fully Recyclable Polyesters
- 5) Redesigned Hybrid Nylons for Optical Clarity and Chemical Recyclability
- 6) Conclusions & Outlook

Chapter 2 consists of an in-depth, critical literature review in which the concept of performance-advantaged, bio-based polymers (PBPs) is presented and exemplified by recent successes from polymer classes with carbon-oxygen (C-O) and carbon-nitrogen (C-N) inter-unit chemical bonds that are accessible from heteroatom-rich, bio-derived feedstocks. Prior to review of the field, a primer to fundamental polymer properties is provided. After discussion of

performance-advantaged properties and promising PBP materials, guiding principles to aid progress in the development of PBPs are presented with a concise discussion of major challenges facing the field.

Chapter 3 reports the re-design of an NHC organocatalyst for recyclability and thermal (de)activation for use in upgrading of biomass-derived furfuraldehydes furfural and 5-hydroxymethyl furfural (HMF). Upgrading of these substrates into C₁₀₋₁₄ furoins was achieved by the selective umpolung self-coupling reaction catalyzed by polystyrene (PS)-supported azolium salts paired with an acetate counterion, which allows a thermal equilibrium between the dormant ion pair and the active NHC state. Together, these features enable catalyst recycling in air with no additional chemicals required. Compared to other supported azolium-acetates, a benzimidazolium bearing a dodecyl chain achieved the highest furoin yields and showed superior recyclability when exposed to air upon filtration. In comparison, HMF self-coupling was less effective in both product yield and catalyst recyclability due to discovered unproductive substrate-catalyst interactions.

Details of selective, organocatalyzed ring-opening polymerization (O-ROP) and depolymerization of a six-five bicyclic lactone, 4,5-*trans*-cyclohexyl-fused γ -butyrolactone (4,5-T6GBL) are presented in Chapter 4. A screening of (thio)urea [(T)U] and organic base pairs revealed unique trends in reactivity for this monomer as well as the most active catalyst pairs, which were employed to produce relatively high molecular weight, low dispersity linear poly(4,5-T6GBL) and copolymers with γ -butyrolactone in a living fashion, enabling thermomechanical characterization. Compared with the metal-catalyzed system, (T)U-base pairs exhibited competitive kinetics, reached higher monomer conversions, and resulting polymers required less purification to attain higher onset decomposition temperature. (T)U-base pairs were selective towards linear polymerization only, whereas triazabicyclodecene can catalyze both polymerization

and (quantitative) depolymerization processes. Cyclic polymers were also selectively formed via NHC-mediated zwitterionic O-ROP.

Chapter 5 reports the results of fundamental investigations into a hybrid lactam monomer for nylon materials designed for chemical recyclability. This hybrid polyamide, nylon 4/6, is based on a bicyclic lactam composed of both high ceiling temperature ϵ -caprolactam and low ceiling temperature pyrrolidone motifs in a hybridized offspring structure. Hybrid nylon 4/6 overcomes tradeoffs in (de)polymerizability and performance properties of the parent nylons and radically alters the physical properties. The resulting nylon 4/6 is stereoregular but non-crystalline and optically clear; it is amorphous but lacks a viscous flow state; it exhibits high polymerizability but is also completely depolymerizable. A 50/50 random copolymer of nylon 4/6 and nylon 4 achieves the greatest synergy in both reactivity and polymer properties of each homopolymer, offering an amorphous nylon with a unique set of properties that are difficult to achieve by nylons, including optical clarity, high glass-transition temperature, melt-processability, and full chemical recyclability.

Chapter 6 consists of a brief discussion of the overall impact of the presented works on their respective fields and greater mission of designing for circularity. An outlook of research towards this mission, including major challenges and opportunities, is also presented.

The dissertation presented hereinafter was conceived in a “journals-format” style, in agreement with the Graduate School guidelines at Colorado State University. The first presented manuscript is a review article which has been published in *Nature Reviews Materials*; the remaining manuscripts are original research articles, two of which have been published as full papers in the peer-reviewed journals *ACS Sustainable Chemistry & Engineering* and *Polymer Chemistry*, and a third full paper has been prepared and submitted to the *Journal of the American Chemical Society*.

Experimental details, including methods, materials characterization, and supporting figures corresponding to each of the individual chapters are consecutively included in Appendixes at the end of this dissertation. This arrangement maintains consistency with the previously published work and provides a readable format of the research presented in the main chapters.

Chapter 2

Bio-Based Polymers with Performance-Advantaged Properties*

2.1. Synopsis

Bio-based compounds with unique chemical functionality can be obtained through selective transformations of plant and other non-fossil, biogenic feedstocks for the development of new polymers to displace those produced from fossil carbon feedstocks. Although substantial efforts have been invested to produce bio-based polymers that are chemically identical to and directly replace those from petroleum, a long-pursued goal is to synthesize new, sustainable, bio-based polymers that either functionally replace or exhibit performance advantages relative to incumbent polymers. Owing to anthropogenic climate change and the environmental consequences of global plastics pollution, the need to realize a bio-based materials economy at scale is critical. To that end, in this Review we describe the concept of performance-advantaged, bio-based polymers (PBPs), highlighting examples wherein superior performance is facilitated by the inherent chemical functionality of bio-based feedstocks. We focus on PBPs with C–O and C–N inter-unit chemical bonds, as these are often readily accessible from bio-based feedstocks, which are

* This dissertation chapter contains the manuscript of a full review article published in *Nature Reviews Materials* [Cywar, R. M.; Rorrer, N. A.; Hoyt, C. B.; Beckham, G. T.; Chen, E. Y.-X. *Nat. Rev. Mater.* **2021**]. This work was authored in part by the National Renewable Energy Laboratory, operated by Alliance for Sustainable Energy, LLC, for the US Department of Energy (DOE) under Contract No. DE-AC36-08GO28308. Funding was provided by the US DOE, Office of Energy Efficiency and Renewable Energy Bioenergy Technologies Office and the US National Science Foundation (NSF-1955482). The views expressed in the article do not necessarily represent the views of the DOE or the US Government. G.T.B. and E.Y.-X.C. prepared the initial draft outline. R.M.C., N.A.R., C.B.H. and G.T.B. wrote the manuscript and designed the figures under the leadership of R.M.C. All authors edited the manuscript prior to submission.

heteroatom-rich relative to petroleum-derived feedstocks. Finally, we outline guiding principles and challenges to aid progress in the development of PBPs.

2.2. Introduction

Synthetic polymers are ubiquitous in modern society owing to their relative ease of synthesis from petroleum-derived intermediates, ability to be formulated into diverse materials, extreme durability and low cost.¹ Monomers for commodity polymer production are typically either direct products from fossil carbon processing or chemically accessible from the primary olefin and aromatic building blocks. It is widely recognized that fossil-based carbon use is leading to anthropogenic climate change,² and polymer production is projected to reach 20% of global fossil fuel consumption by 2050 (ref.³). The detrimental environmental consequences of global plastics pollution are also palpable.⁴ Thus, it is imperative to transition from a fossil-based materials (and energy) economy to a materials economy, ideally circular, founded on building blocks sourced sustainably from plants and other non-fossil, biogenic feedstocks (here, referred to as bio-feedstocks for brevity).^{5–24} This transition presents an opportunity to harness the unique chemistries afforded by heteroatom-rich bio-feedstocks to redesign synthetic polymers.

To facilitate the transition to more sustainable polymers, research efforts have long focused on converting bio-feedstocks into compounds identical to those derived from petroleum.^{6,13,25} Making direct replacement chemicals and polymers is generally considered to be commercially viable, but likely more sustainable in scenarios in which fossil carbon prices are high, or with taxes on fossil carbon that account for the externalities associated with fossil carbon production, consumption and disposal.^{19,26} However, to manufacture direct replacements from bio-feedstocks, selective chemical processes are required to remove chemical functionality afforded naturally by many bio-

feedstocks. Conversely, the production of heteroatom (X)-containing polymers from fossil-based hydrocarbon feedstocks requires the addition of oxygen or nitrogen. The chemical distance measured by H:C and X:C (X = O, N) ratios from fossil-based feedstocks and bio-feedstocks to today's common polymers are exemplified in the van Krevelen diagram shown in Figure 2.1.

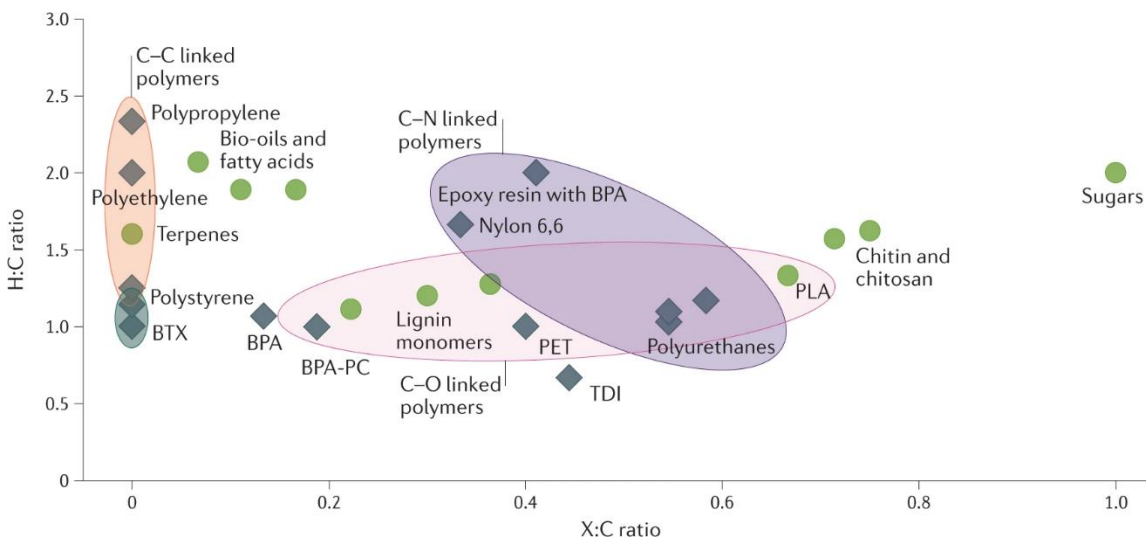


Figure 2.1. Van Krevelen diagram for select polymers. Select fossil-based polymers or feedstocks (black diamonds) and select bio-feedstocks and monomers or polymers (green circles) plotted relative to their heteroatom to carbon ratio (X:C, where X = O, N, among others) and their hydrogen to carbon ratio (H:C). As many C–O and C–N linked polymers and their respective monomers have X:C and H:C ratios similar to those of bio-feedstocks, they are a focus of work in the bio-based polymer field and of this Review. BPA, bisphenol A; BPA-PC, poly(bisphenol A carbonate); BTX, benzene–toluene–xylene; PET, polyethylene terephthalate; PLA, polylactic acid; TDI, toluene diisocyanate.

Although direct replacements can offer straightforward cost and sustainability benchmarks to surpass, the established markets make it challenging for a new bio-feedstock and the associated, capital-intensive manufacturing processes to compete with amortized petrochemical operations solely on a price basis. To compete at scale with fossil-based polymers, we posit that bio-based polymers must exhibit performance-advantaged properties that harness the inherent chemical functionalities of the starting bio-feedstocks. Generalizing to bioproducts (not limited to polymers), Fitzgerald and Bailey defined performance-advantaged bioproducts as bio-based

molecules that do not resemble existing petroleum-derived molecules in structure, and that offer a performance advantage over existing products.^{27,28} For polymers, performance-advantaged attributes include improvements in manufacturability, properties in applications and end-of-life considerations.

In this Review, we highlight progress in leveraging the unique chemical functionalities of bio-feedstocks to synthesize bio-based polymers with performance-advantaged properties. First, we give an overview of bio-feedstocks and describe shortcomings of current synthetic polymers. The majority of the Review highlights recent successes in the development of performance-advantaged, bio-based polymers (PBPs) with C–O or C–N linkages in their backbones. We end by summarizing guiding principles and challenges for the development of such materials.

2.3. Sourcing Bio-Feedstocks

Sustainably sourced feedstocks for the synthesis of PBPs are available across a wide range of forms and volumes, both as natural polymers and as small molecules. We briefly discuss typical feedstocks available on a large scale as polymers or small molecules (Figure 2.2) and describe several transformations that can be applied to these bio-derived intermediates, including those relevant to the PBPs highlighted below. Note that the direct use of naturally occurring polymers as polymeric materials is a major research field but is not covered here.^{12,29,30}

Agricultural crops are used to produce starch and soluble sugars at the commodity scale for use as precursors to a few bio-based chemicals. In many cases in which bio-based polymer precursors are derived from carbohydrates, this availability offers a bio-based feedstock for immediate use at scale.

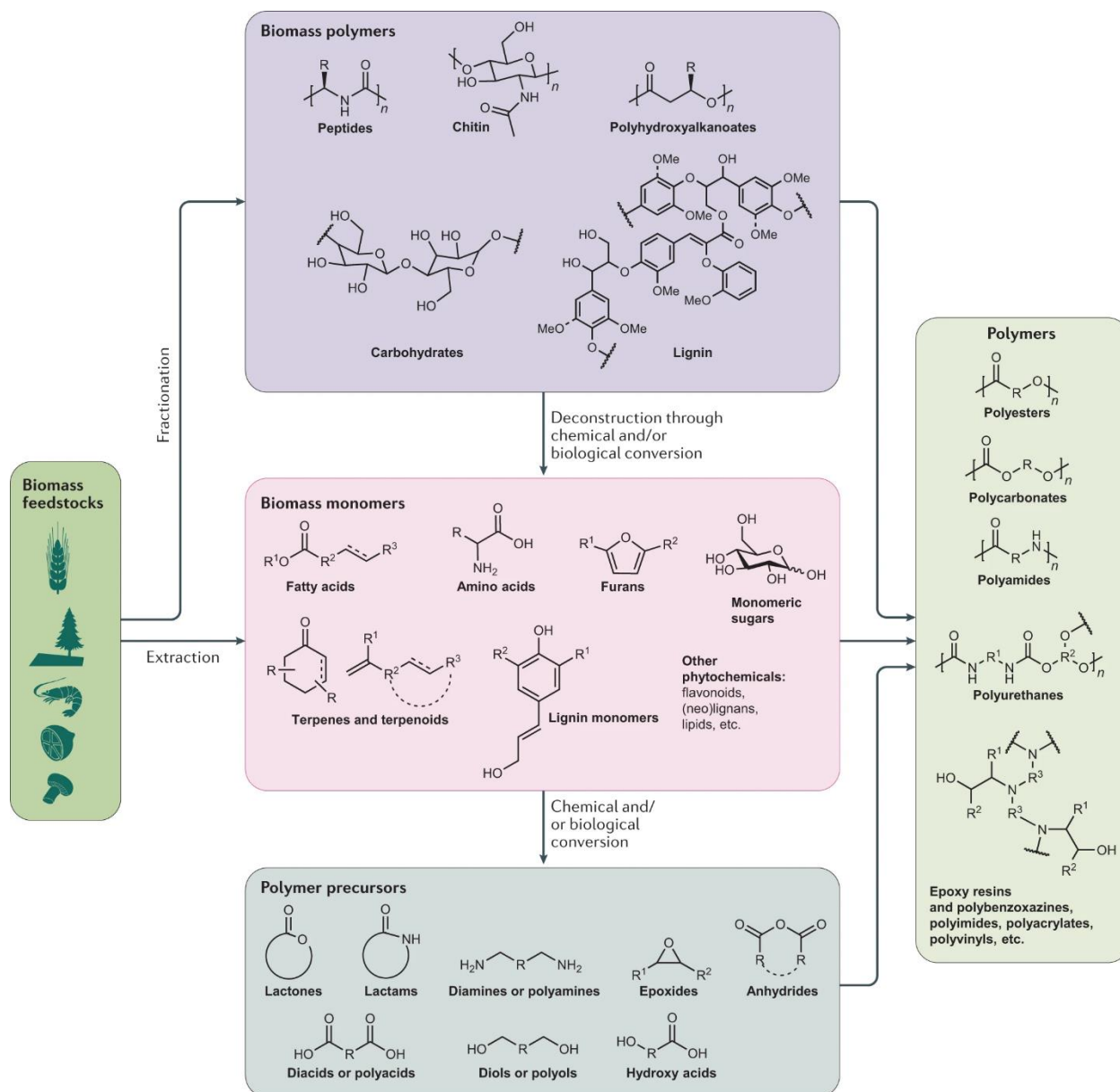


Figure 2.2. Polymers from biomass. A range of biomass feedstocks yield biopolymers, which can be deconstructed into constituent products through chemical and/or biological conversion as well as incorporated directly into polymers. Small molecules can also be extracted directly from the biomass feedstock. These monomeric bio-derived compounds, if not already polymerizable, can be transformed into precursors for polymer synthesis. Structures shown are illustrative and do not fully represent the structural complexity and variety afforded by nature, which can be further compounded through synthetic transformations, and polymer repeating units may vary slightly depending on the particular polymerization strategy.

Beyond starch and soluble sugars, the plant cell-wall polysaccharides, cellulose, hemicellulose³¹ and pectin³², and the aromatic polymer lignin³³ have been pursued as sustainable

feedstocks for more than a century, and with renewed vigor since the 2000s. The development of chemical processes to extract, fractionate and deconstruct plant cell-wall polymers into building blocks is intensely researched. Numerous biological, chemical and thermal processes are used to transform plant cell-wall polymers into small-molecule intermediates, such as carbohydrates, lignin-derived aromatic compounds, pyrolysis-derived intermediates and extractives³⁴ (Figure 2.2). Other plant polymers include cutin and suberin, which are natural polyesters and a readily accessible source of fatty acids and aromatic carboxylic acids.³⁵ Plants also commonly harbor diverse small molecules in the form of phytochemicals, including alkaloids, terpenoids, phenolics and fatty acids, among others, which can often be liberated through mild chemical extraction processes or made as targets of metabolic engineering from more abundant feedstocks. The non-food components of plants, thus, offer a rich source of natural polymers and small molecules for conversion into unique building blocks through selective transformations or direct use (discussed further below).

Besides plants, additional sources of bio-feedstocks include other structural polymers, such as chitin, a polysaccharide found in fungi and arthropod exoskeletons.³⁶ Chitin is a homopolymer of β -1,4-*N*-acetylglucosamine (Figure 2.2) and, thus, has been a focus of the nitrogen-based chemicals and materials field.^{37,38} Chitin can be converted into useful chemicals by methods mirroring those used in the conversion of plant cell-wall polysaccharides.³⁹ Additionally, polysaccharides, proteins and oils common to heterogeneous food-waste streams offer bio-feedstocks that can be fractionated and processed into many of the same building blocks as those from plant cell-wall components.

To convert bio-based feedstocks into building blocks for PBPs often requires additional chemical transformations to obtain the necessary functionality for polymerization. Fortunately,

there is a vast research community focused on selective chemical and biological transformations of bio-feedstocks and small-molecule intermediates into building blocks for new bio-based polymers. As highlighted below, these transformations often involve chemical catalysis,¹³ biological catalysis⁴⁰ or some combination thereof (Figure 2.2).^{20,41–43}

2.4. Polymer Properties

The unique chemical functionality of bio-derived monomers can endow the resulting polymers with performance-advantaged properties. However, before these materials can be scaled up or petrochemical feedstocks replaced, the polymer properties must be characterized and benchmarked relative to the incumbent materials.

Fundamental Polymer Properties. The fundamental properties of bio-based polymers (that is, thermomechanical properties) (Figure 2.3) must be measured and compared with those of typical polymers (Table 2.1) to determine whether they exhibit performance-advantaged properties. In general, polymers must be above a critical molecular weight to experience chain entanglement (M_e) and show consistent properties. The M_e is polymer dependent and can be determined by rheology, hallmarked by the zero-shear viscosity exhibiting a non-linear scaling with molecular weight. Typically, the number and weight-average molecular weights (M_n and M_w , respectively) and chain-length dispersity index (\mathcal{D} , calculated by M_w/M_n) are determined using gel permeation chromatography and expressed in daltons. Thermal properties, which dictate the working temperature window of a polymer, are usually characterized by differential scanning calorimetry, with exothermic and endothermic curves revealing when a material undergoes a glass, melting or crystallizing transition at the temperatures T_g , T_m and T_c , respectively. The thermal decomposition temperature (T_d) is measured by thermogravimetric analysis. Dynamic mechanical analysis reveals

thermal transitions as a function of the storage and loss moduli (E' and E'' , respectively) versus temperature (Figure 2.3.a), illustrating how the glass transition corresponds to softening of a material. For an amorphous, low M_w polymer, the transition to viscous flow occurs immediately, whereas a semi-crystalline polymer has a rubbery plateau between its T_g and T_m and can be used up to the T_m . In terms of mechanical properties, tensile testing (Figure 2.3.b,c) provides a stress (σ)–strain (ϵ) curve, the shape of which (the initial slope is defined as the Young’s modulus, E , and the area underneath as toughness) and the ultimate stress and strain at break (σ_B and ϵ_B , respectively) determine the suitability of a polymer for applications. For example, a material that continues to elongate after reaching maximum stress is considered tough, whereas one that does not is brittle. Although each polymer class (for example, polyesters) or material type (for example, rubbers) has a typical range of thermomechanical properties, the profile can vary depending on functionality, architecture and processing conditions.

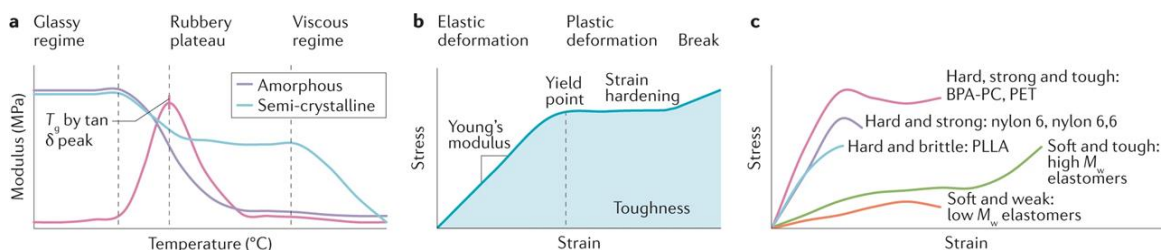


Figure 2.3. Fundamental thermomechanical polymer properties. **a** | Idealized dynamic mechanical analysis plots for amorphous and semi-crystalline polymers with characteristic regions defined. **b** | Idealized stress–strain plot with tensile properties defined. **c** | Idealized stress–strain curves illustrative of common material classes and synthetic polymers. BPA-PC, poly(bisphenol A carbonate); M_w , weight-average molecular weight; PET, polyethylene terephthalate; PLLA, poly-L-lactic acid; T_g , glass transition temperature.

Table 2.1. Thermomechanical properties of common polymers

Polymer	T_g (°C)	T_m (°C)	σ_B (MPa)	E (MPa)	ϵ_B (%)
HDPE	$-140 \leq T_g \leq -100$	130–137	22–31	1,070–1,090	100–1,200
LDPE	< -40	80–115	8.3–34	100–300	100–800
<i>it</i> -PP	$-20 \leq T_g \leq -10$	160–170	31–41	1,140–1,550	100–700
BPA-PC	145–150	–	60–121	2,0658– 2,410	65–107
PET	67–75	245–260	48 ^a –172 ^b	2,757 ^a – 4,136 ^b	100 ^b –500 ^a
PLLA	55–65	160–186	60	1,720	3–6
Nylon 6	40–60 ^c	218–231	50–95	1,500– 3,000 ^c	5–300
Nylon 6,6	50–80 ^c	265–280	35–90 ^c	1,500– 3,500 ^c	5–200

Data for all polymers from the Polymers: A Property Database (mechanical property data obtained with standardized methods from ASTM International and ISO). ϵ_B , strain at break; σ_B , stress at break; E , Young's modulus; HDPE, high-density polyethylene; *it*-PP, isotactic polypropylene; LDPE, low-density polyethylene; BPA-PC, poly(bisphenol A carbonate); PET, poly(ethylene terephthalate); PLLA, poly-l-lactic acid; T_g , glass transition temperature; T_m , melting temperature. ^aAmorphous. ^bBiaxially oriented. ^cMeasured from humid to dry conditions.

Performance-Advantaged Properties. Performance-advantaged properties include improved manufacturability, properties for specific applications and/or end-of-life considerations (such as recyclability or degradability). Importantly, the application properties must be at least on par with those of incumbent materials, and are generally evaluated by the thermomechanical profile. As an example of property enhancement, structurally rigid functional motifs (such as alkenes, ketones, aromatics and bicyclics) often lead to a higher T_g and, thus, such materials can be used at higher temperatures, whereas long alkyl chains ($>C_6$) containing heteroatoms, which are more difficult to obtain from petroleum-based feedstocks, can render greater ductility.^{44–46} These properties, among others such as flame-retardant properties, are often achieved with polymer additive formulations. Using bio-based monomers to form polymers that inherently exhibit these properties avoids the use of often toxic additives (for example, phthalate plasticizers or brominated flame retardants).

Thus, bio-derived monomers could mitigate the toxicological effects associated with polymer manufacturing, use or degradation. Styrene, for example, can yield polymers with robust thermomechanical performance, but its high volatility and toxicity pose health risks.⁴⁷ Similarly, bisphenol A (BPA) imparts favourable properties to polymers owing to its rigidity, but is an endocrine disruptor.^{48–50} In both cases, bio-derived aromatic monomers can serve as advantaged replacements because additional ring substitutions reduce volatility, toxicity and the potential for endocrine disruption.^{51–53} Furthermore, bio-based chemical functionality can facilitate processing, such as faster cure times (that is, the time for crosslinking of individual components to form a network) through amine–ketone condensation compared with typical epoxide–amine chemistries.⁵⁴ The bio-based monomer 1,3-propanediol has replaced 1,4-butanediol and ethylene glycol in some terephthalate polyester products, owing not only to an inexpensive and low-energy production route but also to the resultant changes in polymer morphology that improve the crystallization rate, structure and material elasticity, among other advantages in applications, manufacturing and recycling.^{55,56} Indeed, the prevalence of hydroxy acids, lactones, amines, aldehydes and ketones in bio-based monomers offers unlimited potential to redesign plastics to be chemically recyclable or biodegradable.

To fully capitalize on the unique functionality afforded by bio-feedstocks, it is necessary to establish structure–property relationships. Additionally, new catalysts and synthetic methodologies are needed to accommodate the complex sterics, electronics and functionalities of these monomers. In the following, we further explore how bio-derived functionalities give rise to polymers with performance-advantaged properties, focusing on renewable polymers with oxygen-linked and nitrogen-linked backbones for non-biomedical applications. For these heteroatom-linked polymers, functionality for step-growth polymerization is often more directly accessible

from bio-feedstocks. Chain-growth, ring-opening polymerization (ROP), however, offers more control of the polymerization and often superior polymer properties, as small molecules are removed during monomer synthesis rather than during polymerization. For vinyl addition chain-growth monomers, it is common for an acrylic portion to be installed on the biomolecule, although this is also easily bio-based.⁵⁷ Although not reviewed here, bio-based polymers with hydrocarbon backbones (that is, vinyl and acrylic)^{44,58-62} can also be performance-advantaged. For example, the α -methylene- γ -butyrolactone (MBL; also known as Tulipalin A) family yields acrylic bioplastics with increased thermal and solvent resistance as well as depolymerization selectivity for monomer recovery relative to polymethyl methacrylate, due to stabilization of radical intermediates by the natural pendent lactone motif.^{58,63}

2.5. C-O Linked Polymers

Polyesters.

Polyesters are versatile materials traditionally synthesized by condensation of oxygenated AA/BB or AB monomers (Figure 2.4), and are ideal targets from bioderived monomers, garnering considerable attention.^{16,17,21,23,44,64-68} Microorganisms directly synthesize polyesters for carbon and energy storage as polyhydroxyalkanoates (PHAs)^{69,70} (Figure 2.2), whereas synthetic polyesters are made through step-growth condensation of carboxylates and diols or hydroxy acids, chain-growth ROP of cyclic esters (lactones or lactides) or alternating ring-opening copolymerization (ROCOP) of anhydrides and epoxides.^{21,71} The most widely consumed polyester is polyethylene terephthalate (PET), which is mass produced for textiles and packaging; however, PET persists in the ambient environment for >400 years (ref.⁷²). Bio-based polylactic acid (PLA) is a commercially available and industrially compostable alternative to PET for short-term

packaging applications; the inherently chiral monomer leads to a highly isotactic polymer (poly-L-lactic acid (PLLA)) with improved properties relative to atactic PLA. Sugar-derived polyethylene furanoate (PEF) has been proposed to compete with PET, as its thermal properties are similar but it has $\sim 10\times$ lower oxygen permeability (0.0107 barrer versus 0.114 barrer for PET), which is advantageous for food preservation.⁷³ However, PEF is brittle and does not exhibit strain-hardening, which limits its use in pressurized environments.^{74–76} These examples demonstrate the need for comprehensive benchmarking of bio-based materials. In this section, we discuss examples of performance-advantaged polyesters made by step-growth and ring-opening chemistries.

Step-growth polyesters. Lignin-derived monomers are commonly used to produce semi-aromatic polyesters.^{17,30,44,77,78} Although various PET analogues exhibit T_g values comparable with or higher than that of PET, the mechanical properties are understudied.^{79–83} Thus, there is little evidence to suggest these materials offer advantages over PET in applications. A potential exception is poly(dihydroferulic acid), which is synthesized from an AB monomer and possesses the requisite PET-like thermal properties ($T_g \approx 73$ °C, $T_m \approx 234$ °C (~ 30 °C lower than that of PET), $T_c = 196$ °C), and crystallizes faster, implying processing benefits; however, tensile analysis was not reported.⁷⁹

Another lignin-derived AB monomer, *p*-coumaric acid (Figure 2.4a), has an α,β -unsaturated acid motif that can participate in a post-polymerization, light-initiated cycloaddition (at wavelengths (λ) > 280 nm) to increase the mechanical strength of hyperbranched poly(coumaric-*co*-caffeic acid).⁸⁴ The photoreaction increased σ_B from 50 to 104 MPa and E from 16 to 19 GPa, comparable with those of poly(bisphenol A carbonate) (BPA-PC). Moreover, the potential for biodegradation was demonstrated in soil, or with a combination of accelerated hydrolysis and

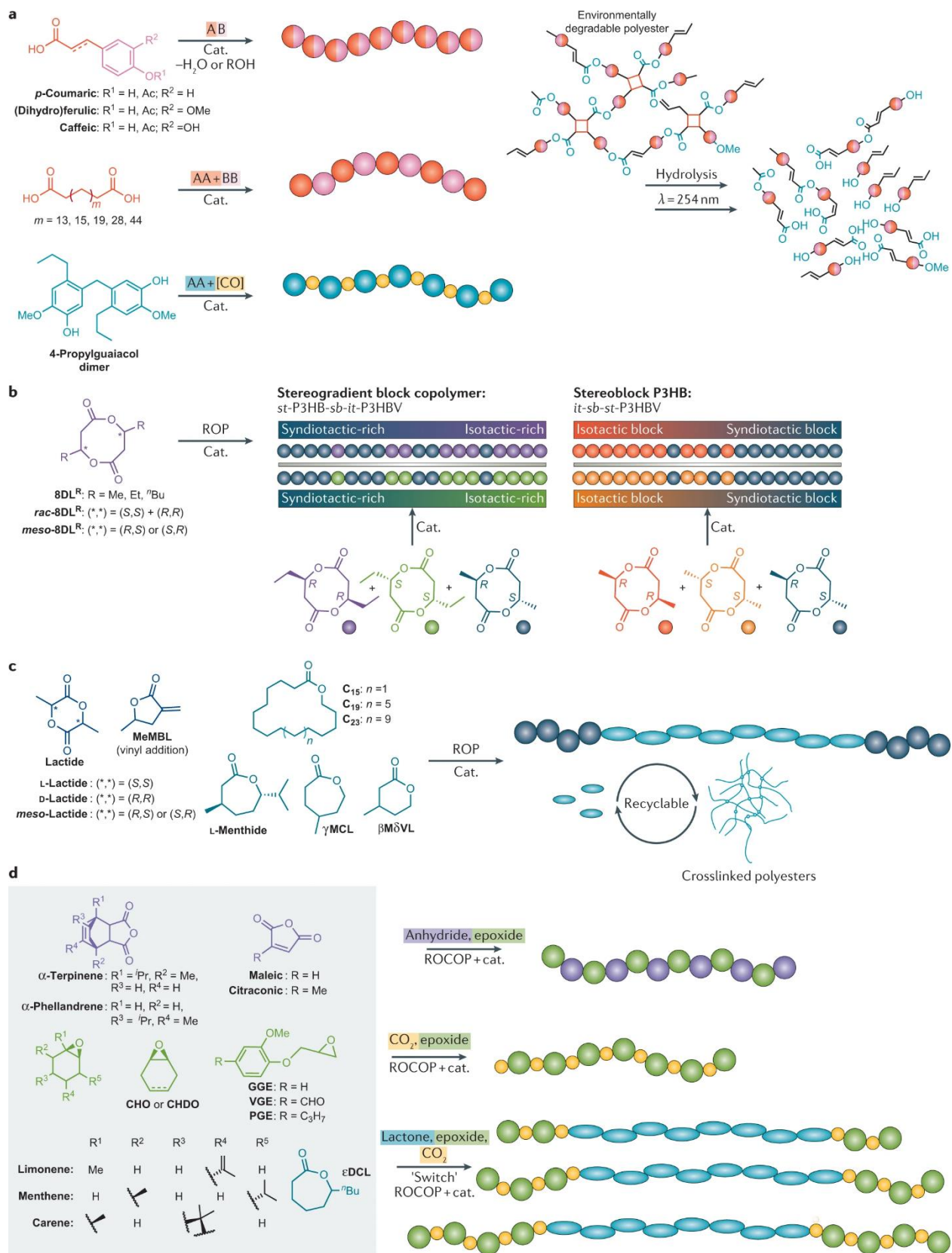


Figure 2.4. Variety of available bio-based polymer architectures with C–O intermonomer

linkages. Examples of bio-derived monomers and polymerization methods for synthesizing C–O linked polymers. **a** | Condensation of AA/BB or AB monomers to form polyesters (red and pink) and polycarbonates (blue and yellow). [CO] refers to a carbonyl-containing co-monomer, such as phosgene or dimethyl carbonate, used to form the carbonate linkage in polycarbonates. Synthesis of the hyperbranched polyester is followed by light-initiated cycloaddition of the α,β -unsaturated moieties to crosslink the polymer shown on the right; accelerated hydrolysis and irradiation at 254 nm results in degradation to small molecules, whereas burying in soil for 10 months leads to gradual biodegradation.⁸⁴ **b** | Selective ring-opening polymerization (ROP) of eight-membered cyclic diolides (8DLR) to form (stereo)block (right) or (stereo)gradient (centre) polyhydroxyalkanoate (PHA) copolymers. Random copolymers are accessible but not shown. **c** | ROP of lactones (soft monomers shown as teal ovals and hard monomers as navy spheres) to polyesters, including crosslinked homopolymers and tri-block copolymers (tri-BCPs). **d** | Ring-opening copolymerization (ROCOP) of anhydrides (purple) and epoxides (green) to polyesters, and CO₂ (yellow) and epoxides to polycarbonates. Switchable ROCOP of lactones, epoxides and CO₂ to produce polyester–polycarbonate BCPs. Epoxide and some anhydride structures shown are derived from terpene in the associated labels and are not the native structures. β M δ VL, β -methyl- δ -valerolactone; γ MCL, γ -methylcaprolactone; ϵ DCL, ϵ -decalactone; CHDO, cyclohexadiene oxide; CHO, cyclohexene oxide; GGE, guaiacol glycidyl ether; *it*, isotactic; MeMBL, γ -methyl- α -methylene- γ -butyrolactone; P3HB, poly(3-hydroxybutyrate); P3HBV, poly(3-hydroxybutyrate-*co*-3-hydroxyvalerate); PGE, propylguaiacol glycidyl ether; *sb*, stereoblock; *st*, syndiotactic; VGE, vanillin glycidyl ether. Panel b adapted with permission from ref.¹⁰⁷, AAAS.

further ultraviolet irradiation ($\lambda = 254$ nm) producing oligomeric and monomeric units ($M_n < 1,000$ Da). Polymers of aliphatic camphoric acid, derived from the oxidation of a bicyclic terpene, exhibit T_g values exceeding that of PET owing to the rigid five-membered ring, and hydrolysis over 14 days yielded monomers and oligomers ($M_n < 600$ Da), even at neutral pH.⁸⁵ Although exploratory, these examples demonstrate how bio-derived functionalities can afford useful thermal and mechanical properties paired with built-in degradation mechanisms.

Trans,trans-muconic acid, which can be obtained from carbohydrates or lignin after facile isomerization of biologically produced *cis,cis*-muconic acid,^{86–89} has furnished unsaturated polyesters for performance-advantaged fiber reinforced plastics.^{52,90} The backbone alkenes in these polyesters allow for reaction with small-molecule crosslinkers, and employing *trans,trans*-muconic acid avoids the use of maleic anhydride to introduce unsaturation and noxious styrene to

crosslink. Relative to maleic anhydride-based polyester resins for fiber-reinforced plastics, muconate-containing polyester materials showed improved strength, thermal properties and adhesion to fibers, because the diene functionality increases the rigidity of the initially linear polymer matrix and provides more crosslinking sites. Additionally, the use of bio-based cinnamic acid with methacrylic acid as branching units showed better compatibility with the unsaturated polyester, and therefore reactivity, than did styrene. In a demonstration of upcycling, *trans,trans*-muconate was polymerized with reclaimed PET oligomers, producing composites that transform US \$0.51 lb⁻¹ waste into a useful US \$2.60 lb⁻¹ product.⁹¹ These composites have attractive mechanical properties and are predicted to save 57% in supply chain energy and decrease greenhouse gas emissions by 40% relative to the preparation of conventional unsaturated polyesters for fiber-reinforced plastics, demonstrating both manufacturing and in-use advantages.

Fatty acids have been transformed into long-chain (C₁₇, C₁₉, C₂₃) aliphatic polyesters (Figure 2.4a) with properties similar to those of low-density polyethylene (LDPE).^{45,92-96} The transformation involves isomerizing alkoxy-carboxylation to give diesters, which subsequently undergo polycondensation with their reduced diol counterparts to form polyesters.^{45,92-96} Even longer-chain C₃₂ and C₄₈ diesters produce polyesters with a higher T_m (120 °C).⁹⁷ The degradability of long-chain aliphatic polyesters is often claimed as an advantage over their comparative polyolefins and is attributed to their likeness to cutin or suberin. A polyester comprising C₁₂ and C₆ monomers showed favourable gas permeability properties, but did not compost at 40 °C over 140 days; only more hydrophilic copolymers with lower crystallinity degraded under the composting conditions.⁹⁸ Polyesters that are more crystalline and hydrophobic would require modification to biodegrade in soil or compost.

PHAs, however, are well known for biodegradability under ambient conditions.^{69,70,99–101} Poly(3-hydroxybutyrate) (P3HB) has exceptional gas barrier properties and outperforms prevalent packaging plastics, because its perfect isotacticity imparts a high degree of crystallinity.¹⁰² However, P3HB is very brittle ($\epsilon_B \approx 3\%$) with a T_m (~ 175 °C) close to the T_d (~ 250 °C), limiting its use.¹⁰¹ Properties can be tailored by incorporating more flexible co-monomers, enabling commercial ventures to begin marketing various PHA products,⁶⁶ whereas converting municipal and agricultural waste into PHAs is an active research area.^{21,99,101,103–105} Synthetic PHAs offer further scope for property enhancement. After 60 years of research, the chemical synthesis of PHAs was finally accomplished by ROP, with the materials rivalling natural PHAs, and with increased control of D and copolymer microstructures (Figure 2.4b).^{106–109} However, the chemical circularity of PHAs needs to be addressed, as degradation in the environment is a fail-safe, leading to loss of value.¹¹⁰

ROP Polyesters. Although many bio-derived functionalities enable straightforward polycondensation of AA/BB or AB monomers, process efficiency can suffer owing to steric and electronic factors as well as competing functionalities of more complex monomers. Precise control of monomer stoichiometry and high temperature and vacuum for long periods can be necessary to reach entanglement Me while fighting thermal degradation. Conversely, ROP of lactones offers exquisite control of the polymerization characteristics (M_n , D , stereoselectivity, microstructure, chain ends and topology), offers tunable kinetics using organometallic and organic catalysts, and can be conducted under mild conditions. Alternating ROCOP has also enabled polyester synthesis from cyclic anhydride and epoxide monomers.^{21,71} Additionally, although all polyesters are inherently hydrolysable, catalytic depolymerization enables lactone recovery when the thermodynamics are well balanced.¹¹¹ ROP further allows for different (co) polymer architectures,

such as random, block, graft, star-shaped and cyclic structures, as well as the inclusion of (reversible) crosslinkers.⁶⁴ Block copolymers (BCPs) can now be screened in high throughput by exploiting the tunable activity of cyclic oxygenate monomers with organocatalysts; for example, 100 unique polymers were produced in just 9 min using a continuous flow reactor.¹¹² Thus, ROP polyesters are often performance-advantaged owing to their modularity and end-of-life options.

The recent success in chemically synthesizing PHAs was inspired by the synthesis of PLA, which proceeds through ROP of a six-membered cyclic monomer comprising two lactic acid units (lactide; monomer shown in Figure 2.4c), with ROP leading to a polymer superior to that produced through hydroxy acid polycondensation. For PHAs, an eight-membered cyclic diolide monomer (8DL^R, R = Me, Et or ⁿBu) (Figure 2.4b) is ring-opened.^{106–108} In contrast to enantiopure L-lactide ROP, whereby a single stereoisomer is polymerized by a non-selective tin catalyst, racemic (*rac*) mixtures of 8DL^R are polymerized by stereoselective catalysts. *Rac*-8DL^{Me} produces perfectly isotactic P3HB under ambient conditions in 1 min, and different 8DL^R monomers can be copolymerized to produce various PHAs. The microstructures and resulting material properties are controlled by the catalyst selectivity and co-8DL^R feed ratios, leading to random, (stereo)block or (stereo)gradient copolymers that are ductile and tough while maintaining high crystallinity. Polymerizing 1:1 *rac:meso*-8DL^{Me} increased the ϵ_B of P3HB sixfold, owing to the syndiotactic stereoblock ($T_m = 157,141$ °C) (Figure 2.4b, right). Elongation of nearly 600% was attained by polymerizing 4:1 *meso*-8DL^{Me}:*rac*-8DL^{Et} to form a syndiotactic P3HB block capped by an isotactic poly(3-hydroxyvalerate) (P3HV) block (Figure 2.4b, center). These microstructures were formed owing to the kinetic preference of the selected catalyst for 8DL^{Me} over 8DL^{Et}, and for the *rac* over the *meso* diastereomer for a given monomer. Compared with P3HB, the P3HB–P3HV copolymer ($T_m = 135$ °C, $\sigma_B = 24$ MPa, $E = 169$ MPa) has a wider processing window and

application space, but maintains polyolefin-like properties. However, the effects of unnatural tacticities require further characterization.¹¹³ The 8DLR monomers are synthesized in four steps from succinate, but there is opportunity to dimerize hydroxy acids by shape-selective catalysis;¹¹⁴ this would enable the circular life cycle of PHAs, which can be hydrolysed to *rac* or enantiopure hydroxy acids.¹¹⁵

ROP of larger lactones is entropy driven and, thus, requires high temperatures. However, enzymatic and coordination catalysis methods have enabled ROP of plant oil-based C₁₅, C₁₉ and C₂₃ lactones.^{21,96,116–122} Reactive extrusion coupled to an enzymatic process was recently demonstrated¹²² and accelerated degradation studies show that the incorporation of smaller (C₆) lactones allows for more rapid hydrolysis by breaking up the hydrophobic backbone.¹¹⁹

Owing to unique sets of bio-derived functionalities, bio-based polyesters show performance advantages in applications such as elastomers and adhesives, wherein non-degradable vinyl polymers dominate.^{64,123,124} ROP of lignocellulose-derived β -methyl- δ -valerolactone (β M δ VL) and γ -methylcaprolactone (γ MCL) (Figure 2.4c) with ester-based crosslinkers produces materials with ϵ_B , σ_B and elasticities on par or superior to those of vulcanized natural rubber bands.^{125,126} Recycling of poly(β M δ VL) recovered 90% monomer, whereas poly(γ MCL) yielded its hydroxy acid when subjected to enzymatic degradation.¹²⁷ Advantages for adhesives beyond competitive adhesive strength include hydrolysability (non-degradable counterparts cause gumming problems in recycling processes), reduced use or elimination of volatiles and toxics, toughness or flexibility and hydrophobicity.^{124,128} Pressure-sensitive adhesives formed through the condensation of fatty acid and sugar-based monomers with 99%+ bio-based content and tunable properties have been commercialized, with a preliminary life cycle analysis showing lower environmental impact compared with polyacrylic tapes.^{123,129} However, ROP offers more opportunities to tune properties

through design of BCPs with specific segment lengths and hardness, by virtue of telechelic end groups and the wide variety of applicable bio-based monomers.⁶⁴

In an ABA tri-BCP approach to pressure-sensitive adhesives, terpene-derived L-menthide (Figure 2.4c) was used as a low T_g central block and PLA as short, hard end blocks.¹²⁸ The backbone substituents suppress crystallization whereas the hard PLA end caps induce the microphase separation necessary for good viscoelasticity. When mixed with a bio-based rosin-ester tackifier, the tri-BCP displayed adhesive properties superior to or comparable with those of styrene-based tapes (with a peel adhesion strength of 3.2 N cm^{-1} versus $1.9\text{--}4.2 \text{ N cm}^{-1}$ for commercial tapes). With hard poly- γ -methyl- α -methylene- γ -butyrolactone (P(MeMBL), a bio-based polyacrylate) as the end caps, similar competitive properties were realized with the added advantage of a heat-fail temperature of $>150 \text{ }^\circ\text{C}$ due to the high thermal stability of poly(α -methylene- γ -butyrolactone)s, surpassing that of non-crosslinked styrenic BCP adhesives.¹³⁰

The most impressive pressure-sensitive adhesive, which does not require tackifier to outperform commercial tapes, is part of a series of ABA polycarbonate-*block*-polyester-*block*-polycarbonate BCPs made by switchable ROCOP catalysis.¹³¹ With an optimized coordination catalyst and reaction conditions, a mixture of bio-based ϵ -decalactone and cyclohexene oxide (to which a bio-based route has been established¹³²) was selectively polymerized to poly(ϵ -decalactone) by ROP until CO_2 was introduced, after which the mechanism switched to epoxide/ CO_2 ROCOP to produce poly(cyclohexane carbonate) (PCHC) end blocks (Figure 2.4d). Tough plastics, elastomers or adhesives are formed depending on only the block lengths. The shortest PCHC block led to an adhesive with a peel strength of 10 N cm^{-1} , which is far higher than those of commercial tapes and other bio-based tri-BCPs. When the polymer is 50 wt% PCHC, a strong and tough plastic is realized ($\sigma_B = 20 \text{ MPa}$, $\epsilon_B = 900\%$), whereas 28 wt% produces an elastic

material with shape recovery. Similarly, a strong, tough plastic with near-ideal elasticity is produced when a recyclable poly(β M δ VL) mid-block is capped by 32% semi-crystalline PLLA ($\sigma_B = 28$ MPa, $\epsilon_B = 1,720\%$), and a similar PLLA content with a γ MCL mid-block has a σ_B of 35 MPa and ϵ_B of 895%.^{133,134} The customizability of oxygenated ABA BCPs, enabled by tunable catalysts, is key to producing these PBPs.

Bio-derived functionalities are apt for epoxide/anhydride ROCOP systems (Figure 2.4d), leading to polyesters with high and tunable T_g values. Epoxidation and Diels–Alder chemistry enable the conversion of bio-derived functionalities to both monomer types, whereas the one-pot cyclization of diacids to anhydrides and subsequent ROCOP with an epoxide has been demonstrated with tandem catalysis.¹³⁵ Epoxides derived from terpenes and 1,4-cyclohexadiene (CHD), a by-product of fatty acid metathesis, undergo ROCOP with phthalic anhydride (Figure 2.4d), affording materials with respectable M_n values of up to 25 kDa and T_g values in the range 59–165 °C (refs^{132,136}). Introducing unsaturation into ROCOP polyesters is reportedly easier with CHD oxide (CHDO) than with maleic anhydride.¹³² Sugar and terpene-based dienes have served as precursors to tricyclic anhydrides by Diels–Alder reaction with maleic anhydride. These anhydrides polymerize with propylene oxide or cyclohexene oxide to form polyesters with T_g values of 66–184 °C (refs^{137,138}). For example, the polyester formed from propylene oxide and the adduct of α -terpinene and maleic anhydride has a T_g of 109 °C ($M_n = 55$ kDa).¹³⁷ Moreover, CO₂ can be added to introduce random carbonate linkages along the backbone and potentially enhance materials.²¹

ROCOP studies have focused on understanding relationships between monomer combinations, catalyst performance (activities and selectivities) and thermal properties, but not on mechanical properties. Although T_g values are high, the proximity of ester linkages (two or three carbons apart)

could curb the strength and ductility.²¹ Thus, research should move towards establishing PBPs using now well-developed ROCOP methods. For example, using ROCOP, polyesters were made from phthalic anhydride, guaiacol glycidyl ether (epoxide) and a small fraction of vanillin glycidyl ether¹³⁹ (Figure 2.4d). Both glycidyl ethers participate in ROCOP, whereas the pendent aldehyde groups on vanillin glycidyl ether can react with a diamine to form reversible imine crosslinks. The resulting crosslinked polyesters are hard and strong, reprocessable and recyclable, with T_g values of ~60–70 °C.

Polycarbonates.

BPA-PC, the most common polycarbonate, is amorphous, hard and tough (Figure 2.3c), with a high T_g (145–150 °C) (Table 2.1), outstanding impact strength and optical clarity, making it a valuable engineering plastic. However, BPA is an endocrine disruptor, and its replacement analogues are also not inert,^{48–51} whereas the co-monomer phosgene is lethal, initiating research into safer alternatives from bio-feedstocks.^{51,140} ROCOP of epoxides/ CO_2 and selective ROP of cyclic carbonates are phosgene-free routes to polycarbonates, but monomer scope is more limited.²¹ In the former, carbonate linkages are only two or three carbons apart, but properties can be modulated by introducing ester linkages. Aliphatic polycarbonates are easily bio-derived and biodegradable,¹⁴¹ but are not engineering plastics. Applications include biomedical materials,^{68,139,142–144} coatings,^{145,146} transparent elastomers^{144,146} or as components of other materials (such as polyethercarbonates and polycarbonate polyols).^{147–149}

Step-growth polycarbonates. Estrogen receptor binding is hampered when phenolics have an *ortho*-methoxy substituent, a common lignin-derived functionality.⁵¹ In human Estrogen receptor studies, the dimer of 4-*n*-propylguaiacol (Figure 2.4a), derived from lignin, shows a pronounced reduction in potency (10–100×) compared with BPA and related analogues. A polycarbonate made

from the 4-*n*-propylguaiacol dimers and triphosgene shows a T_g of 99 °C, but optimization of the low M_n (~5 kDa) could further increase the T_g . Owing to the propyl chains, this polycarbonate is more soluble than those made from the other bisphenols, which is advantageous for processing. However, a higher M_n and mechanical characterization are necessary to establish a performance-advantaged bio-polycarbonate.

Properties competitive with those of BPA-PC have been achieved using isosorbide, a rigid bicyclic diol, and diphenyl carbonate, employing highly active amino acid-based ionic liquid catalysts.¹⁵⁰ High molecular weights ($M_w > 100$ kDa) and yields were reached in 1 h, and the resulting polycarbonate has a T_g of 174 °C. However, owing to brittleness, isosorbide was copolymerized with 1,4-butanediol and 1,4-cyclohexanedimethanol. With 50% isosorbide, the resulting polycarbonate had a T_g of 98 °C with impressive σ_B , ε_B and E values of 57 MPa, 145% and 979 MPa, respectively. These properties show good potential for BPA-PC applications and beyond. An isosorbide-based poly(arylene ether) also outperformed BPA-PC. The bio-based super-engineering plastic is recyclable, transparent and has a high M_n (>100 kDa), exhibiting a high T_g of 212 °C, σ_B of 78 MPa and a low coefficient of thermal expansion.¹⁵¹

ROP Polycarbonates. ROCOP of limonene oxide (LO) or CHDO (Figure 2.4d) and CO₂ produces polycarbonates with high T_g values (~110–120 °C) that are biodegradable and chemically recyclable.^{111,142,143,145,152} When hydroxyl impurities from the limonene source are masked, poly(limonene carbonate) (LO-PC) reaches a T_g of 130 °C — the highest reported for an aliphatic polycarbonate. Upon scaling the synthesis to >1 kg, LO-PC reached a high M_n of >100 kDa, enabling mechanical characterization.¹⁴⁶ This hard and strong polycarbonate has mechanical properties ($\varepsilon_B = 15\%$, $\sigma_B = 55$ MPa) between those of polystyrene and BPA-PC with desirable optical properties. This methodology also used an immobilized chelating agent for catalyst

removal, decreasing solvent use by tenfold during polymer purification. However, LO-PC can discolor in the melt owing to a low T_d . As an additive, ethyl oleate reduces discoloration, but results in a trade-off between rheological and thermomechanical properties.¹⁵³ Both LO-PCs and CHDO-PCs have unsaturated bio-derived functionalities for post-functionalization, which is especially useful for lower M_n polymers. When crosslinked with tri-thiols, the resulting materials have properties important for coatings: high transparency and hardness, solvent and scratch resistance, and good adhesion to metal.¹⁴⁵

Epoxy Resins.

Epoxy resins (epoxies) are widely used thermosets in construction, energy, food and transportation sectors, with their tunability, high T_g , low density, robust mechanical strength and solvent resistance making them suitable for use in coatings^{154,155} and adhesives,¹⁵⁶ or to reinforce other materials.¹⁵⁷ The reliance on BPA and volatile solvents as well as the lack of recyclability have inspired a search for safer, high-performance alternatives with superior end-of-life properties.^{48,51,53,78,158–161} In this regard, bio-based monomers have afforded less toxic epoxies with improved thermomechanical and end-of-life features.^{46,54,154,155,162–175} Epoxy networks comprise an epoxide-containing monomer and a crosslinking monomer (hardener), which provide structural modularity and tunability for specific applications (Figure 2.5a). Rigid aromatic epoxide monomers from lignin can provide high T_g values,¹⁷² although multiple methoxy substituents progressively lower the T_g (refs^{172,176}). Conversely, unsaturated fatty acids can be epoxidized to provide a flexible component when cured with various bio-based hardening agents.^{154,155} For example, varying the bio-based polyacid hardener reacted with epoxidized sucrose soyate (Figure 2.5a) tunes the thermomechanical properties of the epoxy resin and can promote a H₂O-soluble formulation.¹⁵⁵

Dynamic covalent networks could address the waste issue associated with conventional thermosets, as the exchange of bonds in response to heat allows for reprocessing of the network.^{160,161} In a lignin-based example, vanillin and guaiacol were joined in a triphenyl–triepoxymonomer, which was reacted with an anhydride to yield a network with a T_g of 187 °C, which is 30 °C higher than that of the BPA counterpart.¹⁷⁷ The material undergoes dynamic transesterification with an embedded catalyst, self-healing within 10 min, and thus is repairable with a high service temperature. In another example, vanillin was coupled with aminophenol to form an imine-containing monomer before functionalization with epichlorohydrin. Subsequent crosslinking with a diamine produces an imine-containing network (Figure 2.5b).¹⁷⁸ This material is reprocessable and recyclable through heat (no catalyst) or acid hydrolysis, respectively, without notable decreases in thermomechanical properties ($T_g = 71$ °C, $\sigma_B = 46$ MPa, $\epsilon_B = 4.4\%$). Another vanillin–imine network with properties comparable with those of a BPA epoxy was recycled three times without a decline in mechanical properties.¹⁷⁹ An entirely renewable epoxy adhesive was synthesized using ozone-treated kraft lignin with sebacic acid, demonstrating a T_g range of 95–133 °C, reversible adhesion with a lap-shear strength of 6.3 MPa (equivalent to that of the BPA epoxy) and damage repair at 190 °C (ref.¹⁵⁶).

Recyclability and degradability are also advantageous for reinforced epoxy resins. Composite materials endow typical thermosets with mechanical properties for demanding applications but are destined for landfills. Recycling of both polymer and reinforcement components is particularly beneficial when the reinforcements are expensive, such as carbon fiber. Examples of this practice are scarce; however, one example used vanillin coupled with pentaerythritol to produce a rigid spiro-diacetal structure that has acid-catalyzed reversibility, which was exploited to recycle carbon fiber from the composite.¹⁸⁰ This material performed as well as the BPA analog ($T_g = 169$ °C,

a bio-based epoxide-containing monomer (green box) crosslinked with diacid or polyacid (red), or diamine or polyamine (blue).^{154,155,172,174} **b** | Synthesis of an epoxy network containing reversible imine bonds, which are installed during monomer synthesis through the reaction of vanillin (green) with aminophenol (blue), among permanent C–O and C–N linkages. Polymerization of the epoxide monomer with a diamine crosslinker (grey) yields the imine-containing network; this strategy avoids H₂O evolution during network formation.¹⁷⁸ **c** | Formation of a dynamic epoxy network (left and center) with reversible imine bonds from a vanillin-derived epoxide (green, with permanent ring-opened epoxide bonds in navy) and a diamine (purple, with reversible imine bonds in red).¹⁸¹ A composite comprising the dynamic epoxy and carbon fiber can be recycled through acid hydrolysis (right). After 15 h, the epoxy network is completely dissolved (top right), allowing the carbon fiber cloths to be recovered with retention of tensile properties (bottom right, stress–strain plot) and chemical structure (bottom left, Raman spectrum). Panel **b** adapted with permission from ref.¹⁷⁸, ACS. Panel **c** adapted with permission from ref.¹⁸¹, RSC.

$\sigma_B = 87$ MPa, $E = 2.8$ GPa), and the recycled carbon fiber showed no degradation in performance.

In another example, vanillin-based imine chemistry was used to form epoxy and imine crosslinks simultaneously¹⁸¹ (Figure 2.5c). The epoxy network can be reformed or repaired through dynamic imine exchange and degraded by acid hydrolysis to recover the carbon fiber, which fully retained its structural integrity. The reprocessed epoxy also behaved identically to the virgin material ($T_g = 172$ °C, $\sigma_B = 81$ MPa, $E = 2.1$ GPa) and had a higher ϵ_B (15%) than the BPA epoxy analogue (8.6%).

C-O Linked Polymer Summary.

The versatility of bio-based, C–O linked polymers has been well demonstrated, with the most tangible advantages stemming from the use of bio-derived functionalities to enable applications beyond those of commodity thermoplastics and thermosets, or to overcome their specific drawbacks. The role of catalysis in generating performance-advantaged polymers is irrefutable and allows for easy hybridization of polymer types, and entire fields of catalysis have been developed around the polymerization of highly oxygenated bio-based monomers.²¹ The coupling of catalysis to bio-derived functionalities not only enables controlled polymerization, but also rapid and

precision polymerization, which is advantageous to manufacturing. There remain opportunities to further develop catalysts to accommodate the size and complexity of bio-based monomers to control architectures for tailored performance.

There are also enormous health and process benefits associated with C–O linked, bio-based polymers. Phosgene and BPA can be evaded in the manufacturing of polycarbonates, and for epoxies, opportunities for advancement include lower cure temperatures and enhanced degradation to single components for complete circularity. Although polyesters have hydrolysable backbones, biodegradability claims should not be made based on the polyester identity alone. Collaborative studies for promising materials are needed to address degradability beyond accelerated hydrolysis. The importance of this is exemplified by the recalcitrance of PET, and of PLLA in any environment other than industrial composting, leading to public confusion.¹¹⁰ Additionally claims made for performance should be backed by data, from comparisons with control materials tested in parallel rather than with cited data.¹²⁴

2.6. C-N Linked Polymers

Polyamides.

Polyamides are prevalent in high-performance applications, owing to their strength, toughness, durability, and thermal and chemical resistance, and are typically produced by condensation of AA/BB or AB monomers, or ROP of lactams.¹⁸² Aliphatic polyamides, or nylons, are ubiquitous in automotive parts, outdoor gear, industrial fishing equipment and carpet. Drawbacks of conventional nylons are moderate T_g values and a trade-off between strength, T_m and H₂O absorption. Short-chain (C₆) nylons are stronger and higher melting but absorb more H₂O, whereas

long-chain ($\geq C_{10}$) counterparts are more hydrophobic but weaker with a lower T_m . Moisture absorption is beneficial in textiles, whereas dimensional stability is preferred for other applications. Nylon 11 has been produced from castor oil for >70 years and shows advantages over both petroleum-derived short-chain polyamides and nylon 12. Compared with nylon 12, nylon 11 has a higher hydrogen bond density and, thus, exhibits a higher T_m , lower gas permeability (ideal for fuel applications) and improved abrasion and impact resistance. Bio-based sebacic acid (C_{10}) provides a balance between H_2O absorption and strength in nylon^{6,10}. Additionally, nylon 4 is a long sought-after material with cotton-like textile properties, biodegradability and/or chemical recyclability, and straightforward renewability from γ -aminobutyric acid or pyrrolidone; however, low polymerizability and thermal instability hinder its industrial production.¹⁸³

Step-growth Polyamides. Cadaverine (1,5-diaminopentane) is one of few linear diamines with bio-fixed nitrogen, as it is derived directly from the essential amino acid lysine after decarboxylation.^{40,184} In the last decade, the first line of odd–even polyamides has been commercialized, namely nylon 5,X and a series of C_{11-18} diacids. Compared with traditional nylon 6,6, the hydrogen bonding pattern in nylon 5,6 is shifted, leaving more vacant sites (Figure 2.6a). These sites enable improved dyeing while maintaining comparable strength, leading to consistent quality and, ultimately, cost-savings in textile production.^{185–188} Additional in-use advantages of nylon 5,6 fabric over nylon 6,6 include better elastic recovery, antistatic, fire safety and moisture-absorbance properties. When adipic acid is replaced by bio-derived β -keto adipic acid in nylon 6,6, the ketone contributes to an increase in T_g (to 130 °C), a reduction in H_2O uptake and a high T_m (~400 °C); however, melting occurs close to degradation.⁸⁹ Thus, the incorporation of smaller amounts of β -keto adipic acid could enhance conventional nylon 6,6. Bio-based polyamides have largely been based on biobased amino acid or diacid monomers with petroleum-derived diamines,

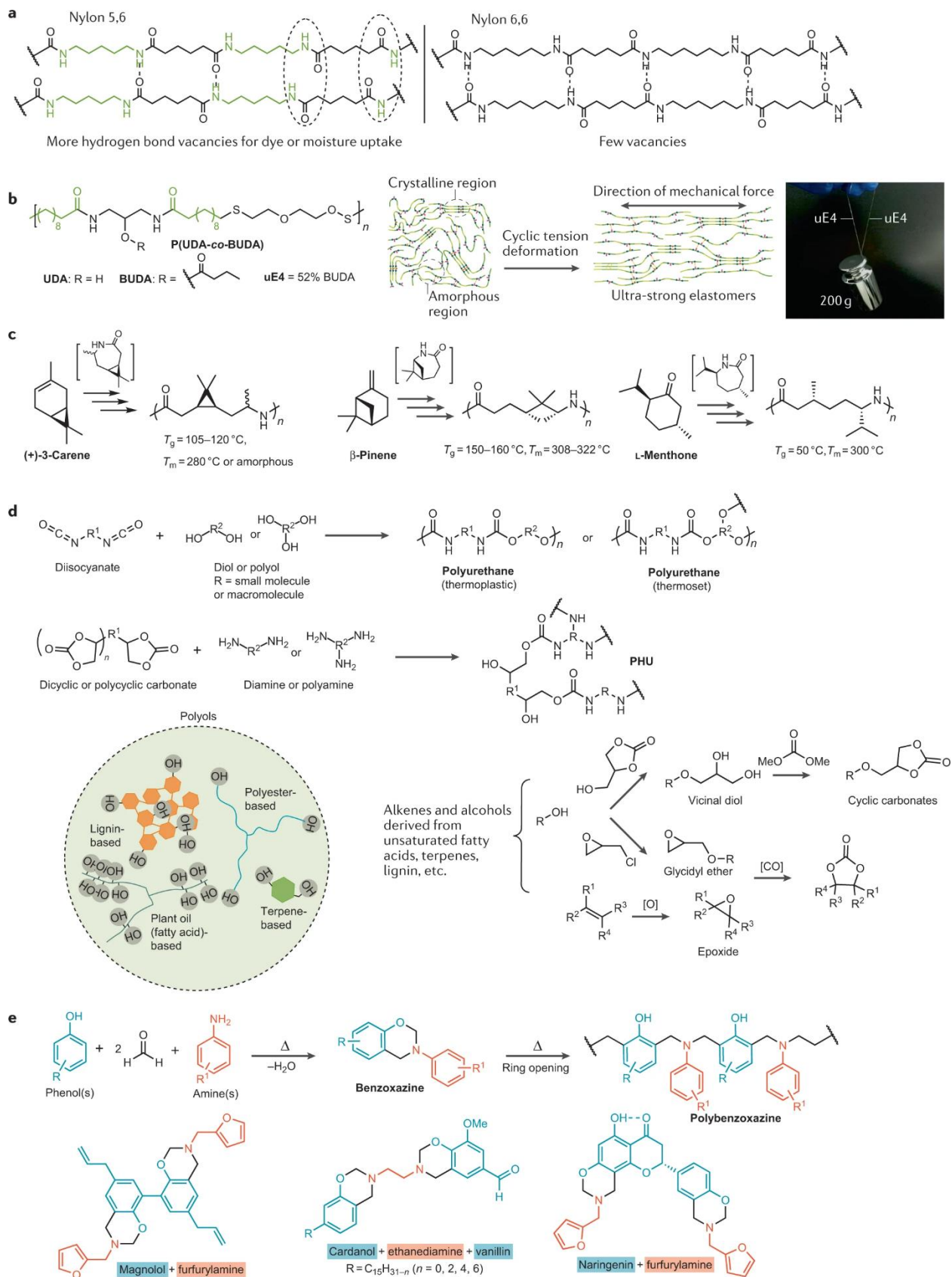


Figure 2.6. Use of bio-derived functionalities in C–N linked polymers. **a** | Comparison of

structures and hydrogen bonding patterns of nylon 5,6 and nylon 6,6, with biobased content shown in green.¹⁸⁶ **b** | Copolymerization of two diene monomers, *N,N'*-(2-hydroxypropane-1,3-diy1)bis(undec-10-enamide) (UDA) and 1,3-di(undec-10-enamido) propan-2-yl butyrate (BUDA), with a dithiol affords the polyimide P(UDA-*co*-BUDA) (bio-based content shown in green).¹⁹⁶ Cyclic tension deformation applied to P(UDA-*co*-BUDA) induces rearrangement of the microstructure to produce ultra-strong elastomers (uEs). uE4 is formed from the P(UDA-*co*-BUDA) with 52% BUDA, and a uE fibre (~135 μm in diameter) is pictured holding a 200-g weight. **c** | Examples of polyamides produced through ring-opening polymerization of terpene-based lactams (substituted caprolactams) and the thermal properties of the polymers. Polymerizability and balance between thermal properties increases from right to left.^{197–201} **d** | Synthesis of polyurethane and polyhydroxyurethane (PHU), and routes to cyclic carbonates for PHU synthesis, with a single starting alcohol shown for simplicity. Examples of polyols for the synthesis of polyurethanes and PHUs are shown in the green circle; polyols derive from the conversion of alkenes present in terpenes and fatty acids from various feedstocks. For PHU synthesis, cyclic carbonate precursors can be prepared directly from alkenes, or through alcohols and polyols. **e** | General synthesis of polybenzoxazine (PBz) (top), and three examples of bio-based benzoxazine monomers (bottom).^{226–228} Panel **b** adapted from ref.¹⁹⁶, CC BY 4.0.

as linear diamines are a less common bio-derived functionality and are typically installed by amination chemistry.^{188–191} Efficient conversion of other functional groups to amines via catalysis can provide sustainable access to polyamides, such as those derived from plant oils.⁹⁶ These polyamides have a low density of amide groups owing to the long aliphatic chains, balancing crystallinity and hydrophobicity for minimized H₂O uptake and further chemical resistance.

Cysteamine (2-aminoethanethiol) is a bifunctional biomolecule that can be used to introduce primary amines through thiol–ene click chemistry.^{189,192,193} For example, cysteamine hydrochloride was added to limonene to form a bulky diamine monomer that was used to plasticize polyamide 6,6 (nylon 6,6) in copolymers.¹⁹² Similarly, AB monomers produced by clicking cysteamine with unsaturated fatty monoesters have been used to realize plasticized copolymers.¹⁹³ The bio-derived functionalities used in these examples impart new features to commodity materials, such as built-in plasticization and hydrophobicity, but mechanical and rheological studies are necessary to fully demonstrate their potential.

Furandicarboxylic acid, or its dimethyl ester, is a common AA monomer for polycondensation, and when polymerized with a diamine produces furan-based polyamides, polyaramids or polyphthalamides.^{194,195} However, melt polycondensation of furanics can lead to undesired oxidation and resin formation. Alternative step-growth methods, such as thiol–ene addition and acyclic diene metathesis polymerization, have been applied to avoid condensation, occurring under milder conditions.^{45,188,193,196} In one demonstration, the production of polyamides by thiol–ene addition polymerization combined clever material design with processing techniques to achieve outstanding properties, with the materials reported to be the strongest elastomers of all long-chain aliphatic polycondensates.¹⁹⁶ Symmetric castor oil-derived monomers featuring a central alcohol or ester flanked by two amide groups with C₁₁ terminal alkene chains, *N,N'*-(2-hydroxypropane-1,3-diyl)bis(undec-10-enamide) (UDA) and 1,3-di(undec-10-enamido)propan-2-yl butyrate (BUDA) (Figure 2.6b, left), were copolymerized with a dithiol. It was hypothesized that nanocrystalline domains, formed through highly localized hydrogen bonding, dispersed throughout an amorphous matrix would lead to exceptional strength. The optimal P(UDA-*co*-BUDA) copolymer, P4, contains 52% UDA and achieves mechanical properties ($E = 150$ MPa, $\sigma_B = 18.4$ MPa, $\epsilon_B = 576\%$ and a toughness of 65 MJ m^{-3} at 17% crystallinity) comparable with or superior to those of commercial aliphatic polyamides and polyesters; however, T_g (24 °C) and T_m (81 °C) are comparatively low. Unidirectional stretching induces alignment of the crystalline domains, forming ultra-strong elastomers (uEs) (Figure 2.6b, center and right). Deformation of P4 to form uE4 increases σ_B sevenfold to 115 MPa, and although ϵ_B decreases to 30%, uE4 maintains a high elastic recovery of 95%. Overcoming the usual trade-off of a weaker material with long-chain monomers, these materials exhibit high strength and toughness for ambient-temperature

applications. Interestingly, by virtue of the clustered crystalline microstructure, these materials fluoresce, which is remarkable for an aliphatic material without chromophores.

ROP Polyamides. ROP of terpene-derived monomers has revealed performance-advantaged polyamides by capitalizing on inherently rigid cyclic structures and chirality.^{188,197,198} Lactam monomers derived from menthone, α -pinene and β -pinene, and (+)-3-carene have been systematically investigated (Figure 2.6c) to determine structure–property relationships, cumulating in the scalable synthesis of high-performance polyamides.^{197–201}

The ketone L-menthone was converted to a lactam through the oxime Beckmann rearrangement (as used industrially in the conversion of cyclohexanone to ϵ -caprolactam for the preparation of nylon 6) and subsequently ring-opened in bulk under typical anionic lactam ROP conditions.¹⁹⁹ The resulting polyamide was produced in low yields (~20%) and had low M_n values (<2 kDa), but exhibited impressive thermal properties ($T_g = 50$ °C, $T_m = 300$ °C). Polyamides of β -pinene lactam were also synthesized employing the oxime route.^{200,201} The structure and stereochemistry of the substituents are retained in the polymer backbone upon bulk ROP (anionic or cationic), and the resulting polyamides were obtained in good yields, with cationic polymerizations leading to higher M_n , albeit still <10 kDa. The T_m (308–322 °C) and thermal stability ($T^d \approx 400$ °C) of poly(β -pinanamide) are comparable with those of the menthone system, but with a much higher T_g of 150–160 °C due to the rigidity and stereoregularity of the backbone cyclobutane ring. However, melt processing is inhibited by the close T_m and T_d values. Polymerization of α -pinene lactam was unsuccessful, as the cyclobutyl ring rearranges, leading to crosslinking side reactions.¹⁹⁸

Polyamides derived from (+)-3-carene, a by-product of the pulping industry, are more promising, reaching much higher M_n values (up to 33 kDa) and yields of up to 77%.¹⁹⁸ The methyl

and geminal-dimethyl cyclopropane substituents, on the same face of the lactam, endow rigidity and hydrophobicity, with the polyamide showing a high T_g of 120 °C and H₂O uptake of 40% relative to that of nylon 6, but no melting transition was observed before decomposition at 400 °C. Monomer stereochemistry was retained, yet the material was amorphous, resulting in transparent films. The effects of (+)-3-carene stereochemistry and its copolymerization with conventional lactams have been investigated to reveal further performance-advantaged polyamides.¹⁹⁷ Diastereomers of the lactam derived from (+)-3-carene were obtained selectively, with large-scale, multistep monomer synthesis demonstrated in a single vessel without purification of the intermediates. The *R* diastereomer has substituents on the same face of the ring, and the substituents in the *S* diastereomer have a *trans* orientation (Figure 2.6c). The change in orientation of the methyl group has a pronounced effect on polymer crystallinity. The polymer derived from the *S* diastereomer is semi-crystalline, with a T_m of up to 280 °C, which is 60 °C higher than that of nylon 6, and a T_g of 105–115 °C (~50 °C higher than that of nylon 6). By contrast, the polymer formed from the *R* diastereomer is amorphous, with a T_g of 115–120 °C. Regardless of some kinetic differences, conversions of almost 90% were achieved for both diastereomers.

In the copolymerization of *S*-carene lactam with caprolactam or laurolactam, differences in the reaction kinetics of the monomers result in gradient copolymer microstructures, which show increased T_g values (increasing linearly with the amount of carene lactam incorporated) and disrupted crystallinities relative to nylon 6 and nylon 12. These properties could enhance the conventional application space, with transparent films, increased working temperature range, chirality and other additive effects achieved by changing the polymer composition. As γ -substituents tend to favor ring-closing, this bio-derived functionality might also provide a thermodynamic driving force for reversibility.

Polyurethanes and Polyhydroxyurethanes.

Polyurethanes are conventionally synthesized from alcohols and isocyanates. Given the propensity for bio-feedstocks to yield hydroxyl groups, polyurethanes are thus obvious candidates for synthesis from bio-based monomers. Polyurethanes can be linear (thermoplastic) or networked (thermoset), and are often used in foams, rigid or flexible, as the reaction of excess isocyanate with H₂O evolves CO₂. Polyurethane monomers and thermomechanical properties vary widely to meet the requirements of diverse applications, from automotive bushings to industrial adhesives. Polyurethanes are often thermosets with long lifetimes, but have limited end-of-life options and use toxic isocyanates.^{78,202} Most polyurethanes are manufactured from flexible diols or polyols and rigid isocyanates (such as toluene diisocyanate). Bio-feedstocks provide access to many aliphatic alcohols, but bio-based phenolics can also be the rigid component (Figure 2.6d).

Direct use of lignin in polyurethanes has received much attention owing to the high phenolic content. There are also diverse lignin feedstocks and numerous modifications performed, typically the conversion of phenols to reactive primary alcohols.³⁰ Generally, lignin-derived polyurethanes have higher compressive strengths than their petroleum counterparts, and, in some cases, can enable biodegradation at lignin loadings as low as 25 wt%.²⁰³ Despite promising features, it is difficult to draw correlations between bio-derived functionalities and material performance because lignin composition varies widely.

Although lignin-based polyurethanes use rigid aromatic polyols, the use of aliphatic polyols is more conventional. Fatty acids can be easily converted to polyols through alkene epoxidation and subsequent hydrolysis.^{204–207} These polyols can then react with aromatic diisocyanates to form polyurethanes that exhibit properties similar to those of polyether-based polyurethanes, for which T_g is in the range 30–50 °C and the mechanical properties are strongly dependent on crosslink

density. The benefit of plant oil-based polyurethanes over polyether-based counterparts is a delay in T_d by up to ~ 75 °C, due to a lower oxygen content. Higher molecular-weight polyols for flexible foams are also produced industrially by hydroformylation and transesterification of polyunsaturated fatty acids.²⁰⁸ Hydroxylterminated polymers, such as polycarbonates¹⁴⁹ and polyesters, can also be used as polyols, and have gained traction industrially. Use of poly(β M δ VL) as a polyol enables chemical recycling of the polyol component,^{127,209} and algae-derived polyester polyols yield a biodegradable polyurethane foam with properties suitable for footwear applications.²¹⁰

Polyhydroxyurethanes (PHUs) offer isocyanate-free routes (Figure 2.6d) to materials that are structurally similar to polyurethanes.^{202,211–213} PHUs form by reaction of amines with cyclic carbonates to give urethane and hydroxyl groups. In general, the urethane group maintains the properties of a polyurethane, whereas the additional hydroxyl can endow better adhesive properties.²¹¹ Cyclic carbonates are not inherent bio-derived functionalities but can be introduced by the carbonation of epoxides, through alkene or alcohol functionalization with epichlorohydrin.⁷⁸ It is possible to avoid toxic epichlorohydrin by alkylation of an alcohol to a vicinal diol, followed by transesterification with dimethyl carbonate (Figure 2.6d).²¹⁴ These alternative routes to cyclic carbonates enable benign manufacturing of PHUs, using green solvents and recoverable catalysts, and have been applied to lignin, but terpenes and fatty acids are also suitable building blocks. Additionally, owing to the hydroxyl groups, PHUs can undergo intermolecular transesterification for material healing.²¹⁵

Some of the earliest bio-based PHUs were synthesized using limonene.²¹⁶ Limonene is first converted to a branched dicyclic carbonate, which is subsequently reacted with C₅–C₆ diamines to form PHUs. The resultant thermosets possess T_g values of 40–70 °C and a favourable E (3–5 GPa),

and are strong but brittle with ϵ_B and σ_B of <2.5% and 53 MPa (ref.²¹⁶), respectively. Use of unpurified limonene carbonate results in plasticization (with a 40 °C decrease in T_g and 45% decrease in E'). Thiol–ene click chemistry provides access to more amine monomers for polyurethanes and PHUs, enabling fully bio-based systems.¹⁹² Carbonated oils can also be implemented in PHUs; for example, the product of carbonated soybean oil and ethylene diamine results in a favourable ϵ_B (80%), but at low σ_B (≤ 1.6 MPa).²¹⁷ Despite the benefits of PHUs over traditional polyurethanes, most studies do not compare against standard petroleum polyurethanes or provide adequate material characterization.

Polyimides.

Polyimides exhibit exceptional thermo-oxidative stability and mechanical properties, solvent and radiation resistance, and low density, making them suitable for aerospace applications.^{218,219} Polyimides are also used in electronics and energy sectors owing to unique dielectric properties. However, the high thermochemical resistance and thermosetting nature of polyimides come with major processing limitations. A pre-polymer formulation must be cured at high temperatures (200–300 °C), which can be complicated by the release of volatiles and incomplete curing. Additionally, polyimides are often colored. These drawbacks limit their integration into technological applications that require low-temperature processing or colorless transparency.²²⁰

More recently, machine learning and genomic engineering have been leveraged to develop bio-based polyimide films with both processing and in-use advantages for various electronics applications.^{57,221,222} These patented polyimides use traditional di-anhydride monomers with bio-based polyamines to realize solution-processable, colorless and transparent materials with outstanding mechanical properties.²²⁰ The exact formulation is undisclosed, but the bio-based components are reportedly responsible for the advantaged properties.^{220,223} For touch sensors, the

high mechanical strength ($E = 3.1$ GPa, $\sigma_B = 117$ GPa for a film 25 μm thick) enables use of thinner films and, thus, full-coverage touch sensing in flexible devices, whereas the high thermal stability ($T_g = 195$ °C, $T_d = 460$ °C)²²³ during annealing with inorganic components leads to better function. Similarly, thin films and the thermal stability expedite the manufacturing of optical filters. Moreover, the material is solderable, eliminating the need for epoxy or acrylic adhesives in printed circuit boards, resulting in a thinner and more flexible system that is completely transparent.

Polybenzoxazines.

Polybenzoxazine (PBz) resins have emerged as high servicetemperature thermosets that can replace phenolic or epoxy resins in aerospace, defense and electronics applications.²²⁴ Benzoxazine monomers are synthesized from a phenol (often BPA), amine and formaldehyde, and then polymerized at high temperatures (160–220 °C) to create tertiary amine connections and regenerate autocatalytic and hydrogen bond-forming phenols across the network (Figure 2.6e). Curing does not require a catalyst, and occurs without by-product evolution, void formation, shrinkage or expansion. PBzs show low flammability, high char yield, strength, low H₂O absorption and high stability towards chemicals and ultraviolet radiation. The use of bio-based monomers has begun to address the high cure temperatures and brittleness,^{225–228} and although promising monomers are not the most abundant, their polymers make a compelling case for them as targets of metabolic engineering.

Chavicol, a bio-based phenol with an allyl group, was used to form PBz resins with a high T_g (350 °C) through additional allyl crosslinking, but required high cure temperatures (230–300 °C).²²⁵ Magnolol — the 2,2'-biphenol dimer of chavicol — has been combined with furfurylamine to form a high-performance PBz.²²⁷ The magnolol–furfurylamine benzoxazine monomer (Figure 2.6e) was synthesized in a 5-min microwave reaction, followed by simultaneous curing of

benzoxazine and allyl functionalities at 160–250 °C (with a polymerization temperature (T_p) of 229 °C). The resulting PBz showed excellent thermal stability with a T_g of 303 °C, which is higher than that of widely used BPA PBzs ($T_g \approx 180$ °C), as well as an onset T_d of 440 °C and a high char yield of 62%. The thermal stability is thought to be enhanced by the participation of the furan ring in crosslinking, in addition to allyl and amine crosslinks, leading to high stiffness ($E' = 2.46$ GPa at room temperature). Additionally, the benzoxazine monomer showed excellent rheological properties with low viscosity (<1 Pa s), providing ample time in the melt before gelling, which is essential for resin transfer molding.

Softness has been induced in PBzs by combining vanillin and cardanol as rigid and flexible components, respectively, within an asymmetric benzoxazine monomer (Figure 2.6e).²²⁶ PBzs formed from cardanol alone have low T_g values, whereas those formed from vanillin cannot be processed because curing occurs close to the monomer T_m . By contrast, the PBz derived from the asymmetric benzoxazine monomer possesses a wide processing window (monomer $T_m = 101$ °C, $T_p = 227$ °C) and a balanced T_g of 129 °C. The E' is 700 MPa, suggesting a much softer material than that formed from magnolol and illustrating how PBz properties can be tailored by judicious use of bio-derived functionalities.

A fully bio-based, performance-advantaged PBz was synthesized from furfurylamine and naringenin, a flavonoid (Figure 2.6e).²²⁸ An autocatalytic free phenol is in place in this system, as naringenin has three phenol groups, one of which is untouched during network formation. Immobilization of the acidic phenol proton by intramolecular hydrogen bonding at low temperatures yields a stable benzoxazine monomer with a long shelf-life. This latent catalytic proton is released upon heating to effect a low T_p of 166 °C; the lowest reported for all pure PBzs. The PBz has a T_g of 286 °C, onset T_d of 361 °C and 64% char yield. Furthermore, the material is

self-extinguishing and non-ignitable with a comparatively low heat release capacity and total heat release compared with BPA-based controls. The addition of 5 mol% naringenin–furfurylamine benzoxazine to a BPA-based PBz modified the properties, decreasing the T_p from 257 to 238 °C and increasing the T_g (from 162 to 178 °C) and onset T_d (from 324 to 344 °C), and also notably improved the flammability metrics.

Polyimines.

Imine bonds confer catalyst-free reprocessability to polyesters and epoxies, but dynamic networks can also be based entirely on this motif. Petroleum-based polyimines serve as recyclable composites for carbon fiber and self-healing matrices for solid-state batteries,^{229–231} but precursor aldehydes are a common bio-derived functionality. Recent examples of bio-based polyimine networks have established structure–property relationships and show good potential for thermoset applications.^{232,233}

An elastomeric material formed from furan dialdehyde and a commercially available mixture of fatty polyamines displays a T_g of –10 °C and a T_d of up to 300 °C, and undergoes rapid stress relaxation at room temperature.²³² The material can be reprocessed with heat or selectively depolymerized in an amine solvent yet remains stable in acidic or basic solutions; this desirable hydrolytic stability is attributed to the hydrophobic amines. Furan dialdehyde, in combination with different amines, has also been used to directly study the relationship between crosslink density and physical properties and to establish relationships between fast stress relaxation and creep resistance, illuminating fundamental design principles for future materials.²³³

Vanillin was dimerized to a dialdehyde by linking the phenols, and the dialdehyde networked with simple aliphatic polyamines to form light-yellow polyimine films.²³⁴ With an increase in

crosslinking, T_g increased from 48 to 64 °C, and all networks were stable up to ~300 °C with high char yields. The films show reasonable toughness, with σ_B and ϵ_B in the ranges 47–57 MPa and 13–16%, respectively. After hot reprocessing, the networks with a higher crosslink density showed better retention of mechanical properties, although the color darkened. The dialdehyde monomers could be recovered by mild heating in strong acid and then used to regenerate light-yellow films. Fire-retardant thermosets have also been achieved by substituting phosphorus oxychloride with three vanillins through their phenols, leaving the aldehydes available for network formation with different amines.²³⁵ The materials demonstrated T_g , σ_B and E of up to 178 °C, 69 MPa and 1.9 GPa, respectively, in combination with flame-retardant properties superior to those of BPA-based thermosets. Although the phosphorus and nitrogen are not directly bio-based, the aromatic ring of vanillin contributes to the base mechanical properties and char formation whereas its phenols provide straightforward access to the aldehyde monomer. Reprocessing was rapid, completed in 2–10 min at temperatures close to the T_g without discoloration of the yellow thermosets. Additionally, high-purity monomer was recovered in up to 77% yield by acid-catalyzed depolymerization. Although bio-derived functionalities can be leveraged to target distinct thermomechanical profiles for recyclable thermoset applications, better balance of stress relaxation and creep deformation must be addressed for materials to have marketable performance advantages.

C-N Linked Polymer Summary.

Bio-derived monomers endow promising material properties and can enhance the property space of conventional C–N linked polymers. These enhancements include circumventing the use of non-benign monomers or additives, advanced architectures (that can inherently incorporate additive effects), superior thermomechanical properties, greater stability, lower flammability and improved

end-of-life options, processing conditions and appearance. Moving forward, it is imperative to test properties directly against petroleum standards and, where possible, use bio-fixed nitrogen monomers, which will hopefully see greater availability in coming years. It is also important to demonstrate performance advantages in the highly specific application environments associated with specialty polymers, which could be further revealed through collaboration with industry.

2.7. Outlook

The inherent functionality of bio-derived compounds can enhance the performance of polymers relative to current petroleum-derived materials. True performance advantages can stimulate industry adoption of biobased materials, yet much work remains to turn this early promise into a viable enterprise. This work includes thorough thermomechanical and rheological characterization of materials, optimization of monomer sourcing and synthesis, demonstration of realistic end-of-life options and production modelling analyses for the most promising systems.²⁴ When designing or evaluating a bio-based material with performance advantages, researchers should consider the guiding principles listed in Figure 2.7.

There are several major challenges in demonstrating PBPs. The first challenge is narrowing down a near infinite combinatorial design space in terms of both monomer combinations and catalyst design. Alongside the hypothesis-driven, combinatorial approach to the selection of comonomers and design of polymer architectures, computational methods such as machine learning and molecular dynamics are emerging as tools to assist in predicting polymer structures with promising properties.^{42,236} A second challenge lies in identifying molecules with hidden performance advantages, such as the ability of naringenin to act autocatalytically during PBz

Obey the principles of green chemistry and engineering

Monomer and polymer synthesis should be guided by the principles of green chemistry, with emphasis on designing for energy efficiency, implementing safer solvents and auxiliaries, maintaining a high atom economy and favouring catalytic reagents over stoichiometric ones.

Identify performance advantages

New bioproducts should be assessed for advantages across manufacturing, application properties and end-of-life considerations (such as recyclability or degradation).

Correlate performance advantages with inherent bio-derived functionalities

Typically, performance advantages are directly related to bio-derived functionality; thus, it is preferable to use fewer chemical transformations in order to retain these bio-derived functionalities. For example, muconic acid can be converted to adipic acid as a direct replacement chemical, or the unsaturated bonds can be retained for additional performance.

Perform characterizations using standardized tests and compare with incumbent materials

Bioproducts should be characterized across a range of properties (including thermomechanical, rheological, optical, barrier and degradability). To claim that a material can serve as a performance-advantaged replacement, it is necessary to report properties relative to the incumbent material under the same synthesis and test conditions, as commercial polymer products will often use trace amounts of co-monomers and/or additives to facilitate processing and optimize properties (such as isophthalates in polyethylene terephthalate (PET)). If not synthesized, data can also be obtained using purchased standards with known compositions.

Validate performance advantages at multiple scales

Once physical properties are established, the performance at different mass scales should be validated. Moreover, promising systems should be subjected to life cycle analyses, techno-economic analyses and supply chain modelling. It is important to avoid assumptions, such as that all bio-based monomers have lower greenhouse gas emissions than petroleum-derived counterparts. Indeed, some bio-based direct replacement chemicals can result in greater greenhouse gas emissions, often due to extensive separations or the disposal of waste by-products²³⁸.

Figure 2.7. Guiding principles for the development of performance-advantaged bioproducts.

formation.²²⁸ Third, ensuring that all requisite properties are at least maintained, if not exceeded, poses a great challenge. As multiple properties are often correlated, an increase in one property might be at the detriment of another. For example, materials with higher T_g may have a wider working temperature window but may be too brittle in practice. Finally, the coupling of performance advantages, especially the coupling of end-of-life considerations with superior

processing or application properties, remains a key challenge. Overcoming these challenges while following the guiding principles will require research at multiple scales and the identification of the optimal products to advance.

This Review has focused on research at the proof-of-concept level, but there are additional considerations when designing commercially viable materials. Challenges associated with bringing a PBP to market include understanding its rheological properties under industrial processing conditions, assessing its performance lifetime under specific application conditions, selecting suitable precursor feedstocks and optimizing the production of these precursors. Introducing new products into an established market presents another set of challenges and opportunities. These challenges include the upfront cost for manufacturing a new material; competing with the incumbent industry, which has a tested foundation; and potential regulatory barriers for certain applications, such as regulatory procedures for food packaging. These challenges are not unique to PBPs but should be acknowledged as barriers to entry for transitioning any new products from laboratory to market.

Lessons can be learned from bioproducts that have already penetrated the market. Examples of products with adequate market penetration include epoxidized soybean oil as a plasticizer, PLA and sebacic acid for nylon 6,10, which have gained traction owing to their avoidance of health risks, compostability and lack of thermal expansion, and lower H₂O permeabilities, respectively. In each case, the performance advantages have facilitated their market penetration. PLA is an example of a material that has overcome several of the above challenges. Although initially postulated to be a widely applicable compostable packaging polymer, high H₂O permeability makes it unsuitable for long-term food and beverage preservation; however, minimal thermal shrinkage makes it ideal as a 3D printing filament. Additionally, to overcome issues associated

with the manufacture of lactic acid, acid-tolerant microbes were developed and simulated moving bed chromatography used to reduce salt waste and remove H₂O. At the time of writing, lactic acid has a market size of 75,000 tons per year, growing at a rate of ~19% per year.²³⁷ Thus, market penetration is possible when a PBP solves a specific problem relative to incumbent materials and manufacturing is optimized to lower cost.

Through further research, the field of performance-advantaged bioproducts has the potential not only to enable the bioeconomy but also to advance numerous scientific and engineering fields. For example, unexplored monomers from biomass offer new structure– property relationships to be studied and invite new catalyst designs and method development. The potential of bio-derived functionalities and their unique combinations within compounds can provide an incentive for the use of biomass feedstocks and, ultimately, bring sustainable polymers to fruition.

References

1. Andrady, A. L. & Neal, M. A. Applications and societal benefits of plastics. *Phil. Trans. R. Soc. B* **364**, 1977-1984 (2009).
2. Davis, S. J., Caldeira, K. & Matthews, H. D. Future CO₂ emissions and climate change from existing energy infrastructure. *Science* **329**, 1330-1333 (2010).
3. World Economic Forum, Ellen MacArthur Foundation & McKinsey. The new plastics economy – rethinking the future of plastics (World Economic Forum, 2016).
4. MacArthur, E. Beyond plastic waste. *Science* **358**, 843-843 (2017).
5. Hermann, B. G., Blok, K. & Patel, M. K. Producing bio-based bulk chemicals using industrial biotechnology saves energy and combats climate change. *Environ. Sci. Technol.* **41**, 7915-7921 (2007).
6. Dodds, D. R. & Gross, R. A. Chemicals from biomass. *Science* **318**, 1250-1251 (2007).
7. Bozell, J. J. & Petersen, G. R. Technology development for the production of biobased products from biorefinery carbohydrates – the US Department of Energy’s “Top 10” revisited. *Green Chem.* **12**, 539-554 (2010).
8. Tuck, C. O., Perez, E., Horvath, I. T., Sheldon, R. A. & Poliakoff, M. Valorization of biomass: deriving more value from waste. *Science* **337**, 695-699 (2012).
9. Shen, L., Worrell, E. & Patel, M. K. Comparing life cycle energy and GHG emissions of bio-based PET, recycled PET, PLA, and man-made cellulose. *Biofuel Bioprod. Biorefin.* **6**, 625-639 (2012).

10. Weiss, M. et al. A review of the environmental impacts of biobased materials. *J. Ind. Ecol.* **16**, S169-S181 (2012).
11. Chen, G.-Q. & Patel, M. K. Plastics derived from biological sources: present and future: a technical and environmental review. *Chem. Rev.* **112**, 2082-2099 (2012).
12. Babu, R. P., O' Connor, K. & Seeram, R. Current progress on bio-based polymers and their future trends. *Prog. Biomater.* **2**, 8-23 (2013).
13. Sheldon, R. A. Green and sustainable manufacture of chemicals from biomass: state of the art. *Green Chem.* **16**, 950-963 (2014).
14. Gandini, A. & Lacerda, T. M. From monomers to polymers from renewable resources: recent advances. *Prog. Polym. Sci.* **48**, 1-39 (2015).
15. Isikgor, F. H. & Becer, C. R. Lignocellulosic biomass: a sustainable platform for the production of bio-based chemicals and polymers. *Polym. Chem.* **6**, 4497-4559 (2015).
16. Zhu, Y., Romain, C. & Williams, C. K. Sustainable polymers from renewable resources. *Nature* **540**, 354-362 (2016).
17. Delidovich, I. et al. Alternative monomers based on lignocellulose and their use for polymer production. *Chem. Rev.* **116**, 1540-1599 (2016).
18. Galbis, J. A., Garcia-Martin, Md. G., de Paz, M. V. & Galbis, E. Synthetic polymers from sugar-based monomers. *Chem. Rev.* **116**, 1600-1636 (2016).
19. Hillmyer, M. A. The promise of plastics from plants. *Science* **358**, 868-870 (2017).

20. Shanks, B. H. & Keeling, P. L. Bioprivileged molecules: creating value from biomass. *Green Chem.* **19**, 3177-3185 (2017).
21. Zhang, X., Fevre, M., Jones, G. O. & Waymouth, R. M. Catalysis as an enabling science for sustainable polymers. *Chem. Rev.* **118**, 839-885 (2018).
22. Debuissy, T., Pollet, E. & Averous, L. Biotic and abiotic synthesis of renewable aliphatic polyesters from short building blocks obtained from biotechnology. *ChemSusChem* **11**, 3836-3870 (2018).
23. Hong, M. & Chen, E. Y.-X. Future directions for sustainable polymers. *Trends Chem.* **1**, 148-151 (2019).
24. Nicholson, S. R., Rorrer, N. A., Carpenter, A. C. & Beckham, G. T. Manufacturing energy and greenhouse gas emissions associated with plastics consumption. *Joule* **5**, 673-686 (2021).
25. Nikolau, B. J., Perera, M. A. D. N., Brachova, L. & Shanks, B. Platform biochemicals for a biorenewable chemical industry. *Plant J.* **54**, 536-545 (2008).
26. Hermann, B. G. & Patel, M. Today's and tomorrow's bio-based bulk chemicals from white biotechnology. *Appl. Biochem. Biotechnol.* **136**, 361-388 (2007).
27. Fitzgerald, N. D. Chemistry challenges to enable a sustainable bioeconomy. *Nat. Rev. Chem.* **1**, 0080 (2017).
28. Fitzgerald, N. & Bailey, A. *Moving Beyond Drop-in Replacements: Performance-advantaged Biobased Chemicals* (US Department of Energy Office of Energy Efficiency and Renewable Energy Bioenergy Technologies Office, 2018).

29. Klemm, D., Heublein, B., Fink, H. P. & Bohn, A. Cellulose: fascinating biopolymer and sustainable raw material. *Angew. Chem. Int. Ed.* **44**, 3358-3393 (2005).
30. Upton, B. M. & Kasko, A. M. Strategies for the conversion of lignin to high-value polymeric materials: review and perspective. *Chem. Rev.* **116**, 2275-2306 (2016).
31. Scheller, H. V. & Ulvskov, P. Hemicelluloses. *Annu. Rev. Plant Biol.* **61**, 263-289 (2010).
32. Mohnen, D. Pectin structure and biosynthesis. *Curr. Opin. Plant Biol.* **11**, 266-277 (2008).
33. Boerjan, W., Ralph, J. & Baucher, M. Lignin biosynthesis. *Annu. Rev. Plant Biol.* **54**, 519-546 (2003).
34. Chundawat, S. P., Beckham, G. T., Himmel, M. E. & Dale, B. E. Deconstruction of lignocellulosic biomass to fuels and chemicals. *Annu. Rev. Chem. Biomol. Eng.* **2**, 121-145 (2011).
35. Pollard, M., Beisson, F., Li, Y. & Ohlrogge, J. B. Building lipid barriers: biosynthesis of cutin and suberin. *Trends Plant Sci.* **13**, 236-246 (2008).
36. Rinaudo, M. Chitin and chitosan: properties and applications. *Prog. Polym. Sci.* **31**, 603-632 (2006).
37. Yan, N. & Chen, X. Sustainability: Don't waste seafood waste. *Nature* **524**, 155-157 (2015).
38. Hülsey, M. J., Yang, H. & Yan, N. Sustainable routes for the synthesis of renewable heteroatom-containing chemicals. *ACS Sus. Chem. Eng.* **6**, 5694-5707 (2018).
39. Ma, X. et al. Upcycling chitin-containing waste into organonitrogen chemicals via an integrated process. *Proc. Natl Acad. Sci. USA* **117**, 7719-7728 (2020).

40. Lee, S. Y. et al. A comprehensive metabolic map for production of bio-based chemicals. *Nat. Catal.* **2**, 18-33 (2019).
41. Wheeldon, I., Christopher, P. & Blanch, H. Integration of heterogeneous and biochemical catalysis for production of fuels and chemicals from biomass. *Curr. Opin. Biotechnol.* **45**, 127-135 (2017).
42. Zhou, X. et al. Computational framework for the identification of bioprivileged molecules. *ACS Sus. Chem. Eng.* **7**, 2414-2428 (2019).
43. Huo, J. & Shanks, B. H. Bioprivileged molecules: integrating biological and chemical catalysis for biomass conversion. *Annu. Rev. Chem. Biomol. Eng.* **11**, 63-85 (2020).
44. Nguyen, H. T. H., Qi, P., Rostagno, M., Feteha, A. & Miller, S. A. The quest for high glass transition temperature bioplastics. *J. Mater. Chem. A* **6**, 9298-9331 (2018).
45. Gandini, A. & Lacerda, T. M. *Polymers from Plant Oils* 2nd edn (Scrivener Publishing, 2019).
46. Mahajan, J. S., O'Dea, R. M., Norris, J. B., Korley, L. T. J. & Epps, T. H. Aromatics from lignocellulosic biomass: a platform for high-performance thermosets. *ACS Sus. Chem. Eng.* **8**, 15072-15096 (2020).
47. Scott, A. Styrene leak in India kills at least 13. *Chemical & Engineering News* <https://cen.acs.org/safety/industrialsafety/Styrene-leak-India-kills-least/98/web/2020/05> (2020).
48. Terasaki, M., Kazama, T., Shiraishi, F. & Makino, M. Identification and estrogenic characterization of impurities in commercial bisphenol A diglycidyl ether (BADGE). *Chemosphere* **65**, 873-880 (2006).

49. Shi, M., Sekulovski, N., MacLean, J. A. & Hayashi, K. Effects of bisphenol A analogues on reproductive functions in mice. *Reprod. Toxicol.* **73**, 280-291 (2017).
50. Ramskov Tetzlaff, C. N., Svingen, T., Vinggaard, A. M., Rosenmai, A. K. & Taxvig, C. Bisphenols B, E, F, and S and 4-cumylphenol induce lipid accumulation in mouse adipocytes similarly to bisphenol A. *Environ. Toxicol.* **35**, 543-552 (2020).
51. Koelewijn, S. F. et al. Sustainable bisphenols from renewable softwood lignin feedstock for polycarbonates and cyanate ester resins. *Green Chem.* **19**, 2561-2570 (2017).
52. Rorrer, N. A., Vardon, D. R., Dorgan, J. R., Gjersing, E. J. & Beckham, G. T. Biomass-derived monomers for performance-differentiated fiber reinforced polymer composites. *Green Chem.* **19**, 2812-2825 (2017).
53. Koelewijn, S. F. et al. Promising bulk production of a potentially benign bisphenol A replacement from a hardwood lignin platform. *Green Chem.* **20**, 1050-1058 (2018).
54. Patel, A., Maiorana, A., Yue, L., Gross, R. A. & Manas-Zloczower, I. Curing kinetics of biobased epoxies for tailored applications. *Macromolecules* **49**, 5315-5324 (2016).
55. Kurian, J. V. A new polymer platform for the future – Sorona® from corn derived 1,3-propanediol. *Polym. Env.* **13**, 159-167 (2005).
56. Sarathchandran, C., Chan, C. H., Karim, S. R. B. A. & Thomas, S. in *Physical Chemistry of Macromolecules* Ch. 19 (eds Chan, C. H., Chia, C. H. & Thomas, S.) 573-617 (Apple Academic, 2014).

57. Bomgardner, M. Is clarity coming for biobased chemicals? *C&EN Glob. Enterp.* **98**, 28-33 (2020).
58. Gowda, R. R. & Chen, E. Y.-X. in *Encyclopedia of Polymer Science and Technology* (Wiley, 2013).
59. Satoh, K. Controlled/living polymerization of renewable vinyl monomers into bio-based polymers. *Polym. J.* **47**, 527-536 (2015).
60. Winnacker, M. & Rieger, B. Recent progress in sustainable polymers obtained from cyclic terpenes: synthesis, properties, and application potential. *ChemSusChem* **8**, 2455-2471 (2015).
61. Kristufek, S. L., Wacker, K. T., Tsao, Y.-Y. T., Su, L. & Wooley, K. L. Monomer design strategies to create natural product-based polymer materials. *Nat. Prod. Rep.* **34**, 433-459 (2017).
62. Winnacker, M. Pinenes: abundant and renewable building blocks for a variety of sustainable polymers. *Angew. Chem. Int. Ed.* **57**, 14362-14371 (2018).
63. Gilsdorf, R. A., Nicki, M. A. & Chen, E. Y. X. High chemical recyclability of vinyl lactone acrylic bioplastics. *Polym. Chem.* **11**, 4942-4950 (2020).
64. Hillmyer, M. A. & Tolman, W. B. Aliphatic polyester block polymers: renewable, degradable, and sustainable. *Acc. Chem. Res.* **47**, 2390-2396 (2014).
65. Munoz-Guerra, S., Lavilla, C., Japu, C. & Martinez de Ilarduya, A. Renewable terephthalate polyesters from carbohydrate-based bicyclic monomers. *Green Chem.* **16**, 1716-1739 (2014).
66. Tullo, A. H. A biopolymer whose time has come. *C&EN Glob. Enterp.* **97**, 20-21 (2019).

67. Martinez de Ilarduya, A. & Munoz Guerra, S. Ring opening polymerization of macrocyclic oligoesters derived from renewable sources. *Polym. Chem.* **11**, 4850-4860 (2020).
68. Gregory, G. L., Lopez-Vidal, E. M. & Buchard, A. Polymers from sugars: cyclic monomer synthesis, ring-opening polymerisation, material properties and applications. *ChemComm* **53**, 2198-2217 (2017).
69. Muhammadi, Shabina, Afzal, M. & Hameed, S. Bacterial polyhydroxyalkanoates-eco-friendly next generation plastic: production, biocompatibility, biodegradation, physical properties and applications. *Green Chem. Lett. Rev.* **8**, 56-77 (2015).
70. Anjum, A. et al. Microbial production of polyhydroxyalkanoates (PHAs) and its copolymers: a review of recent advancements. *Int. J. Biol. Macromol.* **89**, 161-174 (2016).
71. Longo, J. M., Sanford, M. J. & Coates, G. W. Ring-opening copolymerization of epoxides and cyclic anhydrides with discrete metal complexes: structure- property relationships. *Chem. Rev.* **116**, 15167-15197 (2016).
72. Sang, T., Wallis, C. J., Hill, G. & Britovsek, G. J. P. Polyethylene terephthalate degradation under natural and accelerated weathering conditions. *Eur. Polym. J.* **136**, 109873 (2020).
73. Burgess, S. K., Karvan, O., Johnson, J. R., Kriegel, R. M. & Koros, W. J. Oxygen sorption and transport in amorphous poly(ethylene furanoate). *Polymer* **55**, 4748-4756 (2014).
74. Eerhart, A. J. J. E., Faaij, A. P. C. & Patel, M. K. Replacing fossil based PET with biobased PEF; process analysis, energy and GHG balance. *Energy Environ. Sci.* **5**, 6407-6422 (2012).

75. Knoop, R. J. I., Vogelzang, W., van Haveren, J. & van Es, D. S. High molecular weight poly(ethylene-2, 5-furanoate); critical aspects in synthesis and mechanical property determination. *J. Polym. Sci. A Polym. Chem.* **51**, 4191-4199 (2013).
76. Burgess, S. K. et al. Chain mobility, thermal, and mechanical properties of poly(ethylene furanoate) compared to poly(ethylene terephthalate). *Macromolecules* **47**, 1383-1391 (2014).
77. Xu, C., Arancon, R. A. D., Labidi, J. & Luque, R. Lignin depolymerisation strategies: towards valuable chemicals and fuels. *Chem. Soc. Rev.* **43**, 7485-7500 (2014).
78. Fache, M. et al. Vanillin, a promising biobased building-block for monomer synthesis. *Green Chem.* **16**, 1987-1998 (2014).
79. Mialon, L., Pemba, A. G. & Miller, S. A. Biorenewable polyethylene terephthalate mimics derived from lignin and acetic acid. *Green Chem.* **12**, 1704-1706 (2010).
80. Mialon, L., Vanderhenst, R., Pemba, A. G. & Miller, S. A. Polyalkylenehydroxybenzoates (PAHBs): biorenewable aromatic/aliphatic polyesters from lignin. *Macromol. Rapid Commun.* **32**, 1386-1392 (2011).
81. Nguyen, H. T. H., Reis, M. H., Qi, P. & Miller, S. A. Polyethylene ferulate (PEF) and congeners: polystyrene mimics derived from biorenewable aromatics. *Green Chem.* **17**, 4512-4517 (2015).
82. Nguyen, H. T. H., Short, G. N., Qi, P. & Miller, S. A. Copolymerization of lactones and bioaromatics via concurrent ring-opening polymerization/polycondensation. *Green Chem.* **19**, 1877-1888 (2017).

83. Schijndel, J. et al. Repeatable molecularly recyclable semi-aromatic polyesters derived from lignin. *J. Polym. Sci.* **58**, 1655-1663 (2020).
84. Kaneko, T., Thi, T. H., Shi, D. J. & Akashi, M. Environmentally degradable, high-performance thermoplastics from phenolic phytomonomers. *Nat. Mater.* **5**, 966-970 (2006).
85. Nsengiyumva, O. & Miller, S. A. Synthesis, characterization, and water-degradation of biorenewable polyesters derived from natural camphoric acid. *Green Chem.* **21**, 973-978 (2019).
86. Beckham, G. T., Johnson, C. W., Karp, E. M., Salvachua, D. & Vardon, D. R. Opportunities and challenges in biological lignin valorization. *Curr. Opin. Biotechnol.* **42**, 40-53 (2016).
87. Johnson, C. W. et al. Enhancing muconic acid production from glucose and lignin-derived aromatic compounds via increased protocatechuate decarboxylase activity. *Metab. Eng. Commun.* **3**, 111-119 (2016).
88. Settle, A. E. et al. Iodine-catalyzed isomerization of dimethyl muconate. *ChemSusChem* **11**, 1768-1780 (2018).
89. Johnson, C. W. et al. Innovative chemicals and materials from bacterial aromatic catabolic pathways. *Joule* **3**, 1523-1537 (2019).
90. Rorrer, N. A. et al. Renewable unsaturated polyesters from muconic acid. *ACS Sus. Chem. Eng.* **4**, 6867-6876 (2016).
91. Rorrer, N. A. et al. Combining reclaimed PET with bio-based monomers enables plastics upcycling. *Joule* **3**, 1006-1027 (2019).

92. Quinzler, D. & Mecking, S. Linear semicrystalline polyesters from fatty acids by complete feedstock molecule utilization. *Angew. Chem. Int. Ed.* **49**, 4306-4308 (2010).
93. Stempfle, F., Quinzler, D., Heckler, I. & Mecking, S. Long-chain linear C₁₉ and C₂₃ monomers and polycondensates from unsaturated fatty acid esters. *Macromolecules* **44**, 4159-4166 (2011).
94. Stempfle, F., Ritter, B. S., Mulhaupt, R. & Mecking, S. Long-chain aliphatic polyesters from plant oils for injection molding, film extrusion and electrospinning. *Green Chem.* **16**, 2008-2014 (2014).
95. Roesle, P. et al. Synthetic polyester from algae oil. *Angew. Chem. Int. Ed.* **53**, 6800-6804 (2014).
96. Stempfle, F., Ortmann, P. & Mecking, S. Long-chain aliphatic polymers to bridge the gap between semicrystalline polyolefins and traditional polycondensates. *Chem. Rev.* **116**, 4597-4641 (2016).
97. Witt, T., Hausler, M., Kulpa, S. & Mecking, S. Chain multiplication of fatty acids to precise telechelicpolyethylene. *Angew. Chem. Int. Ed.* **56**, 7589-7594 (2017).
98. Genovese, L. et al. Biodegradable long chain aliphatic polyesters containing ether-linkages: synthesis, solid-state, and barrier properties. *Ind. Eng. Chem. Res.* **53**, 10965-10973 (2014).
99. Jiang, G. et al. Carbon sources for polyhydroxyalkanoates and an integrated biorefinery. *Int. J. Mol. Sci.* **17**, 1157 (2016).

100. Wang, S. et al. Biodegradation of poly(3-hydroxybutyrate-co-3-hydroxyhexanoate) plastic under anaerobic sludge and aerobic seawater conditions: gas evolution and microbial diversity. *Environ. Sci. Technol.* **52**, 5700-5709 (2018).
101. Winnacker, M. Polyhydroxyalkanoates: recent advances in their synthesis and applications. *Eur. J. Lipid Sci. Technol.* **121**, 1900101 (2019).
102. Sangroniz, A. et al. Packaging materials with desired mechanical and barrier properties and full chemical recyclability. *Nat. Comm.* **10**, 3559 (2019).
103. Myung, J., Flanagan, J. C. A., Waymouth, R. M. & Criddle, C. S. Methane or methanol-oxidation dependent synthesis of poly(3-hydroxybutyrate-co- 3-hydroxyvalerate) by obligate type II methanotrophs. *Process Biochem.* **51**, 561-567 (2016).
104. Flanagan, J. C. A., Myung, J., Criddle, C. S. & Waymouth, R. M. Poly(hydroxyalkanoate)s from waste biomass: a combined chemical-biological approach. *ChemistrySelect* **1**, 2327-2331 (2016).
105. Myung, J., Flanagan, J. C. A., Waymouth, R. M. & Criddle, C. S. Expanding the range of polyhydroxyalkanoates synthesized by methanotrophic bacteria through the utilization of ω -hydroxyalkanoate co-substrates. *AMB Express* **7**, 118 (2017).
106. Tang, X. & Chen, E. Y.-X. Chemical synthesis of perfectly isotactic and high melting bacterial poly(3-hydroxybutyrate) from bio-sourced racemic cyclic diolide. *Nat. Commun.* **9**, 2345 (2018).
107. Tang, X., Westlie, A. H., Watson, E. M. & Chen, E. Y.-X. Stereosequenced crystalline polyhydroxyalkanoates from diastereomeric monomer mixtures. *Science* **366**, 754-758 (2019).

108. Tang, X. et al. Biodegradable polyhydroxyalkanoates by stereoselective copolymerization of racemic diolides: stereocontrol and polyolefin-like properties. *Angew. Chem. Int. Ed.* **59**, 7881-7890 (2020).
109. Westlie, A. H. & Chen, E. Y.-X. Catalyzed chemical synthesis of unnatural aromatic polyhydroxyalkanoate and aromatic-aliphatic PHAs with record-high glass-transition and decomposition temperatures. *Macromolecules* **53**, 9906-9915 (2020).
110. Haider, T. P., Volker, C., Kramm, J., Landfester, K. & Wurm, F. R. Plastics of the future? The impact of biodegradable polymers on the environment and on society. *Angew. Chem. Int. Ed.* **58**, 50-62 (2019).
111. Coates, G. W. & Getzler, Y. D. Y. L. Chemical recycling to monomer for an ideal, circular polymer economy. *Nat. Rev. Mater.* **5**, 501-516 (2020).
112. Lin, B., Hedrick, J. L., Park, N. H. & Waymouth, R. M. Programmable high-throughput platform for the rapid and scalable synthesis of polyester and polycarbonate libraries. *J. Am. Chem. Soc.* **141**, 8921-8927 (2019).
113. Siracusa, V. Microbial degradation of synthetic biopolymers waste. *Polymers* **11**, 1066 (2019).
114. Dusselier, M., Van Wouwe, P., Dewaele, A., Jacobs, P. A. & Sels, B. F. Shape-selective zeolite catalysis for bioplastics production. *Science* **349**, 78-80 (2015).
115. de Roo, G., Kellerhals, M. B., Ren, Q., Witholt, B. & Kessler, B. Production of chiral *R*-3-hydroxyalkanoic acids and *R*-3-hydroxyalkanoic acid methyl esters via hydrolytic degradation of polyhydroxyalkanoate synthesized by pseudomonads. *Biotechnol. Bioeng.* **77**, 717-722 (2002).

116. van der Meulen, I. et al. Catalytic ring-opening polymerization of renewable macrolactones to high molecular weight polyethylene-like polymers. *Macromolecules* **44**, 4301-4305 (2011).
117. Witt, T. & Mecking, S. Large-ring lactones from plant oils. *Green Chem.* **15**, 2361-2364 (2013).
118. Hodge, P. Entropically driven ring-opening polymerization of strainless organic macrocycles. *Chem. Rev.* **114**, 2278-2312 (2014).
119. Wilson, J. A., Hopkins, S. A., Wright, P. M. & Dove, A. P. Synthesis of ω -pentadecalactone copolymers with independently tunable thermal and degradation behavior. *Macromolecules* **48**, 950-958 (2015).
120. Myers, D. et al. Ring opening polymerization of macrolactones: high conversions and activities using an yttrium catalyst. *Polym. Chem.* **8**, 5780-5785 (2017).
121. Witt, T., Hausler, M. & Mecking, S. No strain, no gain? Enzymatic ring-opening polymerization of strainless aliphatic macrolactones. *Macromol. Rapid Commun.* **38**, 1600638 (2017).
122. Li, C. et al. Lipase-catalyzed ring-opening copolymerization of ω -pentadecalactone and δ -valerolactone by reactive extrusion. *Green Chem.* **22**, 662-668 (2020).
123. Vendamme, R., Schuwer, N. & Eevers, W. Recent synthetic approaches and emerging bio-inspired strategies for the development of sustainable pressure-sensitive adhesives derived from renewable building blocks. *J. Appl. Polym. Sci.* **131**, 40669 (2014).

124. Heinrich, L. A. Future opportunities for bio-based adhesives – advantages beyond renewability. *Green Chem.* **21**, 1866-1888 (2019).
125. Brutman, J. P., De Hoe, G. X., Schneiderman, D. K., Le, T. N. & Hillmyer, M. A. Renewable, degradable, and chemically recyclable cross-linked elastomers. *Ind. Eng. Chem. Res.* **55**, 11097-11106 (2016).
126. De Hoe, G. X. et al. Sustainable polyester elastomers from lactones: synthesis, properties, and enzymatic hydrolyzability. *J. Am. Chem. Soc.* **140**, 963-973 (2018).
127. Schneiderman, D. K. et al. Chemically recyclable biobased polyurethanes. *ACS Macro Lett.* **5**, 515-518 (2016).
128. Shin, J. et al. Pressure-sensitive adhesives from renewable triblock copolymers. *Macromolecules* **44**, 87-94 (2011).
129. Vendamme, R. et al. Interplay between viscoelastic and chemical tunings in fatty-acid-based polyester adhesives: engineering biomass toward functionalized step-growth polymers and soft networks. *Biomacromolecules* **13**, 1933-1944 (2012).
130. Shin, J., Lee, Y., Tolman, W. B. & Hillmyer, M. A. Thermoplastic elastomers derived from menthene and tulipalin A. *Biomacromolecules* **13**, 3833-3840 (2012).
131. Sulley, G. S. et al. Switchable catalysis improves the properties of CO₂-derived polymers: poly(cyclohexene carbonate-*b*- ϵ -decalactone-*b*-cyclohexene carbonate) adhesives, elastomers, and toughened plastics. *J. Am. Chem. Soc.* **142**, 4367-4378 (2020).

132. Winkler, M., Romain, C., Meier, M. A. R. & Williams, C. K. Renewable polycarbonates and polyesters from 1,4-cyclohexadiene. *Green Chem.* **17**, 300-306 (2015).
133. Xiong, M., Schneiderman, D. K., Bates, F. S., Hillmyer, M. A. & Zhang, K. Scalable production of mechanically tunable block polymers from sugar. *Proc. Natl Acad. Sci. USA* **111**, 8357-8362 (2014).
134. Watts, A., Kurokawa, N. & Hillmyer, M. A. Strong, resilient, and sustainable aliphatic polyester thermoplastic elastomers. *Biomacromolecules* **18**, 1845-1854 (2017).
135. Robert, C., de Montigny, F. & Thomas, C. M. Tandem synthesis of alternating polyesters from renewable resources. *Nat. Commun.* **2**, 586 (2011).
136. Pena Carrodeguas, L., Martin, C. & Kleij, A. W. Semiaromatic polyesters derived from renewable terpene oxides with high glass transitions. *Macromolecules* **50**, 5337-5345 (2017).
137. Van Zee, N. J. & Coates, G. W. Alternating copolymerization of propylene oxide with biorenewable terpene-based cyclic anhydrides: a sustainable route to aliphatic polyesters with high glass transition temperatures. *Angew. Chem. Int. Ed.* **54**, 2665-2668 (2015).
138. Sanford, M. J., Pena Carrodeguas, L., Van Zee, N. J., Kleij, A. W. & Coates, G. W. Alternating copolymerization of propylene oxide and cyclohexene oxide with tricyclic anhydrides: access to partially renewable aliphatic polyesters with high glass transition temperatures. *Macromolecules* **49**, 6394-6400 (2016).
139. Snyder, R. L. et al. Mechanically robust and reprocessable imine exchange networks from modular polyester pre-polymers. *Polym. Chem.* **11**, 5346-5355 (2020).

140. Sommerfeld, S. D., Zhang, Z., Costache, M. C., Vega, S. L. & Kohn, J. Enzymatic surface erosion of high tensile strength polycarbonates based on natural phenols. *Biomacromolecules* **15**, 830-836 (2014).
141. Xu, J., Feng, E. & Song, J. Renaissance of aliphatic polycarbonates: new techniques and biomedical applications. *J. Appl. Polym. Sci.* **131**, 39822 (2014).
142. Byrne, C. M., Allen, S. D., Lobkovsky, E. B. & Coates, G. W. Alternating copolymerization of limonene oxide and carbon dioxide. *J. Am. Chem. Soc.* **126**, 11404-11405 (2004).
143. Auriemma, F. et al. Stereocomplexed poly(limonene carbonate): a unique example of the cocrystallization of amorphous enantiomeric polymers. *Angew. Chem. Int. Ed.* **54**, 1215-1218 (2015).
144. Kristufek, T. S. et al. Rapidly-cured isosorbide-based cross-linked polycarbonate elastomers. *Polym. Chem.* **7**, 2639-2644 (2016).
145. Stoser, T. et al. Bio-derived polymers for coating applications: comparing poly(limonene carbonate) and poly(cyclohexadiene carbonate). *Polym. Chem.* **8**, 6099-6105 (2017).
146. Hauenstein, O., Reiter, M., Agarwal, S., Rieger, B. & Greiner, A. Bio-based polycarbonate from limonene oxide and CO₂ with high molecular weight, excellent thermal resistance, hardness and transparency. *Green Chem.* **18**, 760-770 (2016).
147. von der Assen, N. & Bardow, A. Life cycle assessment of polyols for polyurethane production using CO₂ as feedstock: insights from an industrial case study. *Green Chem.* **16**, 3272-3280 (2014).

148. Langanke, J. et al. Carbon dioxide (CO₂) as sustainable feedstock for polyurethane production. *Green Chem.* **16**, 1865-1870 (2014).
149. Allen, S. D. et al. Polycarbonate polyol compositions and methods. US Patent 8,247,520 B2 (2012).
150. Zhang, Z. et al. A non-phosgene process for bioderived polycarbonate with high molecular weight and advanced property profile synthesized using amino acid ionic liquids as catalysts. *Green Chem.* **22**, 2534-2542 (2020).
151. Park, S.-A. et al. Sustainable and recyclable super engineering thermoplastic from biorenewable monomer. *Nat. Commun.* **10**, 2601 (2019).
152. Li, C., Sablong, R. J., van Benthem, R. A. T. M. & Koning, C. E. Unique base-initiated depolymerization of limonene-derived polycarbonates. *ACS Macro Lett.* **6**, 684-688 (2017).
153. Neumann, S., Leitner, L.-C., Schmalz, H., Agarwal, S. & Greiner, A. Unlocking the processability and recyclability of biobased poly(limonene carbonate). *ACS Sus. Chem. Eng.* **8**, 6442-6448 (2020).
154. Ma, S. & Webster, D. C. Naturally occurring acids as cross-linkers to yield VOC-free, high-performance, fully bio-based, degradable thermosets. *Macromolecules* **48**, 7127-7137 (2015).
155. Hevus, I., Ricapito, N. G., Tymoshenko, S., Raja, S. N. & Webster, D. C. Biobased carboxylic acids as components of sustainable and high-performance coating systems. *ACS Sus. Chem. Eng.* **8**, 5750-5762 (2020).

156. Zhang, S. et al. Preparation of a lignin-based vitrimer material and its potential use for recoverable adhesives. *Green Chem.* **20**, 2995-3000 (2018).
157. Toldy, A., Szolnoki, B. & Marosi, G. Flame retardancy of fibre-reinforced epoxy resin composites for aerospace applications. *Polym. Degrad. Stab.* **96**, 371-376 (2011).
158. Maiorana, A., Spinella, S. & Gross, R. A. Bio-based alternative to the diglycidyl ether of bisphenol A with controlled materials properties. *Biomacromolecules* **16**, 1021-1031 (2015).
159. Zago, E. et al. Synthesis of bio-based epoxy monomers from natural allyl- and vinyl phenols and the estimation of their affinity to the estrogen receptor α by molecular docking. *New J. Chem.* **40**, 7701-7710 (2016).
160. Winne, J. M., Leibler, L. & Du Prez, F. E. Dynamic covalent chemistry in polymer networks: a mechanistic perspective. *Polym. Chem.* **10**, 6091-6108 (2019).
161. Scheutz, G. M., Lessard, J. J., Sims, M. B. & Sumerlin, B. S. Adaptable crosslinks in polymeric materials: resolving the intersection of thermoplastics and thermosets. *J. Am. Chem. Soc.* **141**, 16181-16196 (2019).
162. Liu, X. & Zhang, J. High-performance biobased epoxy derived from rosin. *Polym. Int.* **59**, 607-609 (2010).
163. Pan, X., Sengupta, P. & Webster, D. C. High biobased content epoxy-anhydride thermosets from epoxidized sucrose esters of fatty acids. *Biomacromolecules* **12**, 2416-2428 (2011).
164. Chrysanthos, M., Galy, J. & Pascault, J.-P. Preparation and properties of bio-based epoxy networks derived from isosorbide diglycidyl ether. *Polymer* **52**, 3611-3620 (2011).

165. Hong, J., Radojč, D., Ionescu, M., Petrovič, Z. S. & Eastwood, E. Advanced materials from corn: isosorbide-based epoxy resins. *Polym. Chem.* **5**, 5360-5368 (2014).
166. Hu, F., La Scala, J. J., Sadler, J. M. & Palmese, G. R. Synthesis and characterization of thermosetting furan-based epoxy systems. *Macromolecules* **47**, 3332-3342 (2014).
167. Liu, W., Zhou, R., Goh, H. L. S., Huang, S. & Lu, X. From waste to functional additive: toughening epoxy resin with lignin. *ACS Appl. Mater. Interfaces* **6**, 5810-5817 (2014).
168. Qin, J., Liu, H., Zhang, P., Wolcott, M. & Zhang, J. Use of eugenol and rosin as feedstocks for biobased epoxy resins and study of curing and performance properties. *Polym. Int.* **63**, 760-765 (2014).
169. Gandini, A., Lacerda, T. M., Carvalho, A. J. F. & Trovatti, E. Progress of polymers from renewable resources: furans, vegetable oils, and polysaccharides. *Chem. Rev.* **116**, 1637-1669 (2016).
170. Zhang, C., Garrison, T. F., Madbouly, S. A. & Kessler, M. R. Recent advances in vegetable oil-based polymers and their composites. *Prog. Polym. Sci.* **71**, 91-143 (2017).
171. Li, R. et al. Use of hempseed-oil-derived polyacid and rosin-derived anhydride acid as cocuring agents for epoxy materials. *ACS Sus. Chem. Eng.* **6**, 4016-4025 (2018).
172. Zhao, S., Huang, X., Whelton, A. J. & Abu-Omar, M. M. Renewable epoxy thermosets from fully lignin-derived triphenols. *ACS Sus. Chem. Eng.* **6**, 7600-7608 (2018).

173. Ocando, C., Ecochard, Y., Decostanzi, M., Caillol, S. & Averous, L. Dynamic network based on eugenol-derived epoxy as promising sustainable thermoset materials. *Eur. Polym. J.* **135**, 109860 (2020).
174. Hollande, L. et al. Preparation of renewable epoxy-amine resins with tunable thermo-mechanical properties, wettability and degradation abilities from lignocellulose- and plant oils-derived components. *Front. Chem.* **7**, 159 (2019).
175. Gandini, A., Carvalho, A. J. F., Trovatti, E., Kramer, R. K. & Lacerda, T. M. Macromolecular materials based on the application of the Diels-Alder reaction to natural polymers and plant oils. *Eur. J. Lipid Sci. Technol.* **120**, 1700091 (2018).
176. Hernandez, E. D., Bassett, A. W., Sadler, J. M., La Scala, J. J. & Stanzione, J. F. Synthesis and characterization of bio-based epoxy resins derived from vanillyl alcohol. *ACS Sus. Chem. Eng.* **4**, 4328-4339 (2016).
177. Liu, T. et al. A self-healable high glass transition temperature bioepoxy material based on vitrimer chemistry. *Macromolecules* **51**, 5577-5585 (2018).
178. Zhao, S. & Abu-Omar, M. M. Recyclable and malleable epoxy thermoset bearing aromatic imine bonds. *Macromolecules* **51**, 9816-9824 (2018).
179. Yu, Q. et al. Vanillin-based degradable epoxy vitrimers: reprocessability and mechanical properties study. *Eur. Polym. J.* **117**, 55-63 (2019).
180. Ma, S. et al. Readily recyclable, high-performance thermosetting materials based on a lignin-derived spiro diacetal trigger. *J. Mater. Chem. A* **7**, 1233-1243 (2019).

181. Wang, S. et al. Facile in situ preparation of high-performance epoxy vitrimer from renewable resources and its application in nondestructive recyclable carbon fiber composite. *Green Chem.* **21**, 1484-1497 (2019).
182. Marchildon, K. Polyamides – still strong after seventy years. *Macromol. React. Eng.* **5**, 22-54 (2011).
183. Barnes, C. E. Nylon 4 – development and commercialization. *Lenzing. Ber.* **62**, 62-66 (1987).
184. Kim, H. T. et al. Development of metabolically engineered corynebacterium glutamicum for enhanced production of cadaverine and its use for the synthesis of bio-polyamide 510. *ACS Sus. Chem. Eng.* **8**, 129-138 (2020).
185. Lane, J. Terryl, a next-generation fiber: innovative, cost-competitive, biobased polyamide for textiles. *Biofuels Digest* <http://www.biofuelsdigest.com/bdigest/2014/11/10/terryl-a-next-generation-fiberinnovative-cost-competitive-biobased-polyamidefor-textiles/> (2014).
186. Caswell, P. J. Terryl. Presented at the Biotechnology Innovation Organization (BIO) World Congress (2014).
187. Yi, Z., Bingbing, Q. & Chi, L. Blended fiber and preparation method thereof and fabric comprising the blended fiber. CN Patent 105,040,156 A (2014).
188. Winnacker, M. & Rieger, B. Biobased polyamides: recent advances in basic and applied research. *Macromol. Rapid Commun.* **37**, 1391-1413 (2016).

189. Froidevaux, V., Negrell, C., Caillol, S., Pascault, J.-P. & Boutevin, B. Biobased amines: from synthesis to polymers; present and future. *Chem. Rev.* **116**, 14181-14224 (2016).
190. Pinggen, D. et al. Diamines for polymer materials via direct amination of lipid- and lignocellulose-based alcohols with NH₃. *ChemCatChem* **10**, 3027-3033 (2018).
191. Citoler, J., Derrington, S. R., Galman, J. L., Bevinakatti, H. & Turner, N. J. A biocatalytic cascade for the conversion of fatty acids to fatty amines. *Green Chem.* **21**, 4932-4935 (2019).
192. Firdaus, M. & Meier, M. A. R. Renewable polyamides and polyurethanes derived from limonene. *Green Chem.* **15**, 370-380 (2013).
193. Turunc, O., Firdaus, M., Klein, G. & Meier, M. A. R. Fatty acid derived renewable polyamides via thiol-ene additions. *Green Chem.* **14**, 2577-2583 (2012).
194. Jiang, Y., Maniar, D., Woortman, A. J. J., Alberda van Ekenstein, G. O. R. & Loos, K. Enzymatic polymerization of furan-2,5-dicarboxylic acid-based furanic-aliphatic polyamides as sustainable alternatives to polyphthalamides. *Biomacromolecules* **16**, 3674-3685 (2015).
195. Mitiakoudis, A. & Gandini, A. Synthesis and characterization of furanic polyamides. *Macromolecules* **24**, 830-835 (1991).
196. Song, L. et al. Ultra-strong long-chain polyamide elastomers with programmable supramolecular interactions and oriented crystalline microstructures. *Nat. Commun.* **10**, 1315 (2019).
197. Stockmann, P. N. et al. Biobased chiral semi-crystalline or amorphous high-performance polyamides and their scalable stereoselective synthesis. *Nat. Commun.* **11**, 509 (2020).

198. Stockmann, P. N. et al. New bio-polyamides from terpenes: α -pinene and (+)-3-carene as valuable resources for lactam production. *Macromol. Rapid Commun.* **40**, 1800903 (2019).
199. Winnacker, M., Neumeier, M., Zhang, X., Papadakis, C. M. & Rieger, B. Sustainable chiral polyamides with high melting temperature via enhanced anionic polymerization of a menthone-derived lactam. *Macromol. Rapid Commun.* **37**, 851–857 (2016).
200. Winnacker, M., Sag, J., Tischner, A. & Rieger, B. Sustainable, stereoregular, and optically active polyamides via cationic polymerization of ϵ -lactams derived from the terpene β -pinene. *Macromol. Rapid Commun.* **38**, 1600787 (2017).
201. Winnacker, M. & Sag, J. Sustainable terpenebased polyamides via anionic polymerization of a pinene-derived lactam. *ChemComm* **54**, 841–844 (2018).
202. Maisonneuve, L., Lamarzelle, O., Rix, E., Grau, E. & Cramail, H. Isocyanate-free routes to polyurethanes and poly(hydroxy urethane)s. *Chem. Rev.* **115**, 12407–12439 (2015).
203. Luo, X., Xiao, Y., Wu, Q. & Zeng, J. Development of high-performance biodegradable rigid polyurethane foams using all bioresource-based polyols: lignin and soy oil-derived polyols. *Int. J. Biol. Macromol.* **115**, 786–791 (2018).
204. Guo, A., Javni, I. & Petrovic, Z. Rigid polyurethane foams based on soybean oil. *J. Appl. Polym. Sci.* **77**, 467–473 (2000).
205. Zlatanić, A., Lava, C., Zhang, W. & Petrović, Z. S. Effect of structure on properties of polyols and polyurethanes based on different vegetable oils. *J. Polym. Sci. B Polym. Phys.* **42**, 809–819 (2004).

206. Babb, D. A. in *Synthetic Biodegradable Polymers* (eds Rieger, B. et al.) 315-360 (Springer, 2012).
207. Peyrton, J., Chambaretaud, C., Sarbu, A. & Averous, L. Biobased polyurethane foams based on new polyol architectures from microalgae oil. *ACS Sus. Chem. Eng.* **8**, 12187-12196 (2020).
208. Lysenko, Z. et al. Vegetable oil based polyols and polyurethanes made therefrom. WO Patent 2,004,096,882 A1 (2004).
209. Gurusamy-Thangavelu, S. A. et al. Polyurethanes based on renewable polyols from bioderived lactones. *Polym. Chem.* **3**, 2941-2948 (2012).
210. Gunawan, N. R. et al. Rapid biodegradation of renewable polyurethane foams with identification of associated microorganisms and decomposition products. *Bioresour. Technol.* **11**, 100513 (2020).
211. Cornille, A. et al. Promising mechanical and adhesive properties of isocyanate-free poly(hydroxyurethane). *Eur. Polym. J.* **84**, 404-420 (2016).
212. Zhang, K. et al. Non-isocyanate poly(amidehydroxyurethane)s from sustainable resources. *Green Chem.* **18**, 4667-4681 (2016).
213. Carre, C., Ecochard, Y., Caillol, S. & Averous, L. From the synthesis of biobased cyclic carbonate to polyhydroxyurethanes: a promising route towards renewable non-isocyanate polyurethanes. *ChemSusChem* **12**, 3410-3430 (2019).
214. Kuhnel, I., Saake, B. & Lehnen, R. A new environmentally friendly approach to lignin-based cyclic carbonates. *Macromol. Chem. Phys.* **219**, 1700613 (2018).

215. Chen, X., Li, L., Jin, K. & Torkelson, J. M. Reprocessable polyhydroxyurethane networks exhibiting full property recovery and concurrent associative and dissociative dynamic chemistry via transcarbamoylation and reversible cyclic carbonate aminolysis. *Polym. Chem.* **8**, 6349-6355 (2017).
216. Schimpf, V., Ritter, B. S., Weis, P., Parison, K. & Mulhaupt, R. High purity limonene decarbonate as versatile building block for sustainable nonisocyanate polyhydroxyurethane thermosets and thermoplastics. *Macromolecules* **50**, 944-955 (2017).
217. Tamami, B., Sohn, S. & Wilkes, G. L. Incorporation of carbon dioxide into soybean oil and subsequent preparation and studies of nonisocyanate polyurethane networks. *J. Appl. Polym. Sci.* **92**, 883-891 (2004).
218. Liaw, D.-J. et al. Advanced polyimide materials: syntheses, physical properties and applications. *Prog. Polym. Sci.* **37**, 907-974 (2012).
219. Lau, K. S. Y. in *Handbook of Thermoset Plastics* 3rd edn Ch. 10 (eds Dodiuk, H. & Goodman, S. H.) 297-424 (William Andrew Publishing, 2014).
220. McNamara, J., Harvey, J. D., Graham, M. J., Scherger, C. Optically transparent polyimides. WO Patent 2019/156,717 A2 (2019).
221. Serber, Z., et al. Microbial strain improvement by a HTP genomic engineering platform. WO Patent 2017/100,377 A1 (2018).
222. Zymergen. *Zymergen Reimagines Electronics with Breakthrough Bio-fabricated Materials* (Zymergen, 2020).

223. Lane, J. Super clear, super thin, super durable:Zymergen bends it like Beckham, electronics-wise. *Biofuels Digest* <http://www.biofuelsdigest.com/bdigest/2020/04/06/super-clear-super-thin-super-durablezymergen-bends-it-like-beckham-electronics-wise/> (2020).
224. Santhosh Kumar, K. S. & Reghunadhan Nair, C. P. in *Handbook of Thermoset Plastics* 3rd edn Ch. 3 (eds Dodiuk, H. & Goodman, S. H.) 45-73 (William Andrew Publishing, 2014).
225. Dumas, L., Bonnaud, L., Olivier, M., Poorteman, M. & Dubois, P. Chavicol benzoxazine: ultrahigh T_g biobased thermoset with tunable extended network. *Eur. Polym. J.* **81**, 337-346 (2016).
226. Puchot, L. et al. Breaking the symmetry of dibenzoxazines: a paradigm to tailor the design of bio-based thermosets. *Green Chem.* **18**, 3346-3353 (2016).
227. Teng, N. et al. Making benzoxazine greener and stronger: renewable resource, microwave irradiation, green solvent, and excellent thermal properties. *ACS Sus. Chem. Eng.* **7**, 8715-8723 (2019).
228. Zhang, K., Liu, Y., Han, M. & Froimowicz, P. Smart and sustainable design of latent catalyst-containing benzoxazine-bio-resins and application studies. *Green Chem.* **22**, 1209-1219 (2020).
229. Whiteley, J. M., Taynton, P., Zhang, W. & Lee, S.-H. Ultra-thin solid-state Li-ion electrolyte membrane facilitated by a self-healing polymer matrix. *Adv. Mater.* **27**, 6922-6927 (2015).
230. Taynton, P. et al. Re-healable polyimine thermosets: polymer composition and moisture sensitivity. *Polym. Chem.* **7**, 7052-7056 (2016).

231. Taynton, P. et al. Repairable woven carbon fiber composites with full recyclability enabled by malleable polyimine networks. *Adv. Mater.* **28**, 2904-2909 (2016).
232. Dhers, S., Vantomme, G. & Averous, L. A fully bio-based polyimine vitrimer derived from fructose. *Green Chem.* **21**, 1596-1601 (2019).
233. Hajj, R., Duval, A., Dhers, S. & Averous, L. Network design to control polyimine vitrimer properties: physical versus chemical approach. *Macromolecules* **53**, 3796-3805 (2020).
234. Geng, H. et al. Vanillin-based polyschiff vitrimers: reprocessability and chemical recyclability. *ACS Sus. Chem. Eng.* **6**, 15463-15470 (2018).
235. Wang, S. et al. Robust, fire-safe, monomer-recovery, highly malleable thermosets from renewable bioresources. *Macromolecules* **51**, 8001-8012 (2018).
236. Kim, C., Chandrasekaran, A., Huan, T. D., Das, D. & Ramprasad, R. Polymer genome: a data-powered polymer informatics platform for property predictions. *J. Phys. Chem. C.* **122**, 17575-17585 (2018).
237. Hackett, M., Zang, L., Viciu, L. & Masuda, T. *Lactic Acid, Its Salts, and Esters* (IHS Markit, 2018).
238. Montazeri, M., Zaines, G. G., Khanna, V. & Eckelman, M. J. Meta-analysis of life cycle energy and greenhouse gas emissions for priority biobased chemicals. *ACS Sus. Chem. Eng.* **4**, 6443-6454 (2016).

Chapter 3

Thermally Regulated Recyclable Carbene Catalysts for Upgrading of Biomass Furaldehydes[†]

3.1. Synopsis

The upgrading of biomass furaldehydes —furfural (FF) and 5-substituted (R) furfurals (R = CH₂OH, HMF; Me, MF; CH₂OMe, MMF)—into C₁₀₋₁₄ furoins was achieved by the selective umpolung self-coupling reaction catalyzed by polystyrene (PS) supported azolium salts paired with an acetate counterion, which allows a thermal equilibrium between the dormant ion pair and the active *N*-heterocyclic carbene (NHC) states. By regulating the equilibrium with heating to generate sufficient amounts of the active form of the catalyst for catalysis and cooling to deactivate the catalyst for recycling or recovery, such heterogeneous NHC organocatalysis can be performed without stoichiometric quantities of base for NHC catalyst generation and acid for catalyst quenching or recycling. Among several azolium structures investigated, a supported benzimidazolium coupled with a dodecyl chain achieved the highest furoin yields for the self-coupling reactions of FF (>95%) and HMF (>88%). This supported catalyst bearing the long alkyl chain also showed superior recyclability when exposed to air upon filtration, experiencing only a net decrease of ≤ 5% in yield over five cycles of FF self-coupling. In comparison, HMF self-coupling is less effective in both product yield and catalyst recyclability due to unproductive acid-

[†] This dissertation chapter contains the manuscript of a full paper published in *ACS Sustainable Chemistry & Engineering* [Cywar, R. M.; Wang, L.; Chen, E. Y. X. *ACS Sus. Chem. Eng.* **2019**, *7*, 1980-1988]. This work was supported by the U.S. Department of Energy Office of Basic Energy Sciences, grant DE-FG02-10ER16193. We thank Jedediah Wilson and Dr. Ravikumar Ramegowda for discussions. L. Wang collected a few preliminary data, provided guidance during the project, and co-wrote the introduction section.

base interactions between the acetate counterion and the HMF hydroxy proton. This detrimental effect can be overcome by use of substrates MF or MMF, an industrially relevant intermediate in the production of furan-based polyesters.

3.2. Introduction

Furfural (FF) and 5-hydroxymethylfurfural (HMF), produced from dehydration of biorefinery pentose and hexose sugars, have been widely regarded as two of the highest value platform chemicals from biomass.¹⁻⁹ The production of biofuels and fine chemicals from FF and HMF has attracted worldwide interest due to the dwindling of fossil fuel sources and increasing environmental concerns.¹⁻¹⁰ However, the short-chain alkane fuels obtained from FF and HMF exhibit high volatility and low energy densities.^{11, 12} To produce long-chain alkanes for high-quality liquid fuels, FF and HMF need to be upgraded via C–C bond forming, chain-extension reactions.¹³⁻¹⁶ It has been demonstrated that aldol condensation of furfurals with ketones to form condensation intermediates, followed by the hydrodeoxygenation (HDO) process, is a promising strategy to produce long-chain hydrocarbons.^{5, 17-21} A more direct upgrading approach is the *N*-heterocyclic carbene (NHC) catalyzed umpolung self-coupling of FF and HMF into C₁₀ and C₁₂ furoins, respectively.²²⁻³⁰ This route is organically catalyzed and quantitatively atom-economical, as there is no byproduct formation and also requires no coupling partner. The resulting C₁₂ furoin, 5,5'-dihydroxymethyl furoin (DHMF), has been transformed into high-quality jet fuel through the HDO process^{25, 26} and utilized as a renewable difuranic polyol building block or monomer for the synthesis of polyester and polyurethane materials.^{28, 29}

NHCs have emerged as powerful organocatalysts for both organic synthesis and polymerization.³¹⁻³⁴ As most NHCs are highly reactive and sensitive compounds, it has become a common practice to generate NHC catalysts by *in situ* deprotonation of the corresponding azolium salts with a strong base.³⁵⁻³⁷ The catalytic performance of NHCs can be finely tuned by adjusting the steric demand and electronic properties of substituents on the azolium ring. For instance, an NHC derived from the acetate substituted thiazolium, in combination with triethylamine base, catalyzes the self-coupling reaction of FF into C₁₀ furoin in quantitative selectivity and yield.²² NHCs derived from benzimidazolium ([BI]) salts with one or two long-chain alkyl substituents on the nitrogen atoms in the imidazole ring can even catalyze the self-coupling reaction of benzaldehyde in water.^{38,39} Highly efficient and recyclable supported NHC catalyst systems based on long-chain alkyl substituted [BI] salts were also successfully developed for the self-coupling reactions of FF and HMF.⁴⁰⁻⁴³ The catalyst recycling procedure involves activation of the [BI] salt (precatalyst) with a base to generate the NHC catalyst, catalysis in conversion of FF and HMF into C₁₀ and C₁₂ furoins, and recycling of the catalyst by quenching the reaction with HCl to reform the precatalyst, followed by filtration before use in the next cycle.⁴⁰ However, for every catalysis cycle, stoichiometric amounts of base and acid are required, which not only added to the cost but also generated more waste and complicated the product separation. Therefore, it is desirable to develop a thermally regulated, recyclable NHC catalyst system for the self-coupling reactions of FF and HMF where the catalyst generation and recycling can be achieved by simply adjusting the reaction temperature.

In recent years, different approaches have been taken to develop thermally labile NHC-precursors,⁴⁴ such as imidazolium carboxylate⁴⁵⁻⁴⁷ and imidazolium hydrogen carbonate salt.⁴⁸⁻⁵⁰ However, the recycling process of such precatalysts requires further addition of CO₂. In 2012, our

group found that a room-temperature ionic liquid, 1-ethyl-3-methylimidazolium acetate ([EMIM]OAc), can promote the self-coupling reaction of HMF into DHMF in high conversion and selectivity at elevated temperatures.²⁷ The catalyst for this coupling reaction was identified to be the NHC derived from deprotonation at the C-2 position of the imidazole ring by the acetate anion, which exists in an equilibrium with precatalyst [EMIM]OAc.⁵¹⁻⁵³ Although NHC is present in a small amount at room temperature, heating has been found to generate sufficient amounts of the free carbene for characterization, organocatalysis, or stoichiometric reactions.^{27, 51, 52, 54}

Based on this equilibrium, Taton *et al.* subsequently developed thermally recyclable imidazolium acetate precursors of polymer-supported NHCs which were employed in the benzoin condensation reaction. Benzoin yields in the range of 68%–78% were achieved throughout five cycles with their catalyst system.⁵⁴ In this work, we have developed a recyclable NHC catalyst system that is thermally regulated between dormant and active forms for the self-coupling reaction of furfuraldehydes (FAs) into C₁₀₋₁₄ furoins in high selectivity and yield. This recyclable system is derived from a [BI] acetate salt bearing a dodecyl chain which is grafted to a polystyrene (PS) resin, abbreviated as PS-*g*-[BI]-C₁₂-OAc. Figure 3.1 outlines the essential concept of this thermally regulated NHC catalyst system: the dormant state of the supported catalyst system is PS-*g*-[BI]-OAc, which can be thermally activated by heating to 80 °C and shifting the equilibrium towards PS-*g*-NHC, the active form that catalyzes the self-coupling of FAs into furoins. By cooling the system down to room temperature, the equilibrium is shifted back towards the ion pair through protonation of the NHC and recovered through simple filtration to separate it from the furoin products and solvent.

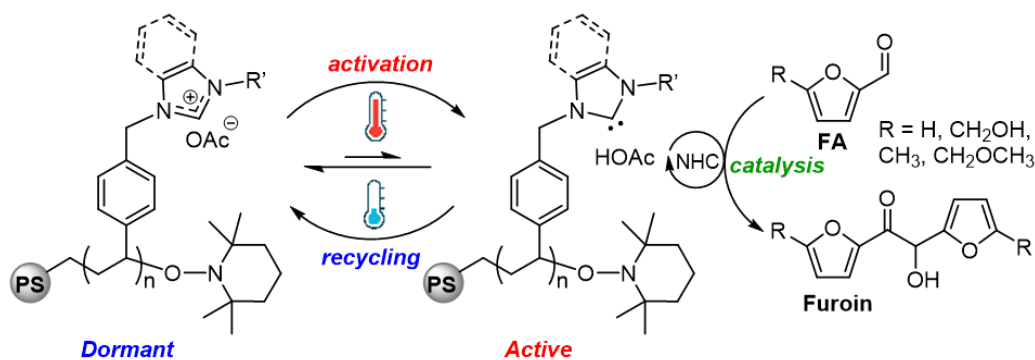


Figure 3.1. Outlined three elementary steps (activation, catalysis, and deactivation or recycling) involved in the thermally regulated, PS-supported [BI]OAc system for self-coupling of FAs to C₁₀₋₁₄ furoins.

3.3. Results and Discussion

Structure-Dependent Orthogonal Reactivity. The weakly basic acetate anion allows for a thermal equilibrium between a hydrogen bonded ion pair form (precatalyst) and the neutral acetic acid-stabilized, free carbene (active species),^{27, 51, 52, 54} which catalyzes the umpolung self-coupling dimerization of FAs to form furoins (Figure 3.2). In this generally accepted mechanism,^{27, 54} nucleophilic attack of a FA by the NHC catalyst generates a carbene-aldehyde tetrahedral zwitterionic intermediate that is protonated by acetic acid to form intermediate **I**, which is then deprotonated by acetate to afford hydroxyl enamine intermediate (**II**).²⁷ This enol intermediate functions as an acyl anion equivalent and attacks a second FA molecule to form zwitterionic intermediate **III**, which undergoes proton transfer and elimination of the NHC catalyst to complete the catalytic cycle (Figure 3.2).

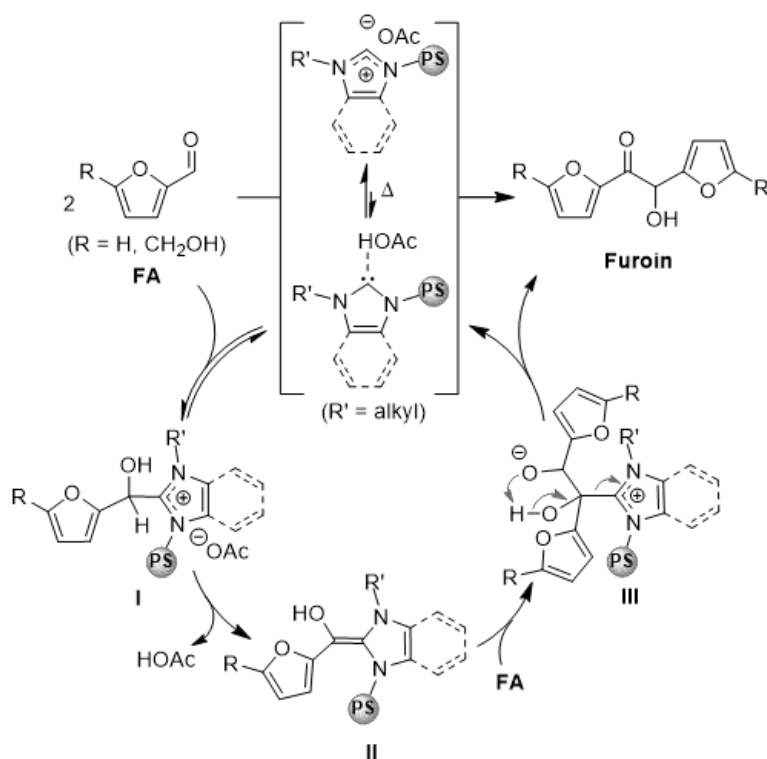
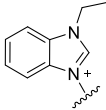
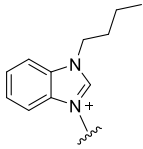
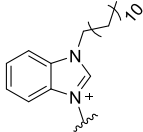
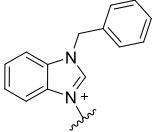
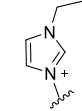
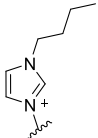
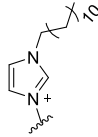
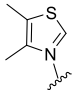
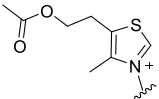


Figure 3.2. Proposed mechanism of FA self-coupling by PS-*g*-[NHC]-C_z-OAc.

Initially, we hypothesized that a catalyst exhibiting orthogonal reactivity (i.e., high activity at elevated temperatures and negligible activity at ambient temperature) would enhance recyclability by shifting the equilibrium more completely towards the dormant ion pair at room temperature, thus preventing the highly reactive free carbene from exposure to air. To identify catalyst structures which might express orthogonality, a range of PS-supported pre-NHC structures in a general formula of PS-*g*-[NHC]-C_z-OAc were prepared; catalyst structures and respective loadings on the resin are located in Table 3.1. Each was screened for self-coupling of FAs at low (25 °C) and high (80 °C) temperatures. Results of FF coupling yields at these two temperatures over a 24 h period are shown in Figure 3.3, where several trends can be observed. For the [BI]-based structures, a

shorter alkyl chain (ethyl) led to sharply decreased activity on going from 80 °C to 25 °C, whereas a longer alkyl chain (butyl, dodecyl) maintained comparably high activity for both temperatures.

Table 3.1. Summary of catalyst structures and respective loadings of grafted azoliums

Structure	Name (PS- <i>g</i> -)	Loading (mmol /g resin)
	[BI]-Et	2.66
	[BI]-Bu	2.16
	[BI]-C ₁₂	1.62 ^a 1.70 ^a 1.73 ^a 1.85 ^a
	[BI]-Bn	2.13
	[IM]-Et	2.33
	[IM]-Bu	2.36
	[IM]-C ₁₂	2.02
	[DMTM]	3.00
	[AcOMeTM] ^b	1.39

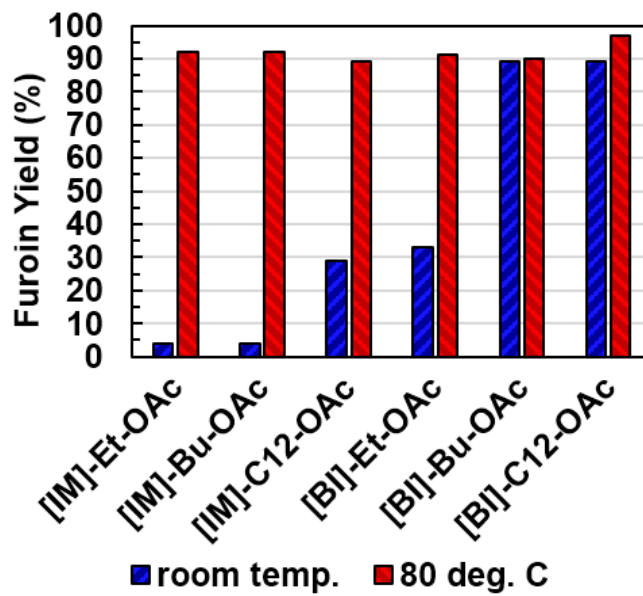


Figure 3.3. Orthogonal reactivity tests of PS-*g*-[NHC]-C_z-OAc catalysts towards the FF self-coupling reaction (24 h).

A longer alkyl chain increases sigma donation to the C-2 site via hyperconjugation,³² which promotes a stronger tendency to the carbene side of the equilibrium at room temperature and leads to high activity even at this low temperature. Imidazolium ([IM]) based structures showed a similar trend of decreasing orthogonality with increasing the alkyl chain length, but it was much less pronounced than the [BI] structures and there was no difference between ethyl and butyl substituents. These results showed that the [IM]-Et structure appeared to exhibit the desired orthogonality, which has also been shown in the literature for this structure incorporated in a copolymer.⁵⁴ However, when subjected to recycling experiments in air, the furoin yield dropped from 91% to 30% on the second cycle. On the other hand, when recycled in an inert atmosphere as a control, no decrease in yield was observed between the first and second cycles. During FF coupling at elevated temperature (80 °C), all [IM]-grafted resins turned deep indigo, and the observed color change was irreversible. When recycled in air, the catalyst changed from indigo to brown, but it

remained indigo when recycled under nitrogen. The color, perhaps due to the ionic/conjugated intermediates **I** and **II** (*c.f.* Figure 3.2), suggests that a fraction of the substrate and catalyst were fixed in the initial steps. Oxidation of the intermediates could be responsible for the decrease in activity after atmospheric recycling.^{31, 33-35, 57} These results suggest that apparent orthogonality cannot predict the recyclability of this system. The use of a weaker base may be able to modulate the highly active [BI]-C₁₂; thus, a trifluoroacetate anion (TFAc, approximately five orders of magnitude less basic than acetate) was investigated for the effect of base strength on apparent orthogonality. However, the ion exchange with this anion is less favorable under typical preparatory conditions.

Recyclability of PS-*g*-[BI]-C₁₂-OAc for FF Self-Coupling. Owing to previous successes with [BI]-C₁₂ chloride salts in base-activated coupling systems,³⁸⁻⁴⁰ this structure motif was investigated for thermal recyclability as the acetate salt. It was found to be both highly active and recyclable toward FF self-coupling, with >95% initial furoin yield and only a 5% net decrease in yield over 5 cycles of FF coupling, regardless of whether the recycling was performed in air or under N₂ atmosphere (Figure 3.4, series **A** and **B**). The furoin product can be crystallized directly out of the THF solution in high purity (Figure S3.10); no further purification is required. High yield (95%) was also observed for a 60 °C, 2 h run with a 10 mol% catalyst loading, and 92% yield was also attained with a 1 mol% catalyst loading in 1 h, demonstrating that even milder temperatures, shorter reaction times, and lower catalyst loadings are sufficient for this reaction. Worth noting here is that controls performed with no catalyst or the chloride precursor PS-*g*-[BI]-C₁₂-Cl showed no background reaction or activity at 80 °C over a 24 h period. The PS-*g*-[BI]-C₁₂-OAc system also showed remarkable room temperature activity, achieving 87% furoin yield in 8 h, signifying that the room and high-temperature reactivities are not orthogonal (*c.f.* Figure 3.3).

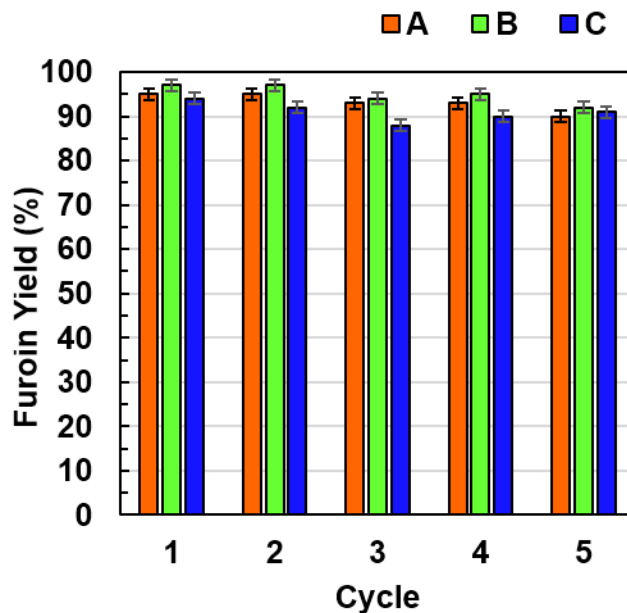


Figure 3.4. Recyclability tests of PS-*g*-[BI]-C₁₂-OAc for the FF self-coupling reaction. **A:** 10 mol%, 80 °C, recycled in air; **B:** 10 mol%, 80 °C, recycled under N₂; **C:** 5 mol%, 80 °C, recycled in air.

However, the room temperature activity was only an initial phenomenon and could not be sustained for subsequent cycles. For cycles 1 and 2 performed at room temperature, the furoin yield dropped from 97 to 50%, but a 3rd cycle at 80 °C returned the furoin yield to 92%. While this catalyst structure was not initially orthogonal, these results demonstrate that the thermal equilibrium plays a significant role in preserving high catalytic activity. However, with incomplete protonation of the NHC at room temperature, traces of acetic acid can be lost to solution during filtration while any carbene is left subject to deactivation by reaction with components of air.^{53,58} Since significant room temperature reactivity is only an initial phenomenon, it led us to question if a small, but potent, amount of the molecular NHC is released from the polymer matrix during the first cycle in THF. The reaction solvent, THF, is known to swell MPR significantly more than the preparatory solvents (MeCN, DCM, MeOH),⁵⁹ and the ¹H NMR spectra of both crude reaction

mixtures and dried furoin products sometimes displayed a small peak between 10.1-10.2 ppm, a chemical shift consistent with the acidic C-2 proton shared by [NHC] and acetate ion.⁵⁴ However, there were no corresponding signals in the alkyl region to account for the long alkyl chain of dodecyl benzimidazole, which cast doubt upon the leaching of molecular catalyst. Therefore, the initial room temperature reactivity phenomenon can be attributed to both deactivated carbene as well as the resulting stoichiometric imbalance of acetate after acetic acid is lost to solution. Acetic acid is known to facilitate the proton transfer steps which lead to the intermediate **II**; without sufficient base, the initial, reversible zwitterionic adduct is less easily converted to productive **II**, and the yield at room temperature suffers greatly, even if the carbene survived exposure to air. This mode of deactivation is also supported by the fact that atmospheric versus inert filtration conditions did not affect net yield loss, as acetic acid could be lost to solution regardless of the atmosphere.

Table 3.2. Recyclability comparison of PS-g-[BI]-C₁₂-OAc and PS-g-[BI]-Bn-OAc for furoin yield of the FF self-coupling.

cycle	[BI]- C ₁₂ -OAc	[BI]- Bn-OAc
1	95%	92%
2	95%	93%
3	93%	89%
4	93%	86%
5	90%	79%

The precatalyst loading was then reduced to 5 mol% to see if there was a pronounced effect on deactivation due to progressive acetic acid loss. While yields were slightly lower overall, the net

yield loss remained similar (Figure 3.4, series C). These results highlight the superior performance of PS-*g*-[BI]-C₁₂-OAc and further corroborate previous hypotheses that the ‘greasy’ dodecyl chain provides a protective, hydrophobic pocket around the reactive site, which contributes to both a higher product yield and better recyclability.³⁸⁻⁴⁰ Effect on yield is clearly visible in the trends displayed in Figure 3.3, and effect on recyclability is further confirmed by the recycling results of PS-*g*-[BI]-Bn-OAc shown in Table 3.2. A benzyl substituent is slightly bulky and non-polar, but not as large or hydrophobic as a dodecyl chain; a 13% net decrease in yield was seen after 5 cycles of FF coupling by the benzyl derivative as compared to only 5% in the case of the dodecyl catalyst. Therefore, the C₁₂ chain clearly plays an important role in preserving the catalyst.

HMF Self-Coupling.

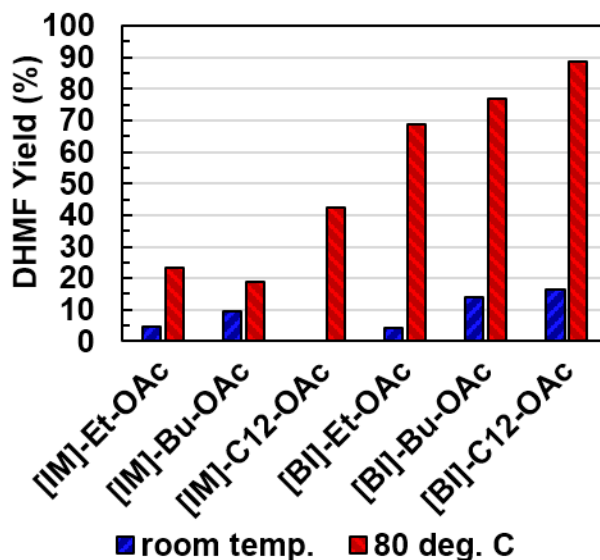
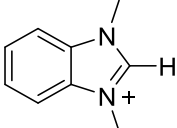
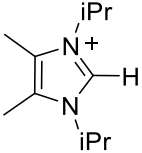
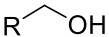
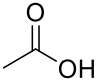


Figure 3.5. Orthogonal reactivity tests of PS-*g*-[NHC]-C_Z-OAc catalysts towards the HMF self-coupling reaction (24 h).

All catalyst structures were less effective for HMF self-coupling than for FF, but the [BI]-based catalysts performed far better than the [IM]-based ones; these trends are illustrated in Figure

3.5. Again, PS-*g*-[BI]-C₁₂-OAc provided the highest DHMF yield of 89% at 80 °C. After unsuccessful attempts to increase the yield, it became apparent that a substrate inhibition-like effect was taking place. These attempts included increasing the catalyst loading up to 20 mol% and adjusting reaction parameters such as temperature and solvent, but all were generally fruitless (Table S3.3). A dibasic succinate counterion was also tested because in a previous study,²² it was shown that two equivalents of base relative to pre-catalyst markedly increased DHMF yield. Since the acetate base is incorporated in precisely one equivalent in this system, a dibasic counterion could possibly provide this extra equivalent. However, the resulting succinate derivatives tested (PS-*g*-[BI]-Et-Succ, PS-*g*-[BI]-C₁₂-Succ) showed negligible difference in reactivity versus the acetate counterparts (Table S3.3).

Table 3.3. Relevant pK_a values.⁶⁰

species	pK_a (DMSO)
	18.6
	24
	30
	12.6

We hypothesize that the difference in reactivities of HMF versus FF, as well as between [BI] and [IM]-based structures towards HMF, are both due to acid-base interactions among the acetate

ion, C-2 proton of the precatalyst, and the hydroxy proton of HMF (illustrated in Figure 3.6, pK_a 's listed in Table 3.3).

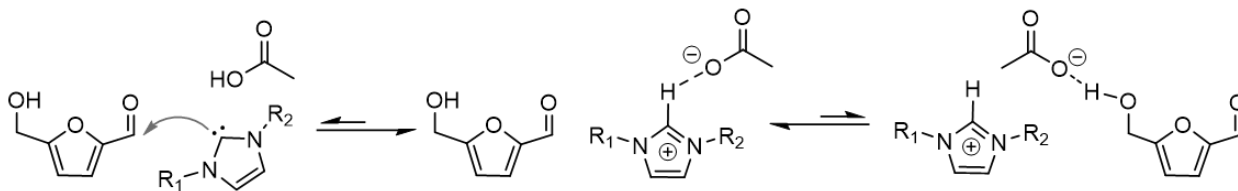


Figure 3.6. Possible acid-base equilibria present in the coupling reaction involving protic HMF.

In the case of FF, there are no acid-base reactions for the acetate to partake in other than at the desired C-2 proton; thus, the reaction proceeds smoothly. For HMF however, the acetate may interact with the hydroxy proton through hydrogen bonding, in addition to the desired C-2 proton as shown in Figure 3.6 and Figure S3.14. This likely explains the lower activity towards HMF in general. In previous work when NHC was generated with a base (e.g. DBU),^{22, 40, 41, 61} acid-base chemistry between the NHC and HMF hydroxy group did not impede reactivity, suggesting that in these coupling systems, the active NHC is indeed more nucleophilic than Brønsted basic, and that the acetate must be the promiscuous species. Our initial report, which employed stoichiometric amounts of the ionic liquid [EMIM]OAc,²⁷ gave good yield (72%) in the presence of HMF's hydroxy proton, but this very interaction can also explain the increase in yield from 72 to 98% when a catalytic amount of Enders TPT (3,4,5-triphenyl-1,2,4-triazole) was used rather than stoichiometric [EMIM]OAc. Additionally, the cross-coupling reaction of FF with HMF proceeds smoothly even in alcohol solvent (ethanol).⁶¹ In the present system, even catalytic quantities of acetate hinder reactivity due to competition between the hydroxy and C-2 protons. Although the hydroxy proton has a higher pK_a (in DMSO solution) than the C-2 proton (Table 3.3),⁶⁰ hydrogen

bonding interactions can still occur. This statement is evidenced by significant changes in chemical shifts and splitting patterns in the NMR spectra of HMF and potassium acetate when mixed in anhydrous DMSO-*d*₆ at room temperature (0.2 or 1.0 equivalents of acetate relative to HMF). These differences are apparent in Figure S3.14 and calculated as Δppm in Tables S3.7-9. The mixtures were also observed to change color from clear (KOAc) or yellow (HMF) to pink (Figure S3.15). Most importantly, the hydroxy proton and adjacent methylene lost triplet and doublet splitting patterns to become broad singlets as the alcohol proton became shared between HMF and the acetate anion.

The large activity difference between [IM] and [BI]-based structures towards HMF self-coupling at 80 °C (Figure 3.5), which was not observed in the case of FF coupling (*c.f.*, Figure 3.3), is likely due to the differing acidities of the C-2 protons in their respective acetate salt forms (Table 3.3). Benzimidazolium ions are significantly more acidic than imidazoliums (by 5.4 p*K*_a units, ~250,000x more acidic), which would make deprotonation at the C-2 site more facile in the case of the former. Therefore, the stronger acidity of [BI] salts allows for a more favorable formation of catalytic NHC in the presence of HMF. In addition, the aforementioned acetate-alcohol interactions are also less significant for [BI] salts due to an 11 p*K*_a unit difference between the C-2 proton of [BI]⁺ and the HMF hydroxy proton; thus, acetate is much less likely to associate with the alcohol. Conversely, the C2-proton of [IM]⁺ and the HMF hydroxy proton have a p*K*_a difference of only 6 units, thus making the acetate-alcohol association more competitive with C-2 deprotonation.

These undesired interactions are also responsible for the poor recyclability of PS-*g*-[BI]-C₁₂-OAc when used for HMF self-coupling, shown in Table 3.4. There was a precipitous drop in yield

Table 3.4. Recyclability tests of PS-*g*-[BI]-C₁₂-OAc for the HMF self-coupling reaction.

Cycle:	1	2	3	4
Yield <i>in-air recycling</i>	84%	62%	57%	^a 66% ^b 29%
Yield <i>air- free recycling</i>	89%	74%	67%	^b 74%

^a after regeneration attempt with AcOH in MeOH^b after regeneration attempt with KOAc in MeOH

after the first cycle: a 14 or 23% decline between the first and second cycles was seen for air-free or atmospheric filtration, respectively. In either case, the standard recycling procedure was discontinued after the third cycle and attempts were made to regenerate the catalyst. To support the hypothesis that acetic acid is lost to solution, this species was given back to the system. As shown in Table 3.4, up to 84% of original catalytic activity could be restored for a fourth cycle by treating the spent catalyst with acetic acid in methanol. Treating with potassium acetate in methanol led to a continued decline in yield to 29%; therefore, it is not likely that a [benz]imidazolium chloride species was reformed by substitution of an HMF alkoxide at a residual benzyl chloride position in the PS resin, because potassium acetate should be an appropriate regenerating agent to exchange a chloride for an acetate anion. On the other hand, if the free carbene were exposed to potassium acetate, there would be no proton provided by the PS-supported system to share between the C-2 carbon and acetate ion, and no counter ion to balance charge with K⁺. Therefore, the regenerating effect of acetic acid confirms that this species is lost to the filtrate during recycling, leaving a free carbene vulnerable to irreversible deactivation.

Because a portion of intact carbene was able to be re-paired with acetic acid after the regeneration experiment, the dodecyl chain was likely responsible for protecting it.

While a method could be developed to incorporate an acetic acid wash after each cycle to maintain DHMF yield, the yield was still inferior to PS-*g*-[BI]-C₁₂-Cl + DBU (94% DHMF), where an acid regeneration is also required.⁴⁰ If C₁₂ furoins are to be produced by the present system, alternate substrates such as 5-methylfurfural (MF) or the industrially relevant methyl ether of HMF (5-methoxymethyl furfural, MMF) are recommended. MMF is currently undergoing scale-up as an intermediate in the production of 2,5-furandicarboxylic acid for commercial poly(ethylene furanoate), a bio-based poly(ethylene terephthalate) substitute.⁶² As such, coupling of MMF to the C₁₂ furoin product aligns with the integrated biorefinery concept.⁹ Coupling experiments performed with both MF and MMF provided the respective C₁₂ and C₁₄ furoin products in very good yields and did not poison the catalyst upon recycling, as expected without the alcohol moiety.

Grafted Thiazolium Catalysts. Previously, we have shown that homogeneous, thiazolium ([TM]) based NHC's catalyze the self-coupling of HMF in near-quantitative yield.²² To investigate the activity of a PS-supported acetate form, we grafted the most active thiazolium structure, 5-(2-acetoxyethyl)-4-methylthiazole (“[AcOMeTM],” shown in Table 3.1) to MPR. During the ion exchange step, the resin was observed to turn orange, and the obtained catalyst was inactive for FF and HMF coupling with yields <10% (Table S3.4). However, it was found to produce furoin in quantitative yield when combined with triethylamine base (Table S3.4). This was clear evidence of an unsuccessful ion exchange step, especially since the higher acidity of thiazolium salts (pK_a 16.5) should facilitate carbene formation from the acetate salt form. The parent chloride, PS-*g*-[AcOMeTM]-Cl, was also observed to decompose during storage in air due to a strong acetic acid odor; this was also confirmed by a headspace analysis. Accordingly, 4,5-dimethylthiazole

([DMTM]) was grafted to avoid the apparent decomposition of the backbone ester substituent. The parent chloride, PS-*g*-[DMTM]-Cl, when activated with a base, was highly active toward both coupling reactions, but again the ion exchange with potassium acetate did not proceed. This could only be combatted when lead acetate in alcohol was used, such that the PbCl₂ precipitated and drove forward the exchange equilibrium. This preparation resulted in a 79% yield of DHMF, confirming the failure of potassium acetate to exchange on a thiazolium chloride. However, this result was still below the yield achieved with PS-*g*-[BI]-C₁₂-OAc or the base-activated [TM] systems (homogeneous or heterogeneous).

3.4. Conclusions

We have developed an efficient, convenient, and thermally regulated catalyst system for the self-coupling reaction of biorefinery platform chemicals, especially FF. Over 90% furoin yield was sustained over five cycles of catalysis with only a 5% net decrease in yield when using the best performing catalyst PS-*g*-[BI]-C₁₂-OAc. The superiority of PS-*g*-[BI]-C₁₂-OAc in terms of both recyclability and yield was demonstrated in this study, by virtue of the ‘greasy’ dodecyl chain providing a hydrophobic pocket that protects any carbene present during filtration from deactivation, and by contributing to increased nucleophilicity required for the umpolung coupling. Benzimidazolium-based catalysts performed better than imidazoliums towards furaldehyde coupling, with longer *N*-alkyl chains contributing to higher activity in both cases. Despite possessing orthogonal reactivity, the imidazolium-based catalyst PS-*g*-[IM]-Et-OAc was not tolerant of air during recycling in this system. Thiazolium structures, while effective catalysts in the PS-supported chloride salt form (which requires base activation), were unable to undergo a successful ion exchange to acetate under normal preparatory conditions. Good yields of the C₁₂

furoin product, DHMF, derived from self-coupling of HMF, could not be sustained due to unfavorable interactions between the acetate base and the hydroxy proton, which impede reactivity and have a poisonous effect that renders the catalyst poorly recyclable. Therefore, use of heterogeneous catalysis for HMF coupling with high yield and good recyclability is best accomplished with the chloride salt, PS-*g*-[BI]-C₁₂-Cl, in combination with a base such as DBU for activation. C₁₂ and C₁₄ furoin products can still be obtained with this system in a recyclable fashion by using MF and MMF substrates, the latter of which is an intermediate in commercial-scale bio-based polyester production.

It is worth noting here that, even with the current best performing catalyst PS-*g*-[BI]-C₁₂-OAc, a gradual decrease in the C₁₀ furoin yield over five cycles of catalysis (~5% net decrease) was still seen, which was attributed to loss of acetic acid during the process so that the active NHC catalyst was not completely deactivated and then regenerated. One design that could overcome this issue is to covalently tether an acetate moiety to the [BI] system. Work in this direction is currently underway.

References

- (1) Bohre, A.; Dutta, S.; Saha, B.; Abu-Omar, M. M., Upgrading Furfurals to Drop-in Biofuels: An Overview. *ACS Sustainable Chem. Eng.* **2015**, *3* (7), 1263-1277.
- (2) Wang, T.; Nolte, M. W.; Shanks, B. H., Catalytic dehydration of C6 carbohydrates for the production of hydroxymethylfurfural (HMF) as a versatile platform chemical. *Green Chem.* **2014**, *16* (2), 548-572.
- (3) Teong, S. P.; Yi, G.; Zhang, Y., Hydroxymethylfurfural production from bioresources: past, present and future. *Green Chem.* **2014**, *16* (4), 2015-2026.
- (4) van Putten, R.-J.; van der Waal, J. C.; de Jong, E.; Rasrendra, C. B.; Heeres, H. J.; de Vries, J. G., Hydroxymethylfurfural, A Versatile Platform Chemical Made from Renewable Resources. *Chem. Rev.* **2013**, *113* (3), 1499-1597.
- (5) Lange, J.-P.; van der Heide, E.; van Buijtenen, J.; Price, R., Furfural—A Promising Platform for Lignocellulosic Biofuels. *ChemSusChem* **2012**, *5* (1), 150-166.
- (6) Rosatella, A. A.; Simeonov, S. P.; Frade, R. F. M.; Afonso, C. A. M., 5-Hydroxymethylfurfural (HMF) as a building block platform: Biological properties, synthesis and synthetic applications. *Green Chem.* **2011**, *13* (4), 754-793.
- (7) Zakrzewska, M. E.; Bogel-Łukasik, E.; Bogel-Łukasik, R., Ionic Liquid-Mediated Formation of 5-Hydroxymethylfurfural—A Promising Biomass-Derived Building Block. *Chem. Rev.* **2011**, *111* (2), 397-417.
- (8) Ståhlberg, T.; Fu, W.; Woodley, J. M.; Riisager, A., Synthesis of 5-(Hydroxymethyl)furfural in Ionic Liquids: Paving the Way to Renewable Chemicals. *ChemSusChem* **2011**, *4* (4), 451-458.

- (9) Bozell, J. J.; Petersen, G. R., Technology development for the production of biobased products from biorefinery carbohydrates—the US Department of Energy’s “Top 10” revisited. *Green Chem.* **2010**, *12* (4), 539-554.
- (10) Huber, G. W.; Chheda, J. N.; Barrett, C. J.; Dumesic, J. A., Production of Liquid Alkanes by Aqueous-Phase Processing of Biomass-Derived Carbohydrates. *Science* **2005**, *308* (5727), 1446.
- (11) King, A. E.; Brooks, T. J.; Tian, Y.-H.; Batista, E. R.; Sutton, A. D., Understanding Ketone Hydrodeoxygenation for the Production of Fuels and Feedstocks From Biomass. *ACS Catal.* **2015**, *5* (2), 1223-1226.
- (12) Sutton, A. D.; Waldie, F. D.; Wu, R.; Schlaf, M.; Pete' Silks Iii, L. A.; Gordon, J. C., The hydrodeoxygenation of bioderived furans into alkanes. *Nat. Chem.* **2013**, *5*, 544.
- (13) Wegenhart, B. L.; Liu, S.; Thom, M.; Stanley, D.; Abu-Omar, M. M., Solvent-Free Methods for Making Acetals Derived from Glycerol and Furfural and Their Use as a Biodiesel Fuel Component. *ACS Catal.* **2012**, *2* (12), 2524-2530.
- (14) Balakrishnan, M.; Sacia, E. R.; Bell, A. T., Etherification and reductive etherification of 5-(hydroxymethyl)furfural: 5-(alkoxymethyl)furfurals and 2,5-bis(alkoxymethyl)furans as potential bio-diesel candidates. *Green Chem.* **2012**, *14* (6), 1626-1634.
- (15) Corma, A.; de la Torre, O.; Renz, M., Production of high quality diesel from cellulose and hemicellulose by the Sylvan process: catalysts and process variables. *Energy Environ. Sci.* **2012**, *5* (4), 6328-6344.
- (16) Corma, A.; de la Torre, O.; Renz, M.; Villandier, N., Production of High-Quality Diesel from Biomass Waste Products. *Angew. Chem. Int. Ed.* **2011**, *50* (10), 2375-2378.

- (17) Imteyaz Alam, M.; De, S.; Dutta, S.; Saha, B., Solid-acid and ionic-liquid catalyzed one-pot transformation of biorenewable substrates into a platform chemical and a promising biofuel. *RSC Adv.* **2012**, *2* (17), 6890-6896.
- (18) Dedsuksophon, W.; Faungnawakij, K.; Champreda, V.; Laosiripojana, N., Hydrolysis/dehydration/aldol-condensation/hydrogenation of lignocellulosic biomass and biomass-derived carbohydrates in the presence of Pd/WO₃-ZrO₂ in a single reactor. *Bioresour. Technol.* **2011**, *102* (2), 2040-2046.
- (19) West, R. M.; Liu, Z. Y.; Peter, M.; Gärtner, C. A.; Dumesic, J. A., Carbon-carbon bond formation for biomass-derived furfurals and ketones by aldol condensation in a biphasic system. *J. Molec. Catal. A: Chem.* **2008**, *296* (1), 18-27.
- (20) Chheda, J. N.; Dumesic, J. A., An overview of dehydration, aldol-condensation and hydrogenation processes for production of liquid alkanes from biomass-derived carbohydrates. *Catal. Today* **2007**, *123* (1), 59-70.
- (21) Barrett, C. J.; Chheda, J. N.; Huber, G. W.; Dumesic, J. A., Single-reactor process for sequential aldol-condensation and hydrogenation of biomass-derived compounds in water. *App. Catal. B: Environ.* **2006**, *66* (1), 111-118.
- (22) Zang, H.; Chen, E. Y. X., Organocatalytic Upgrading of Furfural and 5-Hydroxymethyl Furfural to C₁₀ and C₁₂ Furoins with Quantitative Yield and Atom-Efficiency. *Int. J. Molec. Sci.* **2015**, *16* (4), 7143-7158.
- (23) Wegenhart, B. L.; Yang, L.; Kwan, S. C.; Harris, R.; Kenttämaa, H. I.; Abu-Omar, M. M., From Furfural to Fuel: Synthesis of Furoins by Organocatalysis and their Hydrodeoxygenation by Cascade Catalysis. *ChemSusChem* **2014**, *7* (9), 2742-2747.

- (24) Liu, D.; Chen, E. Y. X., Organocatalysis in biorefining for biomass conversion and upgrading. *Green Chem.* **2014**, *16* (3), 964-981.
- (25) Liu, D.; Chen, E. Y. X., Integrated Catalytic Process for Biomass Conversion and Upgrading to C12 Furoin and Alkane Fuel. *ACS Catal.* **2014**, *4* (5), 1302-1310.
- (26) Liu, D.; Chen, E. Y. X., Diesel and Alkane Fuels From Biomass by Organocatalysis and Metal–Acid Tandem Catalysis. *ChemSusChem* **2013**, *6* (12), 2236-2239.
- (27) Liu, D.; Zhang, Y.; Chen, E. Y. X., Organocatalytic upgrading of the key biorefining building block by a catalytic ionic liquid and N-heterocyclic carbenes. *Green Chem.* **2012**, *14* (10), 2738-2746.
- (28) Mou, Z.; Chen, E. Y. X., Polyesters and Poly(ester-urethane)s from Biobased Difuranic Polyols. *ACS Sustainable Chem. Eng.* **2016**, *4* (12), 7118-7129.
- (29) Mou, Z.; Feng, S.; Chen, E. Y. X., Bio-based difuranic polyol monomers and their derived linear and cross-linked polyurethanes. *Polym. Chem.* **2016**, *7* (8), 1593-1602.
- (30) Zang, H.; Wang, K.; Zhang, M.; Xie, R.; Wang, L.; Chen, E. Y. X., Catalytic coupling of biomass-derived aldehydes into intermediates for biofuels and materials. *Catal. Sci. Technol.* **2018**.
- (31) Flanigan, D. M.; Romanov-Michailidis, F.; White, N. A.; Rovis, T., Organocatalytic Reactions Enabled by N-Heterocyclic Carbenes. *Chem. Rev.* **2015**, *115* (17), 9307-9387.
- (32) Fèvre, M.; Pinaud, J.; Gnanou, Y.; Vignolle, J.; Taton, D., N-Heterocyclic carbenes (NHCs) as organocatalysts and structural components in metal-free polymer synthesis. *Chem. Soc. Rev.* **2013**, *42* (5), 2142-2172.
- (33) Marion, N.; Díez-González, S.; Nolan, S. P., N-Heterocyclic Carbenes as Organocatalysts. *Angew. Chem. Int. Ed.* **2007**, *46* (17), 2988-3000.

- (34) Enders, D.; Niemeier, O.; Henseler, A., Organocatalysis by N-Heterocyclic Carbenes. *Chem. Rev.* **2007**, *107* (12), 5606-5655.
- (35) Hopkinson, M. N.; Richter, C.; Schedler, M.; Glorius, F., An overview of N-heterocyclic carbenes. *Nature* **2014**, *510* (7506), 485-496.
- (36) Benhamou, L.; Chardon, E.; Lavigne, G.; Bellemin-Lapponnaz, S.; César, V., Synthetic Routes to N-Heterocyclic Carbene Precursors. *Chem. Rev.* **2011**, *111* (4), 2705-2733.
- (37) de Frémont, P.; Marion, N.; Nolan, S. P., Carbenes: Synthesis, properties, and organometallic chemistry. *Coord. Chemistry Reviews* **2009**, *253* (7), 862-892.
- (38) Iwamoto, K.-i.; Kimura, H.; Oike, M.; Sato, M., Methylene-bridged bis(benzimidazolium) salt as a highly efficient catalyst for the benzoin reaction in aqueous media. *Org. Biomol. Chem.* **2008**, *6* (5), 912-915.
- (39) Iwamoto, K.-i.; Hamaya, M.; Hashimoto, N.; Kimura, H.; Suzuki, Y.; Sato, M., Benzoin reaction in water as an aqueous medium catalyzed by benzimidazolium salt. *Tetrahedron Lett.* **2006**, *47* (40), 7175-7177.
- (40) Wang, L.; Chen, E. Y. X., Recyclable Supported Carbene Catalysts for High-Yielding Self-Condensation of Furaldehydes into C10 and C12 Furoins. *ACS Catal.* **2015**, *5* (11), 6907-6917.
- (41) Wang, L.; Chen, E. Y. X., An interchangeable homogeneous \rightleftharpoons heterogeneous catalyst system for furfural upgrading. *Green Chem.* **2015**, *17* (12), 5149-5153.
- (42) Yan, B.; Zang, H.; Jiang, Y.; Yu, S.; Chen, E. Y. X., Recyclable montmorillonite-supported thiazolium ionic liquids for high-yielding and solvent-free upgrading of furfural and 5-hydroxymethylfurfural to C10 and C12 furoins. *RSC Adv.* **2016**, *6* (80), 76707-76715.
- (43) Zhong, R.; Lindhorst, A. C.; Groche, F. J.; Kühn, F. E., Immobilization of N-Heterocyclic Carbene Compounds: A Synthetic Perspective. *Chem. Rev.* **2017**, *117* (3), 1970-2058.

- (44) Naumann, S.; Buchmeiser, M. R., Liberation of N-heterocyclic carbenes (NHCs) from thermally labile progenitors: protected NHCs as versatile tools in organo- and polymerization catalysis. *Catal. Sci. Technol.* **2014**, *4* (8), 2466-2479.
- (45) Hans, M.; Delaude, L.; Rodriguez, J.; Coquerel, Y., N-Heterocyclic Carbene Catalyzed Carba-, Sulfa-, and Phospha-Michael Additions with NHC·CO₂ Adducts as Precatalysts. *J. Org. Chem.* **2014**, *79* (6), 2758-2764.
- (46) Delaude, L., Betaine Adducts of N-Heterocyclic Carbenes: Synthesis, Properties, and Reactivity. *Eur. J. Inorg. Chem.* **2009**, *2009* (13), 1681-1699.
- (47) Tudose, A.; Demonceau, A.; Delaude, L., Imidazol(in)ium-2-carboxylates as N-heterocyclic carbene precursors in ruthenium–arene catalysts for olefin metathesis and cyclopropanation. *J. Organomet. Chem.* **2006**, *691* (24), 5356-5365.
- (48) Coupillaud, P.; Vignolle, J.; Mecerreyes, D.; Taton, D., Post-polymerization modification and organocatalysis using reactive statistical poly(ionic liquid)-based copolymers. *Polymer* **2014**, *55* (16), 3404-3414.
- (49) Fèvre, M.; Pinaud, J.; Leteneur, A.; Gnanou, Y.; Vignolle, J.; Taton, D.; Miqueu, K.; Sotiropoulos, J.-M., Imidazol(in)ium Hydrogen Carbonates as a Genuine Source of N-Heterocyclic Carbenes (NHCs): Applications to the Facile Preparation of NHC Metal Complexes and to NHC-Organocatalyzed Molecular and Macromolecular Syntheses. *J. Am. Chem. Soc.* **2012**, *134* (15), 6776-6784.
- (50) Fèvre, M.; Coupillaud, P.; Miqueu, K.; Sotiropoulos, J.-M.; Vignolle, J.; Taton, D., Imidazolium Hydrogen Carbonates versus Imidazolium Carboxylates as Organic Precatalysts for N-Heterocyclic Carbene Catalyzed Reactions. *J. Org. Chem.* **2012**, *77* (22), 10135-10144.

- (51) Hollóczki, O.; Gerhard, D.; Massone, K.; Szarvas, L.; Németh, B.; Veszprémi, T.; Nyulászi, L., Carbenes in ionic liquids. *New J. Chem.* **2010**, *34* (12), 3004-3009.
- (52) Rodríguez, H.; Gurau, G.; Holbrey, J. D.; Rogers, R. D., Reaction of elemental chalcogens with imidazolium acetates to yield imidazole-2-chalcogenones: direct evidence for ionic liquids as proto-carbenes. *Chem. Comm.* **2011**, *47* (11), 3222-3224.
- (53) Gurau, G.; Rodríguez, H.; Kelley, S. P.; Janiczek, P.; Kalb, R. S.; Rogers, R. D., Demonstration of Chemisorption of Carbon Dioxide in 1,3-Dialkylimidazolium Acetate Ionic Liquids. *Angew. Chem. Int. Ed.* **2011**, *50* (50), 12024-12026.
- (54) Lambert, R.; Coupillaud, P.; Wirotius, A.-L.; Vignolle, J.; Taton, D., Imidazolium-Based Poly(Ionic Liquid)s Featuring Acetate Counter Anions: Thermally Latent and Recyclable Precursors of Polymer-Supported N-Heterocyclic Carbenes for Organocatalysis. *Macromol. Rapid Commun.* **2016**, *37* (14), 1143-1149.
- (55) Quiroz-Florentino, H.; Aguilar, R.; Santoyo, B. M.; Díaz, F.; Tamariz, J., Total Syntheses of Natural Furan Derivatives Rehmanones A, B, and C. *Synthesis* **2008**, *2008* (07), 1023-1028.
- (56) Gupta, S.; Chatterjee, A.; Das, S.; Basu, B.; Das, B., Electrical Conductances of 1-Butyl-3-propylimidazolium Bromide and 1-Butyl-3-propylbenzimidazolium Bromide in Water, Methanol, and Acetonitrile at (308, 313, and 318) K at 0.1 MPa. *J. Chem. Eng. Data* **2013**, *58* (1), 1-6.
- (57) Kelemen, Z.; Hollóczki, O.; Nagy, J.; Nyulászi, L., An organocatalytic ionic liquid. *Org. Biomol. Chem.* **2011**, *9* (15), 5362-5364.
- (58) Denk, M. K.; Rodezno, J. M.; Gupta, S.; Lough, A. J., Synthesis and reactivity of subvalent compounds: Part 11. Oxidation, hydrogenation and hydrolysis of stable diamino carbenes. *J. Organomet. Chem.* **2001**, *617-618*, 242-253.

- (59) Santini, R.; Griffith, M. C.; Qi, M., A measure of solvent effects on swelling of resins for solid phase organic synthesis. *Tetrahedron Lett.* **1998**, *39* (49), 8951-8954.
- (60) Bordwell pK_a Table. <http://www.chem.wisc.edu/areas/reich/pkatable/>.
- (61) Wilson, J.; Chen, E. Y. X., Organocatalytic Cross-Coupling of Biofurans to Multifunctional Difuranic C11 Building Blocks. *ACS Sustainable Chem. Eng.* **2016**, *4* (9), 4927-4936.
- (62) Sousa, A. F.; Vilela, C.; Fonseca, A. C.; Matos, M.; Freire, C. S. R.; Gruter, G.-J. M.; Coelho, J. F. J.; Silvestre, A. J. D., Biobased polyesters and other polymers from 2,5-furandicarboxylic acid: a tribute to furan excellency. *Polym. Chem.* **2015**, *6* (33), 5961-5983.

Chapter 4

Selective or living organopolymerization of a six-five bicyclic lactone to produce fully recyclable polyesters[‡]

4.1. Synopsis

Organocatalyzed ring-opening polymerization (O-ROP) of a six-five bicyclic lactone, 4,5-*trans*-cyclohexyl-fused γ -butyrolactone (4,5-T6GBL), can be topologically selective or living at room temperature, depending on catalyst structure. A screening of (thio)urea [(T)U] and organic base pairs revealed unique trends in reactivity for this monomer as well as the most active catalyst pairs, which were employed as received commercially to produce relatively high molecular weight (M_n up to 106 kDa), low dispersity ($D = 1.04$) linear poly(4,5-T6GBL) in a living fashion. The ROP using a hybrid organic/inorganic pair of TU/KOMe in neat conditions led to poly(4,5-T6GBL) with even high molecular weight ($M_n = 215$ kDa, $D = 1.04$). In comparison to the metal-catalyzed system, (T)U-base pairs exhibited competitive kinetics, reached higher monomer conversions, and can be performed in air. In addition, the resulting polymers required less purification to produce materials with higher onset decomposition temperature. (T)U-base pairs were selective towards linear polymerization only, whereas triazabicyclodecene can catalyze both polymerization and (quantitative) depolymerization processes, depending on reaction conditions. Cyclic polymers with $M_n = 41$ -72 kDa were selectively formed via *N*-heterocyclic carbene-mediated zwitterionic O-ROP. The optimal (T)U/base pair pair was used to scale up the polymerization to up to 7.5 g

[‡] This dissertation chapter contains the manuscript of a full paper published in *Polymer Chemistry* [Cywar, R. M.; Zhu, J.-B.; Chen, E. Y. -X. *Polym. Chem.* 2019, 10, 3097-3106]. This work was supported by the United States National Science Foundation, grant CHE-1664915. J.-B. Z. collected preliminary data and provided guidance during the project.

monomer. The resulting P(4,5-T6GBL) by dynamic mechanical and tensile analysis. A series of statistical copolymers with γ -butyrolactone was also prepared and characterized.

4.2. Introduction

Organocatalysis for small molecule and polymer synthesis has evolved steadily over the past two decades, notably in the field of ring-opening polymerization (ROP) of heterocyclic monomers.¹⁻²⁰ The use of organic catalysts has demonstrated certain advantages spanning convenience, economics, environmental concerns, and materials applications.^{1,4-6,9} Not only are organocatalysts considered a sustainable alternative to organometallic complexes¹ for both polymerization and depolymerization,²¹ but their use can also enable polymer applications where metal residues are undesired, such as in biomedical, electronic, and food packaging fields.^{4-6,9}

(Thio)urea [(T)U] species have proved to be highly effective catalysts for organocatalyzed ROP (O-ROP), touting similar or better performance than metal-based catalysts towards the ROP of classical strained rings (e.g. lactones and lactide) in terms of kinetics and selectivity.^{8,14-16} (T)U species catalyze living polymerizations with remarkable selectivity towards polymerization over transesterification (chain transfer), and the mechanism can be modulated by balancing the acidity of the (T)U and the basicity of a co-catalyst.¹⁶ A base that is too weak to deprotonate the (T)U will promote a neutral, ‘cooperative’ mechanism while a stronger organic or alkoxide base will generate a catalytic (T)U anion (Figure 4.1). This mechanistic handle, created by the tunable acidity of the (T)U and selection of commercially available bases, provides a framework for the rational catalyst design employed in recent works as well as this study. New advancements in (T)U catalysis include the bulk polymerization of γ -butyrolactone (GBL) to relatively high molecular

weights and the synthesis of stereoregular polyesters, achieved through clever catalyst design to minimize competitive epimerization pathways.²²⁻²⁵ While (T)U-based catalysts are selective towards the formation of linear polymers, the ability to selectively form cyclic polymers is also desirable.²⁶ In this context, *N*-heterocyclic carbenes (NHCs) produce macrocyclic polyesters free of linear chains via zwitterionic ring-opening polymerization (ZROP).²⁶⁻²⁸ In the absence of initiator, NHCs behave as strong nucleophiles towards lactones, but poor leaving groups in the resulting tetrahedral intermediate. These characteristics, coupled with fast propagation relative to initiation and cyclization, allow relatively high molecular weight cyclic polymers to form regardless of the monomer-to-initiator ratio ($[M]/[I]$).²⁶

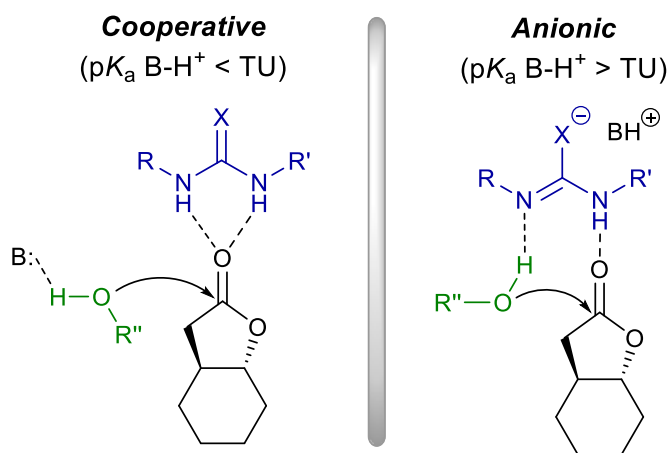


Figure 4.1. Proposed (T)U modes of action in ROP of 4,5-T6GBL.

The need to combat the plastic waste issues that threaten the environment and cause enormous materials value loss to the economy has opened many new avenues in polymer synthesis and degradation research.^{19, 21, 29-40} While viable strategies are being developed to degrade or upcycle pollutant commodity plastics, the transition to a circular plastics economy calls for the innovative

design of new materials with ‘built-in’ recyclability.^{41, 42} The non-strained GBL is intrinsically depolymerizable (i.e., chemically recyclable) due to a low ceiling temperature (T_c), but consequently its polymer, P(GBL), can only be produced at sub-zero temperatures and possesses limited thermostability.^{19, 33} Recent developments in GBL-derivatives have allowed polymerization at room temperature, in addition to enhanced materials properties.^{35, 36} Fusion of an additional ring to the GBL core increases the ring strain, effectively driving the ROP process forward while maintaining complete chemical recyclability of the resulting polymer. When a *trans*-cyclohexane ring is fused at the β, γ (4,5) carbons of GBL, the ring strain energy (ΔH°_p) increases significantly from -5.4 kJ mol^{-1} (GBL) to -18 kJ mol^{-1} (4,5-T6GBL).⁴³ As a result, T_c is also drastically raised. With this shift, ambient temperature is now far below the T_c and polymerization can proceed smoothly to high conversions at $25 \text{ }^\circ\text{C}$.

Recently, we polymerized 4,5-T6GBL by metal-catalyzed coordination ROP, which produced amorphous P(4,5-T6GBL) with M_n up to 89 kDa and a glass-transition temperature (T_g) of $75 \text{ }^\circ\text{C}$, intriguingly similar to that of poly(ethylene terephthalate) (PET).³⁶ The constitutional isomer 3,4-T6GBL can be polymerized to a polymer with M_n exceeding $1 \times 10^6 \text{ Da}$ by a yttrium complex, but the presence of an acidic proton α to the carbonyl at the fusion point of the GBL ring hinders O-ROP by basic catalysts due to rapid isomerization to the non-polymerizable *cis* isomer.³⁵ Here, we report the O-ROP of 4,5-T6GBL, a new monomer in the O-ROP space, to linear and cyclic polymers selectively, as well as the quantitative depolymerization with an organic catalyst. Although both metal and organocatalyzed systems are of a living nature and produce polymers of similar M_n and narrow dispersity on a similar timescale, the organic system reported herein demonstrated several advantages including: 1) higher monomer conversions, 2) reduced polymer purification requirements, 3) increased onset decomposition temperature (T_d), and 4) air stability.

Additionally, (T)U-base catalysis enabled preparation of P(4,5-T6GBL) on a multigram scale for thermomechanical analysis. Statistical copolymers with GBL were also prepared and characterized for the effect of copolymer composition on thermomechanical properties.

4.3. Results and Discussion

Synthesis of Linear P(4,5-T6GBL) via O-ROP

Initial organocatalyst screening. Monomer 4,5-T6GBL, although polymerizable even at room temperature, is still significantly less strained (by more than 4 kJ mol⁻¹) than classical 6 and 7-membered lactones and lactide (see Table S4.1 for ΔH°_p values). The ROP of 4,5-T6GBL by classic anionic initiators produced low molecular weight oligomers with M_n up to only 6.2 kDa (by gel-permeation chromatography, GPC) or 2.6 kDa (by NMR).⁴³ Considering a myriad of organocatalysts available for ROP,² we began our O-ROP study by probing some of the most effective catalyst families for activity and selectivity towards 4,5-T6GBL, which requires powerful catalysts/initiators to render its effective polymerization. We hypothesized that activation of an alcohol initiator alone (by a base) may not be sufficient to afford higher M_n polymers. Likewise, monomer activation alone (by protic acids) may not be sufficient, but *dual activation* could provide the necessary electron deficiency at the monomer carbonyl coupled with increased nucleophilicity of an activated alcohol initiator.² This hypothesis appeared to be correct, as only the bifunctional TU and triazabicyclodecene (TBD) catalysts showed promising preliminary results (Table 4.1). For example, TBD/BnOH mediated well-controlled polymerization, affording a polymer with M_n = 9.14 kDa, initiation efficiency (I^*) = 99%, and D = 1.11 (run 7). However, because this equilibrium polymerization is limited to high monomer concentration conditions⁴⁴ and TBD does

not offer tunability, we extended the investigation by exploring (T)U catalysis.

Table 4.1. Initial screening of organocatalyst families

Run	Cat.	I	[M]/ [Cat.]/[I]	Solvent	Time (h)	Conv. (%)
1	DPP	Ph ₂ CHCH ₂ OH	50/1/1	neat	24	2
2	^t Bu-P ₄	Ph ₂ CHCH ₂ OH	50/1/1	neat	24	5
3	TfOH	BnOH	100/1/1	neat	24	0
4	TU-2	NaOMe	100/3/1	neat	12	53
5	TU-2	NaOMe	100/3/1	THF(5M)	36	26
6	TBD	Ph ₂ CHCH ₂ OH	50/1/1	neat	16	50
7	TBD	BnOH	100/2.5/1	neat	48	64

Inspired by Waymouth's recent study,¹⁶ we screened a matrix of three TU catalyts and three U catalyts (structures shown in Figure 4.2.A) with three different bases (1,8-diazabicyclo[5.4.0]undec-7-ene, DBU; 2-*tert*-butylimino-2-diethylamino-1,3-dimethylperhydro-1,3,2-diazaphosphorine, BEMP; and 1,3-dimesitylimidazol-2-ylidene, IMes). The combination of each (T)U with each base provides different mechanistic scenarios where there is a mismatch in each direction ($pK_a(\text{T)U} > \text{BH}^+$, *cooperative* mechanism; $pK_a(\text{T)U} < \text{BH}^+$, *anionic* mechanism Figure 4.1) in addition to a matched acidity case. The well-matched pairs were predicted to have the highest activity,¹⁷ likely due to effective buffering of the highly basic alkoxide chain end.^{16, 22}

For this initial (T)U/base screening, the monomer conversion was measured at the gel point, but the reaction was allowed to continue for 24 h (or longer for slower systems) to reach maximum conversion. The results in Figure 4.2 (tabulated results can be found in Table S4.2) revealed trends consistent with previous findings regarding (T)U activity¹⁴⁻¹⁶ as well as unique trends in activity for this monomer. Generally, the matched pK_a cases had the highest activity, higher $pK_a(\text{T)U}$'s

A

	TU	TU-1	TU-2	TU-3
Base	pK_a	13.4	16.8	~20
DBU	13.9	14%	13%	6%
BEMP	16.5	6%	61% 7.70 kDa, $\mathcal{D} = 1.04$	70% 8.22 kDa, $\mathcal{D} = 1.04$
IMes	18-24	8%	67% 9.06 kDa, $\mathcal{D} = 1.08$	83% 10.8 kDa, $\mathcal{D} = 1.11$

	U	U-1	U-2	U-3
Base	pK_a	13.8	16.1	18.7
DBU	13.9	73% 8.14 kDa, $\mathcal{D} = 1.08$	68% 7.08 kDa, $\mathcal{D} = 1.08$	20% 3.56 kDa, $\mathcal{D} = 1.40$
BEMP	16.5	69% 7.45 kDa, $\mathcal{D} = 1.07$	81% 9.74 kDa, $\mathcal{D} = 1.10$	82% 10.1 kDa, $\mathcal{D} = 1.09$
IMes	18-24	65% 5.88 kDa, $\mathcal{D} = 1.08$	80% 10.2 kDa, $\mathcal{D} = 1.11$	81% 9.50 kDa, $\mathcal{D} = 1.12$

■ no gelation occurred
 ■ gelation within 24h
 ■ gelation within few hours or minutes

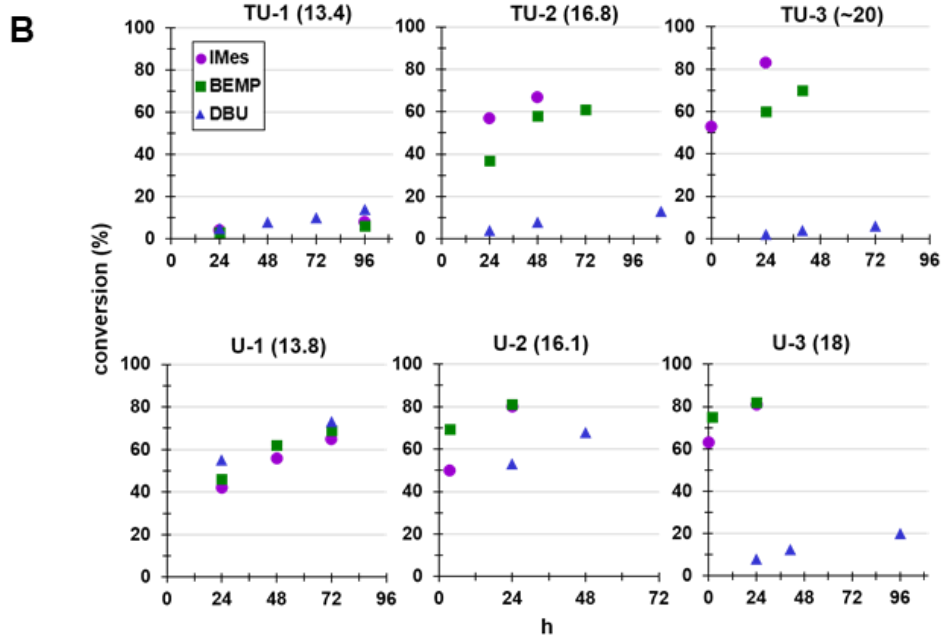


Figure 4.2. General results and trends obtained from (T)U/organic base screening: maximum conversion, M_n , and \mathcal{D} in a matrix presentation (A) and kinetic profiles in time-conversion plots (B).

were most active, and ureas were more active than thioureas with similar pK_a 's (Figure 4.2). Ureas were also more active than TU's with the same substituents: the TU analog of U-1 (pK_a 8.5) resulted in only 10% conversion after 120 h when deprotonated with IMes, while U-1/IMes reached 65% conversion in 72 h. Two catalyst pairs, TU-3/IMes and U-3/IMes, gelled in just one min and led to the highest conversions, thus standing out as the optimal catalyst pairs to employ for subsequent higher degree of polymerization (DP) runs.

These structures were the weakest acids and therefore their anionic, conjugate base forms are the strongest bases; this trend is also consistent with the requirement of high- pK_a (T)U anions for GBL polymerization.^{22, 24} TU-3/IMes was also robust enough to catalyze the polymerization *in air* with equal performance as that performed under nitrogen (Table S4.2). In fact, the dispersities of duplicate in-air runs were closer to 1.00 and the measured M_n values even closer to the theoretical M_n than for the run performed inside the glovebox ($I^* = 92$ or 98 vs 108%), although likely due to quenching the reaction at 6.5 h rather than 24. While (T)U catalysts are selective towards monomer addition over chain transfer,^{14, 15} transesterification could be exacerbated in the gel phase due to limited monomer mobility and close proximity of open-chain ester bonds. As conversion increased, the phase was observed to progress from a viscous fluid to a glassy, impenetrable solid.

Data from this screening provided additional insights to the nature of this monomer system. Distinct sensitivities to base strength were observed among the 6 (T)U catalysts when conversion vs. time was plotted for all aliquots taken during the screening runs (Figure 4.2.B). The urea species displayed much less base sensitivity, generally leading to at least 70% conversion even if slow, while only two TU species reached over 70% conversion. TU-1 and U-1 showed completely opposite activities despite their similar pK_a , and U-2 (pK_a 16.1) still led to 68% conversion after 48 h even when paired with DBU (pK_a 13.9), whereas TU-2 (pK_a 16.8) with DBU largely failed

(13% conversion after 96 h). These distinctions can be explained by neutral urea species acting as stronger H-bond donors than TU's (even if their pK_a values are equal),⁴⁵ and by urea anions acting as stronger bases than TU anions. A neutral TU may be a less effective hydrogen bond donor than a neutral urea with the same substituents or pK_a due to overlap with the large electron cloud of the sulfur atom but is an apparent stronger acid due to increased conjugate base stability. In the anionic form, the large sulfur atom can better stabilize the negative charge, therefore electron density on the basic nitrogen is diminished as compared to a urea anion. U-2 could participate in a cooperative mechanism with DBU because the H-bonding provided by the neutral urea was sufficient to activate the monomer, whereas TU-2 was unsuccessful in this mode. In the case of TU-1 vs. U-1 (pK_a 13.4 and 13.8, respectively) where at least 50% (T)U anion should have been present with each base, the TU-1 was unable to drive polymerization in any scenario while U-1 could, signifying the TU was ineffective in both the neutral and anionic forms. For both TU-3 and U-3, a matched or stronger base was effective for the polymerization, but DBU was not. Being such weak acids ($pK_a > 18$), electrophilic activation of the monomer coupled with the weakest base to activate the alcohol in a cooperative mechanism was not feasible. While neither was successful, U-3 still reached 20% conversion as compared to only 6% for TU-3, once again highlighting urea species' greater H-bond donating ability. It is worth noting here that all mechanistic scenarios can successfully ring-open polymerize more strained monomers such as lactide (LA) and δ -valerolactone (δ -VL) if given enough time to reach completion.¹⁶

Preparation of higher M_n polymers with TU-3/IMes. With the two fastest catalyst pairs [(T)U-3/IMes] in hand, the target DP was raised to 200. Trials with U-3/IMes appeared to suffer a lack of control upon increasing the $[M]/[I]$ ratio, and the resulting polymer M_n values were much lower than expected from the $[M]/[I]$ (Table S4.4). The I^* values were correspondingly high: 180-223%

for a [M]/[I] ratio of 200 and 267% for a [M]/[I] ratio of 500. The U-3/IMes pair was thus abandoned, and higher [M]/[I] ratio trials were continued with TU-3/IMes as this pair displayed greater control over the polymerization with M_n values more closely matched to that predicted by the [M]/[I] ratio (Table 4.2).

Table 4.2. Selected results of polymerization catalyzed by TU-3/IMes

Run	[M]/[TU-3]/[IMes]/[I]	Solvent	Time (h)	Conv. ^a (%)	$M_{n, GPC}$ ^b (kg/mol)	$M_{n, theor.}$ ^c (kg/mol)	I^* (%) ^d	\mathcal{D}^b (M_w/M_n)
1	200/2.5/2.5/1	neat	24	79	21.1	22.0	104	1.02
2	200/5/5/1	Tol 5M	4	61	18.1	17.2	96	1.05
3	200/5/5/1	THF 5M	3	47	13.7	13.7	100	1.13
4 ^e	250/3/1/1	neat	6	74	26.4	26.5	101	1.02
5	500/5/5/1	neat	24	76	39.5	53.1	134	1.03
6	500/10/10/1	neat	6	74	37.4	52.2	140	1.04
7	500/10/10/1	Tol 5M	10	58	28.6	41.0	143	1.04
8	500/10/10/1	THF 5M	10	45	23.8	32.7	137	1.06
9 ^e	1000/5/5/1	neat	18	69	72.6	98.8	136	1.02
10 ^e	1000/10/10/1	neat	7	69	71.8	98.4	137	1.04
11 ^e	2000/20/20/1	neat	16.5	72	106	200	189	1.04

All polymerizations performed in N₂-filled glovebox at ambient temperature with 2 mmol 4,5-T6GBL unless otherwise noted; I = BnOH. ^aMonomer conversion determined by ¹H NMR in CDCl₃. ^bNumber-average molecular weight (M_n) and dispersity index ($\mathcal{D} = M_w/M_n$) determined by gel-permeation chromatography (GPC) at 40 °C in CHCl₃ coupled with a DAWN HELEOS II multi (18)-angle light scattering detector and an Optilab TrEX dRI detector for absolute molecular weights. ^cCalculated based on: $([M]_0/[I]_0) \times \text{Conv.}\% \times (\text{molecular weight of 4,5-T6GBL}) + (\text{molecular weight of I})$, using exact equivalents of monomer measured. ^d $I^* = (M_{n, theor.} / M_{n, GPC}) \times 100$. ^eRuns 4 and 10 used 3 mmol 4,5-T6GBL, run 9 used 4 mmol, and run 11 used 11.5 mmol (1.6 g).

Because (T)U-catalyzed ROPs are known to follow first-order kinetics in both monomer and catalyst concentrations,¹⁴⁻¹⁶ we kept the catalyst concentration at approximately 1 mol% for neat runs and 2 mol% when solvent was used. However, runs with 0.5 mol% or less were still successful on a reasonable timescale (6-24 h, Table 4.2, runs 4 and 9). Using an excess of TU to IMes did not

appear to affect the polymerization appreciably (Table 4.2, run 4 vs. run 1), with both conditions producing P(4,5-T6GBL) with essentially quantitative I^* (101-104%) and extremely low \bar{D} (1.02) values. When tetrahydrofuran (THF) or toluene (Tol) were used at the 200 ratio, the equilibrium was reached in 3-5 h, however, at the expense of lower conversion and thus M_n values. At this ratio, THF led to a relatively broad dispersity of 1.13, and stirring for 24 h led to a more severe broadening to a \bar{D} of 1.21 and reduced I^* (70%). Even a high monomer concentration of 5.0 M limited maximum conversion at room temperature due to the proportional relationship of the polymerization T_c and $[M]$.⁴⁴ For example, when an equilibrated reaction (200/5/5/1, 5.0 M Tol) was moved to a -30 °C environment, the equilibrium conversion increased from 62 to 86%. Overall, the use of solvent had no appreciably positive effect on the polymerization (Table 4.2, runs 2, 3, 7, and 8).

Above target DP500, the I^* value departed from unity (Table 4.2, runs 5-11), but the polymerization remained well controlled ($I^* < 150\%$, $\bar{D} \leq 1.06$) through target DP1000. This phenomenon was also observed in the metal-catalyzed ROP of 4,5-T6GBL, but this organocatalyzed system consistently reached higher conversions.³⁶ Although chain-transfer is likely responsible for obtaining M_n values less than theoretical, a concurrent broadening of dispersity was not observed. We hypothesize that the resulting trans-esterified chains remained as active, or 'alive,' as those initiated by BnOH and continued to add monomer units from the bulk solution at comparable rates. If higher M_n polymers are desired in a shorter timeframe, the catalyst loading can be increased (Table 4.2, run 5-6 and 9-11). Although the target DP2000 run gave an I^* value of 189%, it still produced a polymer with $M_n = 106$ kDa and $\bar{D} = 1.04$ (Table 4.2, run 11), highlighting the robust nature of this system. In comparison, the metal-catalyzed system employing the $[M]/[I]$ of 2000 afforded a polymer with $M_n = 89$ kDa ($I^* = 173\%$, $\bar{D} = 1.02$), albeit

with a lower catalyst loading (0.05 mol%).³⁶ Thus, metal catalysts are still superior in terms of potency towards ROP of this monomer.

Further evidence for living polymerization behavior. The results described above and shown in Table 4.2 and Table S4.2 indicated the polymerization of 4,5-T6GBL by the (T)U/base systems is of a living nature, consistent with the (T)U-catalyzed ROP of typical monomers.^{8, 14-16} The O-ROP of parent monomer GBL is not living, however, due to an additional mode of initiation stemming from an enolized GBL, rather than ring-opening of the first monomer via nucleophilic attack by initiator.^{19, 24}

Besides reaching M_n values close to those expected from $[M]/[I]$ ratios, coupled with low \mathcal{D} values, here we provide three additional lines of evidence to support the characterization of a living polymerization. First, the M_n of the growing chains tracked linearly with monomer conversion as shown in Figure 4.3.A. A slower catalyst pair, U-2/BEMP, was employed to monitor conversion in a wider timeframe than with TU-3/IMes, which gelled quickly. Plots of conversion vs. time and $\ln([M]_0/[M])$ vs. time (Figures 4.3.B and 4.3.C) displayed typical first-order decay and linear trends, respectively, confirming first-order monomer kinetics.

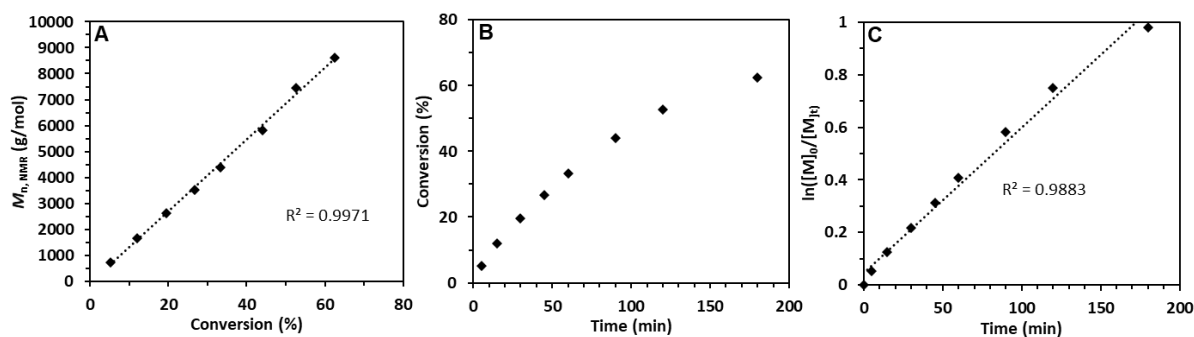


Figure 4.3. Kinetic data of P(4,5-T6GBL) synthesis with $[M]/[U-2]/[BEMP]/[BnOH] = 100/2.5/2.5/1$ at 25 °C.

Second, the matrix-assisted laser desorption/ionization time-of-flight mass spectroscopy (MALDI-TOF MS) chain-end analysis of P(4,5-T6GBL) confirmed the BnO/H moieties remained on the initiating and terminating ends, and thus a linear polymer architecture. The MALDI-TOF MS spectrum of a low M_n polymer prepared by TU-3/BEMP shows the molecular ion peaks are separated by the mass of one monomer unit (140.18 g/mol), as indicated by the slope (140.19) of the line created by plotting m/z (y) vs. number of repeat monomer units (x) (Figure 4.4). The y-intercept corresponds to the mass of the chain ends plus a sodium cation (108.1 + 23.0 g/mol), and close agreement of the plot value (131.9) to the actual value (131.1) suggests the chain-end fidelity typically associated with living polymerizations. Minor peaks visible in the low molecular weight region represent P(4,5-T6GBL) + H⁺, still carrying BnO/H chain ends.

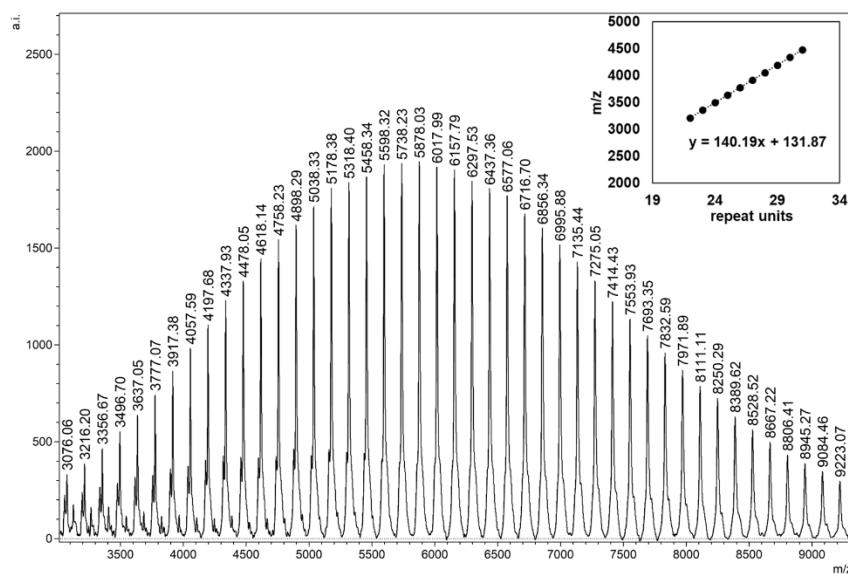


Figure 4.4. MALDI-TOF MS spectrum and chain-end analysis of a linear polymer produced by TU-3/BEMP.

Third, a chain-extension experiment was performed to produce a block copolymer. L-lactide (L-LA) was selected as the second block due to its significantly higher activity in the ROP with a catalyst pair of similar basicity;¹⁶ this condition is required to avoid further conversion of 4,5-

T6GBL after the second monomer is added and perturbs the equilibrium monomer concentration.³⁶ A ratio of 4,5-T6GBL/TU-3/IMes/BnOH = 200/5/5/1 was employed for the first block, with 5.0 M THF conditions to avoid complete gelling but allow equilibrium to be reached before the addition of L-LA. After 4 h and 48% conversion, a 3.88 M THF solution of L-LA was added and quenched after 10 min. The conversion of L-LA was quantitative while that of 4,5-T6GBL increased by 2%, as opposed to 6% for a trial with ϵ -caprolactone which is less active towards a similar catalyst pair.¹⁶ Although the block copolymer structure was not perfect, the characterization data still showed behaviour consistent with an AB block copolymer (the 2% conversion increase corresponds to only four additional 4,5-T6GBL units incorporated into the PLA block). Additionally, no decrease in P(4,5-T6GBL) conversion after further dilution by the L-LA solution is supportive of the capping of this block by PLA. Figure S8 shows the GPC elution profiles of the first block and final block copolymer, P(4,5-T6GBL)-*b*-PLA, with differentiated retention times. Differential scanning calorimetry (DSC) analysis (Figure S4.12) displayed two T_g values corresponding to each block: 56 °C for the PLA block and 71 °C for the P(4,5-T6GBL) block. The thermogravimetric (TGA) analysis (Figure S4.11) revealed a single step decomposition ($T_d = 277$ °C, defined by the temperature of 5% weight loss; $T_{max} = 364$ °C, defined by the peak maximum from a derivative (wt %/°C) vs. temperature (°C) plot); a step-wise decomposition of the individual blocks was not observed due to similar T_d values of the respective homopolymers.

The behavior of this polymerization suggests that the mechanism is in parallel to that of the (T)U catalyzed ROP of typical lactone monomers, which has been studied extensively through kinetic and NMR experiments in addition to computation with density functional theory.^{14, 15} Still, there is more to be learned about these intriguing systems, especially in the roles of the cation and reversible chain end protonation. Figure 4.5 depicts the proposed mechanism of the ROP catalyzed

by TU-3 and IMes, however it should be noted that all possible resonance structures and proton transfers are not shown. There exist many possibilities of proton exchange and hydrogen bonding among the TU anion, organic cation, and chain end, in addition to resonance within the TU anion. Reversible chain-end protonation has been proposed as a buffering mechanism to reduce the basicity of the alkoxide, which could otherwise be a promiscuous species. When the pK_a of the TU is closely matched with the base, there is an even greater opportunity for this dynamic proton exchange throughout the polymerization.

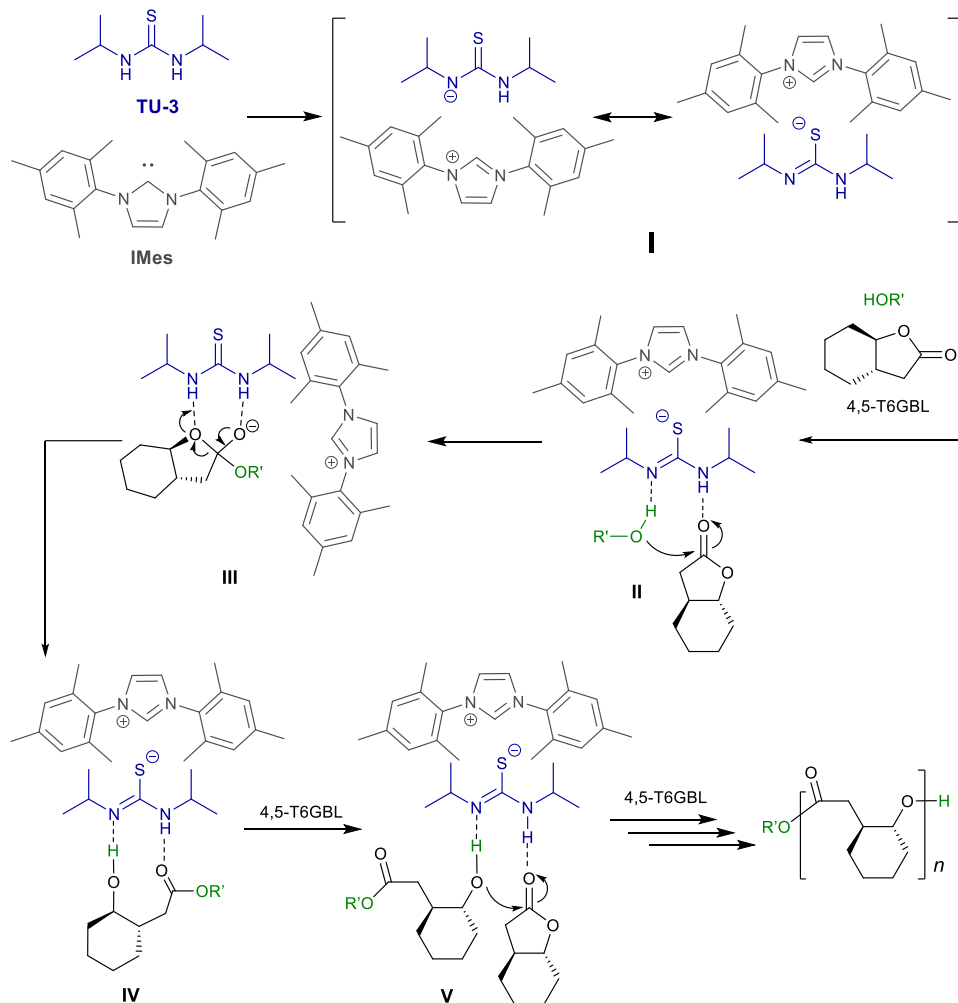


Figure 4.5. Proposed mechanism for the ROP of 4,5-T6GBL by the optimal catalyst pair

The mechanism presented in Figure 4.5 begins with the deprotonation of TU-3 by IMes to form the TU-3 anion and large imidazolium cation. This ion pair (**I**) was typically generated in the presence of monomer and was completely solubilized within 5 min (no reaction ensued until addition of initiator R'OH). Next, the TU-3 anion acts as a bifunctional activator toward both the initiator and monomer, shown in intermediate **II**. Hydrogen bonding of TU-3⁻ to the alcohol and hydrogen bond donation to the monomer carbonyl, simultaneously increase the nucleophilicity and electrophilicity, respectively. The bifunctional nature of the catalyst also draws the two activated species close together, facilitating attack on the carbonyl to form tetrahedral intermediate **III** and the subsequent proton transfer to give ring opening product **IV**. Propagation via transition state **V** continues with the resulting hydroxy chain end becoming activated for further monomer addition. Because the chain end is nearly always engaged in a hydrogen bond with the TU-anion, its basicity is reduced. Zhang *et al.* suggest this can prevent backbiting in the polymerization of GBL, which could also apply to this system.²²

Polymerizations by TU-3/KOMe and TU-3/KH/MeOH. Besides the completely organic system, we also investigated the reactivity of TU-3/KOMe systems toward the ROP of 4,5-T6GBL. In these systems, the initiator and base are conveniently packaged into one reagent: methoxide first deprotonates the TU, and the resulting methanol initiator engages in a hydrogen bond with the TU/K⁺ ion pair. An excess of (T)U is typically used to improve the solubility of the complex, while greater excesses can inhibit the polymerization.¹⁵ A nuance of this system with this monomer is that the initiating complex must be formed and completely solubilized before addition of monomer.

Table 4.3 summarizes selected polymerization results with TU-3/KOMe, which was only successful up to the target DP250. Solution polymerizations exhibited decent control, with $\bar{D} =$

1.07 to 1.16 and $I^* = 91\%$ to 130% (Table 4.3, runs 1, 3, and 5), but the use of solvent limited monomer conversion and therefore polymer M_n . For run 1, equilibrium was reached under 10 min, and further stirring of the reaction up to 1 h resulted in no further monomer conversion but a broadening of \mathcal{D} to 1.30 accompanied with an increase of M_n to 10.8 kDa. A control with only KOMe for the ROP of 4,5-T6GBL was attempted, but prevented by insufficient solubility in THF, toluene, and dichloromethane; in another study, common anionic initiators such as t BuOK afforded only low M_n oligomers.⁴³

Table 4.3. Selected results of polymerization catalyzed by TU-3/KOMe and TU-3/KH/MeOH

Run	[M]/[TU-3]/[KOMe]	Solvent	Time (h)	Conv. (%)	$M_{n,GPC}$ (kg/mol)	$M_{n,theor.}$ (kg/mol)	$I^*(\%)$	\mathcal{D} (M_w/M_n)
1	100/3/1	THF 5M	10 min	58	8.82	7.99	91	1.16
2	250/3/1	neat	24	61	73.7	21.7	29	1.10
3	250/3/1	THF 5M	2.5	61	16.4	21.4	130	1.07
4 ^a	250/3/1 (KH)	neat	6	78	28.0	27.4	98	1.01
5	250/6/1	THF 5M	4.5	53	17.8	18.6	105	1.07
6	250/6/1	neat	6	58	92.9	20.4	22	1.07
7 ^b	250/6/1	neat	6	72	137	25.2	18	1.21
8 ^c	250/6/1	neat	8.5	76	215	26.6	12	1.04

To conduct TU-3/KOMe runs in neat conditions, the complex was first formed in THF and an aliquot was transferred to the reaction vial. After complete removal of solvent *in vacuo*, the reactor was charged with monomer. Runs 2 and 6-8 in Table 4.3 present some surprising results of the neat polymerizations. The polymers obtained from these runs had M_n values much higher than expected, >70 kDa for a [M]/[I] of 250, corresponding to low I^* values (12-29%). After monomer addition, the dried-down complexes were observed to dissolve slowly, for example, run 6 took 7 min to become homogeneous, and gelled in about one h. For run 7, which was performed with the same stoichiometry but larger scale, gelling occurred around the same time as homogeneity (25

min) and the resulting M_n was increased to 137 kDa; further scale-up resulted in a polymer of $M_n = 215$ kDa (run 7). The delay in solvation of the catalyst-initiator complex led us to hypothesize that differential initiation was responsible for the unexpectedly high M_n 's. Only a fraction of initiator was introduced to bulk monomer at a given time, leading to a higher effective $[M]/[I]$ in solution. It is also possible that the overall $[I]$ was also reduced during solvent evacuation by evaporation of methanol. Despite this lack of control, \mathcal{D} values were still relatively narrow ($\mathcal{D} = 1.04 - 1.21$). To test our hypotheses, we performed a control experiment in which the TU anion was solvated by deprotonating with KH in bulk monomer (Table 4.3, run 4). This solution was homogeneous within 5 min and a sample was taken for ^1H NMR analysis to ensure no monomer conversion occurred. No reaction took place until methanol was added to initiate the polymerization, which afforded a polymer of the expected M_n (28.0 kDa, $I^* = 98\%$) and extremely low dispersity of $\mathcal{D} = 1.01$, thus supporting the differential initiation and evaporation hypotheses, which are likely both contributing factors to a higher effective $[M]/[I]$, which appeared to increase further with scale ($[M]$). Increased broadness in comparison to the KH control and the TU-3/IMes system could be due to the introduction of more initiator to an active polymerization, in which it acts as a chain transfer agent or initiates new chains with limited growth.

Overall, the results presented in Tables 4.2 and 4.3 demonstrated four main strategies to obtain P(4,5-T6GBL). First, the TU-3/IMes pair offers an entirely metal-free, living polymerization to obtain relatively high M_n polymers in a reasonable timeframe. Second, the organic/inorganic TU/KOMe system is also effective and is more economical than the use of IMes. Equilibrium is reached quickly, but the requirement to perform the ROP in solution limits the monomer conversion and polymer M_n . Third, the TU/KH/MeOH system allowed the well-controlled bulk ROP, achieving relatively high monomer conversion of 78% and producing P(4,5-T6GBL) with

essentially quantitative efficiency ($I^* = 98\%$) and near unity dispersity ($\mathcal{D} = 1.01$). Fourth, the neat KOMe method offers a convenient and economical way to obtain high M_n polymers, however the resulting M_n cannot be predicted by $[M]/[I]$ ratios. Advantages of the TU-3/IMes system include better catalyst/initiator solubility and the ability to modulate the concentration of active TU anion relative to initiator. In the TU-3/KOMe system, the concentration of TU anion is always equivalent to the alkoxide initiator. Additionally, the use of potassium could be undesired for certain polymer applications.

Synthesis of Cyclic P(4,5-T6GBL) by NHC Catalysts

Next, we turned our attention to the selective synthesis of polymers with a cyclic topology via NHC catalysis. NHC-mediated ZROP has proven to be a powerful method to synthesize cyclic polymers from strained lactones, showing its effectiveness towards 4,5-T6GBL as well. Table 4.4 summarizes the selected results of polymerizations catalyzed by three NHCs of varying nucleophilicity. IMes is the least nucleophilic of the series and did not initiate the polymerization, whereas 1,3-di-*tert*-butylimidazol-2-ylidene (*I*^tBu) and 1,3-diisopropylimidazol-2-ylidene (*I*ⁱPr) were effective catalysts. *I*ⁱPr is more nucleophilic than *I*^tBu, which could account for the markedly higher conversion provided by *I*ⁱPr (74 vs. 56%). The NHC nucleophilicity did not appear to affect the resulting M_n , however (Table 4.4, run 3 vs. 4). As expected, polymer M_n values could not be predicted or controlled, but appeared to cyclize after a certain DP (~300) had been reached; this lack of control also led to broader dispersity ($\mathcal{D} > 1.2$). On the other hand, a higher than average DP of ~510 ($M_n = 72.1$ kDa) was obtained by using a significantly higher $[M]/[NHC]$ ratio of 500 on a larger scale (Table 4.4, run 5 vs. 4).

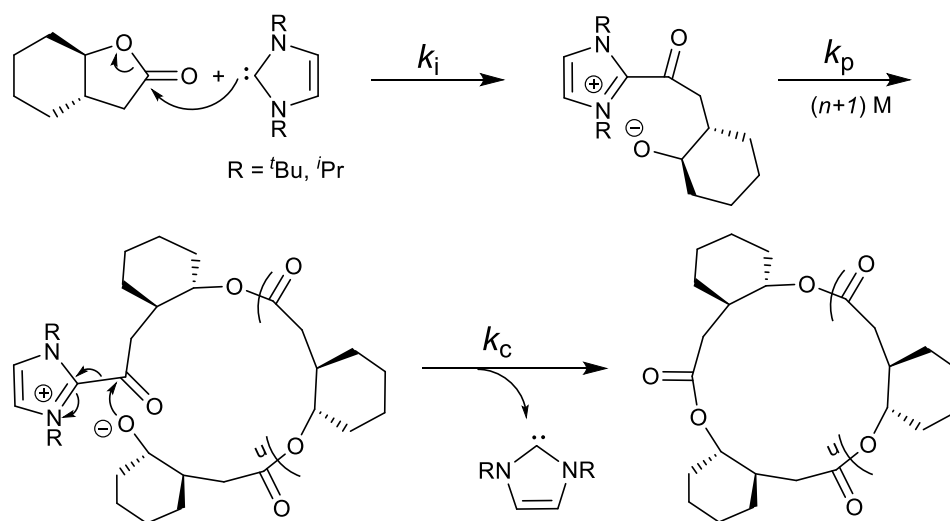
The obtained polymers were confirmed to be cyclic by the absence of end groups in the NMR spectra (Figures S4.13-14), and chain-end analysis of the MALDI-TOF MS spectrum (Figure

Table 4.4. Selected results of NHC catalyzed ZROP

Run	NHC	[M]/[NHC]	Time (h)	Conv. (%)	$M_{n, GPC}$ (kg/mol)	\bar{D} (M_w/M_n)
1	IMes	100/1	24	0	-	-
2	<i>t</i> Bu	50/1	24	68	45.9	1.30
3	<i>t</i> Bu	100/1	24	56	40.6	1.21
4	<i>i</i> Pr	100/1	24	74	42.2	1.38
5	<i>i</i> Pr	500/1	50	64	72.1	1.28

Run 4 used 3 mmol 4,5-T6GBL and run 5 used 10 mmol. See footnotes of Table 2 for explanations and definitions for abbreviations.

S4.18) gave a *y*-intercept (23.7) corresponding to the mass of only a sodium ion and slope of 140.4, indicating the polymer with no end groups. Additionally, cyclic and linear polymers of similar M_n (42.2 and 39.5 kDa, respectively) had a difference of almost two min in the start of elution off the GPC column. The mechanism for the ZROP of 4,5-T6GBL is proposed to be analogous to that of lactone/lactide monomers (Figure 4.6), in which slow initiation and cyclization relative to propagation allows the formation of the macrocyclic polyester.^{11, 26}

**Figure 4.6.** Proposed mechanism of NHC-catalyzed polymerization to cyclic P(4,5-T6GBL).

Polymer Thermal Properties

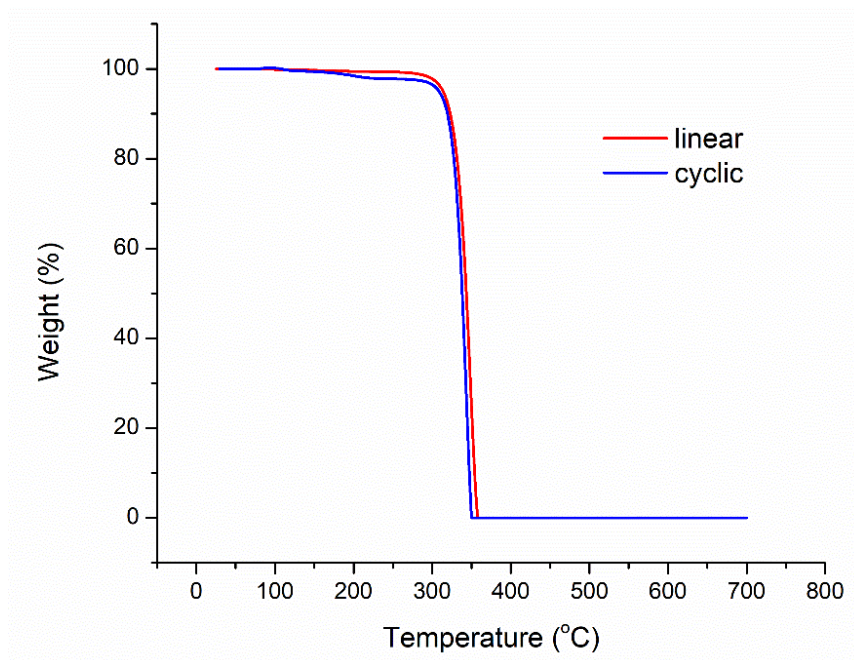


Figure 4.7. TGA curves of linear and cyclic P(4,5-T6GBL) with M_n ~40 kDa produced by the current O-ROP.

Thermal stability of linear and cyclic P(4,5-T6GBL) was compared by TGA, using samples of similar M_n (~40 kDa). An additional sample of linear polymer (~20 kDa) was prepared using $\text{Ph}_2\text{CHCH}_2\text{OH}$ as the initiator to make a direct comparison to the polymers prepared by metal catalysts and analyzed in a previous study,³⁶ which used this initiator and M_n . Cyclic P(4,5-T6GBL) showed a T_d nearly 20 °C higher than the linear polymer in the case of metal-catalyzed ROP ($T_d = 323$ and 304 °C, respectively).³⁶ On the other hand, the cyclic and linear P(4,5-T6GBL) samples of ~40 kDa M_n by the current O-ROP method exhibited the same T_d of 317 °C (Figure 4.7). The T_d of the linear P(4,5-T6GBL) prepared with $\text{Ph}_2\text{CHCH}_2\text{OH}$ initiator and M_n ~20 kDa for direct comparison was 13 °C higher than that of the polymer prepared with a metal catalyst (317 vs 304 °C). The increased thermal stability of the sample prepared by O-ROP highlights

another advantage of organocatalysis. This sample was also precipitated only one additional time after the initial precipitation of the crude polymerization, in contrast to three additional precipitations to remove any metal-based species when metal catalysts were used.³⁶ In this study, we also observed high polymer purity (no monomer or catalyst peaks in NMR spectra) with only one total precipitation and copious washing of the polymer with cold methanol.

Polymer samples were also characterized by DSC analysis to locate the T_g for linear and cyclic polymers (Figures S4.7 and S4.17). The observed T_g 's of 74 and 75 °C for linear and cyclic samples, respectively, are in close agreement with the established values for P(4,5-T6GBL) (75 and 72 °C).³⁶ As expected, no melting transition was observed for these amorphous polymers. In addition, ^{13}C NMR spectrum of the linear polymer (Figure S4.3) exhibited multiple peaks for the carbonyl and stereogenic (β and γ) carbons, also indicative of an atactic polymer microstructure.

Polymer Mechanical Properties

TU-3/KOMe was selected as the catalyst pair to produce high M_n specimens and obtain mechanical properties through dynamic mechanical analysis (DMA) and tensile testing. With 2.5 g monomer, a 250/6/1 initial ratio of [4,5-T6GBL]:[TU-3]:[KOMe] yielded 1.90 g (76% yield) P(4,5-T6GBL) with $M_n = 215$ kDa and $\mathcal{D} = 1.04$. DMA (Figure 4.8) shows that the amorphous material undergoes a steep loss in storage and loss moduli immediately after surpassing the T_g and completely liquifying by ~ 100 °C. At 25 °C, the storage modulus (E') is 1,800 MPa and loss modulus (E'') is 65 MPa. This behavior is similar to P(3,4-T6GBL), which possesses a lower T_g at ~ 50 °C.³⁵

The same method was used to produce polymer for tensile analysis, wherein 7.5 g monomer and a 250/6/1 initial ratio of [4,5-T6GBL]:[TU-3]:[KOMe] yielded 5.4 g (72% yield) P(4,5-T6GBL) with $M_n = 348$ kDa and $\mathcal{D} = 1.10$. Dog-bone shaped specimens were subjected to tensile

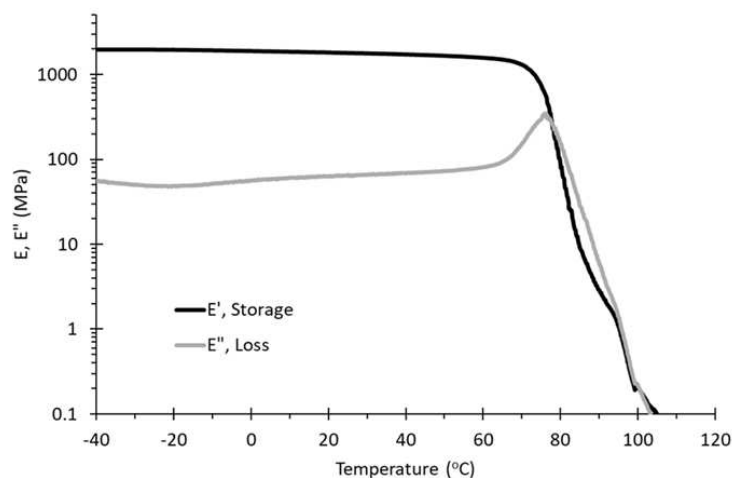


Figure 4.8. DMA of P(4,5-T6GBL) synthesized with TU-3/KOMe ($M_n = 215$ kDa, $\bar{D} = 1.04$)

testing, revealing hard and brittle materials properties (Figure 4.9; strength at break, $\sigma_B = 41 \pm 5$ MPa, elongation at break, $\varepsilon_B = 2.5 \pm 0.2\%$, $n = 3$). The Young's modulus was measured to be 2.3 ± 0.1 GPa. Compared with the constitutional isomer P(3,4-T6GBL), which has $\sigma_B = 26.2$ MPa, $\varepsilon_B = 13\%$, and Young's modulus of 1.85 GPa, P(4,5-T6GBL) is a more rigid plastic with higher ultimate strength but lower elongation.

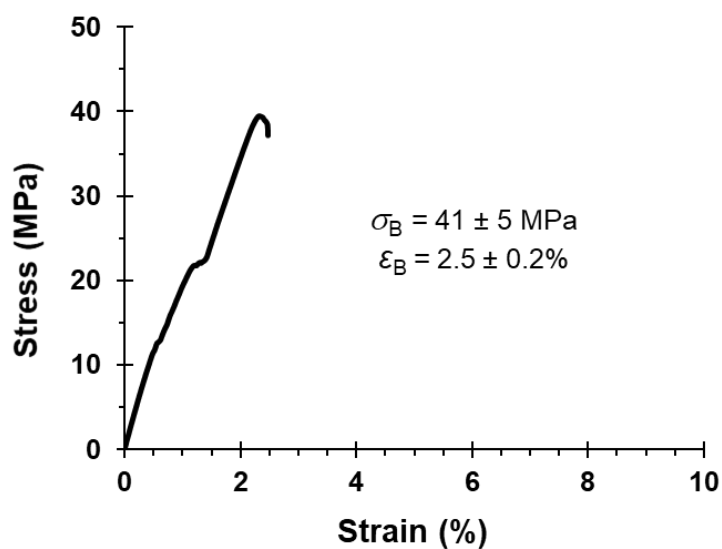


Figure 4.9. Tensile analysis of P(4,5-T6GBL) synthesized with TU-3/KOMe ($M_n = 348$ kDa, $\bar{D} = 1.10$)

Organocatalyzed Depolymerization

With the overarching goal of establishing a circular lifecycle for the P(4,5-T6GBL) material produced by the O-ROP method in mind, we investigated the organocatalyzed depolymerization of P(4,5-T6GBL). The TU-3/IMes pair, which was highly efficient in catalyzing the forward polymerization reaction, was not effective for the depolymerization. Only 8% conversion to monomer was observed after 24 h at 120 °C (0.4 M in toluene), but once again the *selective* nature of (T)U catalysts is highlighted. *t*Bu was also found to be ineffective for depolymerization under the same conditions. TBD has been shown to catalyze the depolymerization of polyesters including P(GBL) and PET,^{21, 32, 33} and proved to be successful for the quantitative and selective depolymerization of P(4,5-T6GBL) at 120 °C (Figure 4.10).

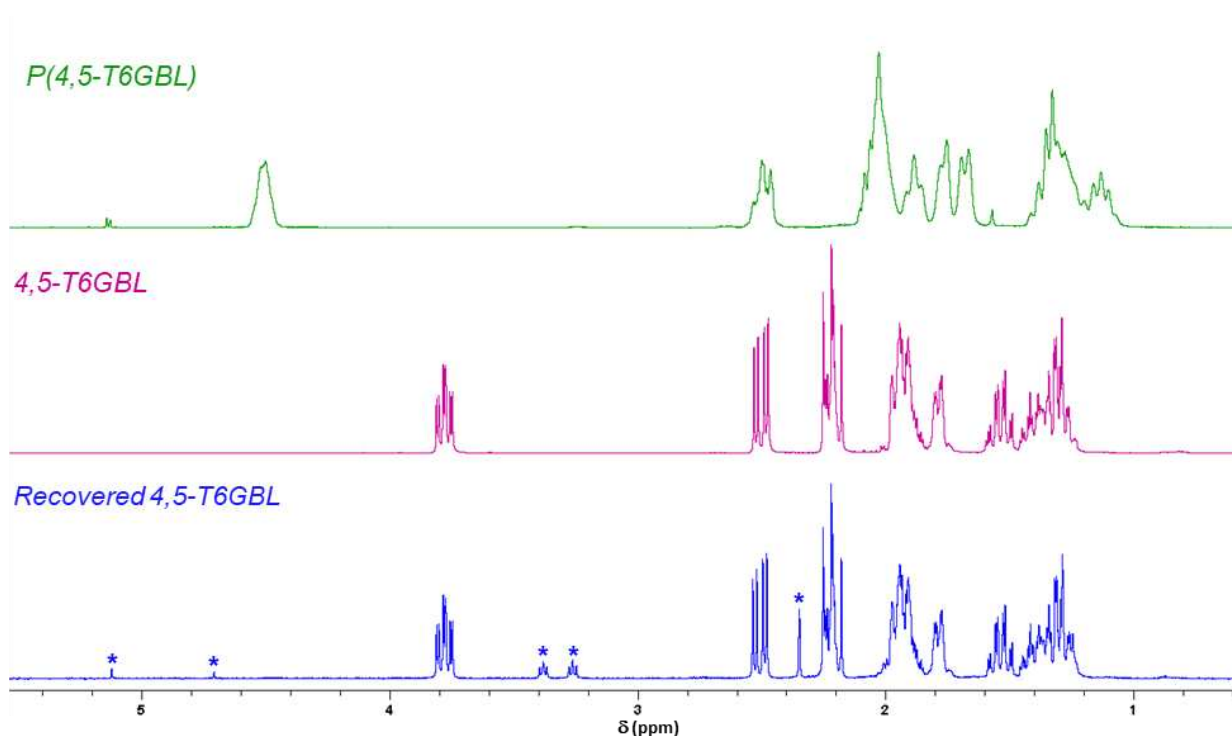


Figure 4.10. NMR (CDCl₃, 25 °C) spectra of starting polymer (top), starting monomer (center), and recovered monomer after depolymerization (bottom). Resonances marked with "*" for quenched TBD-H⁺, BnOH, and residual toluene.

Realizing both the forward and reverse reactions were possible with TBD, we performed a full circle experiment with 100/5/1 [M]/[TBD]/[BnOH]. GPC analysis of an aliquot taken after equilibrium was reached showed the formation of the polymer with $M_n = 7.62$ kDa and $\mathcal{D} = 1.06$. The reaction mixture at that point contained 57% polymer, 43% monomer, and unquenched catalyst; this mixture was subsequently heated to 120 °C and the depolymerization was 98% complete in just 2.5 h. We initially used high dilution conditions to drive the reaction, but the above findings show potential for a solvent-free reactive (vacuum) distillation setup to enable a continuous depolymerization operation.³⁵

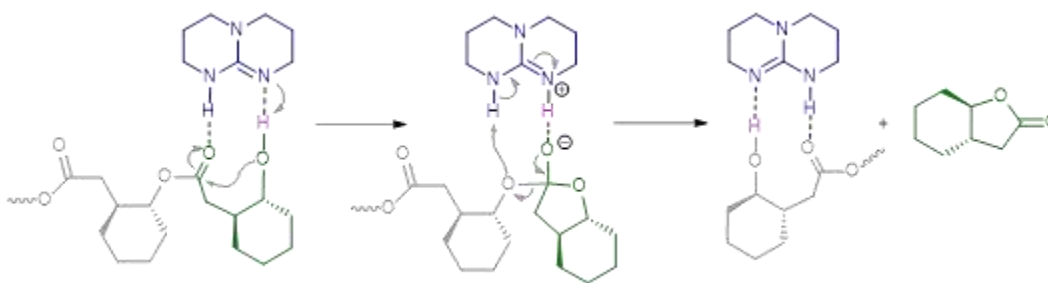


Figure 4.11. Proposed depolymerization mechanism catalyzed by TBD for the quantitative recovery of the stereo-retained monomer.

The mechanism of TBD-catalyzed depolymerization is proposed in Figure 4.11, which is essentially a hydrogen bonding mediated cascade of backbiting reactions down the polymer chain, although some random chain scission may occur. First, the alcohol chain end must become activated through coordination to the basic nitrogen on TBD while the carbonyl of the same monomer unit is electrophilically activated by the acidic site, similar to the standard initiation mechanism of TBD.^{2,21} Next, the dual activation facilitates backbiting and subsequent formation of the thermodynamically stable GBL core of the monomer in a *trans* configuration. No formation of the less strained, more thermodynamically stable *cis* isomer was observed,⁴³ which occurs when

P(4,5-T6GBL) undergoes thermolysis at 300 °C.³⁶ Upon formation of the lactone carbonyl bond, the formed monomer unit is released, and the catalyst regenerated.

Properties of P(4,5-T6GBL)-*co*-GBL Random Copolymers

Random copolymers of 3,4-T6GBL and GBL have been shown to balance materials properties relevant for packaging applications, specifically increasing ductility while maintaining attractive gas permeabilities to O₂ and H₂O vapor.⁴⁶ For example, P(3,4-T6GBL)-*co*-PGBL with 18% GBL shows increased elongation of 150%, reduced T_g of 34 °C, and O₂ and H₂O vapor barrier properties competitive with or superior to commercial packaging materials.

To investigate whether packaging materials with higher T_g could be made from P(4,5-T6GBL)-*co*-PGBL, a series of copolymers were prepared with TU-3/IMes (Table 4.5). Incorporation of 7% or 16% GBL reduced the T_g to 65 and 56 °C, respectively. When a 16% GBL composition was subjected to tensile testing ($M_n = 41$ kDa), a reduction in Young's modulus and σ_B were observed, but GBL incorporation did not increase ϵ_B (ductility), remaining at ~2%.[§]

Table 4.5. Preparation and thermal analysis of P(4,5-T6GBL)-*co*-PGBL

Entry	Reaction ratio 4,5-T6GBL:GBL (4,5- T6GBL:GBL:I)	Polymer Composition (%GBL)	M_n (kDa) ^a	T_g (°C)	T_d (°C)
1	1:10 ^b (100/1000/1)	81	31.0	- 27	257, 2 nd step at 291
2	1:1 (230/230/1)	27	-	32	295
3	3:1 (300/100/1)	16	21.6	56	300
4	10:1 (300/30/1)	7	23.0	65	305

All co-polymerizations employed TU-3/IMes (1 mol% ea.), RT and neat conditions; I = BnOH
^a Determined by GPC in CHCl₃. ^b this run was carried out at -30 °C.

[§] Tensile testing of P(4,5-T6GBL)-*co*-PGBL was conducted by collaborator Dr. Ainara Sangroniz.

4.4. Conclusions

In summary, we have established a convenient and effective method for the organocatalytic polymerization and depolymerization of six-five bicyclic lactone 4,5-T6GBL. Linear polymers with M_n up to 106 kDa and low dispersity D of 1.04 can be selectively prepared using the optimal catalyst pair: 1,3-diisopropylthiourea (TU-3) and IMes, which are commercial reagents and were used with no further purification. The TU catalyzed polymerization exhibited living characteristics, as shown by predictable polymer M_n , low dispersity, kinetic profiling, NMR and MALDI-TOF chain end analysis, as well as the block copolymerization chain extension experiment. TU-3 combined with KOMe also catalyzed the polymerization and, under neat conditions, produced a polymer of $M_n = 137$ kDa in 6 h. TU-3 can also be combined with KH and MeOH, and this combination allowed the well-controlled bulk ROP to achieve high monomer conversion and produce P(4,5-T6GBL) with $I^* = 98\%$ and $D = 1.01$). Linear polymers prepared by the organic systems displayed less purification requirements and higher onset decomposition temperatures (> 13 °C) as compared to those prepared with metal catalysts. Cyclic P(4,5-T6GBL) of $M_n > 40$ kDa can also be produced selectively by nucleophilic NHC catalysts. Guanidine base TBD was found to be effective in catalysing both polymerization and depolymerization of P(4,5-T6GBL). Depolymerization was both quantitative and selective in monomer recovery, with no isomerization to the *cis*-fused isomer. Copolymers with GBL were prepared with TU-3/IMes in an effort to obtain more ductile materials; however, an increase in elongation was not observed for P(4,5-T6GBL)-*co*-PGBL with 16% GBL.

References

1. MacMillan, D. W. C., The advent and development of organocatalysis. *Nature* **2008**, *455*, 304-308.
2. Kieseewetter, M. K.; Shin, E. J.; Hedrick, J. L.; Waymouth, R. M., Organocatalysis: Opportunities and Challenges for Polymer Synthesis. *Macromolecules* **2010**, *43*, 2093-2107.
3. Thomas, C.; Bibal, B., Hydrogen-bonding organocatalysts for ring-opening polymerization. *Green Chem.* **2014**, *16*, 1687-1699.
4. Kamber, N. E.; Jeong, W.; Waymouth, R. M.; Pratt, R. C.; Lohmeijer, B. G. G.; Hedrick, J. L., Organocatalytic Ring-Opening Polymerization. *Chem. Rev.* **2007**, *107*, 5813-5840.
5. Ottou, W. N.; Sardon, H.; Mecerreyes, D.; Vignolle, J.; Taton, D., Update and challenges in organo-mediated polymerization reactions. *Prog. Polym. Sci.* **2016**, *56*, 64-115.
6. Hu, S.; Zhao, J.; Zhang, G.; Schlaad, H., Macromolecular architectures through organocatalysis. *Prog. Polym. Sci.* **2017**, *74*, 34-77.
7. Nederberg, F.; Connor, E. F.; Möller, M.; Glauser, T.; Hedrick, J. L., New Paradigms for Organic Catalysts: The First Organocatalytic Living Polymerization. *Angew. Chem. Int. Ed.* **2001**, *40*, 2712-2715.
8. Dove, A. P.; Pratt, R. C.; Lohmeijer, B. G. G.; Waymouth, R. M.; Hedrick, J. L., Thiourea-Based Bifunctional Organocatalysis: Supramolecular Recognition for Living Polymerization. *J. Am. Chem. Soc.* **2005**, *127*, 13798-13799.
9. Lohmeijer, B. G. G.; Pratt, R. C.; Leibfarth, F.; Logan, J. W.; Long, D. A.; Dove, A. P.; Nederberg, F.; Choi, J.; Wade, C.; Waymouth, R. M.; Hedrick, J. L., Guanidine and Amidine Organocatalysts for Ring-Opening Polymerization of Cyclic Esters. *Macromolecules* **2006**, *39*, 8574-8583.

10. Nyce, G. W.; Glauser, T.; Connor, E. F.; Möck, A.; Waymouth, R. M.; Hedrick, J. L., In Situ Generation of Carbenes: A General and Versatile Platform for Organocatalytic Living Polymerization. *J. Am. Chem. Soc.* **2003**, *125*, 3046-3056.
11. Culkin, D. A.; Jeong, W.; Csihony, S.; Gomez, E. D.; Balsara, N. P.; Hedrick, J. L.; Waymouth, R. M., Zwitterionic Polymerization of Lactide to Cyclic Poly(Lactide) by Using N-Heterocyclic Carbene Organocatalysts. *Angew. Chem. Int. Ed.* **2007**, *46*, 2627-2630.
12. Kieseewetter, M. K.; Scholten, M. D.; Kirn, N.; Weber, R. L.; Hedrick, J. L.; Waymouth, R. M., Cyclic Guanidine Organic Catalysts: What Is Magic About Triazabicyclodecene? *J. Org. Chem.* **2009**, *74*, 9490-9496.
13. Zhu, J.-B.; Chen, E. Y.-X., From meso-Lactide to Isotactic Polylactide: Epimerization by B/N Lewis Pairs and Kinetic Resolution by Organic Catalysts. *J. Am. Chem. Soc.* **2015**, *137*, 12506-12509.
14. Zhang, X.; Jones, G. O.; Hedrick, J. L.; Waymouth, R. M., Fast and selective ring-opening polymerizations by alkoxides and thioureas. *Nat. Chem.* **2016**, *8*, 1047-1053.
15. Lin, B.; Waymouth, R. M., Urea Anions: Simple, Fast, and Selective Catalysts for Ring-Opening Polymerizations. *J. Am. Chem. Soc.* **2017**, *139*, 1645-1652.
16. Lin, B.; Waymouth, R. M., Organic Ring-Opening Polymerization Catalysts: Reactivity Control by Balancing Acidity. *Macromolecules* **2018**, *51*, 2932-2938.
17. Ji, H.-Y.; Wang, B.; Pan, L.; Li, Y.-S., One-Step Access to Sequence-Controlled Block Copolymers by Self-Switchable Organocatalytic Multicomponent Polymerization. *Angew. Chem. Int. Ed.* **2018**, *57*, 16888-16892.
18. Li, H.; Luo, H.; Zhao, J.; Zhang, G., Sequence-Selective Terpolymerization from Monomer Mixtures Using a Simple Organocatalyst. *ACS Macro Lett.* **2018**, *7*, 1420-1425.

19. Hong, M.; Chen, E. Y.-X., Towards Truly Sustainable Polymers: A Metal-Free Recyclable Polyester from Biorenewable Non-Strained γ -Butyrolactone. *Angew. Chem. Int. Ed.* **2016**, *55*, 4188-4193.
20. Khalil, A.; Cammas-Marion, S.; Coulembier, O., Organocatalysis applied to the ring-opening polymerization of β -lactones: A brief overview. *J. Polym. Sci. Part A: Polym. Chem.* **2019**.
21. Jehanno, C.; Pérez-Madrigal, M. M.; Demartean, J.; Sardon, H.; Dove, A. P., Organocatalysis for depolymerisation. *Polym. Chem.* **2019**, *10*, 172-186.
22. Zhang, C.-J.; Hu, L.-F.; Wu, H.-L.; Cao, X.-H.; Zhang, X.-H., Dual Organocatalysts for Highly Active and Selective Synthesis of Linear Poly(γ -butyrolactone)s with High Molecular Weights. *Macromolecules* **2018**, *51*, 8705-8711.
23. Li, M.; Tao, Y.; Tang, J.; Wang, Y.; Zhang, X.; Tao, Y.; Wang, X., Synergetic Organocatalysis for Eliminating Epimerization in Ring-Opening Polymerizations Enables Synthesis of Stereoregular Isotactic Polyester. *J. Am. Chem. Soc.* **2018**, *141*, 281-289.
24. Lin, L.; Han, D.; Qin, J.; Wang, S.; Xiao, M.; Sun, L.; Meng, Y., Nonstrained γ -Butyrolactone to High-Molecular-Weight Poly(γ -butyrolactone): Facile Bulk Polymerization Using Economical Ureas/Alkoxides. *Macromolecules* **2018**, *51*, 9317-9322.
25. Orhan, B.; Tschan, M. J. L.; Wirotius, A.-L.; Dove, A. P.; Coulembier, O.; Taton, D., Iselective Ring-Opening Polymerization of rac-Lactide from Chiral Takemoto's Organocatalysts: Elucidation of Stereocontrol. *ACS Macro Lett.* **2018**, *7*, 1413-1419.
26. Brown, H. A.; Waymouth, R. M., Zwitterionic Ring-Opening Polymerization for the Synthesis of High Molecular Weight Cyclic Polymers. *Acc. Chem. Res.* **2013**, *46*, 2585-2596.

27. Naumann, S.; Dove, A. P., N-Heterocyclic carbenes as organocatalysts for polymerizations: trends and frontiers. *Polym. Chem.* **2015**, *6*, 3185-3200.
28. Crotti, P.; Di Bussolo, V.; Favero, L.; Macchia, F.; Pineschi, M., Yttrium triflate-catalyzed addition of lithium enolates to 1,2-epoxides. Efficient synthesis of γ -hydroxy ketones. *Tet. Lett.* **1994**, *35*, 6537-6540.
29. Hong, M.; Chen, E. Y.-X., Chemically recyclable polymers: a circular economy approach to sustainability. *Green Chem.* **2017**, *19*, 3692-3706.
30. Schneiderman, D. K.; Hillmyer, M. A., 50th Anniversary Perspective: There Is a Great Future in Sustainable Polymers. *Macromolecules* **2017**, *50*, 3733-3749.
31. Fortman, D. J.; Brutman, J. P.; De Hoe, G. X.; Snyder, R. L.; Dichtel, W. R.; Hillmyer, M. A., Approaches to Sustainable and Continually Recyclable Cross-Linked Polymers. *ACS Sus. Chem. Eng.* **2018**, *6*, 11145-11159.
32. Fukushima, K.; Coulembier, O.; Lecuyer, J. M.; Almegren, H. A.; Alabdulrahman, A. M.; Alsewailem, F. D.; McNeil, M. A.; Dubois, P.; Waymouth, R. M.; Horn, H. W.; Rice, J. E.; Hedrick, J. L., Organocatalytic depolymerization of poly(ethylene terephthalate). *J. Polym. Sci. Part A: Polym. Chem.* **2011**, *49*, 1273-1281.
33. Hong, M.; Chen, E. Y.-X., Completely recyclable biopolymers with linear and cyclic topologies via ring-opening polymerization of γ -butyrolactone. *Nat. Chem.* **2016**, *8*, 42-49.
34. Eagan, J. M.; Xu, J.; Girolamo, R. D.; Thurber, C. M.; Macosko, C. W.; LaPointe, A. M.; Bates, F. S.; Coates, G. W., Combining polyethylene and polypropylene: Enhanced performance with PE/iPP multiblock polymers. *Science* **2017**, *355*, 814-816.
35. Zhu, J.-B.; Watson, E. M.; Tang, J.; Chen, E. Y.-X., A synthetic polymer system with repeatable chemical recyclability. *Science* **2018**, *360*, 398-403.

36. Zhu, J.-B.; Chen, E. Y.-X., Living Coordination Polymerization of a Six-Five Bicyclic Lactone to Produce Completely Recyclable Polyester. *Angew. Chem. Int. Ed.* **2018**, *57*, 12558-12562.
37. Tang, J.; Chen, E. Y.-X., Effects of Chain Ends on Thermal and Mechanical Properties and Recyclability of Poly(γ -butyrolactone). *J. Polym. Sci. Part A: Polym. Chem.* **2018**, *56*, 2271-2279.
38. Brutman, J. P.; De Hoe, G. X.; Schneiderman, D. K.; Le, T. N.; Hillmyer, M. A., Renewable, Degradable, and Chemically Recyclable Cross-Linked Elastomers. *Ind. Eng. Chem. Res.* **2016**, *55*, 11097-11106.
39. Rahimi, A.; García, J. M., Chemical recycling of waste plastics for new materials production. *Nat. Rev. Chem.* **2017**, *1*, 0046.
40. Zhang, X.; Fevre, M.; Jones, G. O.; Waymouth, R. M., Catalysis as an Enabling Science for Sustainable Polymers. *Chem. Rev.* **2018**, *118*, 839-885.
41. Tang, X.; Chen, E. Y.-X., Toward Infinitely Recyclable Plastics Derived from Renewable Cyclic Esters. *Chem* **2018**.
42. *The new plastics economy: Rethinking the future of plastics*; World Economic Forum, Ellen MacArthur Foundation, and McKinsey & Company 2016.
43. Haba, O.; Itabashi, H., Ring-opening polymerization of a five-membered lactone trans fused to a cyclohexane ring. *Polym. J.* **2014**, *46*, 89-93.
44. Duda, A.; Kowalski, A., Thermodynamics and Kinetics of Ring-Opening Polymerization. In *Handbook of Ring-Opening Polymerization*, Dubois, P.; Coulembier, O.; Raquez, J.-M., Eds. Wiley-VCH Verlag GmbH & Co. KGaA: Weinheim, Germany, 2009; pp 1-51.

45. Walvoord, R. R.; Huynh, P. N. H.; Kozlowski, M. C., Quantification of Electrophilic Activation by Hydrogen-Bonding Organocatalysts. *J. Am. Chem. Soc.* **2014**, *136*, 16055-16065.
46. Sangroniz, A.; Zhu, J.-B.; Tang, X.; Etxeberria, A.; Chen, E. Y.-X.; Sardon, H., Packaging materials with desired mechanical and barrier properties and full chemical recyclability. *Nat. Comm.* **2019**, *10*, 3559.

Chapter 5

Redesigned Hybrid Nylons for Optical Clarity and Chemical Recyclability**

5.1. Synopsis

Aliphatic polyamides or nylons, such as nylon 6 derived from the high-ceiling temperature (HCT) monomer ϵ -caprolactam, are typically highly crystalline and thermally robust polymers that lack optical clarity and expedient chemical recyclability. On the other hand, nylon 4 derived from the low-ceiling temperature (LCT) monomer pyrrolidone exhibits complete chemical recyclability but it is thermally unstable and not melt-processable. Here we introduce a hybrid nylon, nylon 4/6, based on a bicyclic lactam composed of both HCT ϵ -caprolactam and LCT pyrrolidone motifs in a hybridized offspring structure. Hybrid nylon 4/6 overcomes tradeoffs in (de)polymerizability and performance properties of the parent nylons, while also radically altering the nylon properties. The resulting nylon 4/6 is stereoregular but non-crystalline and optically clear; it is amorphous but lacks a viscous flow state; it exhibits high polymerizability but also high depolymerizability. Intriguingly, a 50/50 random copolymer of nylon 4/6 and nylon 4 achieves the greatest synergy in both reactivity and polymer properties of each homopolymer, offering an amorphous nylon with a unique set of properties that are difficult to achieve by nylons, including optical clarity, high glass-transition temperature, melt-processability, and full chemical recyclability.

** This dissertation chapter contains the manuscript of a full paper submitted to the *Journal of the American Chemical Society* [Cywar, R. M.; Rorrer, N. A.; Mayes, H. B.; Beckham, G. T.; Chen, E. Y.-X. (*Submitted*)]. This work was supported by the U.S. Department of Energy, Office of Energy Efficiency and Renewable Energy, Advanced Manufacturing Office (AMO) and Bioenergy Technologies Office (BETO). This work was performed as part of the BOTTLE™ Consortium, which includes the members from Colorado State University, and funded under contract no. DE-AC36-08GO28308 with the National Renewable Energy Laboratory, operated by Alliance for Sustainable Energy. H.B.M. conducted the computational portion of this work and N.A.R. collected dynamic mechanical analysis data.

5.2. Introduction

Plastic waste accumulation in landfills and the environment calls for solutions to enable a circular plastics economy in which waste plastic becomes a valuable resource.¹⁻⁵ Besides the detrimental effects of plastic pollution and use of finite resources for production, disposal of plastic materials is considered a major loss of value and energy.^{2, 3, 6} Mechanical recycling typically does not yield recycled materials with physical and mechanical properties fit for original applications of the virgin materials.^{4, 7-9} In comparison, chemical recycling delivers monomers which can be repolymerized to virgin-quality polymers.^{4, 10-13}

Significant progress has been made in chemical and biological recycling or upcycling of commodity polymers,^{7-9, 11, 12, 14-20} as well as in the discovery of new monomer-polymer systems with both high polymerizability and depolymerizability for thermoplastics, enabled by low ceiling temperatures (T_c) of heterocyclic monomers.^{10, 13, 21-25} However, achieving requisite thermomechanical properties for packaging or high-performance applications is a major challenge associated with the *redesign*²⁶ of synthetic polymers (from renewable or waste resources) for increased recyclability or environmental degradability.^{10, 21, 27}

In the case of γ -butyrolactone (γ BL)-based polyesters, ring-fusion to an adjacent cyclohexyl ring enhances resulting materials such that high de/polymerizability is achieved in addition to enhanced thermo-mechanical properties relative to P γ BL.^{22, 25, 28, 29} Besides fusion of adjacent rings, *hybridization* has been established as another effective strategy to modulate thermodynamics and physical properties, wherein high and low T_c (HCT and LCT, respectively) monomers are fused into an atom-bridged, fused-ring offspring monomer.²¹ A variety of bicyclic and atom-bridged monomers were first investigated by Hall over 60 years ago while examining the

relationship between ring strain and polymerizability.^{30, 31} Most recently, fused bicyclic monomer systems have been conceptualized to combine the high polymerizability of the HCT parent while maintaining high depolymerizability of the LCT parent and to deliver the resulting hybrid polymer with radically different and/or improved properties than the parents, as demonstrated by Shi *et al.* in the case of a [3.2.1] bicyclic lactone, the offspring of 5 and 7-membered ring lactones.²¹

Chemical recycling could also enable closed-loop lifecycles for high-performance materials such as synthetic textiles, a significant waste stream discarded to landfills.^{32, 33} Nylons, or aliphatic polyamides (PAs), are frequently used fibers for athletic clothing, furnishings, rope, and fishing nets, or as engineering plastics for composites and automotive parts, owing to robust mechanical strength and chemical resistance.³⁴ Chemical recycling of nylon 6 (PA6) to its monomer, HCT 7-membered ring lactam (7-LM or ϵ -caprolactam), has been demonstrated by several strategies in the literature, with significant challenges including: selectivity to 7-LM and subsequent separations, need for using milder conditions, and obtaining 7-LM in a single step.³⁵⁻⁴¹ Commercial depolymerization of nylon 6 is also practiced using steam and high temperatures, resulting in reduced emissions and petroleum use relative to virgin 7-LM manufacturing.^{19, 20}

Like γ BL, the 5-membered lactam (5-LM or 2-pyrrolidone), is a LCT monomer with a T_c of ~ 70 °C in bulk state and nylon 4 (PA4) is reported to have cotton-like textile properties,⁴²⁻⁴⁴ but undergoes concurrent melting and degradation (depolymerization), rendering it unfit for melt-processing. Despite significant efforts, nylon 4 was never commercialized using ring-opening polymerization (ROP).^{43, 45-47} Considering 5-LM can be derived easily from bio-based sources,⁴⁸⁻⁵² and that nylon 4 is both chemically recyclable and biodegradable,^{43, 53-55} this combination of conflicting thermal properties and recyclability or degradability is unfortunate but is all too common for LCT polymers. Thus, it is of both fundamental and applied interests to explore hybrid

HCT/LCT *recyclable-by-design* lactam monomers to produce hybrid nylons that potentially exhibit a set of desired, otherwise conflicting, properties.

In this work, we extend the hybrid HCT/LCT monomer design concept to nylons through fusion of 5-LM and 7-LM parents to the offspring [3.2.1] bicyclic lactam, 6-azabicyclo[3.2.1]octan-7-one, referred to here as 5/7-LM (Figure 5.1). This lactam was first polymerized uncontrollably by Hall in 1958 to give the polymer that was barely characterized, and a footnote stated that monomer was regenerated upon distilling the polymer over an open flame.³¹ Our detailed study, presented here, shows that 5/7-LM and its resulting hybrid nylon 4/6 have both high de/polymerizability and radically different properties than parent polymers, nylon 4 and nylon 6. The unusual properties of nylon 4/6 provided an opportunity to understand the underlying structure-property relationships, which are markedly different than traditional, linear PAs and analogous polyesters. To achieve a chemically recyclable nylon with useful properties, the copolymerization strategy⁵⁶ was utilized with the 5-LM + 5/7-LM pair, affording a unique nylon with synergistic properties that overcome limitations of each homopolymer.

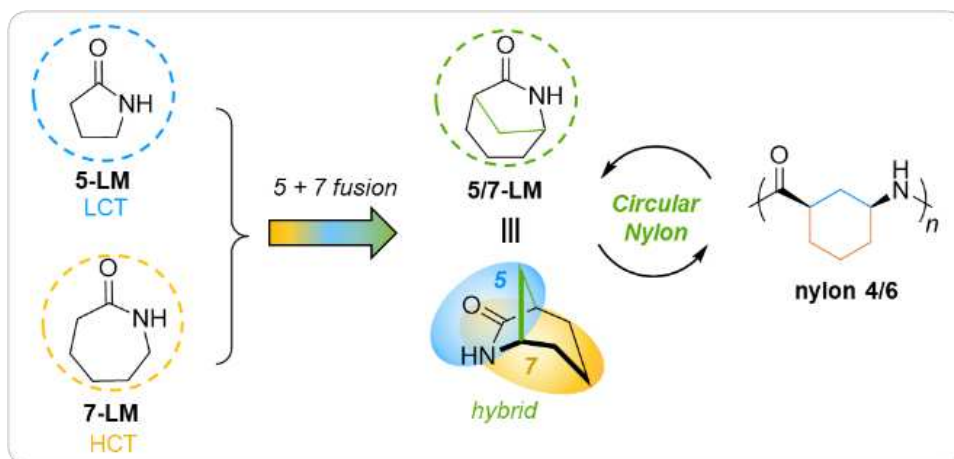


Figure 5.1. Hybridization of LCT 5-LM and HCT 7-LM resulting in 5/7-LM, designed for synergistic de/polymerizability and enhanced properties of circular nylon 4/6.

5.3. Results

Synthesis of Stereoregular Nylon 4/6 and Origins of Stereoregularity.

Polymerization activity of 5/7-LM (a chiral monomer in its racemic (*RS/SR*)-± form) was studied using traditional anionic ring-opening (AROP) conditions for lactams (AROP mechanism: Figure S5.1), including a strong base catalyst and an *N*-acyl substituted activator derived from the 5/7-LM monomer, *N*-benzoyl-5/7-LM (NBzM) to facilitate initiation. The phosphazene superbases ^tBu-P₄, the *N*-heterocyclic carbene 1,3-dimesitylimidazol-2-ylidene (IMes), and the sodium adduct of the monomer (NaM) were compared as base catalysts at [Monomer]:[Base]:[Activator] ratio ([M]/[B]/[A]) of 50/1/1. Isolated yields of purified polymers are reported, which matched well with conversion data when reaction mixtures were analyzed in deuterated trifluoroacetic acid (TFA-*d*). Across all samples, there was no spectral evidence of isomerization to *trans* configuration in the polymer backbone (representative ¹H and ¹³C NMR: Figures S5.10 and S5.12). The structure of nylon 4/6 (Figure 5.1) was further confirmed by COSY and HSQC 2D NMR methods (Figures S5.11 and S5.13).

When ^tBu-P₄ was employed without activator at room temperature (RT, ~23 °C) and 60 °C, nylon 4/6 yield was negligible, but 63% yield was obtained at 120 °C (Table S5.1, entries 1-3). With activator, 82% yield was obtained at RT (Table S5.1, entry 4), indicating that one mode of initiation predominates at lower temperatures (Figure S5.1.B), while two modes can compete at higher temperatures (Figure S5.1.A and S5.1.B). Polymerization at 120 °C was much faster with activator than without, solidifying instantaneously vs. over the course of a few hours.

With NaM as the base (Table S5.1, entries 11-16), more time was required to solidify and reach comparable yields as with ^tBu-P₄, owing to higher basicity and solubility of ^tBu-P₄. The

polymerization by IMes was much slower compared to ^tBu-P₄, presumably due to the similar p*K*_a values of IMes-H⁺ and bicyclic lactams (p*K*_a ~ 24-25 in DMSO).

NMP (*N*-methyl-2-pyrrolidone) is a more effective solvent for the polymerization than THF (tetrahydrofuran). Highly polar NMP offers better stabilization of anionic propagating intermediates and increased monomer solvation (3M in NMP vs. 1M for THF), as higher monomer concentrations shift the monomer-polymer equilibrium more towards polymer. Good yields were maintained from RT to 120 °C with activator and ^tBu-P₄ catalyst in NMP (Table S5.1, entries 4-8, 18, 19), with the best yield of 95% achieved with 3M monomer in NMP carried out at RT for 3 h. Higher molecular weight dispersity (*D*) was observed at RT (>2.0) compared to higher temperatures (<2.0), presumably due to much slower initiation than propagation at RT, with the sample prepared at 120 °C displaying the most unimodal elution profile (Figures S5.14-S5.16). GPC (gel-permeation chromatography) analysis of these nylon samples required them be performed in hexafluoroisopropanol (HFIP); for limited samples of nylon 4/6 samples analyzed, there was good agreement among the *M*_n values measured by GPC (from 5.22 – 12.9 kDa), estimated by ¹H NMR end-group analysis, and calculated theoretically (Table S5.2), indicating that propagation proceeds mostly from activator-initiated chain ends.

Matrix assisted laser desorption ionization-time of flight (MALDI-TOF) spectroscopy revealed a major and minor set of peaks for samples produced at RT, 60, and 120 °C with ^tBu-P₄; as shown in Figure 5.2, the relative intensity of the minor peak set increases with temperature. Both sets are spaced by 125.2 amu, corresponding to the ring-opened 5/7-LM repeating unit, and end-group analysis of the major sets yield y-intercepts corresponding to the sum of the benzoyl initiating end-group and Na⁺ masses (105.12 + 23, Figure S5.17, indicating that the terminal end group is a closed lactam unit which is stable to quenching and purification conditions.⁵⁷ Similar

analysis of the minor sets for samples polymerized at 60 and 120 °C yield intercepts corresponding to the mass of Na⁺ only, indicating these chains were self-initiated (Figure S5.18). For products polymerized at 120 °C, a broad carbonyl peak was observed as a shoulder downfield of the major carbonyl signal, accompanied by additional minor peaks in the aliphatic region for ^tBu-P₄ or NaM (Figures S5.19 and S5.20), which are thought to be the additional end groups from shorter, self-initiated chains which were detected by MALDI-TOF; these peaks also appear in the ¹³C spectrum of polymer produced without activator (Figure S5.21).

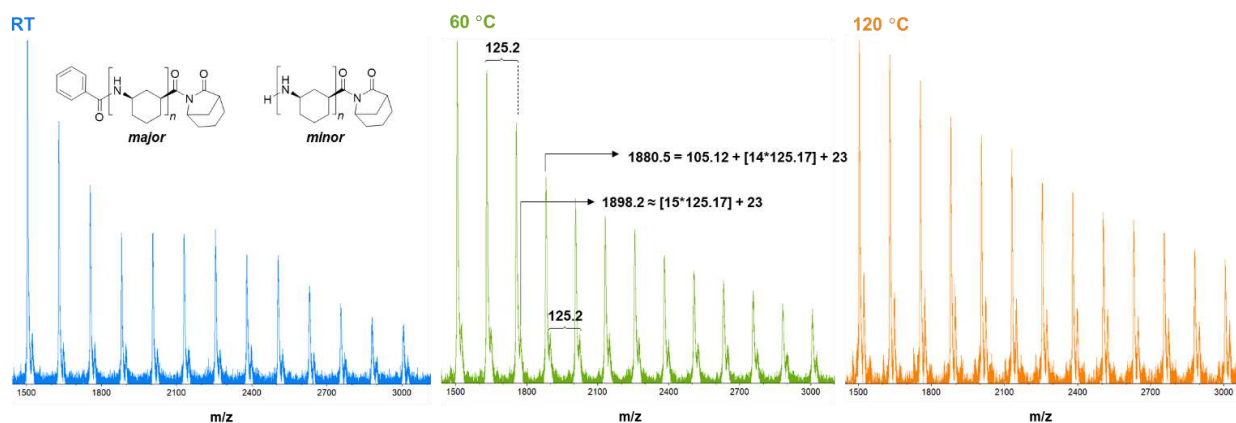


Figure 5.2. MALDI-TOF analysis of nylon 4/6 reveals a major and minor set of peaks corresponding to activator and self-initiated chains, respectively, for polymers produced at 50/1/1 [M]/[B]/[A] at different temperatures in NMP.

In addition to 5/7-LM with the amide connected to the cyclohexyl ring at 1,3-positions, we also prepared its structural isomer 6/6-LM with the amide connected to the cyclohexyl ring at 1,4-positions (Figures S5.6 and S5.7). Using the same conditions as for 5/7-LM, the ROP of 6/6-LM achieved low yields (<20%), forming only low molecular weight oligomers. Thus, the ring strain of 6/6 seems hardly affected by this ring fusion and behaves similarly to the non-strained 6-LM parent (2-piperidone).

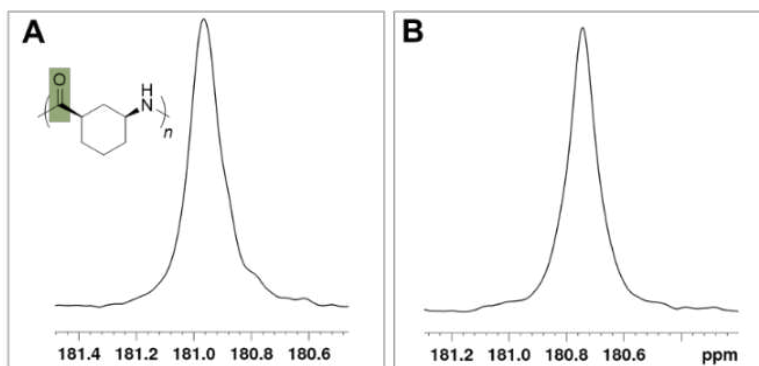


Figure 5.3. ^{13}C NMR analysis (magnified carbonyl region, TFA-*d*) of nylon 4/6 produced with $t\text{Bu-P}_4$ in NMP at RT, from racemic (\pm)-5/7-LM (**A**) and chiral (-)-5/7-LM (**B**, recorded at 55 °C for solubility).

The stereoregularity of the resulting nylon 4/6 materials was analyzed by ^{13}C NMR, zooming in on the carbonyl resonance region of the spectrum that reveals stereosequence information of the chiral monomer repeat units (Figure S5.2). The carbonyl region of ^{13}C NMR spectra of polymer products from $t\text{Bu-P}_4$ reveal a predominant peak at 180.9 ppm in TFA-*d* with trace minor peaks, suggesting a highly stereoregular polymer (Figure 5.3.A), which is confirmed by the chiral polymer prepared from the enantiopure monomer (-)-5/7-LM (Figures S5.5, S5.22 and S5.23, Figure 5.3.B). End-group carbonyl peaks arise further away (175.5, 185.1 ppm) and the minor peaks changed with AROP conditions, indicating changes in tacticity (Figures S5.24-26: effect of base on tacticity; Figure S5.27: overlay). Considering all possible, non-redundant triad stereosequences consisting of three repeat units exclusively in *cis*-configuration (i.e., no epimerization at chiral centers), there are at least three possible carbonyl peaks (Figure S5.2). When NMP was used instead of THF with $t\text{Bu-P}_4$ catalyst, the minor peak was significantly reduced, and three peaks were observed in the IMes-catalyzed polymer product, appearing at 180.9, 180.7, and 180.6 ppm (Figure S5.26).

Next, we investigated the origins of nylon 4/6 stereoregularity. Considering the fundamental step of propagation that proceeds through attack of a bicyclic lactam monomer located on the chain end by a bicyclic lactamate anion (Figure S5.1.C), we hypothesized that this sterically demanding, intermolecular addition scenario provides stereoselectivity through *chain-end control* to produce *erythro*-disyndiotactic or *threo*-disyndiotactic nylon 4/6, corresponding to favored addition of the same or opposite enantiomer, respectively. To test the chain-end control hypothesis, we prepared enantiopure monomer (-)-5/7-LM by chiral resolution crystallization^{58, 59} and subsequently studied its polymerization behavior. Substantially lower polymer yields were obtained from (-)-5/7-LM: AROP at RT by *t*Bu-P₄ in NMP yielded only 23% yield, in stark contrast to the 95% isolated yield from racemic monomer (±)-5/7-LM in the same period of 3 h (Table S5.1, entries 5 and 9). Likewise, 54% yield was obtained from (-)-5/7-LM using NaM, NMP, 60 °C and 24 h, versus 74% from the racemic monomer (Table S5.1, entries 14 and 15). Lower yield and slower kinetics suggest the polymerization suffers when *erythro* is the only possible selectivity; therefore, *threo* attack is likely the more favorable scenario in the polymerization of (±)-5/7-LM.

Unlike the racemic nylon products, the chiral nylon 4/6 materials are insoluble in formic acid, HFIP, and TFA at RT, which is indicative of higher tacticity, but complicated analysis. The chiral polymers dissolved in TFA-*d* at 55 °C for NMR analysis and revealed a single carbonyl peak at 180.7 ppm (Figures 5.2.B, S5.23). Optical rotation of the chiral samples was measured at RT in *m*-cresol. Although only cloudy solutions could be obtained, strong rotation of light was observed relative to the repeating unit (specific rotation, $[\alpha]_D^{23}$, of (-)-*cis*-3-aminocyclohexane carboxylic acid = $-12.0 \pm 1.0^\circ$ in *m*-cresol; $[\alpha]_D^{23}$ of (-)-nylon 4/6 (Table S5.1, entry 10) = $-177.9 \pm 5.5^\circ$ in *m*-cresol), confirming highly enriched or complete *erythro*-disyndiotacticity. The large difference in

magnitude indicates that the chiral polymer also assumes secondary structure in dilute solution.⁶⁰ Higher standard deviation for the chiral polymer may be attributed to incomplete solubility.

To investigate which stereoselectivity is more kinetically favorable, density function theory (DFT) was used to model the propagation step. *Threo* and *erythro* addition of bicyclic lactamate anions to growing chains were modelled for each stereochemical and conformational scenario. For each stereochemical scenario [*RS* addition to *SR* (*threo*), *RS* addition to *RS* (*erythro*)], propagation was modelled with the penultimate monomer in the axial and equatorial conformations for a total of four scenarios, as the geometry of this unit could influence the sterics of monomer addition.

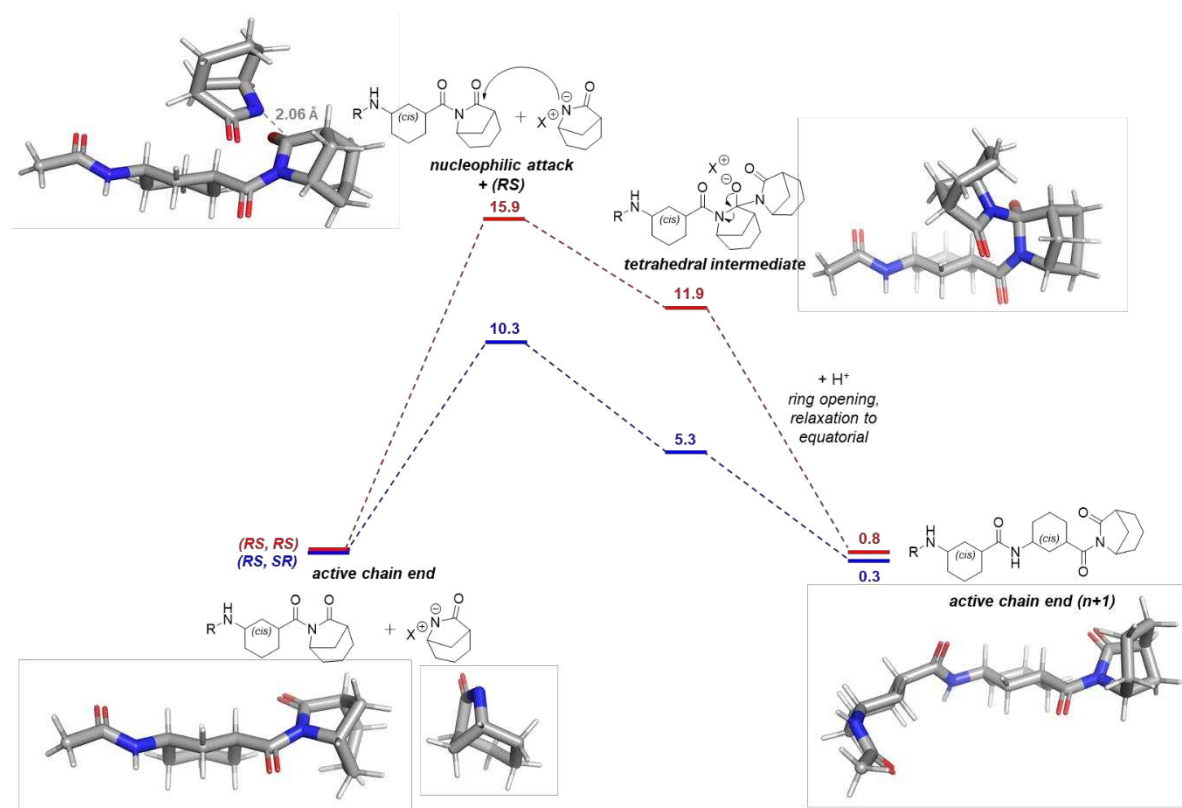


Figure 5.4. Free energy diagram comparing *RS* monomer addition to an *SR*-terminated chain (*threo*, blue) and *RS* monomer addition to an *RS*-terminated chain (*erythro*, red), with 3D representations of the low-energy conformations of model chains used in the DFT calculations for *threo* addition. Values shown are the differences in Gibbs free energy at 100 °C for each reaction step compared to the Gibbs free energy of the reactants, in kcal mol⁻¹, calculated with DFT at the M06-2X2/Def2TZVP level of theory in implicit nitrobenzene.

While the bicyclic lactam is forced into axial conformation, it may relax to equatorial after ring opening. Across all scenarios, the equatorial conformation for the penultimate monomer was found to be in lower energy, relaxing to equatorial once protonated (Figure 5.4). *Threo* attack also showed consistently lower ΔG^\ddagger energies: when comparing addition of an *RS* monomer for *threo* versus *erythro* attack at 100 °C, $\Delta\Delta G^\ddagger = 5.6 \text{ kcal mol}^{-1}$ (Figure 5.4, Table S5.3). These data, together with observed low yields of an *erythro* polymerization, support selectivity to *threo*-disyndiotactic polymer (i.e., alternating enantiomers along the chain) through an inherent *chain-end* control mechanism.

Physical Properties and Chemical Recycling of Nylon 4/6.

Like other PAs, nylon 4/6 was found to be insoluble in all common organic solvents, and only soluble in acidic solvents such as formic acid, TFA, HFIP, and *m*-cresol. Thermogravimetric analysis (TGA) of nylon 4/6 shows an onset decomposition temperature (5% mass loss), $T_{d,5}$ of 357 °C (Figure S5.28), followed by rapid decomposition and leaving zero residue. Neither a glass nor a melting transition (T_g , T_m) was observed by differential scanning calorimetry (DSC) for powdered samples using varied heating and cooling rates (1, 10, 40 °C/min) and scanning slowly (1 °C/min) through degradation (Figure 5.5A). It is common for the T_g of semicrystalline PAs, as well as highly rigid polymers like nylon 4/6, to go undetected by DSC, owing to a small change in free volume during the transition. However, it then came into question whether nylon 4/6 is amorphous or semicrystalline possibly with a $T_m > T_d$ so that a T_m was also not detectable by DSC.

Powder X-ray diffraction of nylon 4/6 showed no sharp peaks (Figure 5.5.B) and a solvent-cast thin film was colorless and completely transparent (Figure 5.5.C). This additional evidence confirmed that nylon 4/6 is an amorphous PA. The chiral polymer sample (-)-nylon 4/6 also did

not show a T_g or a T_m . The nylon 4/6 film was brittle and could not be analyzed by dynamic mechanical analysis (DMA) for T_g by the $\tan\delta$ peak ($T_{g(\text{DMA})}$). However, a T_g at 176 °C was observed in a first DSC scan when the thin film sample was heated at 40 °C/min (Figure S5.29), but this was difficult to reproduce for both subsequent heating cycles and for fresh samples. When repeated, the same film produced T_g -like signals at 146 and 199 °C during the first scans (Figures S5.30 and S5.31). Applying the Fox equation to a random copolymer (*vide infra*) of 5/7-LM and 5-LM (using ‘dry’ $T_{g(\text{DMA})}$ of nylon 4 = 81 °C⁶¹) resulted in an estimated T_g of ~200 °C for nylon 4/6, which is consistent with the observed DSC T_g values, considering DMA-determined T_g values from $\tan\delta$ peaks are typically higher than those observed by DSC, and the observation that >150 °C was required to fully dry samples.

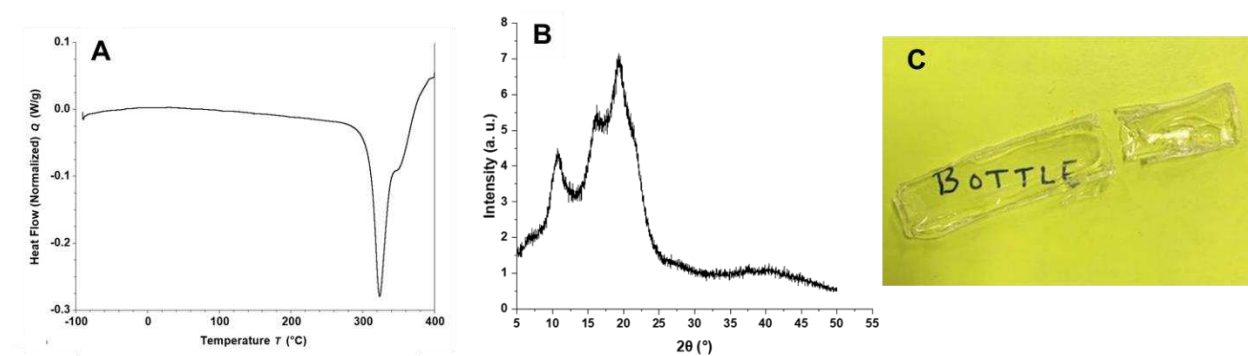


Figure 5.5. Stereoregular nylon 4/6 as an amorphous, transparent PA material. **A)** a second DSC scan (1 °C/min, exo up) through degradation at $T_{\text{peak}} = 324$ °C; **B)** powder XRD of a sample produced by ^tBu-P₄ at 60 °C in NMP; **C)** optically clear, brittle thin film sample.

Curiously, when this amorphous and rigid PA is heated through degradation at the bench, it does *not* enter viscous flow (liquify) above the T_g , as would be typical of an amorphous polymer. This unusual property implies a strongly H-bonded system, despite the lack of crystallites. FTIR was utilized to further characterize H-bonding. Nylon 4/6 was found to have a *lower* frequency

Amide A band ($\sim 3200\text{-}3300\text{ cm}^{-1}$, N-H stretching) compared to nylon 6 and nylon 4 samples by 14 and 11 cm^{-1} , respectively (Figures S5.33-35, Table S5.4), suggesting a shorter hydrogen bond length.^{62, 63}

Thermodynamic parameters for 5/7-LM ($[M]_{\text{eq}}$, ΔH_p° , ΔS_p° , and T_c) were obtained from a Van 't Hoff plot displaying $\ln[M]_{\text{eq}}$ as a function of $1/T(\text{K})$ (Figure S5.36). The $[M]_{\text{eq}}$ values of parallel reactions ($[M]_{\text{eq}} = 0.96\text{ M}$) were measured by LC-MS, as a traditional equilibrium experiment monitored by ^1H NMR was unsuccessful due to overlapping, soluble oligomer peaks at low conversion (higher temperatures) and polymer precipitation at higher conversions (lower temperatures), which reduced NMR resolution. Using the equation $\ln([M]_{\text{eq}}) = \frac{\Delta H_p^\circ}{RT} - \frac{\Delta S_p^\circ}{R}$, thermodynamic parameters were found to be $\Delta H_p^\circ = -10.0\text{ kJ mol}^{-1}$ and $\Delta S_p^\circ = -20.1\text{ J mol}^{-1}\text{ K}^{-1}$, with a $T_c = 498\text{ K}$ ($225\text{ }^\circ\text{C}$) at $[M] = 1.0\text{ M}$. The ΔG_p values calculated by DFT are near-zero at 25, 100, and 120 $^\circ\text{C}$ (Table S5.3), consistent with ΔG_p values calculated at these temperatures using experimentally determined ΔH_p° and ΔS_p° values in the Gibb's free energy equation, including the trend of higher ΔG_p , and thus decreasing driving force with increasing temperature. Given the near-zero ΔG_p values, polymer precipitation clearly plays a large role in driving the polymerization forward.

To test chemical recyclability nylon 4/6 through depolymerization at the bench, high temperature and low vacuum were applied to samples in a glass sublimator (Figure S5.37) which enabled condensation of recycling products for quantification and analysis. First, a thermolysis was run from 400-475 $^\circ\text{C}$, resulting in quantitative mass recovery relative to the starting polymer, but the recovered 5/7-LM was impure (Figure S5.38). To reduce recycling temperature and improve selectivity to monomer, two approaches were compared. Method 1 is Lewis acid catalysis

by ZnCl_2 , to activate carbonyls as electrophiles for amine backbiting, and Method 2 an acid pretreatment by HCl to produce carboxylic acid end groups for electrophilic attack. ZnCl_2 was chosen for its strong Lewis acidity, high thermal stability, and previously demonstrated success for catalyzed polyester depolymerization.²⁵ When 20 wt.% was adsorbed to the polymer surface, the $T_{d,5}$ decreased by 51 °C, resulting in a smooth TGA decomposition profile (Figure S5.39). For Method 2, after a 90 min reflux in 1 M HCl, the onset decomposition temperature was reduced; however, the curve was not entirely shifted to a lower temperature range as with Method 1, and left residue.

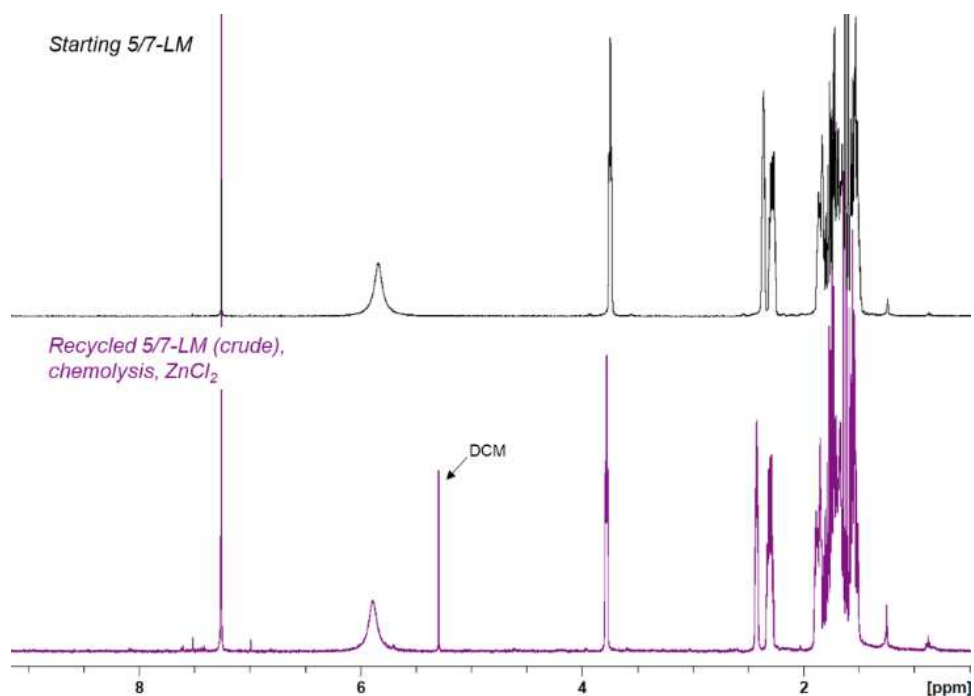


Figure 5.6. Starting monomer and crude, recovered monomer after chemolysis with 20 wt.% ZnCl_2

Employing Method 1 with ZnCl_2 (20 wt.%) at a mantle temperature of 290 °C resulted in 93-98% mass recovery relative to the starting polymer over several trials. A ring of sublimate also condensed on the reactor walls (Figure S5.37), which was not combined with the product collected

from the condenser. The crude product (Figure 5.6) showed to be in good purity by ^1H NMR (integrated spectrum: Figure S5.40) but was sticky and contained zinc species which co-sublimed, as well as a small fraction of activator and impurities which contributed to over-integration in the 1.50-2.36 ppm region. Re-subliming the monomer at 55 °C and filtering off insoluble particles with diethyl ether resulted in highly pure 5/7-LM (integrated spectrum: Figure S5.41) in 70% isolated yield, with normal integrations and which repolymerized identically to a control with fresh monomer (NaM/60 °C/24 h, 75% yield for both). A control was also performed in which nylon 4/6 without ZnCl_2 was held at 290 °C overnight, resulting in no depolymerization and demonstrating the importance of catalysis in chemical recycling of this nylon.

Synergies of Copolymers of Nylon 4/6 and Nylon 4.

Considering the high recyclability but the non-melt-processability (low thermal stability) of nylon 4 and the balanced de/polymerizability, high thermal stability, and optical clarity of nylon 4/6, we were intrigued by the possibility of developing synergistic copolymers of nylons 4 and 4/6 that could render the copolymer not only chemically recyclable but also melt-processable and optically clear. To this end, we investigated the copolymerization of 5-LM and 5/7-LM (Table 5.1), performed at RT and in neat for mixtures containing over 75 mol% 5-LM. At and above 50% 5/7-LM, minimal NMP was used to dissolve monomers for a high concentration polymerization (30-60 M). At the outset, a 50/1/1 $[\text{M}_{\text{tot}}]/[\text{B}]/[\text{A}]$ ratio was applied with $^t\text{Bu-P}_4$ catalyst to obtain a spectrum of copolymer compositions, with 5/7-LM incorporation ranging from 0 to 90% (Table 5.1, entries 1-7). All reactions solidified within 1 min, including the 5-LM homopolymerization, and isolated yields up to 90% were obtained. Incorporation of 5/7-LM, determined by ^1H NMR, tracked well with monomer feed ratios for both the 50/1/1 and 250/5/1 ratios (Figures S5.42-52),

Table 5.1. Selected results from copolymerization of 5-LM and 5/7-LM.

Entry	5-LM:5/7-LM	[M]/[B]/[A]	Base	Time (h)	Yield (%)	%5/7-LM incorp.	M_n , GPC ^a	\bar{D} ^b	$T_{d,5}$ ^c (°C)
1	100:0	50/1/1	^t BuP ₄	1.5	78	-	5.00	1.64	286
2	95:5	50/1/1	^t BuP ₄	1.5	77	7			287
3	85:15	50/1/1	^t BuP ₄	1.5	75	17	5.32	1.11	291
4	85:15	50/1/1	Na5LM	1.5	59	20			
5	75:25	50/1/1	^t BuP ₄	1.5	77	30			292
6	50:50	50/1/1	^t BuP ₄	1.5	41	54	7.19	1.08	314
7	15:85	50/1/1	^t BuP ₄	1.5	90	90	9.15	1.36	333
8	100:0	250/5/1	Na5LM	24	53	0	17.8	2.52	289
9	85:15	250/5/1	Na5LM	24	64	15	18.7	1.37	297
10	75:25	250/5/1	Na5LM	24	58	25			296
11	50:50	250/5/1	Na5LM	24	71	48	22.3	1.49	309
12	50:50	250/5/1	Na5LM	24	93	51			316
13	15:85	250/5/1	Na5LM	24	49	80			320

Entries 1-7 were performed with 250-500 mg total monomers, entries 8-11 and 13 were performed with 2-3 g, and entry 12 was performed with 10 g. ^{a,b}Determined by GPC in HFIP assuming 100% mass recovery. ^cDetermined by TGA.

as similar conversions were reached for both monomers when checked. Kinetics were not performed due to rapid solidification, but ¹³C NMR spectra show statistical distributions of many sequence peaks, indicative of a random copolymer microstructure and a loss of chain end-controlled stereoselectivity for the 5/7-LM units (Figures S5.54-56). The observed smooth, unimodal TGA decomposition profiles are also consistent with the random copolymer structure (Figures S5.57-67). The copolymerization was subsequently scaled up to a 250/5/1 [M]/[B]/[A] ratio and 2-3 g total monomers using Na5LM as the base, all solidifying within 10 min, but left to continue polymerizing for 24 h. Although ^tBu-P₄ provided narrower \bar{D} copolymers, sodium is a much more economical base. The higher [M]/[A] ratio was successful for obtaining copolymers with $M_n > 15$ kDa for all copolymer compositions, enabling reliable thermal and mechanical characterizations.

Across all copolymerizations, narrower D values (1.08 – 1.49) were obtained for copolymers relative to each homopolymer (GPC traces: Figures S5.68-72). When the 50:50 monomer ratio was scaled up to 10 g monomers, the highest isolated polymer yield of 91% was obtained.

Nylon 4 and nylon 4/6-*co*-nylon 4 samples produced with the 50/1/1 ratio were analyzed by simultaneous DSC-TGA (SDT, Figures S5.73-75) to visualize proximity of melting and onset degradation. Nylon 4 melting ($T_m = 258$ °C) is concurrent with onset degradation ($T_{d,5(SDT)} = 263$ °C). When 17% 5/7-LM is incorporated, the T_m decreases to 245 °C and the heat flow curve returns to baseline briefly before onset decomposition at $T_{d,5(SDT)} = 276$ °C. At 54% 5/7-LM incorporation, a small endotherm is present just above 200 °C with a $T_{d,5(SDT)} = 309$ °C. This gain in thermal stability is exactly the average of the two parent $T_{d,5(SDT)}$ values. The trend of increased T_d and widened processing window is illustrated by the overlaid SDT curves in Figure S5.76. Relative to nylon 4, crystallinity was reduced at ~15% and ~25% 5/7-LM incorporations and essentially eliminated above ~50%, for which no thermal transitions were observed after the first DSC heating scans (Figures S5.77-83). The low M_n copolymer with ~50% 5/7-LM incorporation showed a first scan endotherm at 204 °C (Figure S5.80), but this was not observed for the higher M_n copolymers with ~50% 5/7-LM incorporation (Figures S5.81 and S82). Like the homopolymers, copolymer T_g were not detectable by DSC.

To further probe thermal stability, the spectrum of copolymers of varied compositions made at the 250/5/1 ratio was subjected to one-hour isothermal holds at a theoretical processing temperature (Figure 5.7). Incorporation of 5/7-LM clearly increases thermal stability of nylon 4 and its copolymers. Specifically, an isothermal hold of nylon 4 at its T_m (258 °C) for 1 h results in ~80% loss by weight due to thermal degradation. It was difficult to gauge a real processing temperature for the amorphous ~50% 5/7-LM compositions by DSC alone; however, a sample was

observed to liquify on a hot surface at ~ 225 °C, and it showed much enhanced stability at 250 °C, losing only about 9% weight after 1 h. After 1 h at 230 °C, only 4% was lost (Figure S5.84).

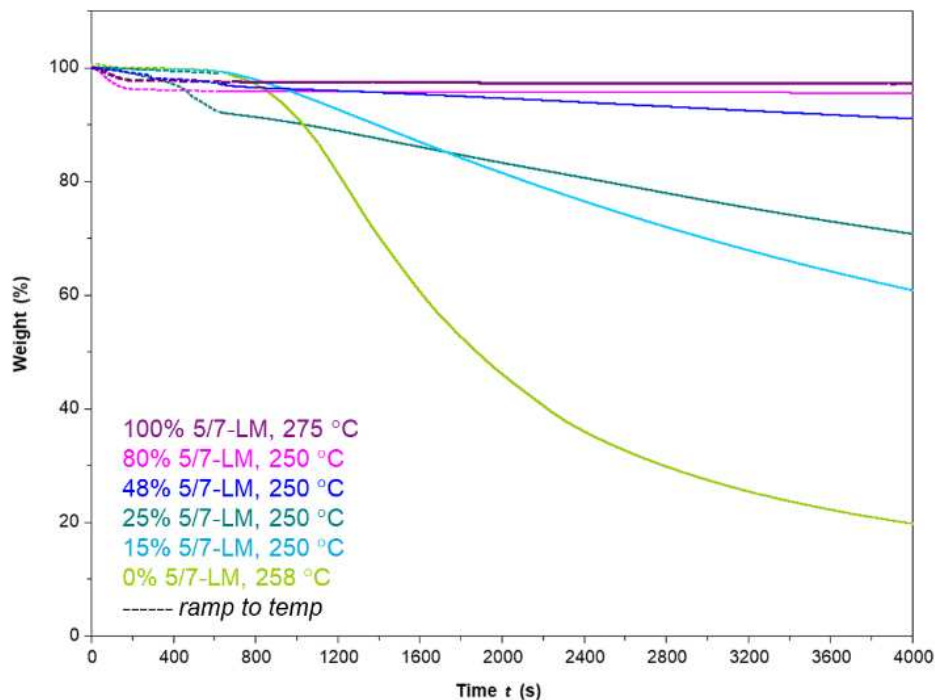


Figure 5.7. Isothermal holds of copolymers of varied compositions at processing-relevant temperatures for 1 h.

As expected, the copolymer with a higher 5/7-LM incorporation of 80% shows higher thermal stability at 250 °C, with negligible mass loss after 1 h. FTIR spectra of copolymer samples show Amide A band peaks at lower frequencies than nylon 4 (Figures S5.85 and S5.86), with the 54% 5/7-LM composition having an almost identical peak to nylon 4/6 homopolymer (Table S5.4).

To demonstrate that the covalently bound copolymer structure was responsible for the increase in thermal stability, a 50:50 physical blend of nylon 4 and nylon 4/6 was prepared by solvent casting. The two homopolymers were in fact *immiscible*, creating a cloudy solution and phase-separating upon drying (Figure 5.8, left). In sharp contrast, the random copolymer nylon 4/6-co-

nylon 4 of the 50/50 composition develops a homogenous film and is optically clear. The TGA profile of the physical blend shows a two-step decomposition profile, corresponding to individual component nylon 4 (first step) and nylon 4/6 (second step) in the blend, whereas the random copolymer displays a single, narrow decomposition profile (Figure 5.8, right).

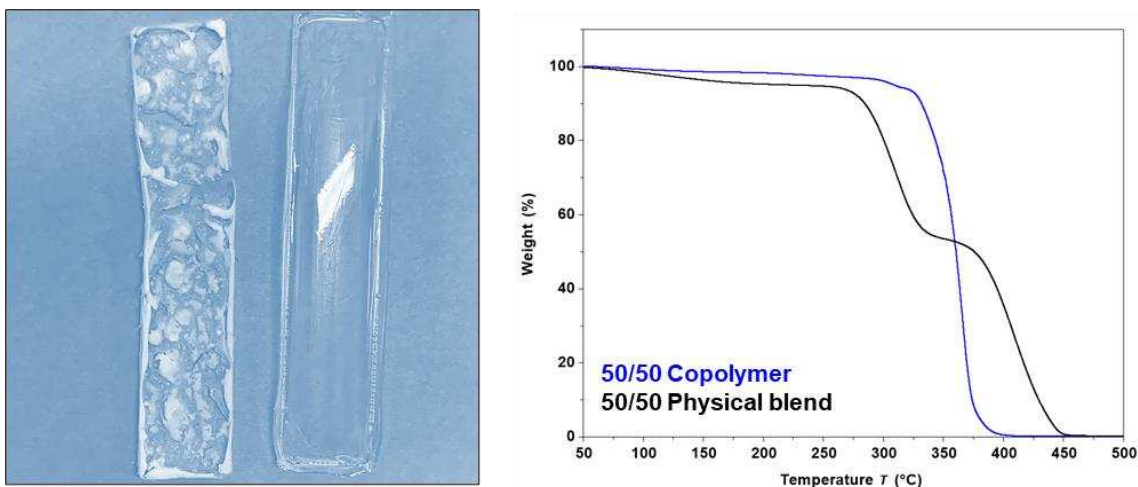


Figure 5.8. Physical blend of 50/50 nylon 4/6 and nylon 4 compared to the ~50/50 random copolymer. Top: solvent-cast thin films with physical blend on left, copolymer on right (the white streak is a reflection of light). Bottom: TGA profiles of each sample.

Thin films for DMA were prepared from samples produced at the 250:5:1 ratio. A decrease in crystallinity is visually apparent (Figure S5.87), with the copolymer of 48% 5/7-LM composition becoming optically clear. Nylon 4 thin films were too brittle and failed during testing, but has been found to have a dry $T_{g(\text{DMA})} = 81\text{ }^{\circ}\text{C}$.⁶¹ Water-dependent shifts in the $\tan\delta$ curve (the ratio of storage to loss moduli) were observed for the copolymers, where air-equilibrated samples show lower $\tan\delta$ peak values ($T_{g(\text{DMA})}$) in a first heating scan followed by an increase in storage modulus and higher $T_{g(\text{DMA})}$ during a second heating scan, representing the ‘dry’ $T_{g(\text{DMA})}$. For the 48% 5/7-LM composition (Figure 5.9.A and B), the two $T_{g(\text{DMA})}$ values are 76 °C apart at 80 and 156 °C. For 25% 5/7-LM, $T_{g(\text{DMA})}$ are only 15 °C apart at 85 and 100 °C (Figures S5.88 and S5.89). The overall

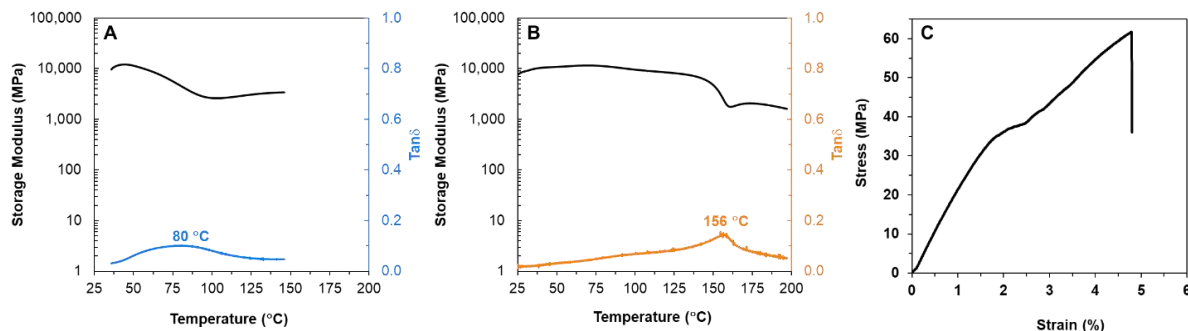


Figure 5.9. Mechanical analysis of ~50/50 nylon 4/6-co-nylon 4 thin films. **A)** First heating scan of DMA at 5 °C/min, 1 Hz; **B)** Second heating scan of DMA at 5 °C/min, 1 Hz; **C)** Representative stress-strain curve (RT, 5 mm/min).

low $\tan\delta$ intensities are indicative of stiff materials. The copolymer with 48% 5/7-LM also exhibits a rubbery plateau above the T_g for both heating scans, uncommon for amorphous materials of low to medium molecular weight. Curiously, the storage modulus of the 25% 5/7-LM composition is much lower than that of the 48% 5/7-LM copolymer and nylon 6 (Figure S5.90), further highlighting the synergy of a ~50/50 composition. Tensile analysis of ~50/50 nylon 4/6-co-nylon 4 thin films shows a high Young's modulus (2278 ± 381 MPa), an ultimate stress of 54 ± 5 MPa, an elongation at ultimate stress of $4.4 \pm 1.3\%$, and an elongation at break of 2.4-13.4% (Figure S5.91 and Table S5.5); the stress-strain curve shown in Figure 5.9.C best represents the average data.

To observe water absorption behavior, films were submerged for 24 h and weighed after patting dry (Figure S5.92). The 48% 5/7-LM copolymer absorbed a similar amount of water to nylon 4 (28 and 23%, respectively), and both became more flexible owing to plasticization by water. In contrast, the 15% composition unexpectedly absorbed 53% of its original mass, also becoming extremely soft and tearing apart while immersed.

A similar approach to recycling developed for nylon 5/7 was employed here for the chemical recycling of ~50/50 copolymer samples, using 10 wt.% ZnCl₂ adsorbed to the polymer powder and subjected to an external mantle temperature = 300 °C and low vacuum in a glass sublimator with a cryogenic condenser at -78 °C (5-LM melting point = 24 °C). TGA of the ZnCl₂-copolymer mixture showed a 71 °C drop in $T_{d,10}$ (Figure S5.93) to 264 °C, at which the polymer is liquified. Quantitative monomer recovery relative to starting polymer mass was obtained and the crude product was highly pure with a nearly identical ratio of 5/7-LM to 5-LM monomers as starting polymer (integrated spectrum: Figure S5.94), but possibly contained some Zn species (NMR silent). The crude recycling product (Figure 5.10) crystallized upon cooling under a layer of pentane. After decanting, small impurity peaks in the ¹H NMR were reduced, however with a slight loss of 5/7-LM (integrated spectrum: Figure S5.95).

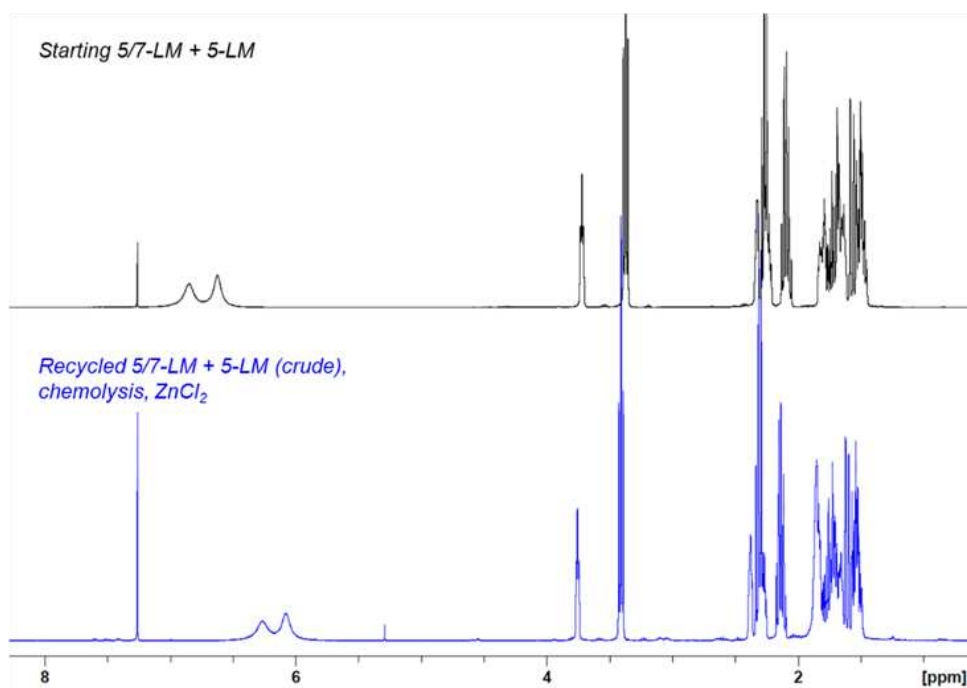


Figure 5.10. Starting monomers and crude, recycled monomers after chemolysis with 10 wt.% ZnCl₂.

5.4. Discussion

The hybrid monomer design through HCT/LCT monomer hybridization aims to attain the high polymerizability of the HCT parent while maintaining the selective depolymerizability of the LCT parent, thereby overcoming property tradeoffs in a single monomer structure. In this work, as a result of [5+7] fusion, 5/7-LM shows good polymerization activity in solution across the tested temperature range of RT-120 °C, with an observed tradeoff for higher yield and narrower \bar{D} at lower and higher temperatures, respectively, when using the organic superbases ^tBu-P₄. Racemic 5/7-LM polymerization exhibits chain-end control stereoselectivity to *threo*-disyndiotactic nylon 4/6, the kinetic product, but its high tacticity does *not* result in crystallinity. Nylon 4/6 can be selectively recycled to monomer via thermolysis, with Lewis acid catalyst ZnCl₂ lowering the required temperature and improving selectivity. This amorphous, stereoregular nylon exhibits a high T_g (estimated to be ~200 °C) and is optically clear; it was also found to lack a viscous flow state, remaining as a solid through degradation. The experimentally determined thermodynamic parameters for 5/7-LM are in good agreement with analogous bicyclic monomers.^{21, 64} The calculated negative ΔH_p° and ΔS_p° values are consistent with strained ring monomers exhibiting thermodynamic reversibility (i.e., moderate T_c values), with ΔH_p° between those reported for 5-LM and 7-LM.⁴² Again, the derived ΔG_p values for different polymerization temperatures are in good agreement with those calculated by DFT. The estimated T_c also reflects the observed tendencies to polymerize or depolymerize below or above this temperature, respectively.

The unusual combination of properties provided an intriguing opportunity to understand the underlying structure-property relationships in nylon 4/6 for both fundamental understanding and for the benefit of future hybrid monomer design. The first unusual combination is that nylon 4/6 is a highly stereoregular, yet amorphous PA. Both PAs and most stereoregular polymers tend to

be semicrystalline, enabled by long-range order across polymer chains; however, even the chiral nylon 4/6 derived from the enantiopure monomer did not exhibit a T_m . The second unusual combination is amorphicity without a viscous flow state above the T_g . Typically, amorphous polymers undergo a steep loss in storage and loss moduli after passing through the T_g , resulting in liquification. These phenomena suggest that inter- or intramolecular forces hold nylon 4/6 chains in a solid state.

We hypothesized that both crystallization and liquification in nylon 4/6 are prevented by a unique capability for *intra-monomer* H-bonding. Each 1,3-*cis*-cyclohexyl unit of the backbone can assume an di-axial or di-equatorial conformation, and in the axial conformation, the 1,3-C=O and -NH are positioned in close proximity. Diaxial interactions, which are usually destabilizing, could be more favorable here due to formation of an H-bond. Such a configuration would also create a kink in the chain, preventing an elongated chain conformation and hindering chain alignment.

To gain insight to chain conformation and rationalize physical properties, DFT was employed to model lowest energy conformations of representative nylon 4/6 trimers with 2° amide end groups (Figure 5.11). For both *threo* and *erythro*-disyndiotactic trimers, the equatorial conformations were found to have identical free energies, within numerical error, and 3.7~4.6 kcal mol⁻¹ lower in free energy than their axial conformations at 100 °C (Figure 5.11), indicating no *thermodynamic* driving force favoring one polymer tacticity. In the axial conformation, the lowest energy rotamers aligned the amide hydrogen toward the oxygen to enable hydrogen bonding. However, this *intra-monomer* hydrogen bond's N-H-O angle is 151-153°, far from the ideal 180°, and the O-H distance is extremely close at 1.84-1.87Å (typical H-bond lengths are ~2.0-3.0Å). The stabilizing contribution of this weak H-bond is insufficient to offset the strain of the di-axial steric interactions, which perturb the angle of the C1-C2-C3 ring bond from the ideal 109.5° for this sp³

bond to $\sim 116^\circ$, with other angles also strained to a lesser extent (Figure S5.96). Taking into account these energetic differences, a Boltzmann distribution of conformations at 300K would be $\sim 800:1$ equatorial:axial, $\sim 150:1$ at 400K, $\sim 50:1$ at 500K, and $\sim 1.2:1$ at 600K.

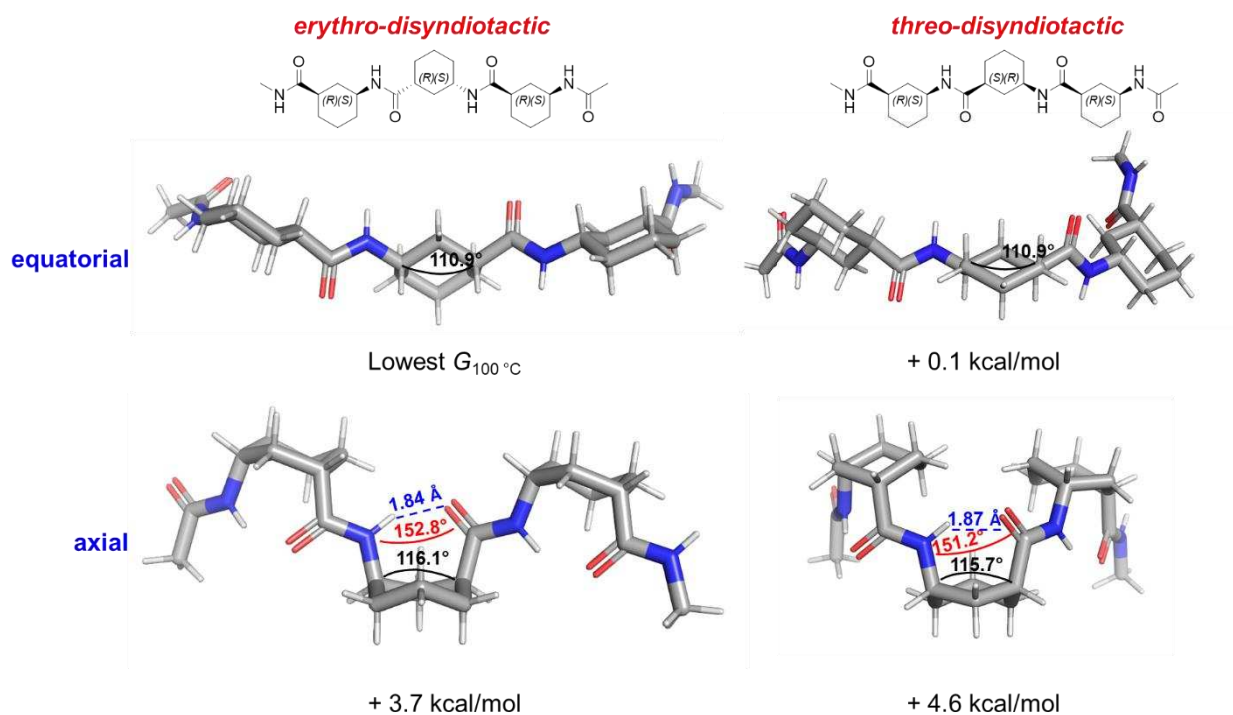


Figure 5.11. Lowest energy conformations and relative free energy differences for representative nylon 4/6 trimers, calculated with DFT at the M06-2X2/Def2TZVP level of theory in implicit nitrobenzene at 100°C.

With these modeling data in hand, we propose that viscous flow is prevented by the increasing content of axial sites at elevated temperatures, especially when close to degradation (recycling) at 600K. Generation of weak, intra-monomer 1,3-diaxial H-bonds at elevated temperatures is thought to provide stabilization which ultimately prevents liquification. Conversion to axial near the T_d also mirrors the positioning of bonds in the bicyclic 5/7-LM, facilitating ring-closing for recycling. For crystallization, even a few axial sites could create kinks in the chain that contribute to disruption of long-range order required for crystallization; however, at room temperature, other

factors likely dominate, such as stereodefects and an irregular backbone pattern due to accommodation for interchain H-bonds among amides.

Interestingly, both a PA and polyester analog to nylon 4/6 are semicrystalline. The PA analog, from ring-opening of 8-oxa-6-azabicyclo[3.2.1]octan-7-one, which contains an ether bond between C1 and C3 in the resulting polymer backbone, has a T_m close to T_d , and was proposed to exist in an equatorial conformation.⁶⁵⁻⁶⁷ The direct lactone analog of 5/7-LM, 6-oxabicyclo[3.2.1]octan-7-one, results in a crystalline polyester when the backbone is entirely *cis*,²¹ and also likely exists in an all-equatorial conformation. These behaviors suggest that chain-packing is indeed hindered in nylon 4/6, despite a primarily equatorial arrangement at RT.

To capitalize on the advantageous properties of nylon 4/6, including its chemical recyclability, high T_g , optical clarity, and thermal stability, we pursued nylon 4-based copolymers through copolymerization with 5-LM. The LCT 5-LM could potentially serve as a ‘trojan horse’ in the HCT 7-LM in copolymers if random copolymers are obtained,^{68, 69} however, in a recent report, days-long reactions were required for the 5-LM + 7-LM copolymerization to achieve sufficient M_n , and neither isothermal stability nor recycling was studied.⁶⁸ In stark contrast, the current copolymerization of 5/7-LM with 5-LM readily produces statistically random nylon 4 copolymer, nylon 4/6-*co*-nylon 4.

Nylon 4 is thermally unstable, owing to concurrent melting and degradation which prevents melt-processing. Again, this combination of properties is unfortunate considering the sustainable aspects of bio-renewability, chemical recyclability, and biodegradability. Regarding the synthesis of 5/7-LM, the precursor *m*-aminobenzoic acid has been recognized as a valuable bioproduct to target through fermentation, which been demonstrated in low titer from a co-culture of *E. Coli* but remains a challenge.⁷⁰

Besides obtaining the desired random copolymer microstructure, 5/7-LM and 5-LM showed synergistic reactivity. Relative to homopolymers, higher M_n and narrower \mathcal{D} copolymers were obtained, suggesting improved control of the polymerization. Both nylon 4/6 and nylon 4 precipitated from reactions at low M_n , creating heterogeneous mixtures with the active chain ends becoming occluded. With a 50/50 comonomer mixture in particular, the reaction mixture remained homogeneous throughout the entire polymerization (a gel which eventually solidifies), which should facilitate continued monomer addition. With increased control of the polymerization, higher M_n copolymer was realized for reliable thermal and mechanical analysis.

Copolymer nylon 4/6-*co*-nylon 4 also showed synergistic properties relative to the parents, nylon 4/6 and nylon 4. Interestingly, these two homopolymers were immiscible, and a eutectic drop in T_m is achieved for copolymers while maintaining high T_g values. The nylon 4/6 and nylon 4 prepared in this study were rather brittle and thin films could not be tested on DMA. Thermal analysis of a compositional spectrum of nylon 4/6-*co*-nylon 4 clearly showed that 5/7-LM improves thermal stability of nylon 4. Although the ~15% and ~25% 5/7-LM compositions show marked improvement and are semicrystalline, they are likely not stable enough for melt-processing and are softer materials. Unexpectedly high water uptake of the 15% composition also rendered it soft and weak when immersed. In contrast, the ~50% 5/7-LM composition was much more thermally stable and behaved as a typical PA when submerged in water, becoming plasticized. Moreover, the ~50/50 composition shows a rubbery plateau in DMA, which is unusual for an amorphous material of low to medium molecular weight and suggests adequate H-bonding is present within the polymer despite a lack of crystallites. The enhanced thermal stability and thermomechanical properties are thus promising for processing techniques like injection molding or melt-spinning.



Figure 5.12. Photographs of thin films of nylon 4/6-*co*-nylon 4 in ~50/50 composition.

The ~50/50 nylon 4/6-*co*-nylon 4 composition (Figure 5.12) is a strong, stiff, amorphous, optically clear, and thermally stable PA exhibiting a rubbery plateau and full chemical recyclability. The material readily absorbs atmospheric moisture, with both ‘ambient’ and ‘dry’ $T_{g(\text{DMA})}$ values (80 and 156 °C, respectively) higher than nylon 6 (40-60 °C). The high Young’s modulus is also comparable to that of nylon 6.⁷¹ In addition to typical nylon applications such as fibers, this material could potentially be used for clear coatings and composites, with the same solvent resistance as typical nylons but higher temperature resistance.

Future work on this copolymer includes study of the effect of chain endcaps (both initiating and terminating),^{47, 72, 73} thermal stabilizers, and plasticizers on thermomechanical properties. For larger-scale recycling, we envision a depolymerization process where liquified polymer is passed over a fixed catalyst bed and the reformed comonomer products are immediately condensed. Furthermore, as nylon 4 has been found to biodegrade in soil and marine environments,^{53, 54} and nylon 4/6 also has a four-carbon backbone, biodegradation of ~50/50 nylon 4/6-*co*-nylon 4 is under long-term study. Exploration of additional hybridized lactams, including those resulting from different ring fusions or containing multiple functionalities, merits continued investigation.

References

1. Sheldon, R. A.; Norton, M., Green chemistry and the plastic pollution challenge: towards a circular economy. *Green Chem.* **2020**, *22*, 6310-6322.
2. Hong, M.; Chen, E. Y.-X., Future Directions for Sustainable Polymers. *Trends Chem.* **2019**, *1*, 148-151.
3. *The New Plastics Economy — Rethinking the future of plastics*; World Economic Forum, Ellen MacArthur Foundation and McKinsey & Company: 2016.
4. Rahimi, A.; García, J. M., Chemical recycling of waste plastics for new materials production. *Nat. Rev. Chem.* **2017**, *1*, 0046.
5. Hundertmark, T.; Mayer, M.; McNally, C.; Simons, T. J.; Witte, C. How plastics waste recycling could transform the chemical industry 2018. <https://www.mckinsey.com/industries/chemicals/our-insights/how-plastics-waste-recycling-could-transform-the-chemical-industry#> (accessed August 9, 2021).
6. Nicholson, S. R.; Rorrer, N. A.; Carpenter, A. C.; Beckham, G. T., Manufacturing energy and greenhouse gas emissions associated with plastics consumption. *Joule* **2021**.
7. Worch, J. C.; Dove, A. P., 100th Anniversary of Macromolecular Science Viewpoint: Toward Catalytic Chemical Recycling of Waste (and Future) Plastics. *ACS Macro Lett.* **2020**, *9*, 1494-1506.
8. Garcia, J. M.; Robertson, M. L., The future of plastics recycling. *Science* **2017**, *358*, 870-872.

9. Payne, J.; Jones, M. D., The Chemical Recycling of Polyesters for a Circular Plastics Economy: Challenges and Emerging Opportunities. *ChemSusChem* **2021**, *14*.
10. Coates, G. W.; Getzler, Y. D. Y. L., Chemical recycling to monomer for an ideal, circular polymer economy. *Nat. Rev. Mater.* **2020**, *5*, 501-516.
11. Thiounn, T.; Smith, R. C., Advances and approaches for chemical recycling of plastic waste. *J. Polym. Sci.* **2020**, *58*, 1347-1364.
12. Vollmer, I.; Jenks, M. J. F.; Roelands, M. C. P.; White, R. J.; van Harmelen, T.; de Wild, P.; van der Laan, G. P.; Meirer, F.; Keurentjes, J. T. F.; Weckhuysen, B. M., Beyond Mechanical Recycling: Giving New Life to Plastic Waste. *Angew. Chem. Int. Ed.* **2020**, *59*, 15402-15423.
13. Hong, M.; Chen, E. Y. X., Chemically recyclable polymers: a circular economy approach to sustainability. *Green Chem.* **2017**, *19*, 3692-3706.
14. Ellis, L. D.; Rorrer, N. A.; Sullivan, K. P.; Otto, M.; McGeehan, J. E.; Román-Leshkov, Y.; Wierckx, N.; Beckham, G. T., Chemical and biological catalysis for plastics recycling and upcycling. *Nat. Catal.* **2021**, *4*, 539-556.
15. Fernandes, A. C., Reductive depolymerization as an efficient methodology for the conversion of plastic waste into value-added compounds. *Green Chem.* **2021**.
16. Rorrer, J. E.; Beckham, G. T.; Román-Leshkov, Y., Conversion of Polyolefin Waste to Liquid Alkanes with Ru-Based Catalysts under Mild Conditions. *JACS Au* **2021**, *1*, 8-12.
17. Knott, B. C.; Erickson, E.; Allen, M. D.; Gado, J. E.; Graham, R.; Kearns, F. L.; Pardo, I.; Topuzlu, E.; Anderson, J. J.; Austin, H. P.; Dominick, G.; Johnson, C. W.; Rorrer, N. A.; Szostkiewicz, C. J.; Copié, V.; Payne, C. M.; Woodcock, H. L.; Donohoe, B. S.; Beckham, G.

- T.; McGeehan, J. E., Characterization and engineering of a two-enzyme system for plastics depolymerization. *Proc. Natl. Acad. Sci. U.S.A.* **2020**, *117*, 25476-25485.
18. Rorrer, N. A.; Nicholson, S.; Carpenter, A.; Bidy, M. J.; Grundl, N. J.; Beckham, G. T., Combining Reclaimed PET with Bio-based Monomers Enables Plastics Upcycling. *Joule* **2019**, *3*, 1006-1027.
19. *Shaw Industries Sustainability Report*; 2008.
20. <https://www.econyl.com/the-process/>.
21. Shi, C.; Li, Z.-C.; Caporaso, L.; Cavallo, L.; Falivene, L.; Chen, E. Y. X., Hybrid monomer design for unifying conflicting polymerizability, recyclability, and performance properties. *Chem.* **2021**, *7*, 670-685.
22. Liu, Y.; Wu, J.; Hu, X.; Zhu, N.; Guo, K., Advances, Challenges, and Opportunities of Poly(γ -butyrolactone)-Based Recyclable Polymers. *ACS Macro Lett.* **2021**, *10*, 284-296.
23. Shi, C.; McGraw, M. L.; Li, Z.-C.; Cavallo, L.; Falivene, L.; Chen, E. Y.-X., High-performance pan-tactic polythioesters with intrinsic crystallinity and chemical recyclability. *Sci. Adv.* **2020**, *6*, eabc0495.
24. Tang, X.; Chen, E. Y. X., Toward Infinitely Recyclable Plastics Derived from Renewable Cyclic Esters. *Chem.* **2019**, *5*, 284-312.
25. Zhu, J.-B.; Watson, E. M.; Tang, J.; Chen, E. Y. X., A synthetic polymer system with repeatable chemical recyclability. *Science* **2018**, *360*, 398-403.

26. Shi, C.; Reilly, L. T.; Kumar, V. S. P.; Coile, M. W.; Nicholson, S. R.; Broadbelt, L. J.; Beckham, G. T.; Chen, E. Y.-X., Design Principles for Intrinsically Circular Polymers with Tunable Properties. *Chem.* **2021**.
27. Cywar, R. M.; Rorrer, N. A.; Hoyt, C. B.; Beckham, G. T.; Chen, E. Y. X., Bio-based polymers with performance-advantaged properties. *Nat. Rev. Mater.* **2021**.
28. Cywar, R. M.; Zhu, J.-B.; Chen, E. Y. X., Selective or living organopolymerization of a six-five bicyclic lactone to produce fully recyclable polyesters. *Polym. Chem.* **2019**, 3097-3106
29. Zhu, J.-B.; Chen, E. Y.-X., Living Coordination Polymerization of a Six-Five Bicyclic Lactone to Produce Completely Recyclable Polyester. *Angew. Chem. Int. Ed.* **2018**, 57, 12558-12562.
30. Hall, H. K., Synthesis and Polymerization of Atom-bridged Bicyclic Lactams. *J. Amer. Chem. Soc.* **1960**, 82, 1209-1215.
31. Hall, H. K., Polymerization and Ring Strain in Bridged Bicyclic Compounds. *J. of the Amer. Chem. Soc.* **1958**, 80, 6412-6420.
32. Leal Filho, W.; Ellams, D.; Han, S.; Tyler, D.; Boiten, V. J.; Paço, A.; Moora, H.; Balogun, A.-L., A review of the socio-economic advantages of textile recycling. *J. Clean. Prod.* **2019**, 218, 10-20.
33. Payne, A., 6 - Open- and closed-loop recycling of textile and apparel products. In *Handbook of Life Cycle Assessment (LCA) of Textiles and Clothing*, Muthu, S. S., Ed. Woodhead Publishing: 2015; pp 103-123.

34. Marchildon, K., Polyamides – Still Strong After Seventy Years. *Macromol. React. Eng.* **2011**, *5*, 22-54.
35. Kumar, A.; von Wolff, N.; Rauch, M.; Zou, Y.-Q.; Shmul, G.; Ben-David, Y.; Leitus, G.; Avram, L.; Milstein, D., Hydrogenative Depolymerization of Nylons. *J. Amer. Chem. Soc.* **2020**, *142*, 14267-14275.
36. Kamimura, A.; Shiramatsu, Y.; Kawamoto, T., Depolymerization of polyamide 6 in hydrophilic ionic liquids. *Green Energy Environ.* **2019**, *4*, 166-170.
37. Alberti, C.; Figueira, R.; Hofmann, M.; Koschke, S.; Enthaler, S., Chemical Recycling of End-of-Life Polyamide 6 via Ring Closing Depolymerization. *ChemistrySelect* **2019**, *4*, 12638-12642.
38. Chen, J.; Li, Z.; Jin, L.; Ni, P.; Liu, G.; He, H.; Zhang, J.; Dong, J.; Ruan, R. J. J. o. M. C.; Management, W., Catalytic hydrothermal depolymerization of nylon 6. **2010**, *12*, 321-325.
39. Kamimura, A.; Yamamoto, S., An Efficient Method To Depolymerize Polyamide Plastics: A New Use of Ionic Liquids. *Org. Lett.* **2007**, *9*, 2533-2535.
40. Bockhorn, H.; Donner, S.; Gernsbeck, M.; Hornung, A.; Hornung, U., Pyrolysis of polyamide 6 under catalytic conditions and its application to reutilization of carpets. *J. Anal. Appl. Pyrolysis* **2001**, *58-59*, 79-94.
41. Czernik, S.; Elam, C. C.; Evans, R. J.; Meglen, R. R.; Moens, L.; Tatsumoto, K., Catalytic pyrolysis of nylon-6 to recover caprolactam. *J. Anal. Appl. Pyrolysis* **1998**, *46*, 51-64.

42. Russo, S.; Casazza, E., 4.14 - Ring-Opening Polymerization of Cyclic Amides (Lactams). In *Polymer Science: A Comprehensive Reference*, Matyjaszewski, K.; Möller, M., Eds. Elsevier: Amsterdam, 2012; pp 331-396.
43. Barnes, C., Nylon 4 - Development and Commercialization. *Lenzinger Ber.* 1987, pp 62-66.
44. Fries, T.; Bělohávková, J.; Roda, J.; Králíček, J., Polymerization of lactams. *Polym. Bull.* **1984**, *12*, 87-91.
45. Bour, E. H. J. P.; Warnier, J. M. M.; Brouwers, J. A. L. Preparation of poly-2-pyrrolidone with N-(2-caprolactim)-caprolactam accelerator. 4362862, 1982.
46. Schirawski, G., Untersuchungen zur anionischen polymerisation von pyrrolidon. *Makromol. Chem.* **1972**, *161*, 57-68.
47. Roda, J.; Brožek, J.; Králíček, J., Polymerization of lactams, 37. Isolation and characterization of alkali carboxylates of 2-pyrrolidone. *Makromol. Chem. Rapid Comm.* **1980**, *1*, 165-169.
48. Grewal, J.; Khare, S. K., 2-Pyrrolidone synthesis from γ -aminobutyric acid produced by *Lactobacillus brevis* under solid-state fermentation utilizing toxic deoiled cottonseed cake. *Bioprocess Biosyst. Eng.* **2017**, *40*, 145-152.
49. De Schouwer, F.; Claes, L.; Claes, N.; Bals, S.; Degrève, J.; De Vos, D. E., Pd-catalyzed decarboxylation of glutamic acid and pyroglutamic acid to bio-based 2-pyrrolidone. *Green Chem.* **2015**, *17*, 2263-2270.

50. Tanielyan, S. K.; More, S. R.; Augustine, R. L.; Tosukhowong, T.; Ozmeral, C.; Roffi, K.; Shmorhun, M.; Glas, J., Hydrogenation of Succinimide to 2-Pyrrolidone Over Solid Catalysts. *Top. Catal.* **2014**, *57*, 1582-1587.
51. Yamano, N.; Kawasaki, N.; Takeda, S.; Nakayama, A., Production of 2-Pyrrolidone from Biobased Glutamate by Using *Escherichia coli*. *J. Polym. Environ.* **2013**, *21*, 528-533.
52. Delhomme, C.; Weuster-Botz, D.; Kühn, F. E., Succinic acid from renewable resources as a C4 building-block chemical—a review of the catalytic possibilities in aqueous media. *Green Chem.* **2009**, *11*, 13-26.
53. Yamano, N.; Kawasaki, N.; Ida, S.; Nakayama, A., Biodegradation of polyamide 4 in seawater. *Polym. Degrad. Stab.* **2019**, *166*, 230-236.
54. Tachibana, K.; Hashimoto, K.; Yoshikawa, M.; Okawa, H., Isolation and characterization of microorganisms degrading nylon 4 in the composted soil. *Polym. Degrad. Stab.* **2010**, *95*, 912-917.
55. Yamano, N.; Nakayama, A.; Kawasaki, N.; Yamamoto, N.; Aiba, S., Mechanism and Characterization of Polyamide 4 Degradation by *Pseudomonas* sp. *J. Polym. Environ.* **2008**, *16*, 141-146.
56. Sangroniz, A.; Zhu, J.-B.; Tang, X.; Etxeberria, A.; Chen, E. Y. X.; Sardon, H., Packaging materials with desired mechanical and barrier properties and full chemical recyclability. *Nat. Comm.* **2019**, *10*, 3559.

57. Winnacker, M.; Neumeier, M.; Zhang, X.; Papadakis, C. M.; Rieger, B., Sustainable Chiral Polyamides with High Melting Temperature via Enhanced Anionic Polymerization of a Menthone-Derived Lactam. *Macromol. Rapid Commun.* **2016**, *37*, 851-857.
58. Amorín, M.; Castedo, L.; Granja, J. R., Self-Assembled Peptide Tubelets with 7 Å Pores. *Chem. Eur. J.* **2005**, *11*, 6543-6551.
59. Amorín, M.; Castedo, L.; Granja, J. R., New Cyclic Peptide Assemblies with Hydrophobic Cavities: The Structural and Thermodynamic Basis of a New Class of Peptide Nanotubes. *J. Amer. Chem. Soc.* **2003**, *125*, 2844-2845.
60. Miyake, G. M.; DiRocco, D. A.; Liu, Q.; Oberg, K. M.; Bayram, E.; Finke, R. G.; Rovis, T.; Chen, E. Y. X., Stereospecific Polymerization of Chiral Oxazolidinone-Functionalized Alkenes. *Macromolecules* **2010**, *43*, 7504-7514.
61. Bellinger, M. A.; Ng, C.-W. A.; Macknight, W. J., Effects of water on the mechanical relaxation in polyamide 4. *Acta Polym.* **1995**, *46*, 361-366.
62. Wu, Y.; Xu, Y.; Wang, D.; Zhao, Y.; Weng, S.; Xu, D.; Wu, J., FT-IR spectroscopic investigation on the interaction between nylon 66 and lithium salts. *J. Appl. Polym. Sci.* **2004**, *91*, 2869-2875.
63. Krimm, S.; Bandekar, J., Vibrational Spectroscopy and Conformation of Peptides, Polypeptides, and Proteins. In *Advances in Protein Chemistry*, Anfinsen, C. B.; Edsall, J. T.; Richards, F. M., Eds. Academic Press: 1986; Vol. 38, pp 181-364.
64. Hashimoto, K.; Sumitomo, H.; Shinoda, H.; Washio, A., Equilibrium anionic polymerization of bicyclic oxalactam. *J. Polym. Sci. C: Polym. Lett.* **1989**, *27*, 307-311.

65. Hashimoto, K.; Sumitomo, H.; Washio, A., Preparation of monodisperse hydrophilic polyamide by anionic polymerization of bicyclic oxalactam. *J. Polym. Sci. A: Polym. Chem.* **1989**, *27*, 1915-1923.
66. Hashimoto, K.; Sumitomo, H., Synthesis and Polymerization of an Optically Active Bicyclic Oxalactam. A Novel Hydrophilic Polyamide Membrane Prepared from (+)-(1R,5S)-8-Oxa-6-azabicyclo[3.2.1]octan-7-one. *Macromolecules* **1980**, *13*, 786-791.
67. Sumitomo, H.; Hashimoto, K., Polymerization of Bicyclic Oxalactam. A Novel Polyamide Poly(tetrahydropyran-2,6-diyiminocarbonyl). *Macromolecules* **1977**, *10*, 1327-1331.
68. kim, N. C.; Kamal, T.; Park, S.-y.; Cho, C.-G.; Kim, J.-H.; Yoo, Y.-T.; Nam, S. W.; Jeon, B. S.; Kim, Y. J., Preparation, chemical, and thermal characterization of nylon 4/6 copolymers by anionic ring opening polymerization of 2-Pyrrolidone and ϵ -Caprolactam. *Fibers Polym.* **2014**, *15*, 899-907.
69. Schirawski, G., Untersuchungen zur copolymerisation von pyrrolidon und caprolactam. *Makromol. Chem.* **1972**, *161*, 69-83.
70. Zhang, H.; Stephanopoulos, G., Co-culture engineering for microbial biosynthesis of 3-amino-benzoic acid in Escherichia coli. *Biotechnol. J.* **2016**, *11*, 981-987.
71. PA6. <https://designerdata.nl/materials/plastics/thermo-plastics/polyamide-6> (accessed August 9, 2021).
72. Tang, J.; Chen, E. Y.-X., Effects of Chain Ends on Thermal and Mechanical Properties and Recyclability of Poly(γ -butyrolactone). *J. Polym. Sci. A: Polym. Chem.* **2018**, *56*, 2271-2279.

73. Tachibana, K.; Hashimoto, K.; Tansho, N.; Okawa, H., Chemical modification of chain end in nylon 4 and improvement of its thermal stability. *J. Polym. Sci. A: Polym. Chem.* **2011**, *49*, 2495-2503.
74. Towns, J.; Cockerill, T.; Dahan, M.; Foster, I.; Gaither, K.; Grimshaw, A.; Hazlewood, V.; Lathrop, S.; Lifka, D.; Peterson, G. D.; Roskies, R.; Scott, J. R.; Wilkens-Diehr, N., XSEDE: Accelerating Scientific Discovery. *Comput. Sci. Eng.* **2014**, *16*, 62-74.

Chapter 6

Conclusions and Outlook

6.1. Conclusions and Outlook

The need to transition to a circular carbon and materials economy has become increasingly clear.¹⁻³ The realization of carbon-neutral bio-based products (e.g., chemicals and materials including polymers) relies not only on replacing petroleum-derived building blocks with those derived from plants, but the discovery of new materials with enhanced properties and sustainable lifecycles relative to petroleum-derived products.⁴⁻¹¹ Product end-of-life (recyclability or degradability), can also be directly addressed during the design phase of new, sustainable materials as shown in this work.

Industrial chemical processes, particularly for biorefining, should also be designed for sustainability with considerations such as atom economy, waste generation, and energy use.^{12, 13} Catalyzed chemical processes inherently reduce waste relative to use of stoichiometric reagents, and heterogeneous (or supported) catalysts have the advantage of facile separation. In many cases, heterogeneous catalysts can be re-used or regenerated. However, many are based on precious metals which are non-renewable resources.¹⁴ On the other hand, organic catalysts are considered a sustainable alternative.¹⁵⁻¹⁷ Organocatalysis also offers unique selectivities, steric and electronic tunability, and yields products free of metal residues. Thus, it is important to adapt homogeneous organocatalysts to heterogeneous for a long lifetime.¹⁸

The umpolung coupling reaction of biorefinery platform furfuraldehydes by NHC organocatalysis enables their chain-extension to C₁₀-C₁₄ furoin products which can be used as fuel intermediates

or multifunctional monomers.¹² To design a recyclable NHC for this atom-economic coupling, approaches including grafting onto silica or polymer resin and clay intercalation have been taken, by way of the easily functionalized azolium nitrogen sites.¹⁹⁻²¹ However, all of these supported forms require stoichiometric base for pre-catalyst activation to generate the air-sensitive NHC, and strong acid to quench it prior to recycling in air. A thermally activated, polymer supported NHC has been developed which catalyzes furfural coupling in maintained high yield over 5 cycles of use after recycling in-air, based on the thermal equilibrium between an acetate salt and NHC-acetic acid pair.²² A hydrophobic C₁₂ substituent proved superior to other (benz)imidazolium structures for both yield and recycling, showing that orthogonal reactivity (i.e. high activity and high temperature, low activity at room temperature) alone was insufficient for predicting a recyclable catalyst. Instead, the hydrophobic pocket provided by the C₁₂ chain provides protection from oxygen and moisture and demonstrated superior catalytic activity, due to being a both a good nucleophile (via hyperconjugation) and a good leaving group (via steric hindrance).

The discovery of acid-base interactions between the acetate counterion and the alcohol proton of HMF led to lower initial yields (97% vs 89% for the optimal catalyst, PS-*g*-[BI]-C₁₂-OAc) and much worse recyclability. This limitation has two important implications. First, this interaction led to increased loss of acetic acid post-reaction and contributed to reduced catalytic performance in future cycles. Thus, in future generations of this thermally-activated, PS-NHC, the counterion could be covalently tethered in a zwitterionic form. This insight is important because even with furfural substrate, traces of acetic acid can still be lost during each recycle due to incomplete conversion to the acetate salt at room temperature. Second, the detrimental acid-base interaction highlights some limitation of HMF as a substrate. The use of etherified HMF circumvented the issue, and these substrates have also shown superior characteristics as biorefinery chemical

intermediates. For example, EMF/MMF are high-boiling liquids with longer shelf lives than HMF, and result in higher yields of furan dicarboxylic acid (a monomer for bio-based poly(ethylene furanoate)).²³ Further research into sustainable and efficient ways to convert biomass and HMF to the etherified C₆ furaldehydes is needed.

In designing useful plastics with complete chemical recyclability,²⁴ two ring-fused bicyclic monomers with moderate T_c values were explored for balanced (de)polymerization-performance properties.^{25, 26} Ring-opening polymerization (ROP) of the lactone and lactam monomers (4,5-T6GBL and 5/7-LM) with organic and benign alkali metal salt catalysts produced polymers with sufficient M_n for thermomechanical characterization in a sustainable fashion. The structure-property relationships of the resulting, completely depolymerizable materials, and those of copolymers, were examined in detail. Owing to cyclohexane rings fused to the polymer backbone, both the polyester P(4,5-T6GBL) and polyamide nylon 4/6 were rigid materials. The new materials contribute to a growing family of recyclable monomer-polymer systems based on moderate T_c values, allowing both polymerization and depolymerization at accessible temperatures.

Selective O-ROP of 4,5-T6GBL allowed for the synthesis of linear polyesters in a living fashion, via thiourea/base pair catalysis, or to cyclic polyesters via nucleophilic NHCs.²⁶ After screening for the most active catalyst pair, the optimal structures 1,3-diisopropylthiourea and IMes (or KOMe) were employed to reach relatively high M_n (up to 106 kDa). These catalysts are commercially available and were used as received. The screening revealed many interesting kinetic trends and provided insights to the reactivity of (thio)urea/base pairs with a moderate T_c monomer. Pairs with well-matched pK_a values catalyzed the polymerization controllably, and with trends revealing a threshold level of activation required for successful polymerization based on base strength of the (thio)urea anion. Compared to the metal-catalyzed system,²⁷ organocatalysis

provided several advantages. Recyclable polymers with higher decomposition temperatures were attained with less purification, higher M_n reached, and polymerization kinetics were competitive. Furthermore, organocatalyzed depolymerization by the guanidine TBD was quantitative and selective to the *trans* isomer only. The mechanical properties of the highest M_n P(4,5-T6GBL) samples were used for dynamic mechanical and tensile analysis ($\epsilon_b = 2.5 \pm 0.2\%$, $\sigma_b = 41 \pm 5$ MPa). It is an amorphous material ($T_g = 75$ °C) and undergoes steep loss in storage and loss moduli immediately after surpassing the T_g . Interestingly, the incorporation of GBL in random copolymers did not result in enhanced ductility, whereas the effect of GBL incorporation was dramatic for the constitutional isomer P(3,4-T6GBL).²⁸ Overall, P(3,4-T6GBL) proved to be a superior material for packaging applications. The advantages of organocatalysis for the synthesis of P(4,5-T6GBL) were clear, however there is potential to explore heterogenization of (thio)urea, NHC, and guanidine catalysts for polymer synthesis. Supported versions of these catalysts have been demonstrated but are primarily employed in small molecule transformations.²⁹⁻³¹

The lactam monomer examined was designed by the hybridization strategy.^{25, 32} The LCT monomer pyrrolidone (5-LM) is ‘hybridized’ with HCT ϵ -caprolactam (7-LM) to create a fused ring offspring monomer (5/7-LM) which contains both 5 and 7-membered lactams. The offspring monomer maintains high polymerizability of the HCT parent while retaining the depolymerizability (recyclability) of the LCT parent while exhibiting vastly different properties. Unlike the parent nylons, the resulting nylon 4/6 material is stereoregular and amorphous (optically clear) with high T_g (~200 °C), brittle, and lacks a viscous flow state prior to degradation. Density functional theory (DFT) calculations revealed that *threo*-disyndiotactic polymers were the kinetically-preferred products of the chain-end control mechanism which involves a sterically encumbered intermediate. DFT also provided insight into likely chain conformations, supporting

the hypothesis that weak, 1,3-diaxial hydrogen-bond interactions stabilize the polymer at elevated temperatures.

Hybrid 5/7-LM was subsequently used as a co-monomer with 5-LM to prepare random copolymers. Nylon 4, which is easily bio-based, chemically recyclable, and biodegradable, unfortunately degrades (recycles to monomer) at its melting temperature and thus cannot be melt-processed (e.g., extrusion, injection molding). This hybrid monomer behaved as a ‘trojan horse’ for introducing thermal stability and lowering processing temperatures of nylon 4 copolymers, with a ~50/50 copolymer composition showing the greatest synergy in both reactivity and properties. A physical blend of nylon 4 and nylon 4/6 is immiscible, but the synergistic ~50/50 copolymer has high T_g (80-156 °C), is optically clear, and melt-processable as indicated by stability during isothermal holds at theoretical processing temperatures. As both comonomers are chemically recyclable, the copolymer also demonstrated full chemical recyclability. Nylon 4/6-*co*-nylon 4 was shown to be a stiff material ($\sigma_b = 54 \pm 5$ MPa at $\epsilon_b = 4.4 \pm 1.3\%$) with storage and Young’s moduli comparable to those of industrial nylon 6, and has potential for plasticization in more humid environments.

This new, fully recyclable nylon material shows potential for both typical nylon applications like fibers as well as optically clear coatings or composite matrices with excellent solvent resistance; the development of high-performance composite components with circular lifecycles is a critical need and the topic has received increasing research attention in recent years.⁴ Similar to PGBL and nylon 4, there is potential to study the effect of both initiating and terminating chain end functionalities of nylon 4/6-*co*-nylon 4 on the thermal stability.^{33, 34}

Recent successes in the re-design of synthetic polymers have only scratched the surface of possibilities for bio-based and recyclable-by-design materials.^{1, 4, 25, 32, 35-39} Not only do these new materials demonstrate sustainable and circular lifecycles but also show competitive and tunable physical properties, when compared to petroleum-derived incumbent materials. Each compelling example contributes structure-property relationship information useful for further property enhancement, and broadly illustrates that barriers to a circular economy do not arise from a lack of innovation. In fact, it is possible if synergistic new technologies (i.e., intrinsically recyclable polymers and advanced robotic sorting of post-consumer plastics) can be adopted by industry, government, and society. As eloquently stated by Chen in 2021, “the arguments that today’s plastics are much cheaper and that new plastics contaminate recycling streams neglect environmental, financial, and social triple bottom-line accountability. It will be critically important for the plastics industry to embrace this new plastics revolution. Sacrificing some short-term profitability in order to transition to a circular plastics economy will require courage, commitment, and strategic planning. Achieving a sustainable plastic future preserving natural resources and the environment for future generations depends on doing so.”⁴⁰

References

1. Coates, G. W.; Getzler, Y. D. Y. L., Chemical recycling to monomer for an ideal, circular polymer economy. *Nat. Rev. Mater.* **2020**, *5*, 501–516.
2. Hatti-Kaul, R.; Nilsson, L. J.; Zhang, B.; Rehnberg, N.; Lundmark, S., Designing Biobased Recyclable Polymers for Plastics. *Trends Biotechnol.* **2020**, *38*, 50-67.
3. *The New Plastics Economy — Rethinking the future of plastics*; World Economic Forum, Ellen MacArthur Foundation and McKinsey & Company: 2016.
4. Cywar, R. M.; Rorrer, N. A.; Hoyt, C. B.; Beckham, G. T.; Chen, E. Y. X., Bio-based polymers with performance-advantaged properties. *Nat. Rev. Mater.* **2021**, DOI: 10.1038/s41578-021-00363-3
5. Huo, J.; Shanks, B. H., Bioprivileged Molecules: Integrating Biological and Chemical Catalysis for Biomass Conversion. *Annu. Rev. Chem. Biomol. Eng.* **2020**, *11*, 63-85.
6. Fitzgerald, N.; Bailey, A. *Moving Beyond Drop-In Replacements: Performance-Advantaged Biobased Chemicals*; US Department of Energy Office of Energy Efficiency and Renewable Energy Bioenergy Technologies Office: 2018.
7. Hillmyer, M. A., The promise of plastics from plants. *Science* **2017**, *358*, 868-870.
8. Fitzgerald, N. D., Chemistry challenges to enable a sustainable bioeconomy. *Nat. Rev. Chem.* **2017**, *1*, 1-3.
9. Shanks, B. H.; Keeling, P. L., Bioprivileged molecules: creating value from biomass. *Green Chem.* **2017**, *19*, 3177-3185.
10. Zhu, Y.; Romain, C.; Williams, C. K., Sustainable polymers from renewable resources. *Nature* **2016**, *540*, 354-362.

11. Hermann, B. G.; Blok, K.; Patel, M. K., Producing Bio-Based Bulk Chemicals Using Industrial Biotechnology Saves Energy and Combats Climate Change. *Environ. Sci. Technol.* **2007**, *41*, 7915-7921.
12. Liu, D.; Chen, E. Y. X., Organocatalysis in biorefining for biomass conversion and upgrading. *Green Chem.* **2014**, *16*, 964-981.
13. Anastas, P.; Eghbali, N., Green Chemistry: Principles and Practice. *Chem. Soc. Rev.* **2010**, *39*, 301-312.
14. Supanchaiyamat, N.; Hunt, A. J., Conservation of Critical Elements of the Periodic Table. *ChemSusChem* **2019**, *12*, 397-403.
15. Naumann, S.; Dove, A. P., N-Heterocyclic carbenes as organocatalysts for polymerizations: trends and frontiers. *Polym. Chem.* **2015**, *6*, 3185-3200.
16. Kiesewetter, M. K.; Shin, E. J.; Hedrick, J. L.; Waymouth, R. M., Organocatalysis: Opportunities and Challenges for Polymer Synthesis. *Macromolecules* **2010**, *43*, 2093-2107.
17. MacMillan, D. W. C., The advent and development of organocatalysis. *Nature* **2008**, *455*, 304-308.
18. Shaikh, I. R., Organocatalysis: Key Trends in Green Synthetic Chemistry, Challenges, Scope towards Heterogenization, and Importance from Research and Industrial Point of View. *J. Catal.* **2014**, *2014*, 402860.
19. Lambert, R.; Coupillaud, P.; Wirotius, A.-L.; Vignolle, J.; Taton, D., Imidazolium-Based Poly(Ionic Liquid)s Featuring Acetate Counter Anions: Thermally Latent and Recyclable Precursors of Polymer-Supported N-Heterocyclic Carbenes for Organocatalysis. *Macromol. Rapid Commun.* **2016**, *37*, 1143-1149.

20. Wang, L.; Chen, E. Y. X., Recyclable Supported Carbene Catalysts for High-Yielding Self-Condensation of Furaldehydes into C10 and C12 Furoins. *ACS Catal.* **2015**, *5*, 6907-6917.
21. Wang, L.; Chen, E. Y. X., An interchangeable homogeneous \leftrightarrow heterogeneous catalyst system for furfural upgrading. *Green Chem.* **2015**, *17*, 5149-5153.
22. Cywar, R. M.; Wang, L.; Chen, E. Y. X., Thermally Regulated Recyclable Carbene Catalysts for Upgrading of Biomass Furaldehydes. *ACS Sus. Chem. Eng.* **2019**, *7*, 1980-1988.
23. Diego, C. M. d.; Schammel, W. P.; Dam, M. A.; Johannes, G.; Gruter, M. Method for the preparation of 2,5-furandicarboxylic acid and esters thereof. WO2011/043660A2, 2011.
24. Shi, C.; Reilly, L. T.; Kumar, V. S. P.; Coile, M. W.; Nicholson, S. R.; Broadbelt, L. J.; Beckham, G. T.; Chen, E. Y.-X., Design Principles for Intrinsically Circular Polymers with Tunable Properties. *Chem.* **2021**.
25. Cywar, R. M.; Rorrer, N. A.; Mayes, H. B.; Beckham, G. T.; Chen, E. Y.-X., Redesigned hybrid nylons for optical clarity and chemical recyclability. (*Submitted*) **2021**.
26. Cywar, R. M.; Zhu, J.-B.; Chen, E. Y. X., Selective or living organopolymerization of a six-five bicyclic lactone to produce fully recyclable polyesters. *Polym. Chem.* **2019**, *10*, 3097-3106.
27. Zhu, J.-B.; Chen, E. Y. X., Living Coordination Polymerization of a Six-Five Bicyclic Lactone to Produce Completely Recyclable Polyester. *Angew. Chem. Int. Ed.* **2018**, *57*, 12558-12562.
28. Sangroniz, A.; Zhu, J.-B.; Tang, X.; Etxeberria, A.; Chen, E. Y.-X.; Sardon, H., Packaging materials with desired mechanical and barrier properties and full chemical recyclability. *Nat. Comm.* **2019**, *10*, 3559.

29. Andrés, J. M.; Ceballos, M.; Maestro, A.; Sanz, I.; Pedrosa, R., Supported bifunctional thioureas as recoverable and reusable catalysts for enantioselective nitro-Michael reactions. *Beilstein J. Org. Chem.* **2016**, *12*, 628-635.
30. Luan, Y.; Zheng, N.; Qi, Y.; Tang, J.; Wang, G., Merging metal–organic framework catalysis with organocatalysis: A thiourea functionalized heterogeneous catalyst at the nanoscale. *Catal. Sci. Technol.* **2014**, *4*, 925-929.
31. Yang, Y.-C.; Leung, D. Y. C.; Toy, P. H., Rasta Resin-TBD as a Reusable Catalyst for Transesterification Reactions. *Synlett* **2013**, *24*, 1870-1874.
32. Shi, C.; Li, Z.-C.; Caporaso, L.; Cavallo, L.; Falivene, L.; Chen, E. Y. X., Hybrid monomer design for unifying conflicting polymerizability, recyclability, and performance properties. *Chem.* **2021**, *7*, 670-685.
33. Tang, J.; Chen, E. Y.-X., Effects of Chain Ends on Thermal and Mechanical Properties and Recyclability of Poly(γ -butyrolactone). *J. Polym. Sci. A. Polym. Chem.* **2018**, *56*, 2271-2279.
34. Tachibana, K.; Hashimoto, K.; Tansho, N.; Okawa, H., Chemical modification of chain end in nylon 4 and improvement of its thermal stability. *J. Polym. Sci. A. Polym. Chem.* **2011**, *49*, 2495-2503.
35. Liu, Y.; Wu, J.; Hu, X.; Zhu, N.; Guo, K., Advances, Challenges, and Opportunities of Poly(γ -butyrolactone)-Based Recyclable Polymers. *ACS Macro Lett.* **2021**, *10*, 284-296.
36. Shi, C.; McGraw, M. L.; Li, Z.-C.; Cavallo, L.; Falivene, L.; Chen, E. Y.-X., High-performance pan-tactic polythioesters with intrinsic crystallinity and chemical recyclability. *Sci. Adv.* **2020**, *6*, eabc0495.
37. Tang, X.; Chen, E. Y. X., Toward Infinitely Recyclable Plastics Derived from Renewable Cyclic Esters. *Chem.* **2019**, *5*, 284-312.

38. Zhu, J.-B.; Watson, E. M.; Tang, J.; Chen, E. Y. X., A synthetic polymer system with repeatable chemical recyclability. *Science* **2018**, *360*, 398-403.
39. Wang, Y.; Li, M.; Chen, J.; Tao, Y.; Wang, X., O-to-S Substitution Enables Dovetailing Conflicting Cyclizability, Polymerizability, and Recyclability: Dithiolactone vs. Dilactone. *Angew. Chem. Int. Ed.* **2021**, *60*, 22547-22553.
40. Iacovidou, E.; Geyer, R.; Kalow, J.; Palardy, J.; Dunn, J.; Hoellein, T.; Xiong, B.; Chen, E. Y. X., Toward a circular economy for plastics. *One Earth* **2021**, *4*, 591-594.

Appendix A

Experimental Details and Supporting Information for Chapter 3

A.1. Materials and Methods

Materials. All oxygen and moisture sensitive manipulations were carried out in a nitrogen or argon-filled glovebox or under nitrogen atmosphere using standard Schlenk techniques. Tetrahydrofuran (THF) was dried over metallic sodium/potassium alloy for 24 h at room temperature in an inert atmosphere, filtered, and distilled under nitrogen before use. Anhydrous acetonitrile (Aldrich), methanol (Fisher Scientific), and DMSO- d_6 were dried over 3 or 4 Å, pre-activated molecular sieves. Furfural (TCI), 5-methyl furfural (MF, Alfa Aesar), and DMSO were dried over calcium hydride and vacuum distilled prior to use. 5-Hydroxymethylfurfural (HMF) (Ark Pharm, Acros Organics), Merrifield's peptide resin (MPR, Aldrich, 200-400 mesh, 3.5-4.5 mmol/g Cl⁻ loading, 1% cross-linked), benzimidazole (Acros Organics), 1-bromododecane (Aldrich), 1-bromoethane (Aldrich), 1-bromobutane (Aldrich), benzyl chloride (Aldrich), imidazole (Aldrich), 1-ethyl imidazole (TCI), 1-butyl imidazole (Alfa Aesar), 2-(4-methyl-5-thiazolyl)ethyl acetate (Alfa Aesar), 4,5-dimethylthiazole (Matrix Scientific), 1-ethyl-3-methylimidazolium acetate (Alfa Aesar), potassium acetate (Fisher Scientific), potassium hydroxide (Fisher Scientific), potassium trifluoroacetate (Oakwood Chemical), lead (II) acetate (Fisher Scientific, 2% w/v in alcohol), and dichloromethane (Fisher Scientific) were used as received. Potassium succinate was prepared by titration of succinic acid (aq.) with potassium hydroxide (aq.), followed by evaporation of the water and drying under vacuum at 60 °C for 72 h. The literature procedure¹ was followed to prepare 5-methoxymethyl furfural (MMF) from HMF.

Methods. ^1H and ^{13}C NMR spectra were recorded on a Varian Inova or Bruker 400 MHz spectrometer. Fourier transform infrared (FT-IR) spectroscopy was performed on a Thermo Scientific (Nicolet iS50) FT-IR spectrometer equipped with a diamond attenuated total reflectance (ATR) at room temperature in the range of 550–4000 cm^{-1} . Thermogravimetric analysis (TGA) was performed under nitrogen atmosphere at a heating rate of 10 $^{\circ}\text{C}/\text{min}$ from 20 to 800 $^{\circ}\text{C}$ using TA Q-series Q50, TA Instruments.

Preparation of Alkylated [Benz]imidazoles (pre-[NHC]'s). Literature procedures² were adapted for these preparations. Imidazole or benzimidazole (25 mmol) was dispersed in acetonitrile (1.25 M), along with 2 equivalents of KOH (crushed pellets) and 1 equivalent alkyl halide. The mixture was brought to reflux for 4 h. After cooling to room temperature, the solids were filtered off through a pad of Celite and washed with dichloromethane (DCM). The solvent was removed by rotary evaporation, and to the residue, 20 mL dichloromethane were added. The organic phase was washed twice with distilled water, followed by brine, then dried with Na_2SO_4 , filtered, and evaporated to yield the products: 1-ethylbenzimidazole, 84% yield; 1-butylbenzimidazole, 90% yield; 1-dodecylbenzimidazole, 97% yield; 1-benzylbenzimidazole, 85% yield; 1-dodecylimidazole, 89% yield. ^1H NMR spectra of all prepared [benz]imidazoles can be found in the Supporting Information.

Preparation of Polystyrene (PS)-Grafted, Pre-[NHC] Chloride Salts. Merrifield's peptide resin (MPR) (3.00 g) and pre-[NHC] (12.5 mmol, 9-10 mmol excess relative to Cl^-) were dispersed in anhydrous acetonitrile and the mixture was stirred under N_2 reflux for 72 h.³ The resulting PS-*g*-[XY]-*C*_Z-Cl (XY = pre-[NHC] heterocycle, where [IM] = imidazolium, [BI] = benzimidazolium, [TM] = thiazolium, and Z = alkyl substituent) was filtered, washed with copious DCM, and dried at 60 $^{\circ}\text{C}$ under vacuum overnight. To determine the amount of pre-[NHC] grafted, the mass gained

by the resin was converted to mmol and divided by the total mass of the dried, grafted resin to arrive at a mmol pre-[NHC]/g resin loading value. The loadings range from 1.4-2.4 mmol/g resin; specific loadings for each prepared resin can be found in Table 1. Note that solid state ^{13}C NMR and SEM characterization of such grafted chloride salts were performed in our previous study.³

Ion Exchange of PS-*g*-[XY]-C_z-Cl to PS-*g*-[XY]-C_z-OAc. Potassium acetate (4.87 g, 49.6 mmol, 5 equiv. relative to grafted pre-[NHC]) was dissolved in anhydrous methanol (1.65 M) and the grafted resin (5.84 g, 9.91 mmol [BI]-C₁₂) was added. The mixture was capped with a septum, a nitrogen inlet needle attached, and the mixture was stirred for approximately 24 h at room temperature. The resin was filtered, washed with methanol, and dried under vacuum at room temperature overnight. In the case of PS-*g*-[DMTM]-Cl, ion exchange required the use of Pb(OAc)₂: 36 ml of 2% w/v Pb(OAc)₂ in alcohol (5 equiv. acetate relative to grafted pre-[NHC]) was mixed with 0.25 g PS-*g*-[DMTM]-Cl (0.75 mmol [DMTM]-Cl) and stirred under nitrogen for 24 h. The solution became progressively yellow as precipitate formed. The resin was filtered and stirred with anhydrous DMSO for 1 h, filtered again and washed with DMSO, followed by drying in the vacuum oven at 50 °C for 24 h.

Typical Procedure for Furfural and HMF Self-Coupling Reactions by PS-*g*-[XY]-C_z-OAc. Furfural (1.00 g, 10.4 mmol), THF (10.4 ml, 1.0 M), and PS-*g*-[BI]-C₁₂-OAc (0.613 g, 1.04 mmol [BI]-C₁₂) were added to a thick-walled glass pressure reactor and sealed inside a nitrogen-filled glovebox. The reactor was then heated to 80 °C for 8 h. The NMR spectrum of the reaction mixture was used to determine conversion after cooling to room temperature, and the resulting coupling products, C₁₀ furoin and C₁₂ DHMF, were characterized by ^1H NMR according to literature values.^{4, 5} For isolation of the coupling products, the reaction mixture was filtered and solvent evaporated. Remaining furfural or MF was removed by heating the C₁₀ furoin product in

a vacuum oven, isolated furoin yields 97% and 71%, respectively. The product of MF coupling, 5,5'-dimethyl furoin (DMF),⁶ was characterized by ¹H and ¹³C NMR. The C₁₂ DHMF⁵ product was separated from remaining HMF by washing with toluene; isolated yield: 78%. The C₁₄ product of MMF coupling, 5,5'-dimethoxymethyl furoin (DMMF), was isolated by flash chromatography (1:1 hexanes:ethyl acetate) and characterized by NMR. ¹H NMR (400 MHz, CDCl₃): δ 7.20-7.21 (d, *J* = 3.60 Hz, 1H, Furan-*H*), 6.43-6.44 (d, *J* = 3.60, 1H, Furan-*H*), 6.31-6.32 (d, *J* = 3.20, 1H, Furan-*H*), 6.25-6.26 (d, *J* = 3.20, 1H, Furan-*H*), 5.74 (s, 1H, *CHOH*), 4.42 (s, 2H, Furan-*CH*₂*O*), 4.31-4.32 (d, *J* = 2.80 Hz, 2H, Furan-*CH*₂*O*), 3.79-3.89 (m, 1H, *CHOH*), 3.35 (s, 3H, -*OCH*₃), 3.28 (s, 3H, -*OCH*₃). ¹³C NMR (400 MHz, CDCl₃): δ 184.0, 158.1, 152.5, 151.5, 149.1, 121.2, 111.2, 110.4, 109.8, 69.3, 66.4, 66.2, 58.6, 57.8.

For recycling experiments, the catalyst was filtered either in air or under nitrogen inside the glovebox, washed with anhydrous THF, and dried under vacuum at room temperature overnight before use in the next cycle. The 10 mol% recycles used 1.00 g furfural for each of the 5 cycles, while the 5 mol% recycles were scaled down according to the mass of recovered catalyst since any loss would have an exponential effect on the stoichiometry of the reaction. After the 3rd cycles of HMF coupling reactions for both air-free and in-air recycling experiments, regeneration attempts were performed by stirring the recycled PS-supported catalyst for 8 h with 5 equivalents acetic acid or potassium acetate in methanol (1.0 M). Recycling experiments with MF and MMF started with 275 and 145 mg substrate, respectively.

A.2.

Table S3.1. Batch-to-batch assessment of grafted catalyst PS-g-[BI]-C₁₂-OAc

batch (mmol [BI]-C₁₂/g PS)	furfural coupling yield (10 mol%, 80 C, 8h, THF)
1.62	95%
1.70	95%
1.76	97%
1.85	97%
standard deviation	±1%

Table S3.2. Run-to-run assessment of (same batch) PS-g-[BI]-C₁₂-OAc

batch (mmol [BI]-C₁₂/g PS)	furfural coupling yield (10 mol%, 80 C, 2h, THF)
1.76	94%
1.76	93%
1.76	93%
standard deviation	±0.6%

Table S3.3 Selected attempts to increase DHMF yield with various PS-supported catalyst structures.

catalyst (PS-g-)	reaction temp.	time	solvent	yield
[BI]-C ₁₂ -OAc (20 mol%)	80 °C	8 h	THF	85%
[BI]-Et-Succ (10 mol%)	80 °C	8 h	THF	67%
[BI]-C ₁₂ -Succ (10 mol%)	80 °C	8 h	THF	84%
[BI]-C ₁₂ -OAc (10 mol%)	60 °C, microwave	1 h	THF	52%
[BI]-C ₁₂ -OAc	80 °C	4 h	Neat	40%
[BI]-C ₁₂ -OAc	80 °C	8 h	EtOH	66%
[IM]-Bu-OAc	120 °C	24 h	THF	27%

Table S3.4. Results of couplings attempted with thiazolium based catalysts

catalyst (PS-g-)	reaction temp.	time	solvent	yield
[AcOMeTM]-Cl (10 mol%) + NEt ₃ (20 mol%)	100 °C	3 h	neat	96% DHMF
[AcOMeTM]-OAc (10 mol%) ^a	80 °C	24 h	THF	5% FF; 1% DHMF
[AcOMeTM]-OAc (10 mol%) ^a + NEt ₃ (20 mol%)	100 °C	3 h	neat	100% FF
[DMTM]-Cl (10 mol%) + NEt ₃ (20 mol%)	100 °C	3 h	neat	95% DHMF
[DMTM]-OAc (10 mol%) ^a	80 °C	24 h	THF	4% DHMF
[DMTM]-OAc (10 mol%) ^b	80 °C	24 h	THF	80% DHMF
[DMTM]-OTFAc (10 mol%)	80 °C	24 h	THF	14% DHMF

^a Ion-exchanged with 5 eq. KOAc in MeOH^b Ion-exchanged with Pb(OAc)₂ in alcohol solution (Fisher, 2% w/v)**Table S3.5.** Results of 5-methylfurfural coupling experiments

Cycle	Yield (NMR)
1	89%
2	88%
3	92%*

*3rd cycle was run with a different scale.**Table S3.6.** Results of 5-methoxymethylfurfural coupling experiments

Cycle	Yield (NMR)
1	81%
2	85%*

*2nd cycle was run with a different scale.

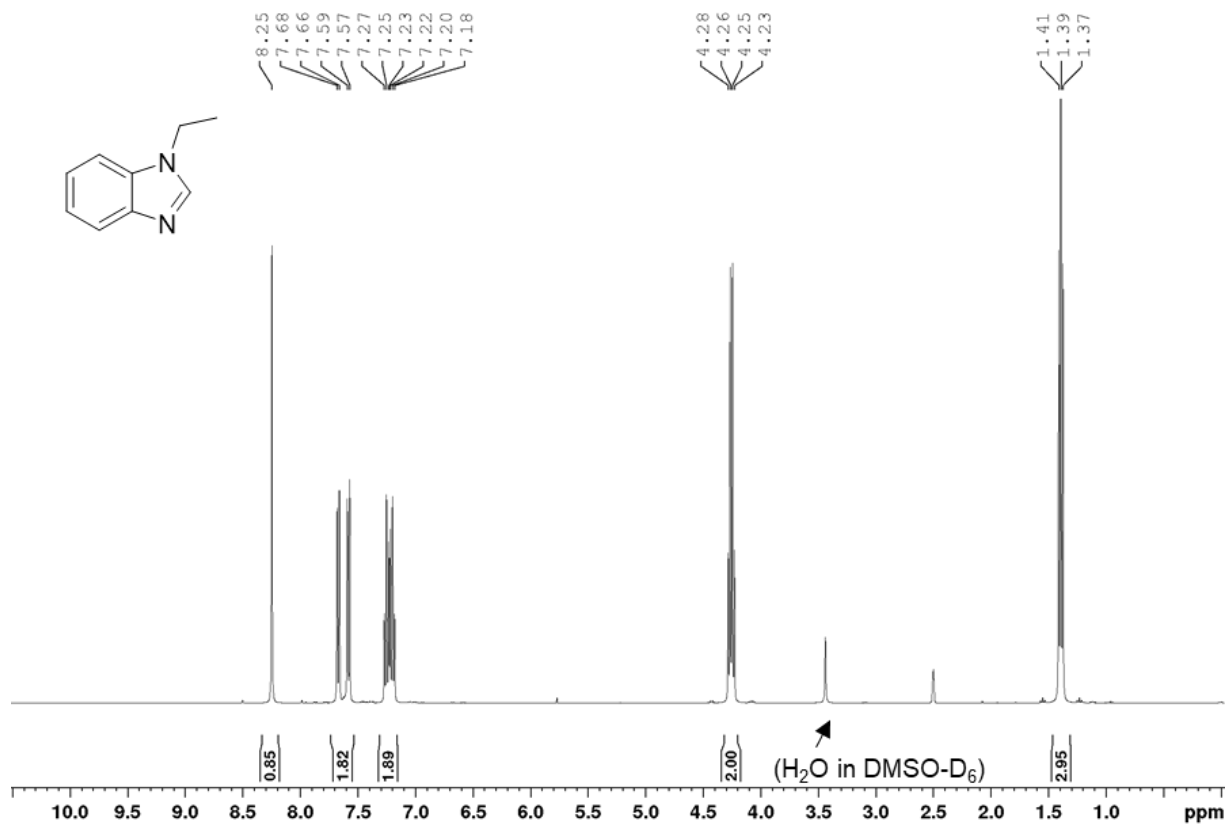


Figure S3.1. ^1H NMR (400 MHz, $(\text{CD}_3)_2\text{SO}$) spectrum of 1-ethylbenzimidazole

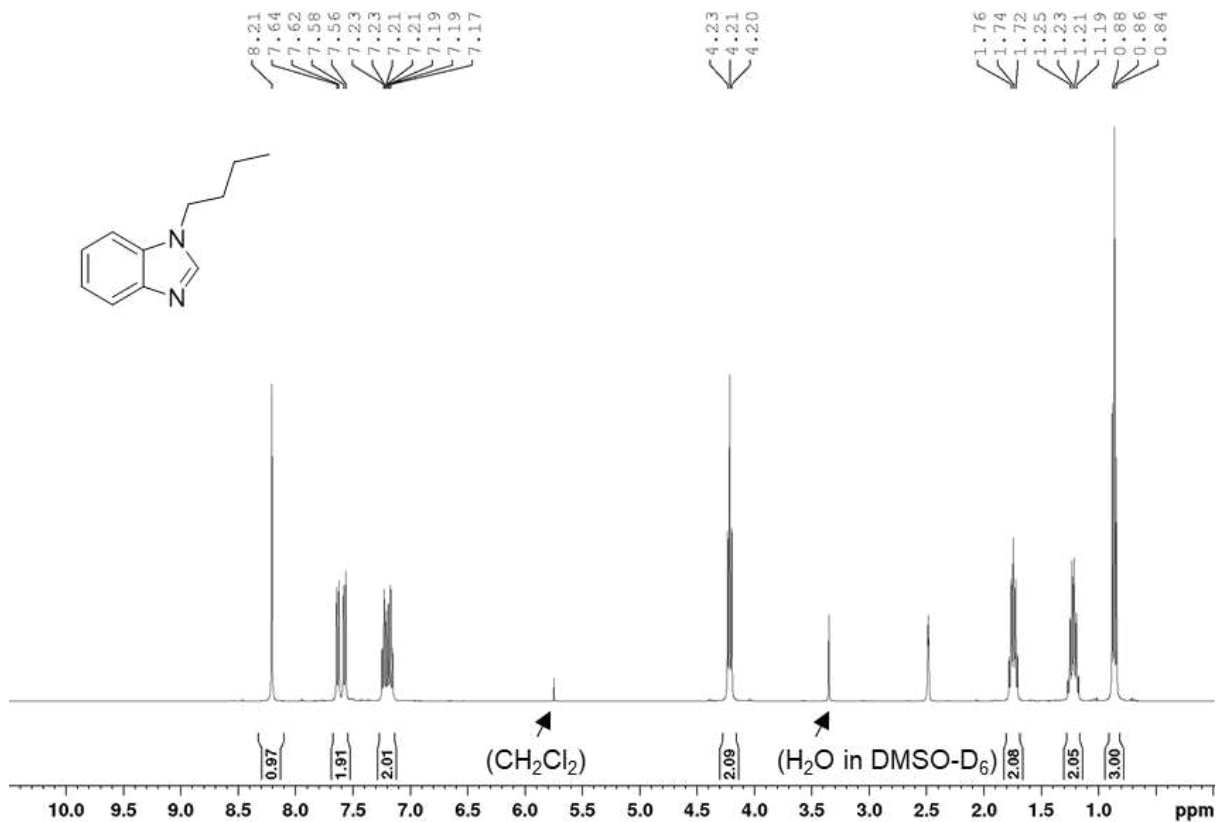


Figure S3.2. ¹H NMR (400 MHz, (CD₃)₂SO) spectrum of 1-*n*-butylbenzimidazole

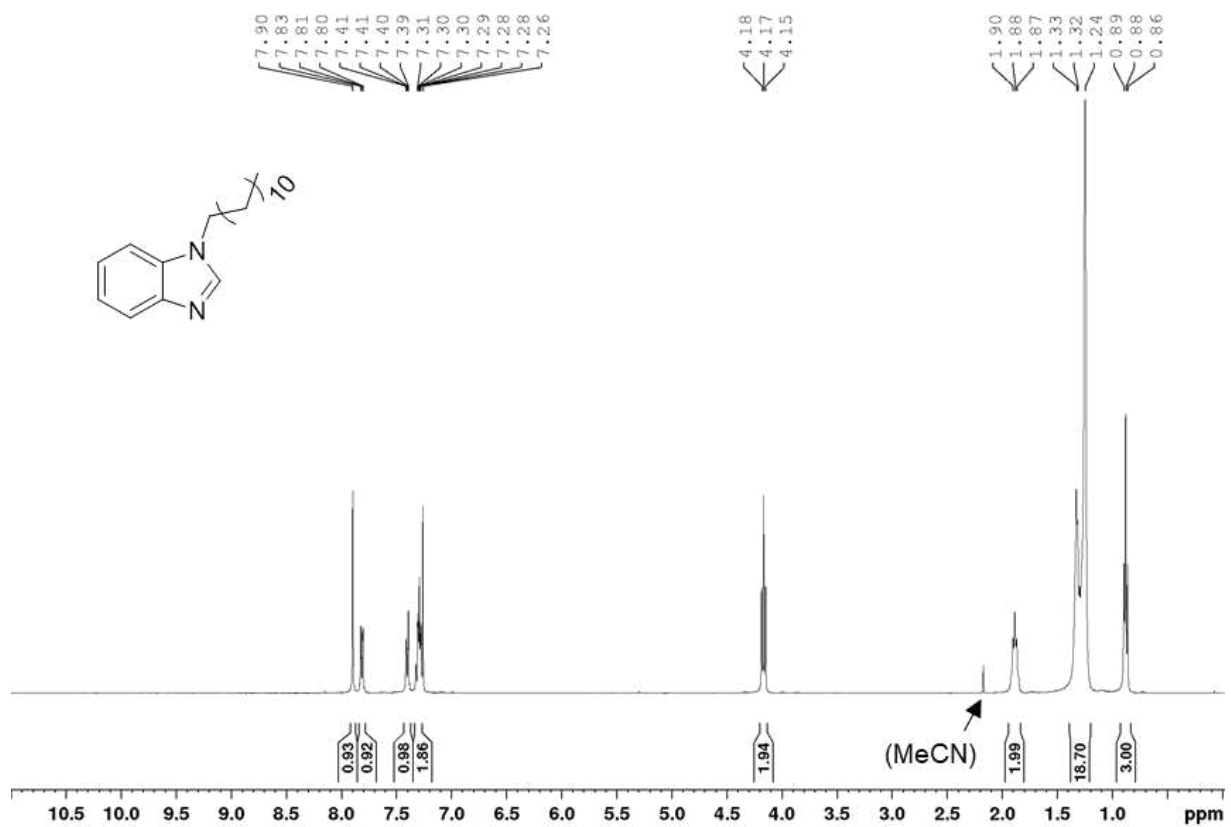


Figure S3.3. ¹H NMR (400 MHz, CDCl₃) spectrum of 1-dodecylbenzimidazole

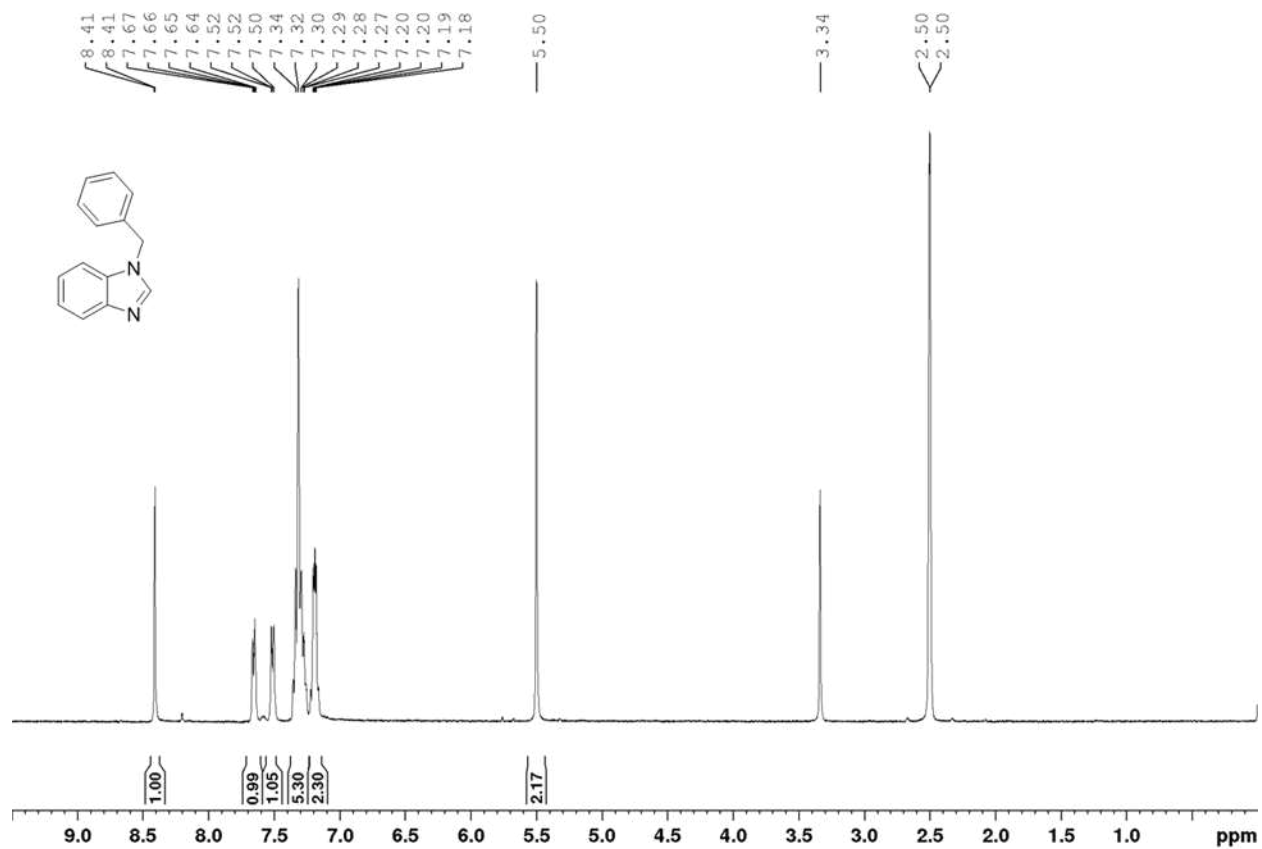


Figure S3.4. ¹H NMR (400 MHz, (CD₃)₂SO) spectrum of 1-benzylbenzimidazole

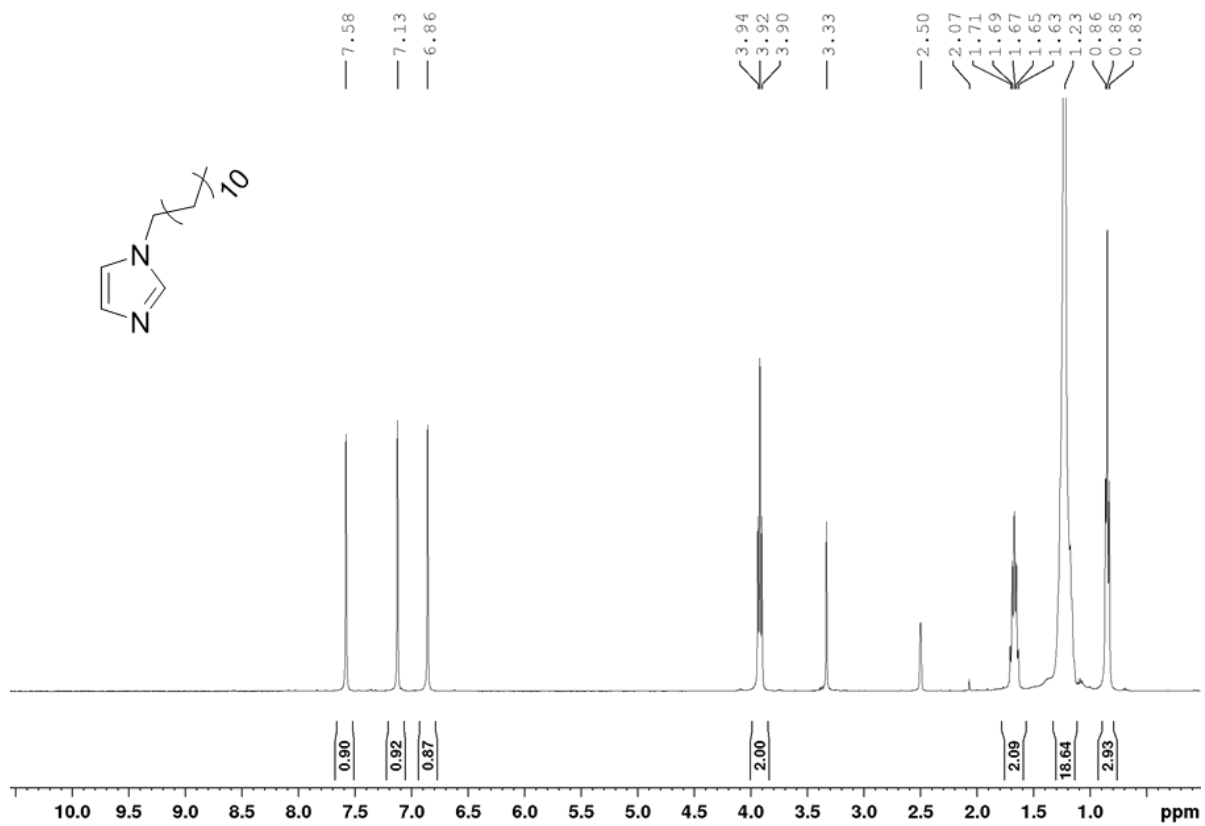


Figure S3.5. ¹H NMR (400 MHz, (CD₃)₂SO) spectrum of 1-dodecylimidazole

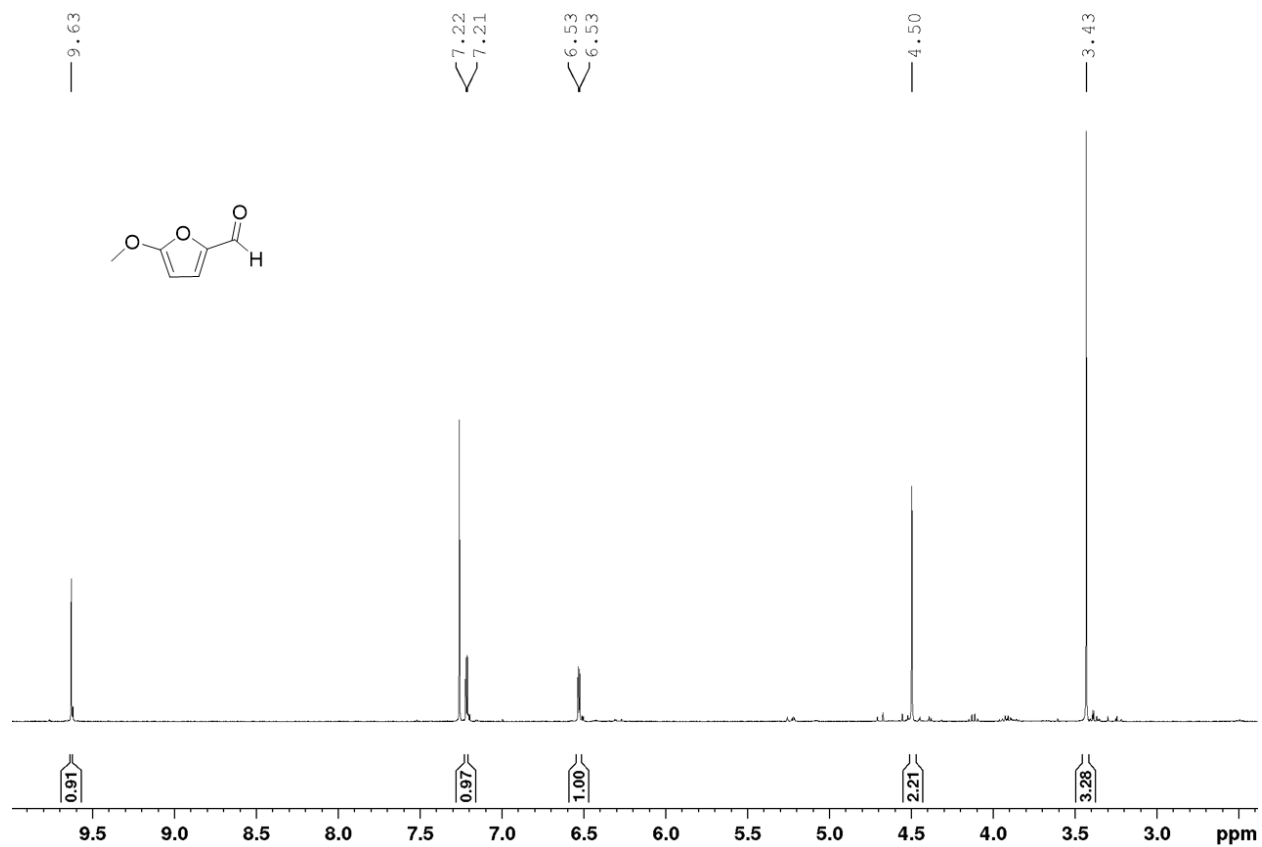


Figure S3.6. ¹H NMR of 5-methoxymethyl furfural

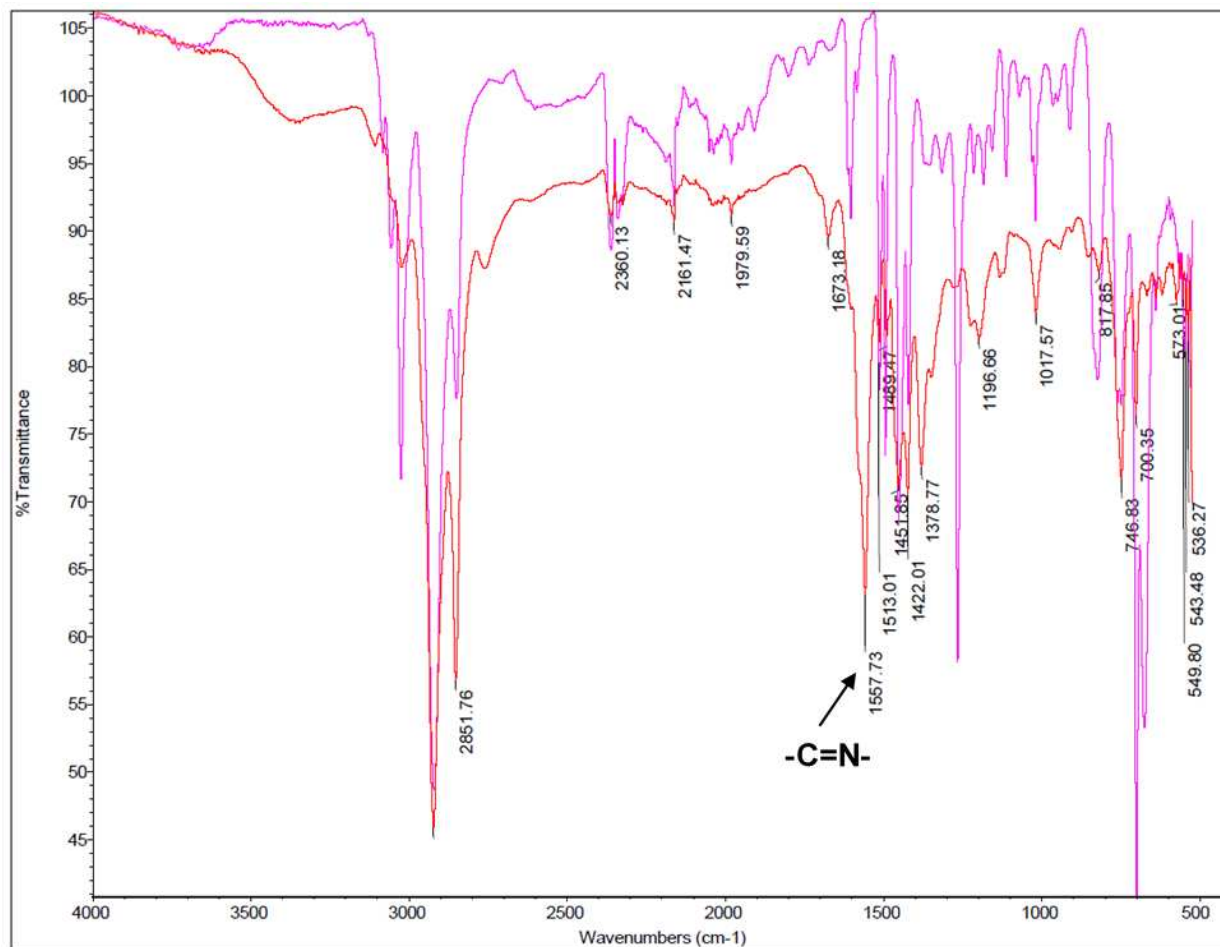


Figure S3.7. IR spectra of Merrifield's Peptide Resin (chloromethylated polystyrene, pink) and grafted PS-g-[BI]-C₁₂-OAc (red).

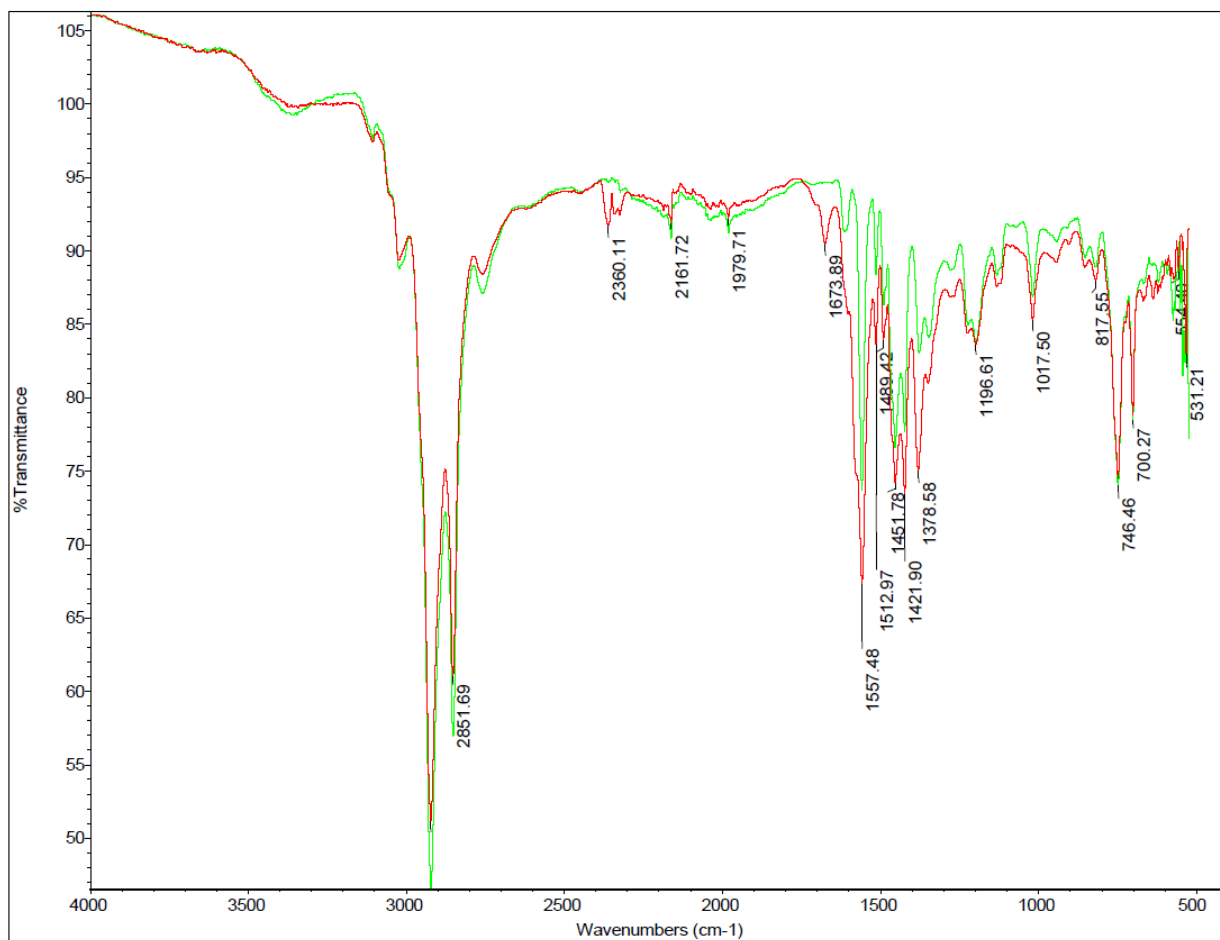


Figure S3.8. IR spectra of PS-g-[BI]-C₁₂-Cl (green) and PS-g-[BI]-C₁₂-OAc (red).

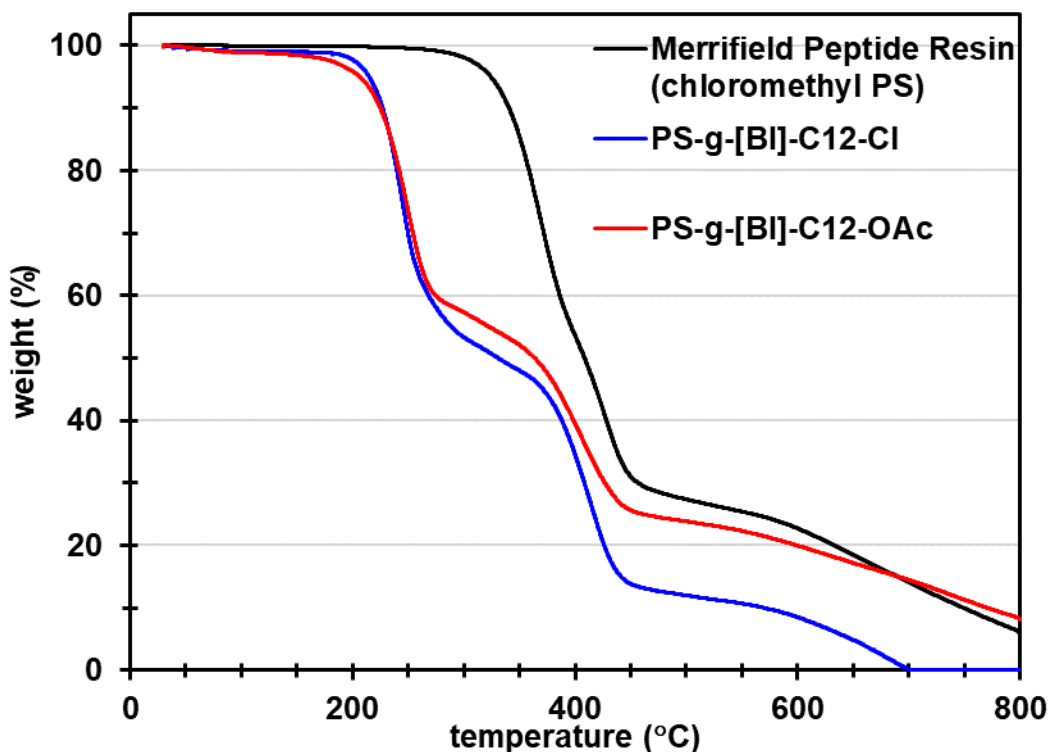


Figure S3.9. TGA Curves of bare resin and grafted species

Merrifield Peptide Resin (chloromethyl PS)

Onset decomposition (5% mass loss): 324.1 °C

PS-g-[BI]-C12-Cl:

Onset decomposition (5% mass loss): 214.9 °C

1st step: 138.9 to 326.1 °C; 48.5% mass lost

2nd step: 326.1 to 529.4 °C; 39.3% mass lost

PS-g-[BI]-C12-OAc:

Onset decomposition (5% mass loss): 206.7 °C

1st step: 115.0 to 316.4 °C; 43.2% mass lost

2nd step: 316.4 to 496.5 °C; 31.7% mass lost

- The 1st decomposition steps for chloride and acetate [BI] salts represent decomposition of the grafted [BI]-C₁₂ species; the 2nd step represents PS decomposition
- Approximately 13% more residue is left after the 2nd decomposition step for the salt bearing acetate anion than chloride anion

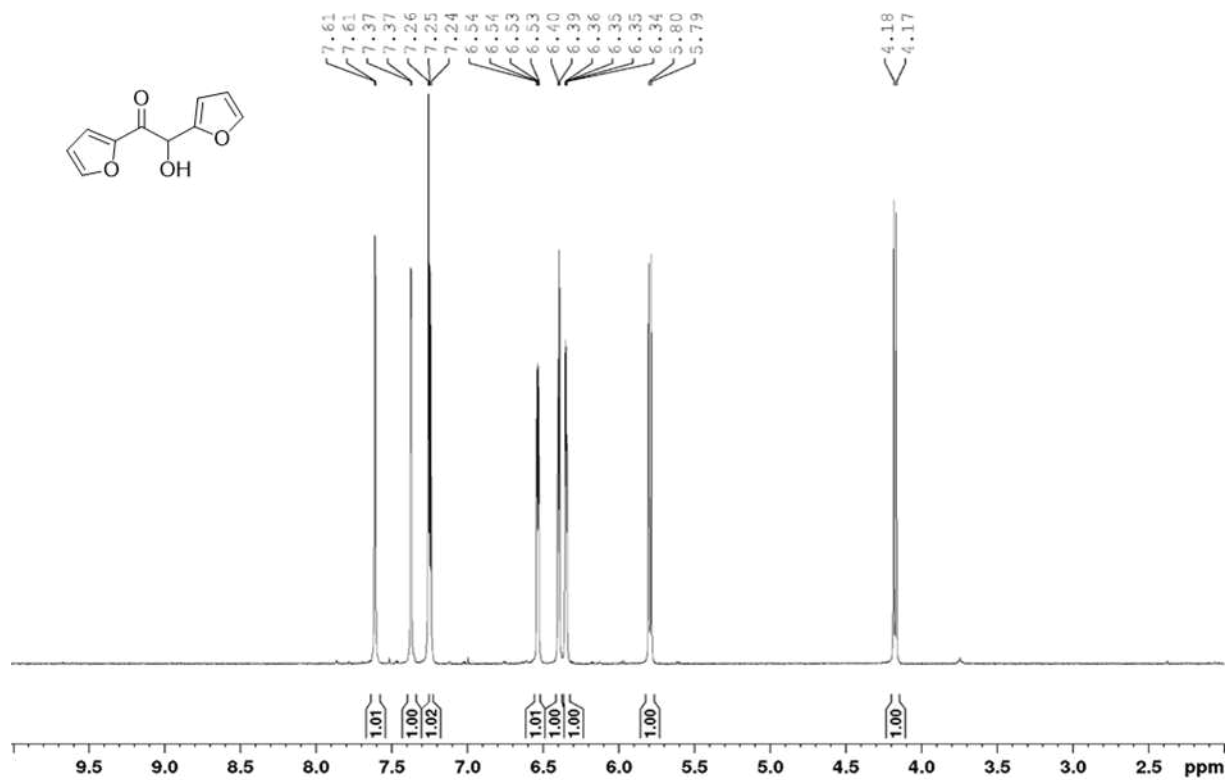


Figure S3.10. $^1\text{H NMR}$ (400 MHz, CDCl_3) spectrum of furoin product (isolated)

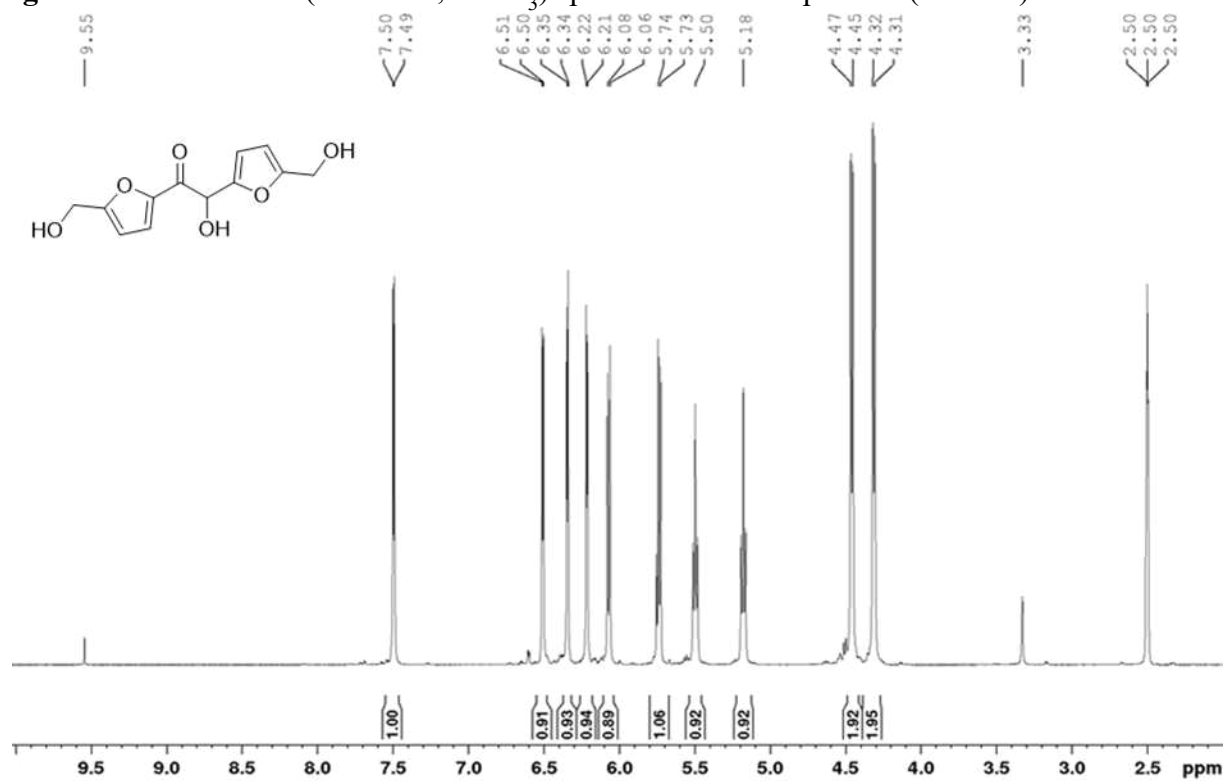


Figure S3.11. $^1\text{H NMR}$ (400 MHz, $(\text{CD}_3)_2\text{SO}$) spectrum of DHMF product (isolated)

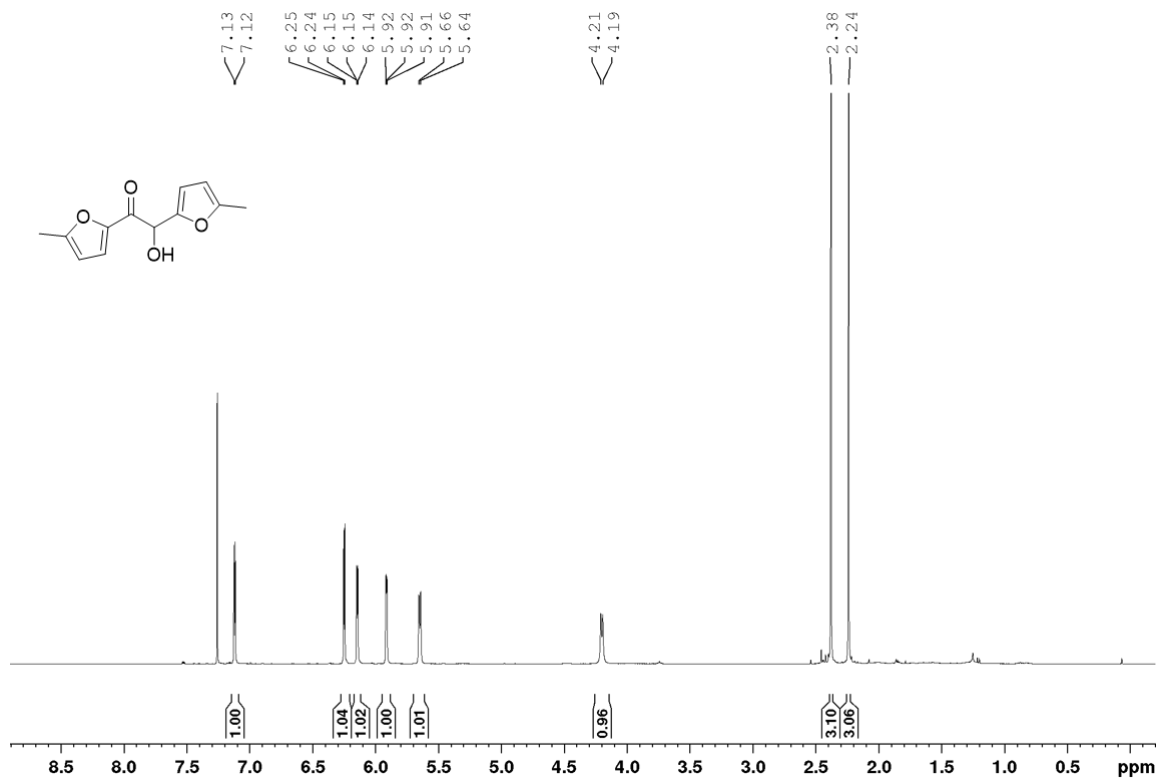


Figure S3.12. ¹H NMR (400 MHz, CDCl₃) spectrum of DMF product (isolated)

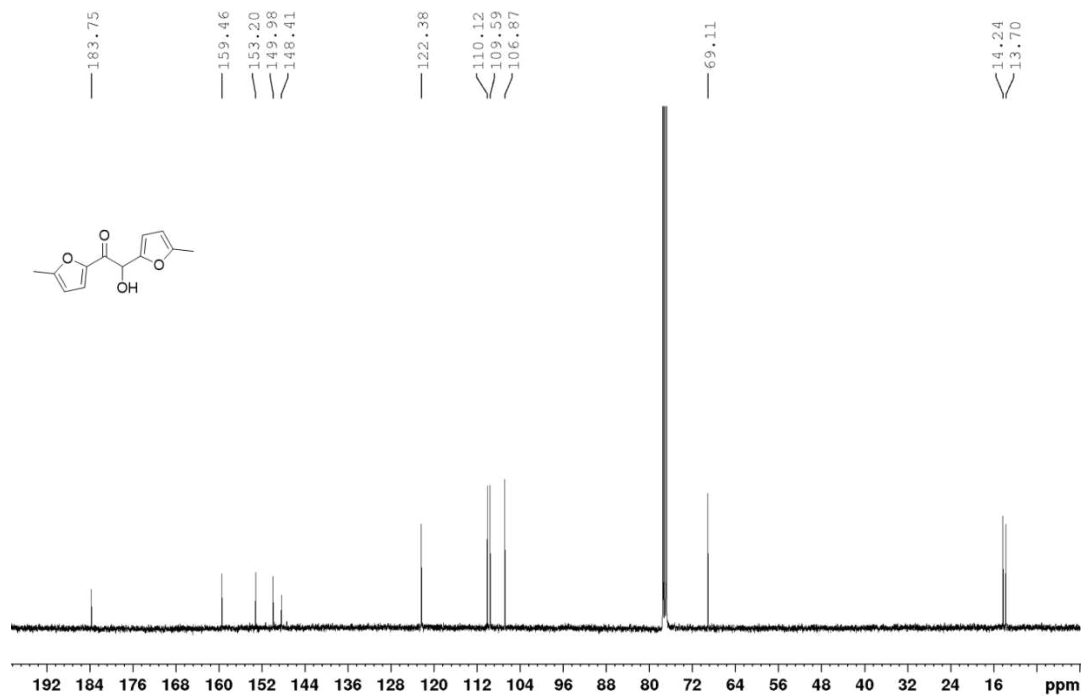


Figure S3.13. ¹³C NMR (400 MHz, CDCl₃) spectrum of DMF product (isolated)

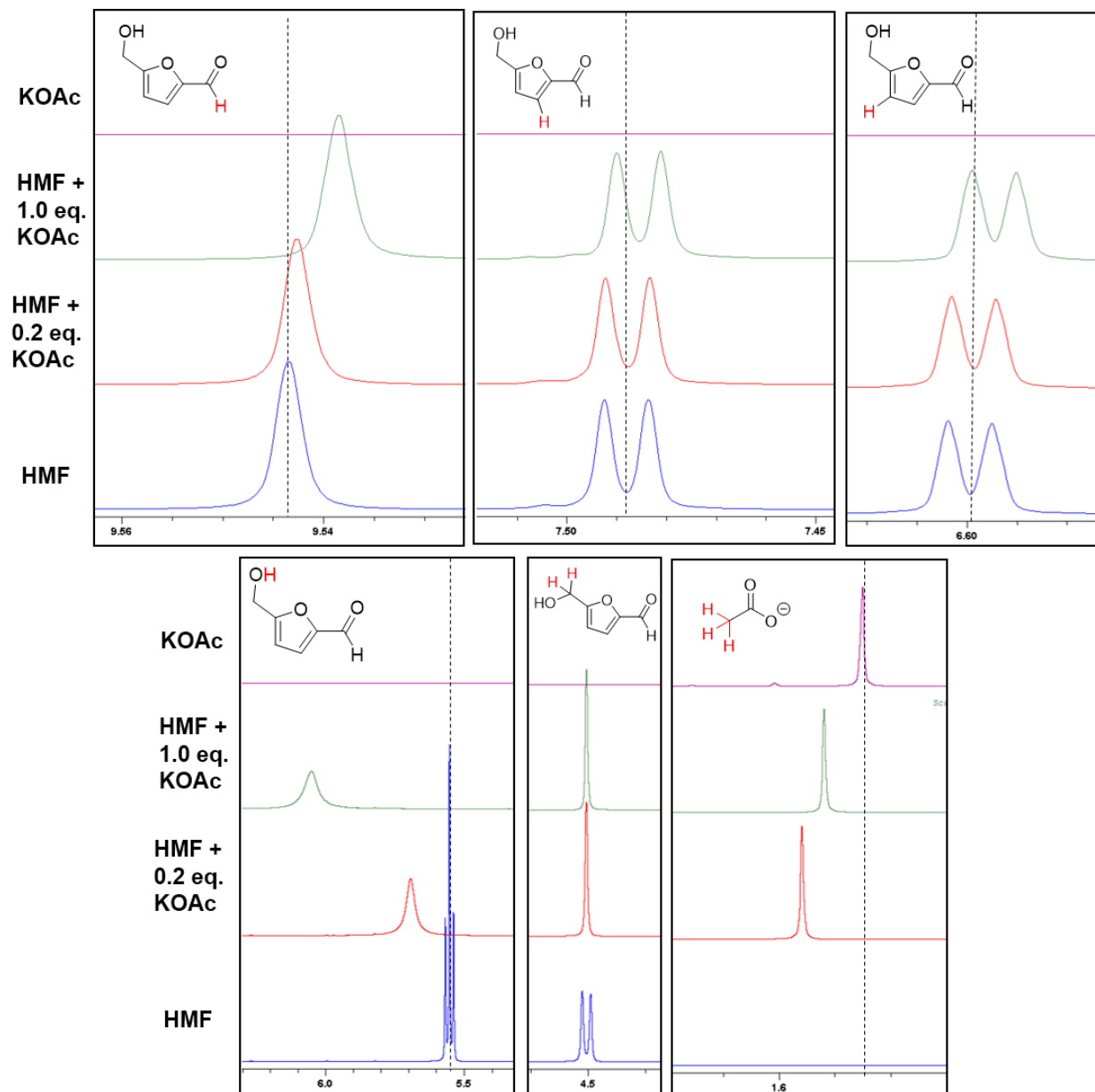


Figure S3.14. Interactions of acetate and alcohol in ^1H NMR (DMSO- d_6)

Table S3.7. ^1H NMR (DMSO- d_6) chemical shift changes of HMF-Acetate mixtures relative to HMF standard

HMF ^1H Chemical Shifts (ppm)					
	HMF	HMF + 0.2 eq KOAc	Δppm	HMF + 1.0 eq KOAc	Δppm
HMF-CHO	9.544	9.543	-0.001	9.539	-0.005
HMF-FuranH	7.488	7.488	-0.000	7.485	-0.003
HMF-FuranH	6.599	6.599	-0.000	6.595	-0.004
HMF-CH ₂	4.504	4.504	0.000	4.503	-0.001
HMF-OH	5.554	5.693	0.139	6.050	0.497

Δppm = ppm values observed in mixture – ppm values observed in standard

Table S3.8. ^1H NMR (DMSO- d_6) chemical shift changes of HMF-Acetate mixtures relative to KOAc standard

KOAc ^1H Chemical Shifts (ppm)					
	KOAc	HMF + 0.2 eq KOAc	Δppm	HMF + 1.0 eq KOAc	Δppm
KOCCH ₃	1.525	1.560	0.035	1.580	0.055
*H--OCCH ₃	-	12.4865	-	12.5292	-

*this new peak is close to baseline, integrates to <0.1%

Table S3.9. ^{13}C NMR (DMSO- d_6) chemical shift changes of HMF-Acetate mixtures relative to KOAc standard

KOAc ^{13}C Chemical Shifts (ppm)					
	KOAc	HMF + 0.2 eq KOAc	Δppm	HMF + 1.0 eq KOAc	Δppm
KOCCH ₃	26.30	not detected	-	25.78	-0.52
KOCCH ₃	172.95	not detected	-	173.31	0.36

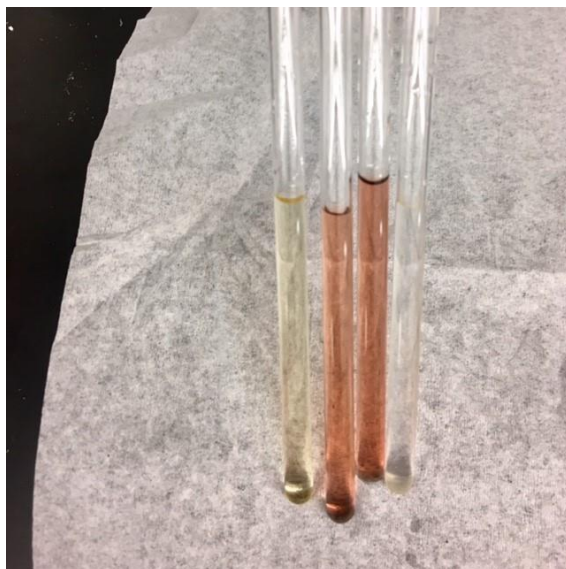


Figure S3.15. Color change of HMF-Acetate mixtures vs. standards in anhydrous $\text{DMSO-}d_6$.
Left to right: HMF only, HMF + 0.2 eq. acetate, HMF + 1.0 eq. acetate, KOAc only.

References

1. Quiroz-Florentino, H.; Aguilar, R.; Santoyo, B. M.; Díaz, F.; Tamariz, J., Total Syntheses of Natural Furan Derivatives Rehmanones A, B, and C. *Synthesis* **2008**, *2008*, 1023-1028.
2. Gupta, S.; Chatterjee, A.; Das, S.; Basu, B.; Das, B., Electrical Conductances of 1-Butyl-3-propylimidazolium Bromide and 1-Butyl-3-propylbenzimidazolium Bromide in Water, Methanol, and Acetonitrile at (308, 313, and 318) K at 0.1 MPa. *J. Chem. Eng. Data* **2013**, *58*, 1-6.
3. Wang, L.; Chen, E. Y. X., Recyclable Supported Carbene Catalysts for High-Yielding Self-Condensation of Furaldehydes into C10 and C12 Furoins. *ACS Catal.* **2015**, *5*, 6907-6917.
4. Liu, D.; Zhang, Y.; Chen, E. Y. X., Organocatalytic upgrading of the key biorefining building block by a catalytic ionic liquid and N-heterocyclic carbenes. *Green Chem.* **2012**, *14*, 2738-2746.
5. Mou, Z.; Feng, S.; Chen, E. Y. X., Bio-based difuranic polyol monomers and their derived linear and cross-linked polyurethanes. *Polym. Chem.* **2016**, *7*, 1593-1602.
6. Mou, Z.; Chen, E. Y. X., Polyesters and Poly(ester-urethane)s from Biobased Difuranic Polyols. *ACS Sus. Chem. Eng.* **2016**, *4*, 7118-7129.

Appendix B

Experimental Details and Supporting Information for Chapter 4

B.1. Materials and Methods

Materials. Air and moisture sensitive materials and syntheses were handled and performed in flame-dried Schlenk-type glassware on a dual-manifold Schlenk line or in an N₂-filled glovebox. High-performance liquid chromatography (HPLC)-grade organic solvents were first sparged extensively with nitrogen during filling of 20 L solvent reservoirs and then dried by passage through activated alumina (for THF), followed by passage through Q-5 supported copper catalyst stainless steel columns (for toluene). THF was further dried by stirring over sodium-potassium alloy for 24 h at room temperature followed by filtration and distillation under N₂; toluene was further dried by stirring with flame-activated CaH₂ for 24 hours followed by distillation under N₂. Anhydrous ethanol (Pharmco Aaper) was used as received and stored over activated 3Å molecular sieves. Benzyl alcohol (Sigma Aldrich), CDCl₃ (Cambridge Isotope Laboratories), and aniline (Alfa Aesar) were dried and distilled over CaH₂ before use. Thiourea and urea catalysts were synthesized and purified according to literature procedure;¹ cyclohexylamine (Alfa Aesar), phenylisocyanate (Beantown Chemical), phenylisothiocyanate (TCI), 3,5-bis(trifluoromethyl)phenyl isocyanate (TCI), 3,5-bis(trifluoromethyl)phenyl isothiocyanate (TCI), 3,5-bis(trifluoromethyl)aniline (Alfa Aesar), and 1,3-diisopropyl thiourea (Sigma Aldrich) were used as received, and 1,3-diphenyl urea (TCI) was recrystallized from ethyl acetate before use. NHC 1,3-isopropylimidazol-2-ylidene (IPr) was synthesized according to literature procedure.² L-Lactide (Sigma Aldrich) was purified by sublimation. Cyclohexene oxide (TCI), diethyl

malonate (Beantown Chemical), sodium ethoxide (Beantown Chemical), potassium hydroxide (Fisher), 1,3-dimesitylimidazol-2-ylidene (IMes, TCI), 1,3-di-*tert*-butylimidazol-2-ylidene (tBu, TCI), 2-*tert*-butylimino-2-diethylamino-1,3-dimethylperhydro-1,3,2-diazaphosphorine (BEMP, Sigma Aldrich), 1,8-diazabicyclo[5.4.0]undec-7-ene (DBU, Beantown Chemical), and potassium methoxide (KOMe 95%, Sigma Aldrich) were used as received. γ -Butyrolactone (Sigma Aldrich) was dried and distilled over CaH₂ and stored in the glovebox.

Methods. Absolute Molecular Weight Measurements. Polymer absolute weight-average molecular weight (M_w), number-average molecular weight (M_n), and dispersity indices ($D = M_w/M_n$) were measured via gel-permeation chromatography (GPC). The GPC instrument consisted of an Agilent HPLC system equipped with one guard column and two PLgel 5 μ m mixed-C gel permeation columns, coupled with Wyatt DAWN HELEOS II multi (18)-angle light scattering and Wyatt Optilab TrEX dRI detectors. The analysis was performed at 40 °C using chloroform as the eluent at a flow rate of 1.0 mL/min, using Wyatt ASTRA 7.1.2 molecular weight characterization software. The refractive index increments (dn/dc) of the linear and cyclic P(4,5-T6GBL) used were 0.0706 ± 0.0004 mL/g and 0.0718 ± 0.0014 mL/g, respectively, determined in a previous study.³ The AB block copolymer was analyzed by exact concentration in place of a dn/dc value.

Spectroscopic Characterizations. Low M_n samples were analyzed by matrix-assisted laser desorption/ionization time-of-flight mass spectroscopy (MALDI-TOF MS). An Ultraflex MALDI-TOF mass spectrometer (Bruker Daltonics) was operated in positive ion, reflector mode using a Nd:YAG laser at 355 nm and 25 kV accelerating voltage. A thin layer of a 1% NaI solution was first deposited on the target plate, followed by a mixture of 10 μ L sample and matrix (dithranol, 20mg/mL in MeOH, 10% AAC). External calibration was done using a peptide

calibration mixture (4 to 6 peptides) on the same sample plate. The raw data was processed using mMass software.

NMR spectra were recorded on a Bruker 400 MHz (FT 400 MHz, ^1H ; 100 MHz, ^{13}C). Chemical shifts were referenced to internal solvent resonances and reported as parts per million relative to SiMe_4 .

Thermal Analysis. Decomposition onset temperatures (T_d) and maximum rate decomposition temperatures (T_{max}) of the polymers were measured by thermal gravimetric analysis (TGA) on a Q50TGA Analyzer, TA Instrument. Polymer samples were heated from room temperatures to 700 °C at a heating rate of 10 °C/min. Values of T_{max} were obtained from derivative (wt %/°C) vs. temperature (°C) plots and defined by the peak maximum, while T_d values were obtained from wt% vs. temperature (°C) plots and defined by the temperature of 5% weight loss. The glass-transition temperature (T_g) of purified and thoroughly dried polymer samples were measured by differential scanning calorimetry (DSC) on an Auto Q20, TA Instrument. All T_g values were obtained from a second scan (10 °C/min) after the thermal history was removed by the first scan (10 °C/min).

Mechanical Analysis. Dynamic mechanical analysis (DMA) was performed on a TA Instruments DMA Q800 operating in tension film mode at a strain of 0.10% and frequency of 1 Hz. Thin film samples (approx. dimensions L x W x D = 30 mm x 13 mm x 0.6 mm) were placed in the clamps and heated from -40 °C through material failure at 3 °C/min. Tensile testing was performed on an Instron 5966 tensiometer with a 10 kN load cell and 5 mm/min strain rate.

Preparation of Monomer 4,5-T6GBL. The literature procedure⁴ was modified for the preparation of 4,5-T6GBL. To a 1 L, 3-neck flask equipped with a stir bar, addition funnel, and reflux condenser was added 14.8 g (218 mmol, 1.09 equiv.) sodium ethoxide and 160 mL

anhydrous ethanol under a nitrogen atmosphere. The mixture was stirred vigorously for 1 h to completely dissolve ethoxide. Diethyl malonate (31.9 mL, 210 mmol, 1.05 equiv.) was added to the addition funnel via syringe, dripped into the reaction flask over 30 min and stirred another 90 min to ensure complete enolate formation. Cyclohexene oxide (20.2 mL, 200 mmol, 1 equiv.) was then added to the addition funnel via syringe and dripped in over 15 min. The temperature was raised to 70 °C and the mixture solidified after approximately 30 min. Stirring was turned off and the reaction was heated for 3 h. After cooling to room temperature, 320 mL DI H₂O was added in portions to dissolve the solid, followed by 45.2 g KOH (80.5 mmol, 3.5 equiv. considering 85% KOH purity). Ethanol was completely removed via azeotropic distillation and the hydrolysis refluxed overnight. After cooling, the basic mixture was stirred vigorously with 250 mL ether for 1-1.5 h, ensuring interfacial mixing. The layers were separated with a separatory funnel and the extraction process was repeated. The aqueous layer was acidified to pH 1-2 with concentrated HCl and extracted with ethyl acetate (4 x 250 mL). The combined organic layer was washed with brine, dried over Na₂SO₄, and solvent was evaporated to yield the carboxylic acid. The isolated carboxylic acid was decarboxylated by heating to 185 °C under reflux until CO₂ evolution ceased (approx. 2 h), with distillation of acetic acid byproduct and residual solvents. The temperature was raised to 205 °C for 5 min before distilling under vacuum to yield 55% 4,5-T6GBL over 3 steps. Vacuum distillation from CaH₂ (b.p. 62-65 °C at 75 mTorr) was performed to yield polymerization-grade monomer (Figure S4.1).

General Polymerization Procedures. Polymerizations were performed inside a nitrogen-filled glovebox at ambient temperature unless otherwise noted. In a typical polymerization, catalysts were measured directly into a 5 mL glass vial equipped with a micro stir bar, followed by the monomer. This mixture was stirred until homogenous and the polymerization was initiated by

addition of benzyl alcohol (BnOH) via auto pipettor (for the initial (T)U screening) or a glass syringe (for all other runs). For polymerizations employing KOMe, a stock solution of (T)U and KOMe was prepared; for neat conditions, solvent was removed from the stock solution aliquot *in vacuo* before monomer was added. For the runs performed in air (Table S4.2, run 1-AIR-A and B), all reagents were measured outside the glovebox. Aliquots were taken at given time *t* from the reaction and quenched with benzoic acid (~5 mg) in 0.6 ml CDCl₃ to determine conversion by ¹H NMR. After a desired time period, the polymerization was quenched by the addition of excess benzoic acid (~25 mg) in CHCl₃ (~3 mL). After agitation, the dissolved polymer was precipitated into cold methanol (50 mL for 2 mmol scale polymerizations) and allowed to settle for 24 h before filtration and washing with cold MeOH. Polymers were dried in a vacuum oven at 50-60 °C for 24 h; samples used for thermal analysis and depolymerization experiments were further purified by dissolving in CHCl₃ and re-precipitating into cold MeOH, followed by filtration and drying in the vacuum oven at 60 °C for 24 h.

Polymerization of 4,5-T6GBL with (T)U/Base/ROH (Table S4.2, Entry 1). To a 5 mL vial containing a stir bar was added 3.9 mg Di^{*i*}PrTU (0.05 mmol) and 7.4 mg IMes (0.05 mmol), followed by 0.272 g (1.94 mmol) monomer. The mixture was stirred until homogeneous (5-10 min), then 1.0 μl (9.7 μmol) BnOH was injected to initiate the polymerization.

Polymerization of 4,5-T6GBL with TU/KOMe (Table 4.3, Entry 1). A stock solution was made with 10.0 mg (0.143 mmol) KOMe, 68.6 mg (0.428 mmol) Di^{*i*}PrTU and 1.0 mL THF. To a separate vial equipped with a stir bar and Teflon-lined cap, 0.280 g (2.0 mmol) 4,5-T6GBL was added. To stirred monomer was added 140 μL stock solution to initiate the polymerization.

Polymerization of 4,5-T6GBL with NHC (Table 4.4, Entry 2). To a 5 mL vial containing a stir bar was added 7.2 mg (0.04 mmol) *i*Bu, followed by 280.4 mg (2.00 mmol) 4,5-T6GBL. The reaction stirred until gelation and was quenched after 24 h.

Synthesis of Block Copolymer. To a 5 mL vial containing a stir bar was added 7.8 mg TU-3, 14.8 mg IMes, 0.272 g 4,5-T6GBL, and 145 μ L THF. After all solids were dissolved, the polymerization was initiated by injection of 1.0 μ L BnOH. After 4 h, an aliquot was removed for NMR and GPC analysis. A solution of 0.280 g lactide in 500 μ L THF was added with vigorous stirring and quenched after 10 min.

Depolymerization Procedure. Inside the N₂-filled glovebox, a 10 mL thick-walled pressure reactor was loaded with 55 mg polymer sample and aliquot (1 mL) of catalyst in toluene (10.9 mg/mL). The sealed reactor was removed from the glovebox and heated at 120 °C for 24 h. The reactor was cooled slightly before being opened and quenched with benzoic acid while hot. When monitored for conversion over time, 100 mg polymer sample and a pressure vessel equipped with a sidearm were used.

Synthesis of Random Copolymers with GBL (Table 4.4, Entry 3). To a 5 mL vial containing a stir bar was added 5.6 mg Di^{*i*}PrTU (0.035 mmol) and 10.6 mg IMes (0.035 mmol), followed by 74.6 mg (2.20 mmol) GBL and 364 mg 4,5-T6GBL (2.60 mmol). The mixture was stirred until homogeneous (5-10 min), then 0.9 μ L (0.009 mmol) BnOH was injected to initiate the polymerization.

Preparation of P(4,5-T6GBL) Thin Film and Dog Bone Specimens. A Carver compression molder was used to hot press polymer samples. For thin films, a thin stainless steel rectangular mold (0.6 mm thickness) containing 1.8 g polymer sample was placed between aluminum plates lined with PTFE sheets. The mold assembly was placed in the hot press and heated to ~100 °C for

~10 min under 5,000 psi pressure and allowed to cool slowly under pressure. Rectangular films were cut with sharp blades. For dog-bone specimens, a stainless steel rectangular mold (1 mm thick) was filled with 5.4 g polymer and pressed under the same conditions as films. A Qualitest ASTM type V cutting die and manual clicker press was used to cut out dog-bone shaped specimens.

B.2.

Table S4.1. Enthalpy (ΔH_p°) and entropy (ΔS_p°) of polymerization for various lactone monomers⁵⁻⁷

Monomer	Ring Size	ΔH_p° (kJ mol ⁻¹)	ΔS_p° (J mol ⁻¹ K ⁻¹)
β -propiolactone	4	-75	-55
γ -butyrolactone	5	-5.4	-40
3,4-T6GBL	5+6	-20	-75
4,5-T6GBL	5+6	-18	-65
δ -valerolactone	6	-27	-65
L-Lactide	6	-29	-41
ϵ -caprolactone	7	-14	-10

Table S4.2. Detailed results of initial (T)U/organic base screening

Entry	Catalyst(s)	Time (h) (gel)	Conv. (%) ^a	M_n , GPC (kg/mol) ^b	M_n , theor (kg/mol) ^c	\mathcal{D} (M_w/M_n) ^b
1	TU-3/IMes	(1 min) 24	(53) 83	10.8	11.7	1.11
1-AIR-A	TU-3/IMes	(5 min) 6.5	(53) 76	11.7	10.7	1.07
1-AIR-B	TU-3/IMes	(5 min) 7	(51) 78	11.2	11.0	1.05
2	TU-3/BEMP	(18) 40	(60) 70	8.22	9.92	1.04
3	TU-3/DBU	110	6	-	-	-
4	U-3/ IMes	(1 min) 24	(63) 81	9.50	11.5	1.12
5	U-3/ BEMP	(2) 24	(75) 82	10.1	11.6	1.09
6	U-3/ DBU	96	20	3.56	2.91	1.40
7	TU-2/IMes	(24) 48	(57) 67	9.06	9.50	1.08
8	TU-2/BEMP	(48) 72	(58) 61	7.70	8.66	1.04
9	TU-2/DBU	110	13	-	-	-
10	U-2/IMes	(3) 24	(50) 80	10.2	11.3	1.11
11	U-2/BEMP	(3.5) 24	(69) 81	9.74	11.5	1.10
12	U-2/DBU	(24) 48	(53) 68	7.08	9.64	1.08
13	U-1/IMes	(24) 72	(42) 65	5.88	9.22	1.08
14	U-1/BEMP	(24) 72	(46) 69	7.45	9.78	1.07
15	U-1/DBU	(24) 72	(55) 73	8.14	10.3	1.08
16	TU-1/IMes	96	8	-	-	-
17	TU-1/BEMP	96	6	-	-	-
18	TU-1/DBU	96	14	-	-	-

All polymerizations performed inside N₂-filled glovebox (except 1-AIR) at room temperature with 2 mmol monomer, no solvent and [M]/[(T)U]/[Base]/[I] = 100/2.5/2.5/1; I = BnOH. ^a Monomer conversion determined by ¹H NMR in CDCl₃. ^b M_n and \mathcal{D} values determined by GPC at 40 °C in CHCl₃. ^c Calculated based on: ([M]₀/[I]₀) × Conv.% × (molecular weight of 4,5-T6GBL) + (molecular weight of I).

Table S4.3. Controls without (T)U

Entry	Base	[M]/[B]/[I]	Time (h)	Conv. (%) ^a
1	IMes	100/2.5/1	96	20%
2	BEMP	100/2.5/1	96	0%
3	DBU	100/2.5/1	96	0%

All polymerizations performed inside N₂-filled glovebox at room temperature with 2 mmol monomer, no solvent, and I = BnOH. ^a Monomer conversion determined by ¹H NMR in CDCl₃

Table S4.4. Higher DP trials with U-3/IMes

Entry	[M]/[U-3]/[IMes]/[I]	Time (h) (gel)	Conv. (%) ^a	<i>M</i> _{n, GPC} (kg/mol) ^b	<i>M</i> _{n, theor} (kg/mol) ^c	<i>D</i> (<i>M</i> _w / <i>M</i> _n) ^b	<i>I</i> [*] (%) ^d
1	200/1/1/1	(1 h) 24	(47) 71	8.93	19.9	1.06	223
2	200/2.5/2.5/1	(7 min) 24	(55) 83	13.0	23.4	1.11	180
3	200/5/5/1	(0 min) 24	(58) 88	13.8	25.3	1.18	183
4	500/2.5/2.5/1	(20 min) 24	(41) 71	19.0	50.7	1.07	267

All polymerizations performed inside N₂-filled glovebox at room temperature with 2 mmol monomer, no solvent and I = BnOH. ^a Monomer conversion determined by ¹H NMR in CDCl₃. ^b *M*_n and *D* values determined by GPC at 40 °C in CHCl₃. ^c Calculated based on: ([M]₀/[I]₀) × Conv.% × (molecular weight of 4,5-T6GBL) + (molecular weight of I), using exact equivalents of monomer measured. ^d *I*^{*} = (*M*_{n, theor} / *M*_{n, GPC}) × 100

Table S4.5. Organocatalytic depolymerization of P(4,5-T6GBL)

Run	Catalyst	Cat. Loading (mol%)	Solvent	Temp. (°C)	Time (h)	Conv. (%) ^a
1	<i>t</i> Bu	2	Tol 0.4 M	120	24	0
2	TU-3/IMes	2	Tol 0.4 M	120	24	8
3	TBD	2	Tol 0.4 M	120	24	100
4	TBD	2	THF 0.4 M	80	24	50
5	TBD	1	Tol 1.0 M	120	10	96

^a Polymer conversion determined by ¹H NMR in CDCl₃.

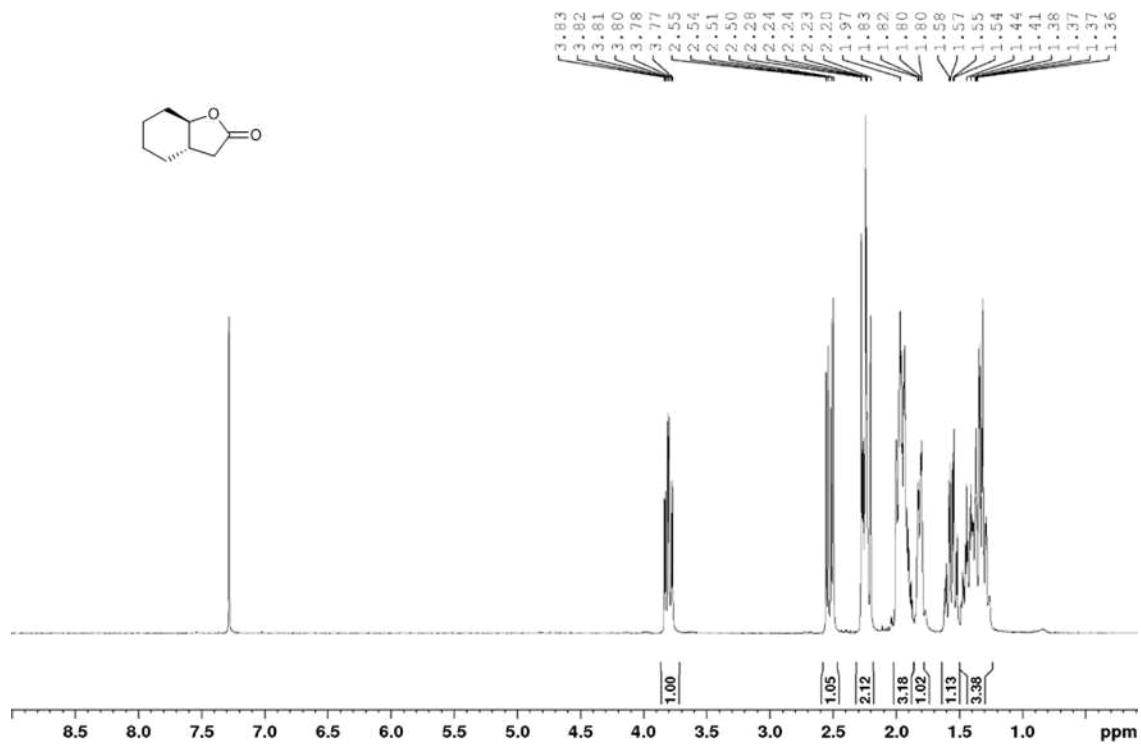


Figure S4.1. ^1H NMR (CDCl_3 , 25 $^\circ\text{C}$) spectrum of 4,5-T6GBL.

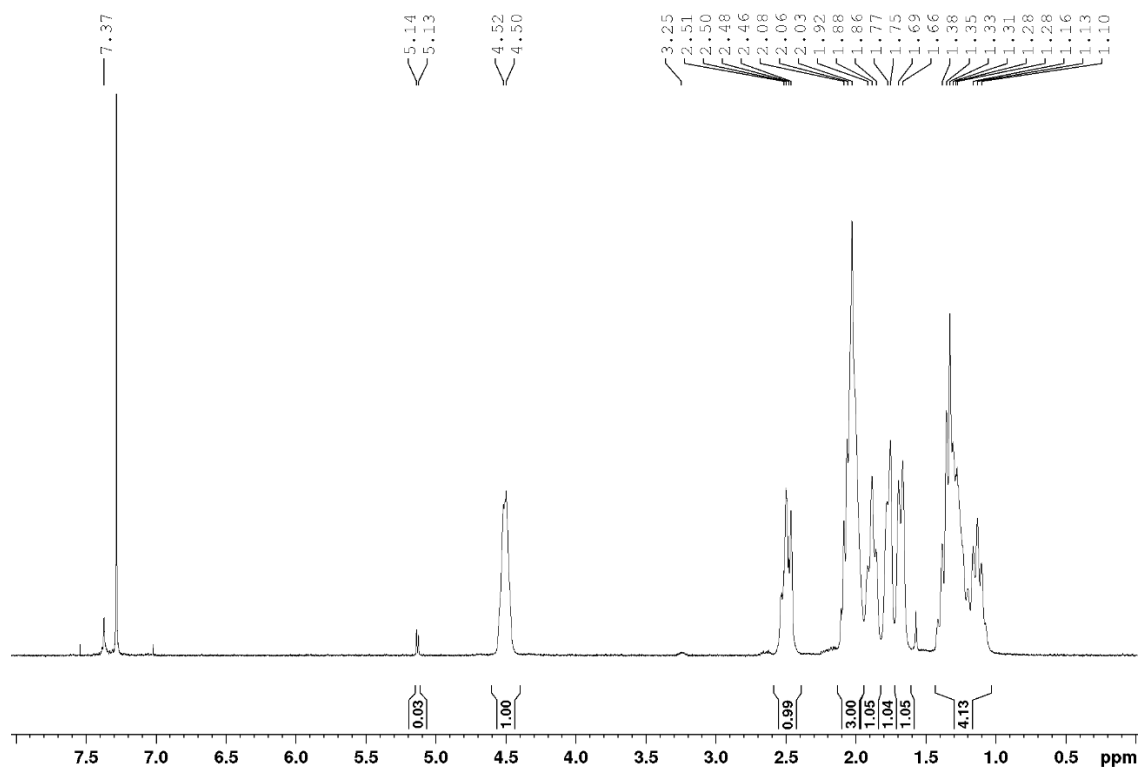


Figure S4.2. ^1H NMR (CDCl_3 , 25 $^\circ\text{C}$) spectrum of linear P(4,5-T6GBL) obtained by $[\text{M}]/[\text{U-3}]/[\text{IMes}]/[\text{BnOH}] = 100/2.5/2.5/1$.

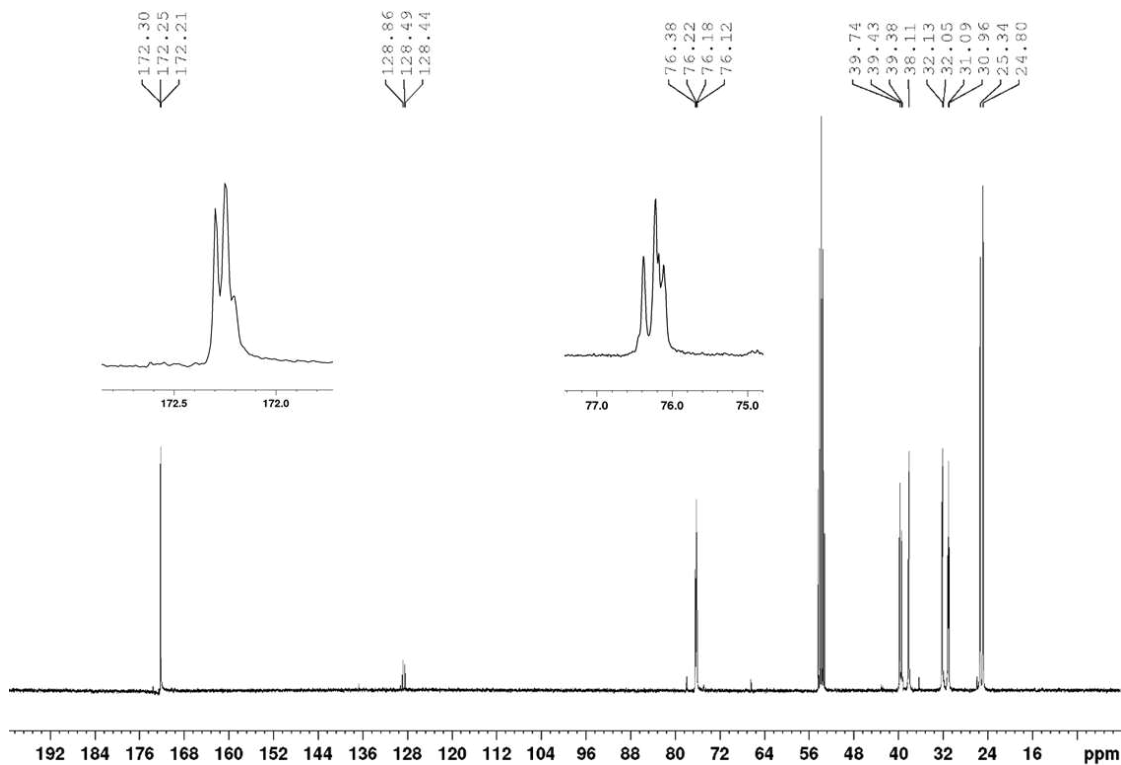


Figure S4.3. ^{13}C NMR (CD_2Cl_2 , $25\text{ }^\circ\text{C}$) spectrum of linear P(4,5-T6GBL) obtained by $[\text{M}]/[\text{U-3}]/[\text{IMes}]/[\text{BnOH}] = 100/2.5/2.5/1$.

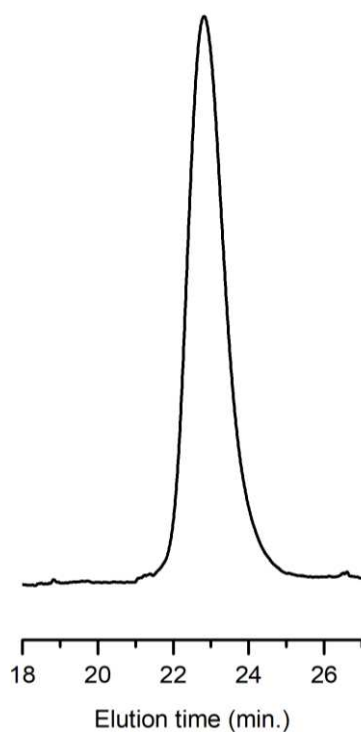


Figure S4.4. GPC trace of linear P(4,5-T6GBL) prepared by $[M]/[U-3]/[IMes]/[BnOH] = 100/2.5/2.5/1$, $M_n = 10.1$ kDa, $D = 1.09$.

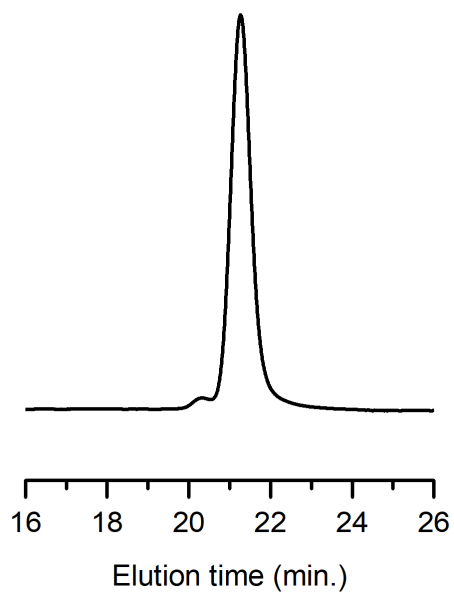


Figure S4.5. GPC trace of linear P(4,5-T6GBL) prepared by $[M]/[TU-3]/[IMes]/[BnOH] = 500/5/5/1$, $M_n = 39.5$ kDa, $D = 1.03$.

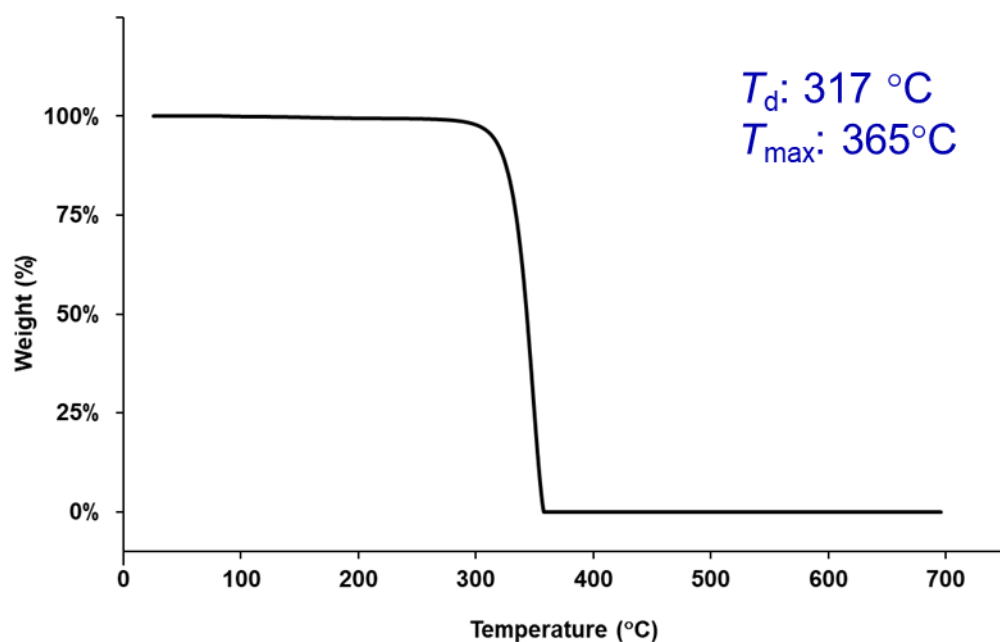


Figure S4.6. TGA curve of P(4,5-T6GBL) obtained by $[M]/[TU-3]/[IMes]/[Ph_2CHCH_2OH] = 200/5/5/1$, $M_n = 21.5$ kDa, $D = 1.03$.

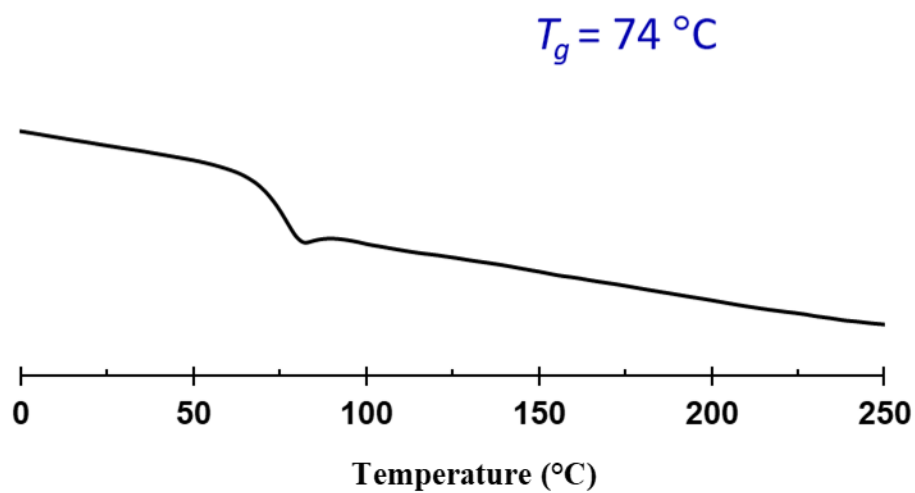


Figure S4.7. DSC curve of P(4,5-T6GBL) obtained by $[M]/[TU-3]/[KOME] = 250/3/1$, $M_n = 90$ kDa, $D = 1.07$.

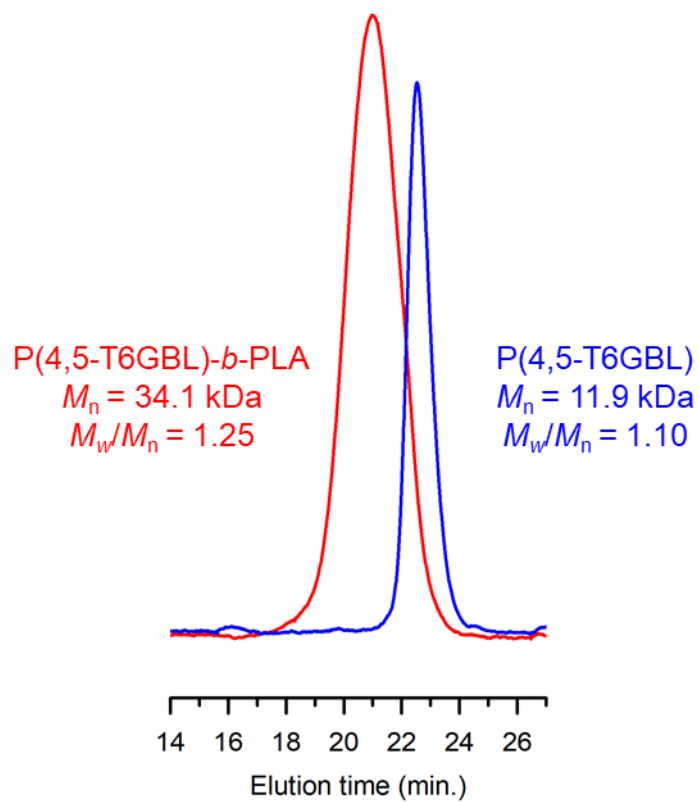


Figure S4.8. GPC traces of linear P(4,5-T6GBL) before and after chain extension via block copolymerization.

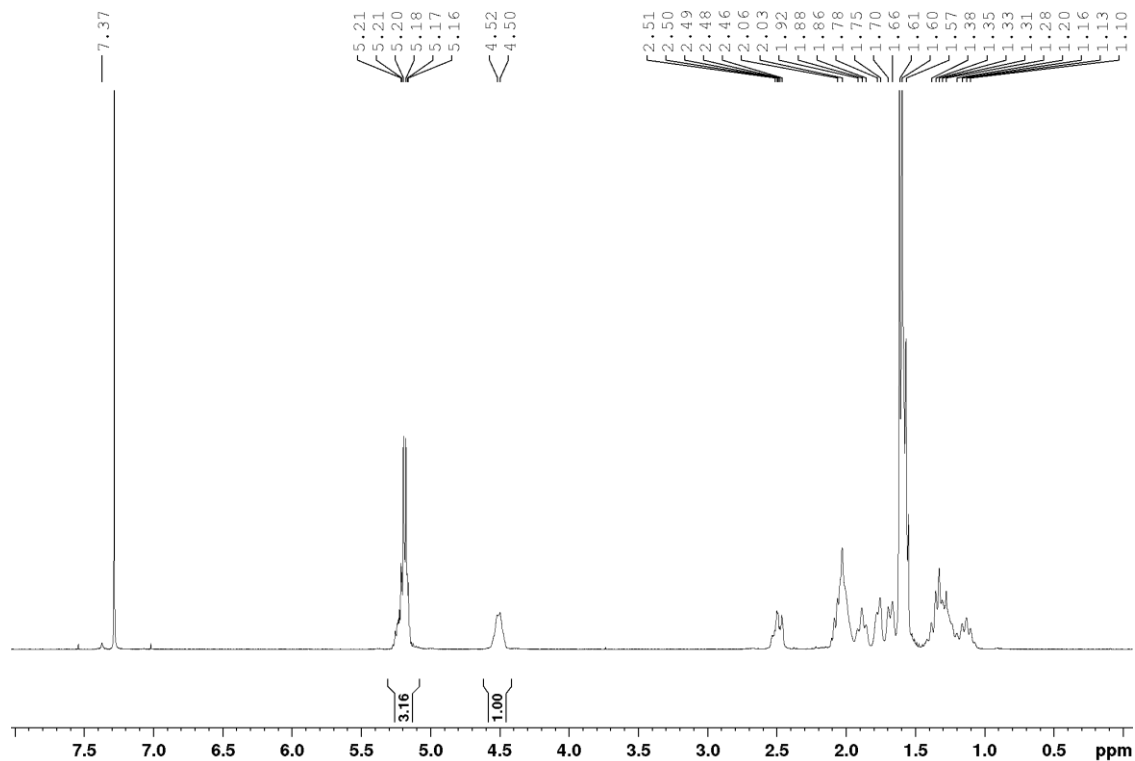


Figure S4.9. ^1H NMR (CD_2Cl_2 , 25 $^\circ\text{C}$) spectrum of isolated P(4,5-T6GBL)-*co*-PLA.

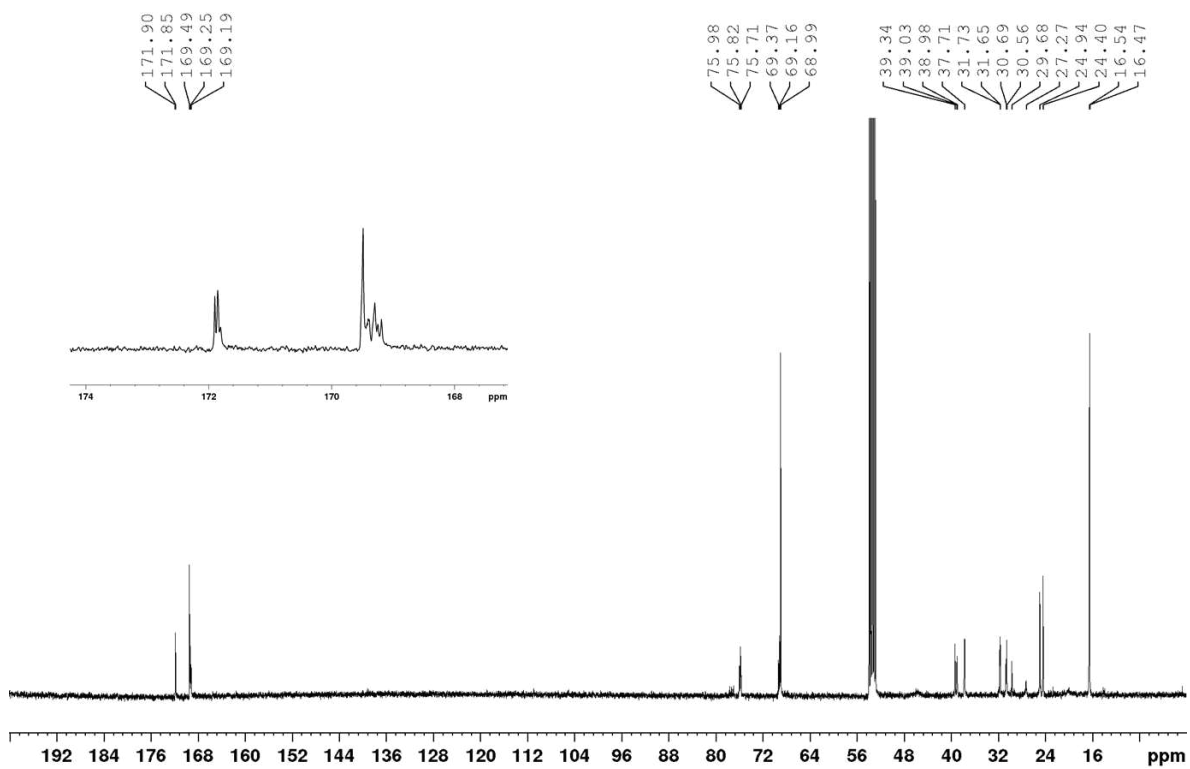


Figure S4.10. ^{13}C NMR (CDCl_3 , 25 $^\circ\text{C}$) spectrum of isolated P(4,5-T6GBL)-*co*-PLA.

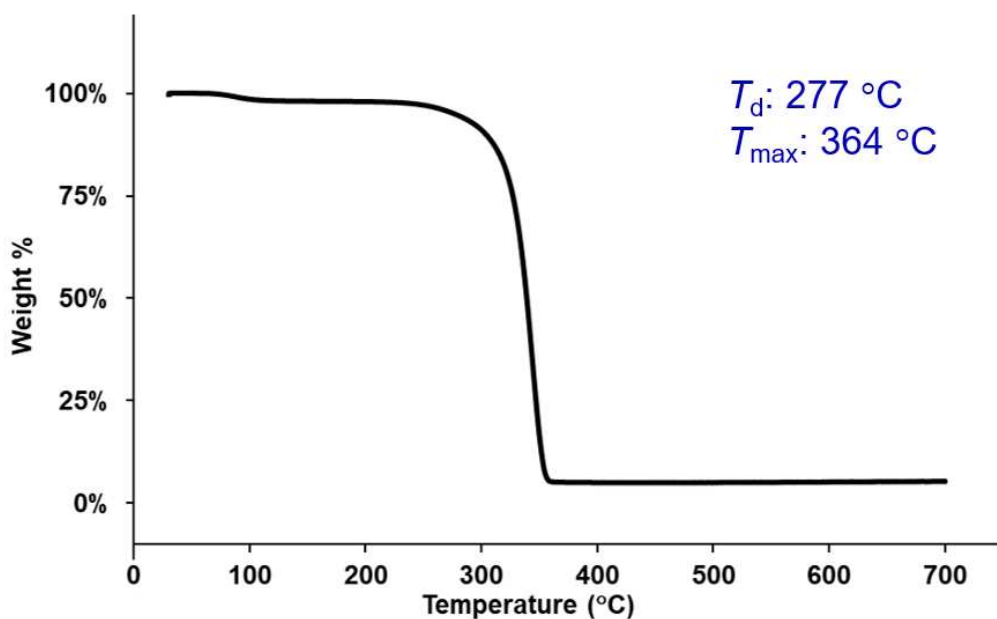


Figure S4.11. TGA curve of P(4,5-T6GBL)-*co*-PLA, $M_n = 34.1$ kDa, $D = 1.25$.

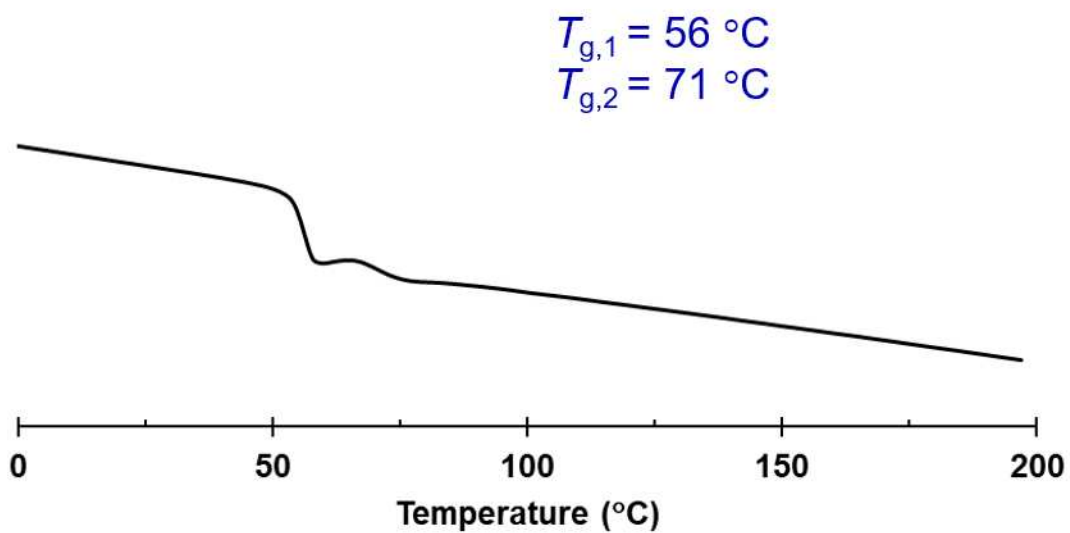


Figure S4.12. DSC curve of P(4,5-T6GBL)-*co*-P(LA).

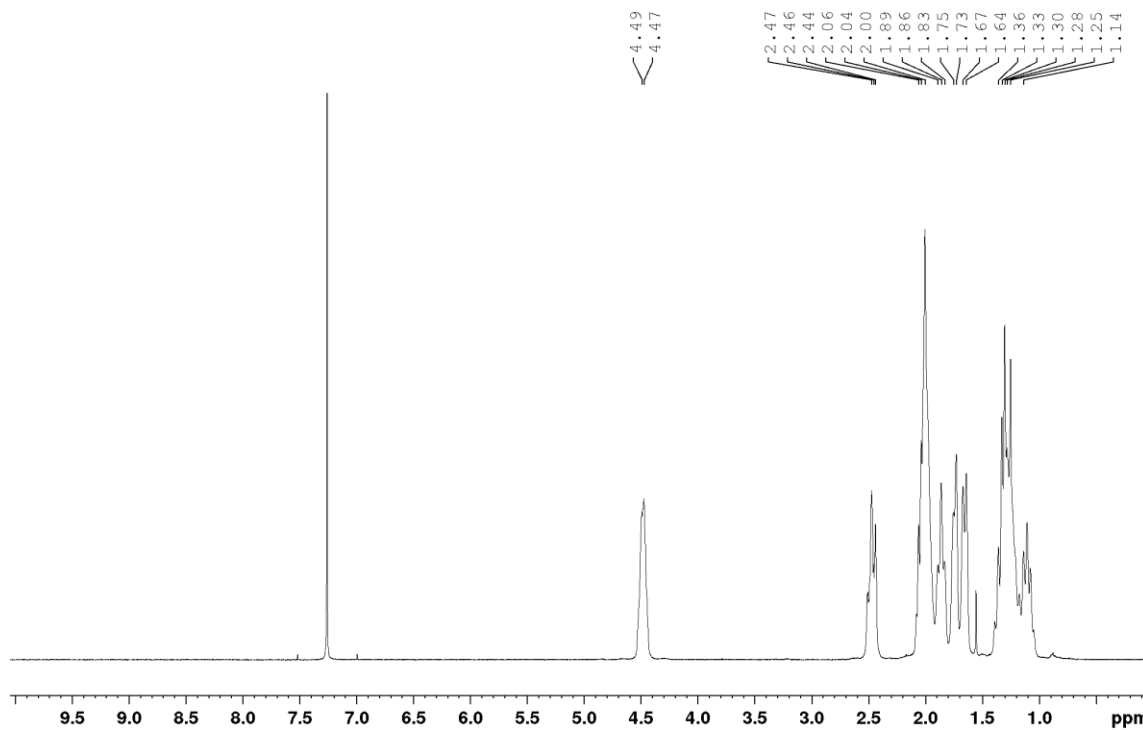


Figure S4.13. ^1H NMR (CDCl_3 , 25 °C) spectrum of cyclic P(4,5-T6GBL) obtained by $[\text{M}]/[\text{I}^t\text{Bu}] = 100/1$.

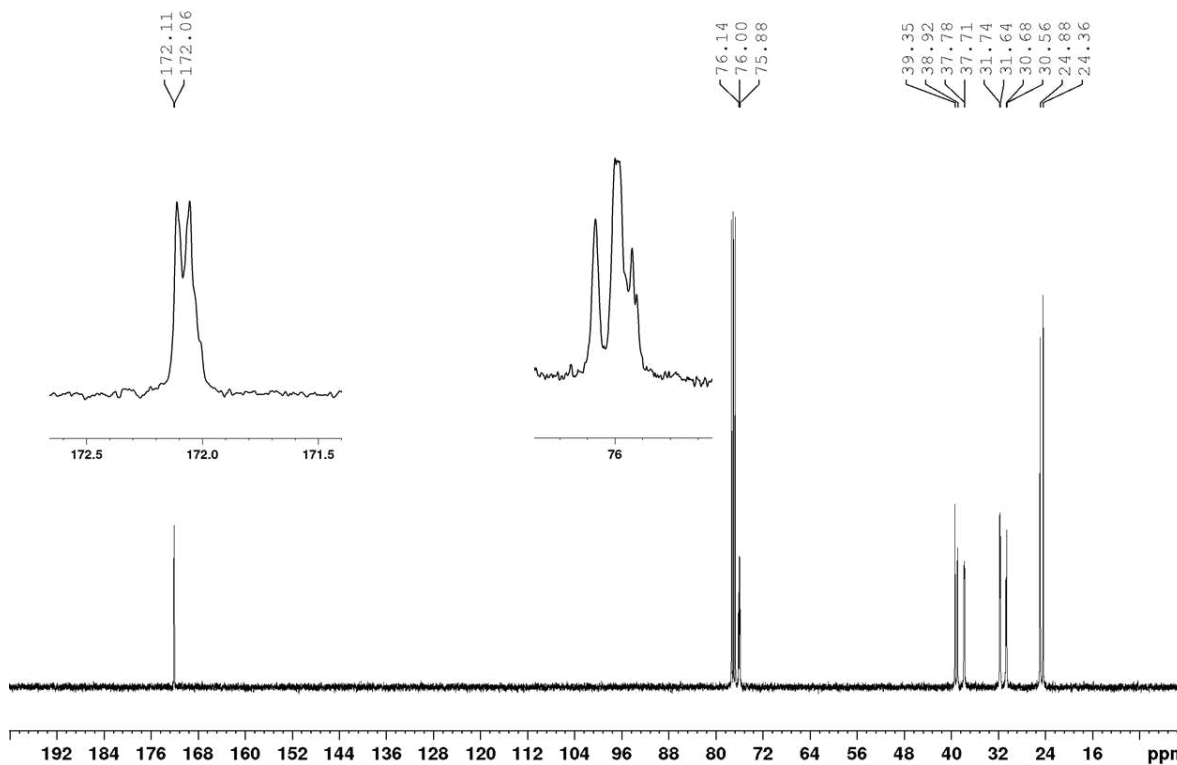


Figure S4.14 ^{13}C NMR (CDCl_3 , 25 °C) spectrum of cyclic P(4,5-T6GBL) obtained by $[\text{M}]/[\text{I}^t\text{Bu}] = 100/1$.

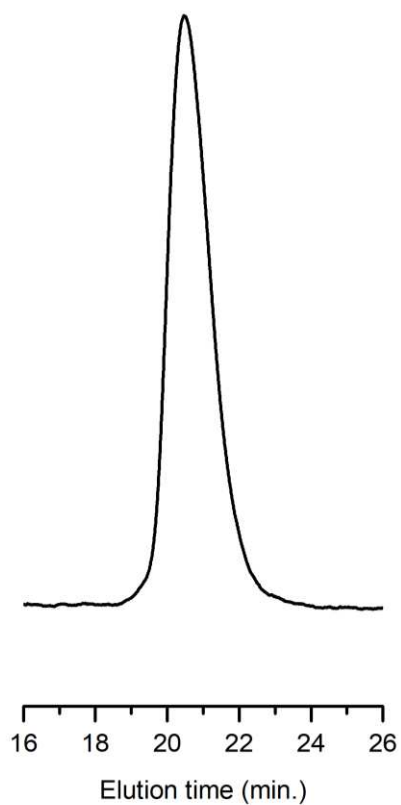


Figure S4.15. GPC trace of cyclic P(4,5-T6GBL) obtained by $[M]/[I'Bu] = 100/1$, $M_n = 40.6$ kDa, $\mathcal{D} = 1.21$.

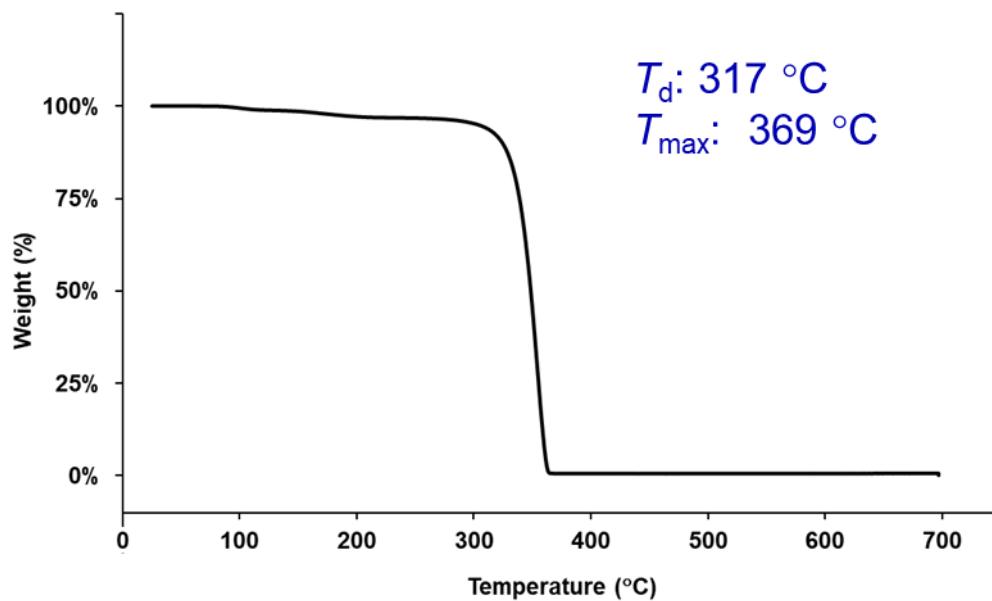


Figure S4.16. TGA curve of cyclic P(4,5-T6GBL) obtained by $[M]/[I'Bu] = 100/1$, $M_n = 40.6\text{ kDa}$, $\bar{D} = 1.21$.

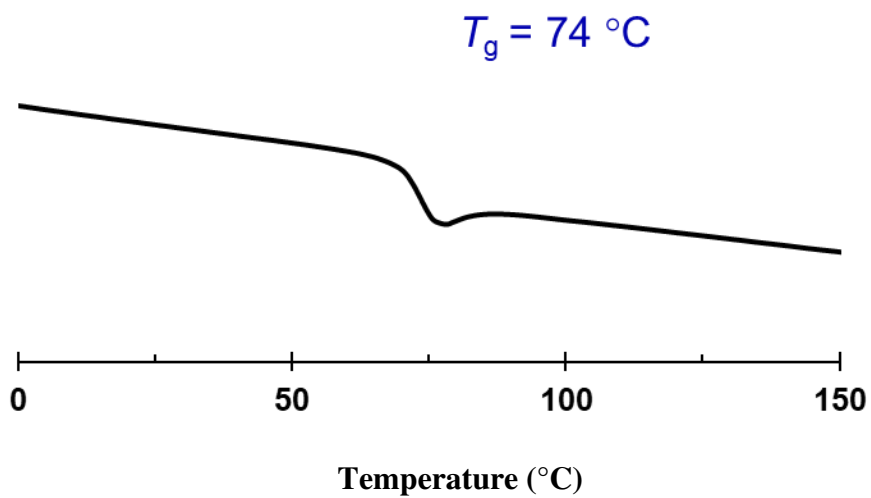


Figure S4.17. DSC curve of cyclic P(4,5-T6GBL) obtained by $[M]/[I'Bu] = 100/1$.

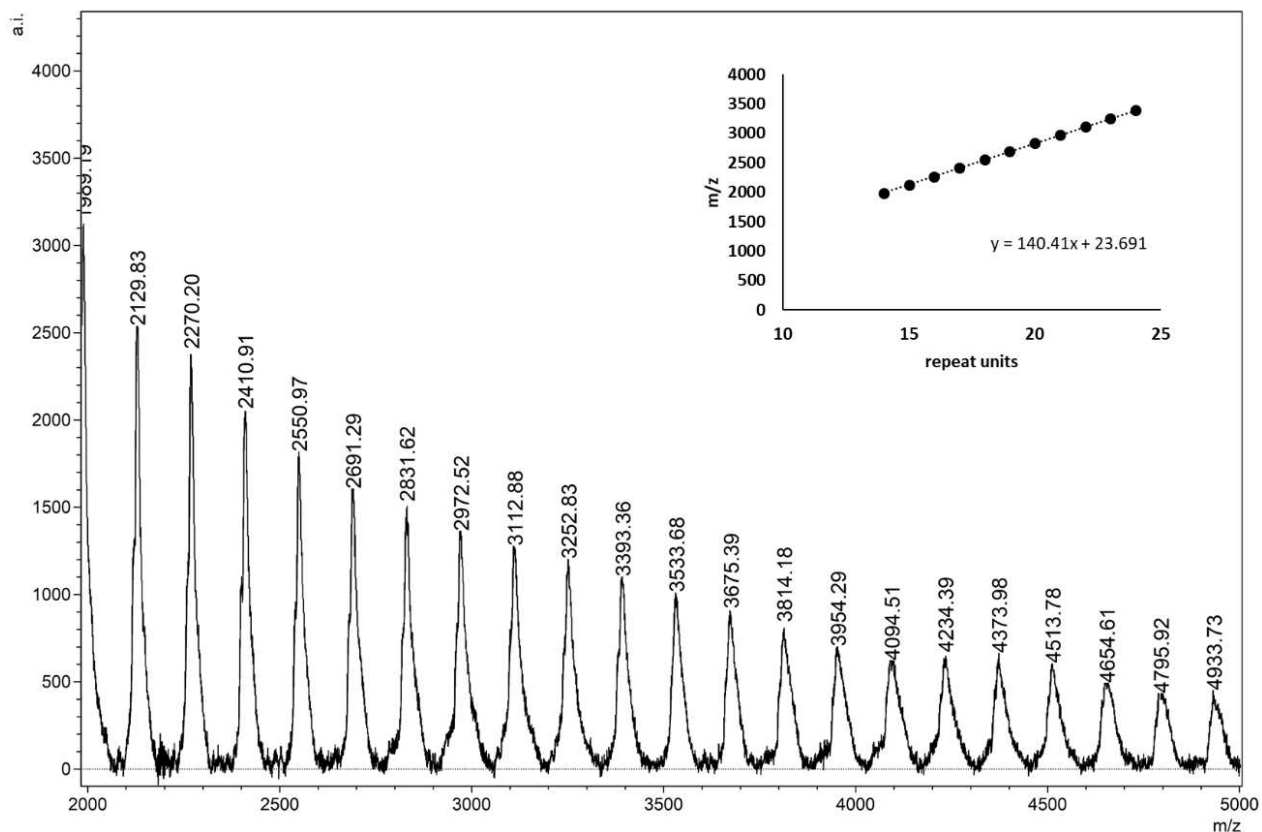


Figure S4.18. MALDI-TOF spectrum cyclic P(4,5-T6GBL) obtained by $[M]/[I^tBu] = 100/1$.

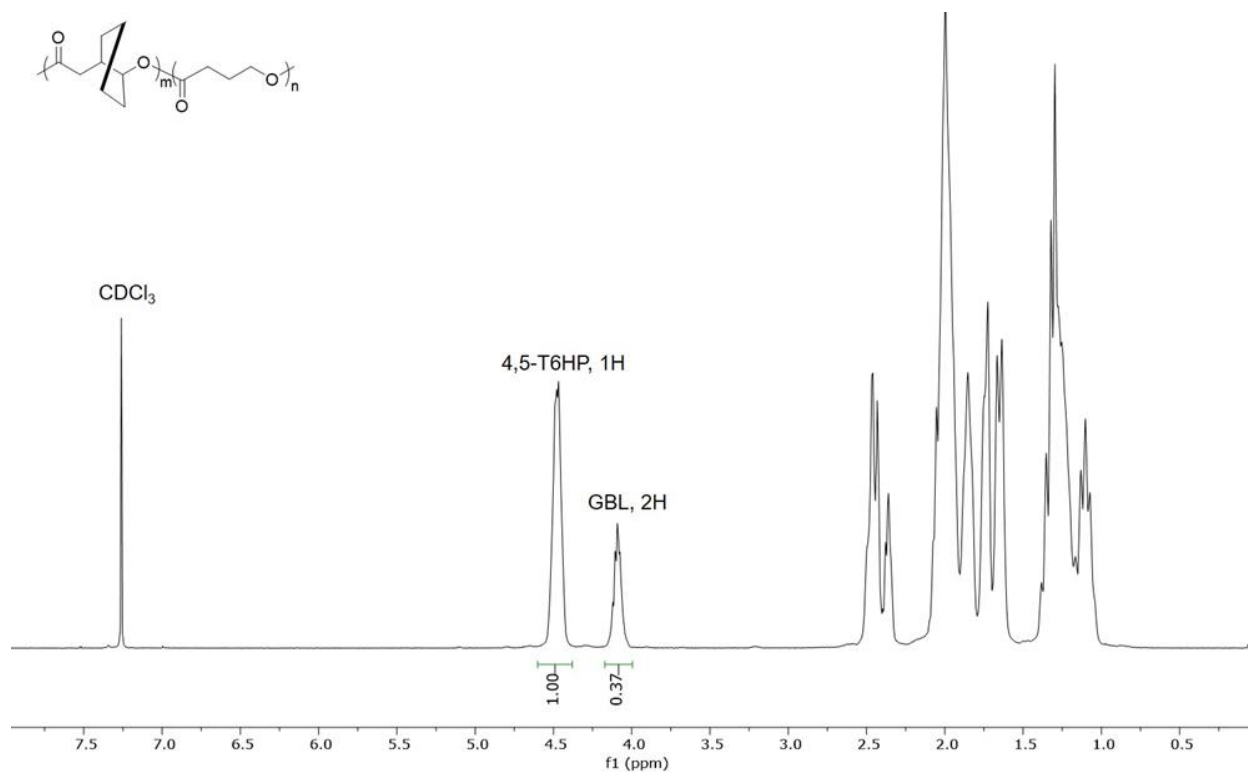


Figure S4.19. ¹H NMR (CDCl₃) of P(4,5-T6GBL)-*co*-PGBL with 16% GBL.

References

1. Lin, B.; Waymouth, R. M., Organic Ring-Opening Polymerization Catalysts: Reactivity Control by Balancing Acidity. *Macromolecules* **2018**, *51*, 2932-2938.
2. Niehues, M.; Erker, G.; Kehr, G.; Schwab, P.; Fröhlich, R.; Blacque, O.; Berke, H., Synthesis and Structural Features of Arduengo Carbene Complexes of Group 4 Metallocene Cations. *Organometallics* **2002**, *21*, 2905-2911.
3. Zhu, J.-B.; Chen, E. Y.-X., Living Coordination Polymerization of a Six-Five Bicyclic Lactone to Produce Completely Recyclable Polyester. *Angew. Chem. Int. Ed.* **2018**, *57*, 12558-12562.
4. Newman, M. S.; VanderWerf, C. A., Isomeric Lactone Pairs Related to Cyclohexanone-2-acetic Acid¹. *J. Am. Chem. Soc.* **1945**, *67*, 233-237.
5. Schneiderman, D. K.; Hillmyer, M. A., Aliphatic Polyester Block Polymer Design. *Macromolecules* **2016**, *49*, 2419-2428.
6. Haba, O.; Itabashi, H., Ring-opening polymerization of a five-membered lactone trans fused to a cyclohexane ring. *Polym. J.* **2014**, *46*, 89-93.
7. Zhu, J.-B.; Watson, E. M.; Tang, J.; Chen, E. Y.-X., A synthetic polymer system with repeatable chemical recyclability. *Science* **2018**, *360*, 398-403.

Appendix C

Experimental Details and Supporting Information for Chapter 5

C.1. Materials and Methods

Materials. Air and moisture-sensitive reactions were conducted in oven-dried glassware on a dual manifold N₂/vacuum Schlenk line or inside an N₂-filled glovebox.

The following reagents were used as received: *meta*-aminobenzoic acid (Sigma), *para*-aminobenzoic acid (Sigma), *cis*-3-aminocyclohexane carboxylic acid (TCI), Rh/C (5 wt.% Rh loading, Sigma), NaH (60 wt.% dispersion in mineral oil, Sigma), 1-*tert*-Butyl-4,4,4-tris(dimethylamino)-2,2-bis[tris(dimethylamino)-phosphoranylideneamino]-2λ⁵,4λ⁵-catenadi(phosphazene) (tBu-P₄, Sigma), 1,3-dimesitylimidazol-2-ylidene (IMes, TCI), Benzoyl chloride (Acros AcroSeal 99%), *N,N*-diisopropylethylamine (Hünig's base, TCI >99%), (*R*)-(+)-1-Phenylethylamine (TCI >99%), citric acid (Sigma), and ZnCl₂ (Sigma, anhydrous).

The following solvents were used as received: Dowtherm A (Sigma), diethyl ether (VWR, HiPerSolv Chromanorm stabilized by ethanol), acetone (VWR), formic acid (Sigma, >98%), *N*-methylpyrrolidone (NMP, Sigma anhydrous SureSeal 99.5%), tetrahydrofuran (THF, Sigma anhydrous SureSeal ≥99.9%), Methyl-THF (Sigma, stored over 4Å molecular sieves), trifluoroacetic acid (TFA, TCI), 2-Pyrrolidone (5-LM, Sigma, ≥99%, stored over 4Å molecular sieves), trifluoroacetic acid-deuterated (TFA-*d*, Cambridge Isotope Laboratories), hexafluoroisopropanol (HFIP, Chem Impex), *m*-cresol (TCI), dichloromethane (DCM, VWR), acetonitrile (Fisher Scientific HPLC grade, stored over 4Å molecular sieves), hexanes (VWR), pentane (Sigma), and heptane (VWR).

AmberChrom® 50WX4 ion exchange resin (Sigma, H⁺ form) was pre-cleaned by stirring in ethanol and then DI H₂O until rinses were clear and the resin was stored damp.

Nylon 6 sheeting (thickness 0.6 mm) was purchased from GoodFellows (M_n 35.9 kDa, $D = 1.28$, $T_{g, DSC} = 43$ °C, $T_m = 222$ °C, crystallinity = 19%, $T_{d,5} = 402$ °C).

Methods.

Spectroscopic Characterizations. NMR spectra were recorded on a Bruker 300 or 400 MHz (FT 300 or 400 MHz, ¹H; 100 MHz, ¹³C). Chemical shifts were referenced to internal solvent resonances and reported as parts per million relative to tetramethylsilane (TMS). For ¹³C samples recorded in CDCl₃, internal solvent resonance was set to 77.36 ppm for axis calibration (corresponding to center of triplet signal). For ¹H and ¹³C samples recorded in TFA-*d*, internal solvent resonance was set to 11.50 ppm for ¹H and 112.416 ppm for ¹³C (corresponding to the furthest upfield of the 8 TFA-*d* ¹³C resonances) for axis calibration. ¹³C spectra of polyamides were recorded in TFA-*d* using a d1 delay of 6 seconds and 7,168 scans at 30 °C unless otherwise noted.

Polyamide samples were analyzed by matrix-assisted laser desorption/ionization time-of-flight mass spectroscopy (MALDI-TOF MS) using an Ultraflex MALDI-TOF mass spectrometer (Bruker Daltonics) in linear mode using a Nd:YAG laser at 355 nm and 25 kV accelerating voltage. The sample spots (~3 mg/mL in *m*-cresol) were deposited onto the target plate, air-dried, and then vacuum dried at 50 °C, followed by matrix deposition (α -cyano-4-hydroxycinnamic acid (HCCA), 10 mg/ml in acetonitrile/water/TFA (50.0%/47.5%/2.5%)) and air-drying. External calibration was performed with peptide calibration mixture (4-6 peptides) spotted on the same plate. Data was processed using mMass software.

Fourier Transform Infrared (FTIR) spectra of bulk polymers (as-precipitated, moisture-equilibrated) were recorded on a Thermo Scientific Nicolet iS50 FTIR spectrometer with single

reflectance ATR. Powder x-ray diffraction pattern was obtained with a Bruker D8 Discover DaVinci Powder X-ray Diffractometer with CuK α radiation and LYNXEYE-XE-T energy discriminating detector; scan of $2\theta = 5\text{--}50^\circ$ with a step size of 0.02° and a count time of 1.3 sec/step. The finely powdered polymer sample was obtained by liquid N₂ cooling and grinding in a mortar and pestle.

LC/DAD/MS analysis was employed for Quantitation of 5/7-LM containing samples, performed on an Agilent 1100 LC system (Agilent Technologies, Santa Clara, CA) equipped with a diode array detector (DAD) and a G6120A single quadropole mass spectrometer. Each sample and standard were injected at a volume of 2 μL on a Phenomenex Luna C18(2)-HST 100A" column 25 μm , 2.0 x 100 mm column (Phenomenex, Torrance, CA). The column temperature was maintained at 45 $^\circ\text{C}$ and the buffer used to separate the analytes of interest was 0.16% formic acid in water (A)/acetonitrile (B). A gradient program was used to separate the analytes of interest: (A) = 100% and (B) = 0% at time $t = 0$; (A) = 100% and (B) = 0% at $t = 1$ min; (A) = 50% and (B) = 50% at $t = 7.67$ min; (A) = 30% and (B) = 70% at $t = 9.33$ min; (A) = 30% and (B) = 70% at $t = 10.67$ min; (A) = 100% and (B) = 0% at $t = 10.68$ min; (A) = 100% and (B) = 0% at $t = 13$ min. The flow rate was held constant at 0.50 mL min^{-1} resulting in a run time of 13 minutes. The 5/7-LM standard was used to construct a calibration curve between the ranges of 5 – 250 $\mu\text{g mL}^{-1}$. The mass spectrometer was scanned from 50-350 m/z with a gas temperature of 350 $^\circ\text{C}$, drying gas flow at 12.0 l/min, nebulizer pressure of 35psig, and a VCap of 3000v in positive mode utilizing electrospray. The total ion chromatogram (TIC) and retention time was used to identify and quantitate the analyte of interest. A minimum of 7 calibration levels were used for each analyte with an r^2 coefficient of .995 or better. A check calibration standard (CCS) was analyzed every 10 samples to ensure the integrity of the initial calibration

Absolute Molecular Weight Measurements. Gel permeation chromatography (GPC) was used to determine number and weight-average molecular weights (M_n , M_w) of homo- and copolyamide samples on a Wyatt MiniDAWN TREOS system equipped with Multi Angle Light Scattering (MALS, 3 angles) and Refractive Index (RI, 658 nm) detectors. Polymer concentrations of 2.0 mg/ml in HFIP were injected at a volume of 50 μ L into the system at a flow rate of 0.4 mL/min through the column at 40 °C. Astra software was used to determine M_n , M_w , and dispersity index (M_w/M_n) with calibration based on polystyrene standards and assuming 100% mass recovery.

Thermal Analysis. Thermogravimetric analysis (TGA) was performed with a TA Instruments TGA-5500 at a heating ramp rate of 20 °C/min under N₂. Dynamic Scanning Calorimetry (DSC) was conducted using a TA Instruments DSC-Q2000. Simultaneous DSC/TGA (SDT) was performed with TA Instruments SDT-0650 at a heating ramp rate of 10 °C/min under N₂. Data were processed using Trios software.

Thin film preparation. Approximately 0.67 g copolymer was dissolved in 4-6 ml formic acid and the viscous solution was pipetted into 3 Teflon bar molds (0.5" (w) x 2 3/8" (l) x 1/8" (h)). The mold was covered with a cardboard box and evaporated overnight. After 18-24h, the films (\approx 0.25 mm thick) could be removed with forceps and were clamped between glass microscope slides with binder clips and further dried in the vacuum oven (90-100 °C, 24-48h). Before any test, the films were allowed to equilibrate with atmospheric moisture for 48+ hours.

Water sorption. ASTM D570-98 was followed. Thin films were dried at 90 °C in the vacuum oven for 24h and cut into 3 roughly equal pieces (\sim 50 mg ea.) and weighed. The samples were immersed in DI water for 24 hours, then removed and placed on a Kimwipe, patted dry and weighed again.

Dynamic Mechanical Analysis (DMA). A TA Instruments DMA Q800 was used to obtain storage and loss moduli as a function of temperature (from ambient to 150+°C) and frequency (0.1 Hz to 10 Hz). A temperature ramp rate of 5°C/min was utilized, and data is plotted at a frequency of 1 Hz. A dual cantilever fixture was utilized to test the samples under flexion with a deformation of 1 mm (1000 μm) to ensure a consistent DMA wave form for the rigid samples. Moisture-equilibrated thin films that were approximately 35mm x 12 mm x 0.5mm (LxWxT) were subjected to two heating cycles to observe the ‘wet’ and ‘dry’ T_g values by the $\tan\delta$ peak for first and second heating scans, respectively. When necessary, tests were stopped during the rubbery plateau to avoid melting inside the instrument.

Tensile Testing. Rectangular thin films were tested on an Instron 5900 Series tensiometer equipped with a 1 kN load cell at 5 mm/min and room temperature (~ 23 °C). Prior to testing, vacuum oven-dried samples were equilibrated in air for 48-72h. Raw data was converted to stress (MPa) vs. strain (% elongation) by Bluehill Universal Software on the Instron. Resulting stress-strain data was averaged for $n = 5$ samples (width ≈ 12 mm, length ≈ 60 mm, thickness 0.25-0.30 mm) (Table S5.5).

DFT Calculations. All calculations were completed using Gaussian 16 Rev. C.01¹ using the M06-2X²/Def2TZVP^{3, 4} level of theory. All structures were optimized using implicit solvent parameters for nitrobenzene ($\epsilon=34.809$) and the Polarizable Continuum Model (PCM) with the integral equation formalism variant (IEFPCM).^{5, 6} The calculations included the keyword “CPHF=Grid=Fine” and, for the implicit solvent, “PDENS=7.0”, as these integration grid specifications removed many erroneous low wavenumber frequencies. All local minima were verified to have zero imaginary frequencies. All transition state structures exactly one imaginary frequency and verified to connect the local minima (reactants and products) shown by following

the intrinsic reaction coordinates⁷ in both directions for the default number of steps and step size, following by geometry optimization. Rotamer searches were performed to search for low-energy conformations and the conformations reported are those with the lowest Gibbs free energies as calculated at 25, 100, and 120 °C using physical constant values for fundamental physical constants reported in the NIST Standard Reference Database 121⁸ and scaling vibrational frequencies by 0.9505.⁹

Small molecule syntheses.

*Synthesis of aminocyclohexane carboxylic acids (1,3 or 1,4-ACHA) from aminobenzoic acids.*¹⁰ To a pressure vessel was added *m*-aminobenzoic acid (10.0g, 72.9 mmol), 150 mL 30% ethanol/water, 4.5 mL acetic acid, and 1.00 g Rh/C (5% Rh loading). After N₂ purging, H₂ was charged to 1500 psi and the reactor was stirred overnight at 60 °C. Once cooled to room temperature, pressure was vented, and the mixture filtered and washed with water. The volume was reduced to ~75mL and poured into 250 mL acetone to precipitate the product overnight. The product was filtered and washed with acetone and dried in the vacuum oven at 50 °C for 48h. ¹H NMR spectra (D₂O) matched literature data.

1,3-ACHA: 87% yield, approx. 85/15 cis/trans ratio.

1,4-ACHA: 85% yield, approx. 85/15 cis/trans ratio.

*Synthesis of fused lactams (5/7-LM and 6/6-LM).*¹⁰ 3-ACHA (15.0 g, 104.8 mmol) was added to a 100 mL round bottom flask with a stir bar and 45 mL Dowtherm A, and a Dean-Stark trap with condenser were attached. Air was removed from the with 3 cycles of brief evacuation and N₂ backfill. Using a thermocouple-controlled heating mantle, the reaction was heated to 260 °C and refluxed until clear (30-60 min.) and cooled under N₂. The mixture was precipitated into 7X excess

of heptane and chilled overnight before filtration and washing with cold heptane to yield crude lactam.

5/7-LM from hydrogenation product (*cis/trans* mixture): 37% yield, purified by sublimation.

5/7-LM from pure *cis*-3-ACHA: 79% yield, purified by dissolving in HPLC-grade acetone, filtration, and rotary evaporation ^1H NMR (400 MHz, CDCl_3) δ (ppm): 5.75 (bs, N-H) 3.75 (t, $J = 4.702$, 1H), 2.38 (m, 1H), 2.28 (m, 1H), 1.47-1.90 (m, 7H), Figure S5.3. ^{13}C NMR (100 MHz, CDCl_3) δ (ppm): 180.62, 52.15, 40.46, 39.36, 28.57, 26.32, 18.64, Figure S5.4.

6/6-LM from hydrogenation (*cis/trans* mixture): 75% yield, purified by sublimation

^1H NMR (400 MHz, CDCl_3) δ (ppm): 6.35 (bs, N-H), 3.61 (br, 1H), 2.53 (br, 1H), 1.58-1.95 (m, 7H), Figure S5.6. ^{13}C NMR (100 MHz, CDCl_3) δ (ppm): 178.77, 47.91, 38.13, 27.92, 24.24, Figure S5.7.

Preparation of (-)-5/7-LM via chiral resolution of cis-3-ACHA.^{11, 12} Racemic (*rac*) 3-ACHA was Boc-protected and the product recrystallized. *Rac*-Boc-3-ACHA was resolved with (+)-phenylethylamine, which was added to the hot solution in 2:1 CHCl_3 :hexanes. Upon cooling, the entire mixture solidified and was re-boiled with additional solvent to dissolve one diastereomeric salt and filtration was performed hot. To ensure separation, the isolated filtrate was re-boiled in 2:1 CHCl_3 :hexanes and hot-filtered again. The soluble diastereomer salt in the filtrate was re-protonated with citric acid in a separatory funnel and extracted with DCM.

A DCM solution of (*rel-R,S*)-3-ACHA was deprotected with excess TFA. After rotary evaporation, the resulting ammonium salt was neutralized with AmberChrom® 50WX4 ion exchange resin. The resin was prepared by stirring in absolute ethanol and filtering with ethanol and DI H_2O until filtrate was clear. The damp resin (~1.5x excess based on theoretical H^+ equivalents) was loaded into a burette and a concentrated aqueous solution of substrate was loaded

on top. One bed volume (BV) of DI H₂O was used to rinse the column, proceeded by elution with 5BV 1M aq. pyridine. After rotary evaporation and complete drying, (rel-*R,S*)-3-ACHA was subjected to the same cyclization procedure as *rac* to obtain (-)-5/7/LM. ¹H NMR (400 MHz, CDCl₃) δ (ppm): 5.52 (bs, N-H) 3.75 (t, *J* = 4.768, 1H), 2.39 (m, 1H), 2.28 (m, 1H), 1.47-1.90 (m, 7H), Figure S5.5.

Specific rotation of chiral products (10 cm path):

$[\alpha]_D^{23}$ (rel-*R,S*)-Boc-3-ACHA = -53° in MeOH (lit. = -50°)

$[\alpha]_D^{23}$ (rel-*R,S*)-5/7-LM: -20°

*Synthesis of N-benzoyl-5/7LM (NBzM, Activator).*¹³ A 100 mL Schlenk flask containing 40 mL anhydrous 2-methyl-THF was cooled on an ice bath for 30 mins and 0.220g NaH (60% dispersion in mineral oil, 9.19 mmol, 1.15 eq.) was added under N₂ flow and stirred for 2h. Benzoyl chloride (1.16 mL, 9.99 mmol, 1.25 eq.) was added dropwise via syringe and the ice bath was removed. The reaction stirred overnight and was quenched with cold DI H₂O. The product was extracted with DCM and purified by recrystallization in 75/25 heptane/methyl isobutyl ketone to yield 49% NBzM.

¹H NMR (400 MHz, CDCl₃) δ (ppm): 7.38-7.65 (m, 5H), 4.60 (t, *J* = 4.860, 1H), 2.65 (bt, 1H), 2.32 (m, 1H), 1.57-1.98 (m, 7H), Figure S5.8. ¹³C NMR (100 MHz, CDCl₃) δ (ppm): 176.42, 170.20, 134.95, 132.05, 129.16, 128.04, 56.66, 43.16, 35.81, 27.28, 26.96, 18.68, Figure S5.9.

Synthesis of sodium lactamate salts of 5/7-LM (NaM) and 5-LM (Na5LM). In a 10 mL Schlenk flask inside the glovebox, 158 mg NaH (60% dispersion in mineral oil, 3.99 mmol, 1.0 eq.) was added to 2 mL anhydrous THF. 5/7-LM (500 mg, 3.99 mmol 1.0 eq) was dissolved in 4 mL anhydrous THF and added slowly to the NaH then stirred overnight. Outside the glovebox, the

resulting salt was washed with anhydrous THF and hexanes to remove excess lactam and mineral oil, then dried in the vacuum oven at 60 °C.

Typical polymerization procedures.

With ^tBu-P₄ catalyst for a [Monomer]/[Catalyst]/[Activator] ratio of 50/1/1. Inside the glovebox, a 4 mL glass vial was loaded with 200.0 mg 5/7-LM (1.60 mmol), 7.3 mg NBzM (0.032 mmol) and 0.53 mL NMP (3M). If elevated temperature was required, the mixture was brought to the desired temperature in an aluminum heat block before catalyst addition. To start the polymerization, 40 μL ~0.8M ^tBu-P₄ in hexane was injected to the stirring mixture and the vial was capped. After the desired reaction time, the polymerization was removed from the glovebox and ~1 mL formic acid was added to quench and dissolve the polymer. The formic acid solution was precipitated into diethyl ether or acetone, centrifuged, and re-centrifuged with fresh ether. Precipitation was repeated twice more, drying polymer in between. Isolated yield was recorded after drying at 100 °C in the vacuum oven for 24h.

With Na⁺ catalyst for a [Monomer]/[Catalyst]/[Activator] ratio of 50/1/1. Inside the glovebox, a 4 mL glass vial was loaded 225.3 mg 5/7-LM (1.80 mmol), 8.3 mg NBzM (0.036 mmol) and 0.60 mL NMP (3M). If elevated temperature was required the mixture was brought to the desired temperature in an aluminum heat block before catalyst addition. To start the polymerization, 5.3 mg NaM (0.036 mmol, finely powdered) was added to the stirring mixture and the vial was capped. After the desired reaction time, the polymerization was removed from the glovebox and ~1 mL formic acid was added to quench and dissolve the polymer. The formic acid solution was precipitated into wet acetone (10-20% water to aid in sodium removal), centrifuged, and re-centrifuged fresh acetone. Precipitation was repeated twice more, once more to wet acetone and

finally to diethyl ether, drying polymer in between. Isolated yield was recorded after drying at 100 °C in the vacuum oven for 24h.

Copolymerization with 5-LM. The same procedure as described above for homopolymerization was employed for copolymerizations with 5-LM. When the monomer feed contained 75% or more 5-LM, no solvent was necessary; minimum NMP was used for 50% or less 5-LM. For the 250/5/1 ratio, Na5LM (finely powdered) was employed as the base.

Polymerizations for Van 't Hoff Analysis

To determine temperature-dependence of $[M]_{eq}$, polymerizations were run in parallel at 75, 90, 105, and 120 °C. Heating blocks or oil baths were pre-heated for at least one hour prior to starting the experiment. Inside the glovebox, a stock solution (stock 1) was prepared containing 33:1 molar equivalents of 5/7-LM to NBzM using 820.5 mg 5/7-LM, 44.7 mg NBzM, and 6.2 mL NMP. A second stock solution, stock 2, was prepared in a 4 mL vial sealed with a rubber septum screw cap, containing 194.8 mg IMes and 2.0 mL NMP, which was heated briefly to 60 °C to aid solubilization. To each of 5, 4 mL reaction vials equipped with a stir bar was transferred 1.0 mL stock 1 via a glass 1.0 mL gastight syringe and the vials were sealed with rubber septum screw caps. To the vial labeled 'control' was added 100 μ L blank NMP. The remaining 4 reaction vials were heated for 2 minutes before injection of 100 μ L stock 2 via a 100 μ L glass syringe to initiate the 33:1:1 $[M]:[B]:[A]$ polymerization at the desired temperature ($[M]_0 = 0.96$ M).

After 18 hours, each vial (including the control) was quenched with 5 μ L formic acid, also injected through the septa. After cooling, each was diluted with 2.0 mL acetonitrile via automatic pipette and centrifuged (dilution factor DF = 2.81). Two further dilutions were performed into acetonitrile (DF = 15, 10) before LC/DAD/MS analysis.

Recycling procedures

Nylon 4/6 recycling with ZnCl₂. Inside the glovebox, 275 mg nylon 4/6 was added to a glass sublimator with a water condenser. The powder or fine granules were pre-wet with anhydrous THF (0.2 mL) and then coated in a ZnCl₂-THF solution (20 wt.% ZnCl, 55 mg in 0.2 mL THF). The sublimator was sealed and attached to the Schlenk line, where vacuum was pulled carefully to evaporate the THF. It was necessary to open the apparatus briefly to move all polymer to the bottom and clean the condenser. After re-assembly, condenser lines were opened, and the temperature of the thermocouple-controlled heating mantle was held at 290 °C for 18h (vacuum ~20 mTorr). Crude product was rinsed into a tared round bottom flask with DCM, which was removed by rotary evaporation and weighed for crude yield. A new DCM solution was then transferred into a round-bottom sublimator, evaporated, and the crude product (Figure S5.40) re-sublimed at 55 °C (vacuum ~20 mTorr). The re-sublimed monomer was dissolved in 1.0 mL diethyl ether and filtered through a 0.2 μm syringe filter to yield 70% (193 mg) 5/7-LM (Figure S5.41) which was subjected to re-polymerization against a control with fresh 5/7-LM.

Nylon 4/6-co-nylon 4 recycling with ZnCl₂. Inside the glovebox, 250 mg powdered nylon 4/6-co-nylon 4 (51% 5/7-LM) was added to a glass sublimator with a cryogenic condenser. The powder was pre-wet with anhydrous THF (0.2 mL) and then coated in a ZnCl₂-THF solution (10 wt.% ZnCl₂, 25 mg in 0.2 mL THF). The sublimator was sealed and attached to the Schlenk line, where vacuum was pulled carefully to evaporate the THF. The apparatus was briefly opened to move all polymer to the bottom and clean the condenser. The condenser was filled with dry ice/isopropanol, and the temperature of the thermocouple-controlled heating mantle was held at 300 °C for 3h. Crude product was rinsed into a round bottom flask with DCM and solvent was removed carefully by rotary evaporation to avoid loss of volatile 5-LM (water bath temperature 18 °C, 250 mbar

pressure), yielding 249 mg products (Figure S5.94). A layer of pentane was added to the products, which crystallized at 4 °C and the pentane was decanted while cold (Figure S5.95), yielding 235 mg.

C.2.

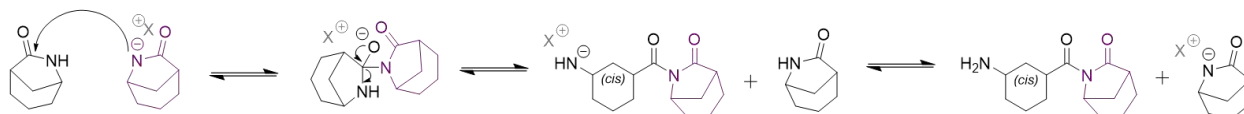


Figure S5.1.A. Monomer Initiation

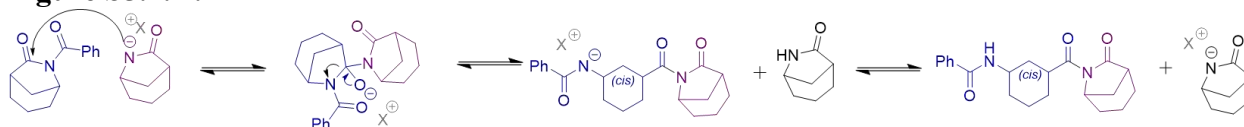
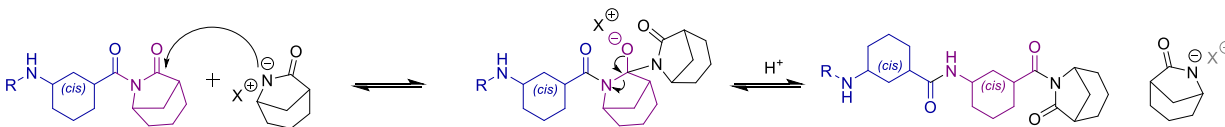


Figure S5.1.B. Activated Initiation



R = H or C₆H₅

Figure S5.1.C. Propagation

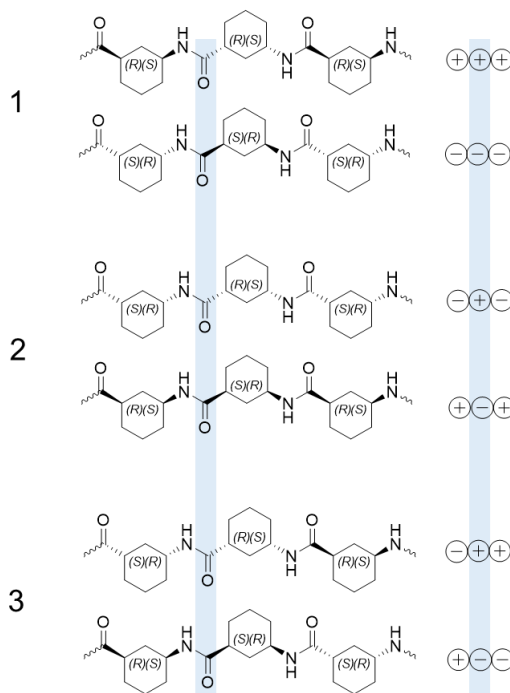


Figure S5.2. ¹³C NMR stereo-sequence peaks

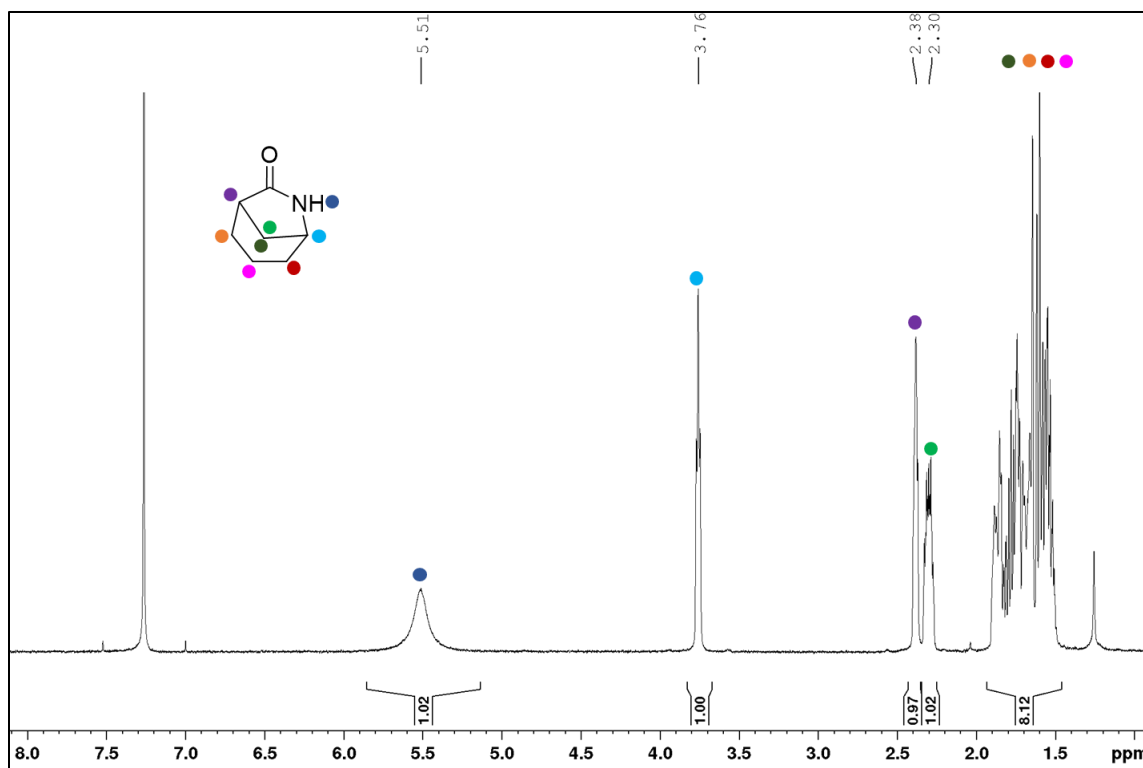


Figure S5.3. ^1H NMR (CDCl_3) of (\pm)-5/7-LM

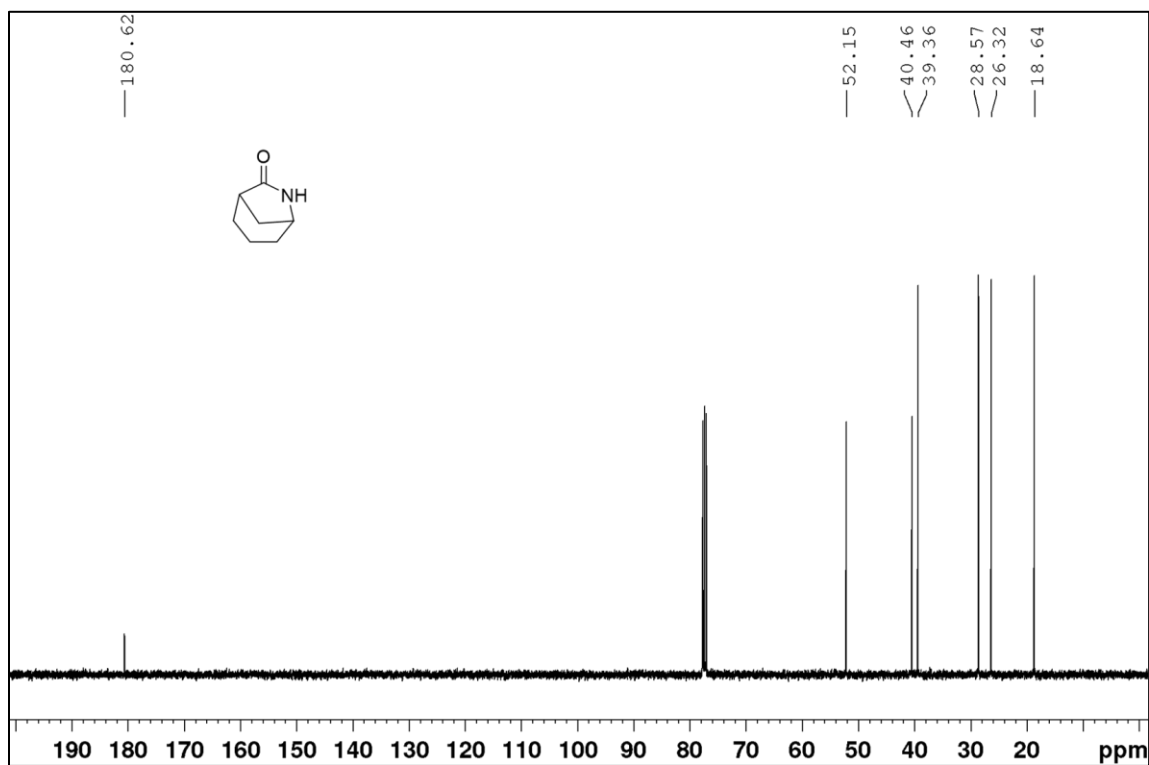


Figure S5.4. ^{13}C NMR (CDCl_3) of (\pm)-5/7-LM

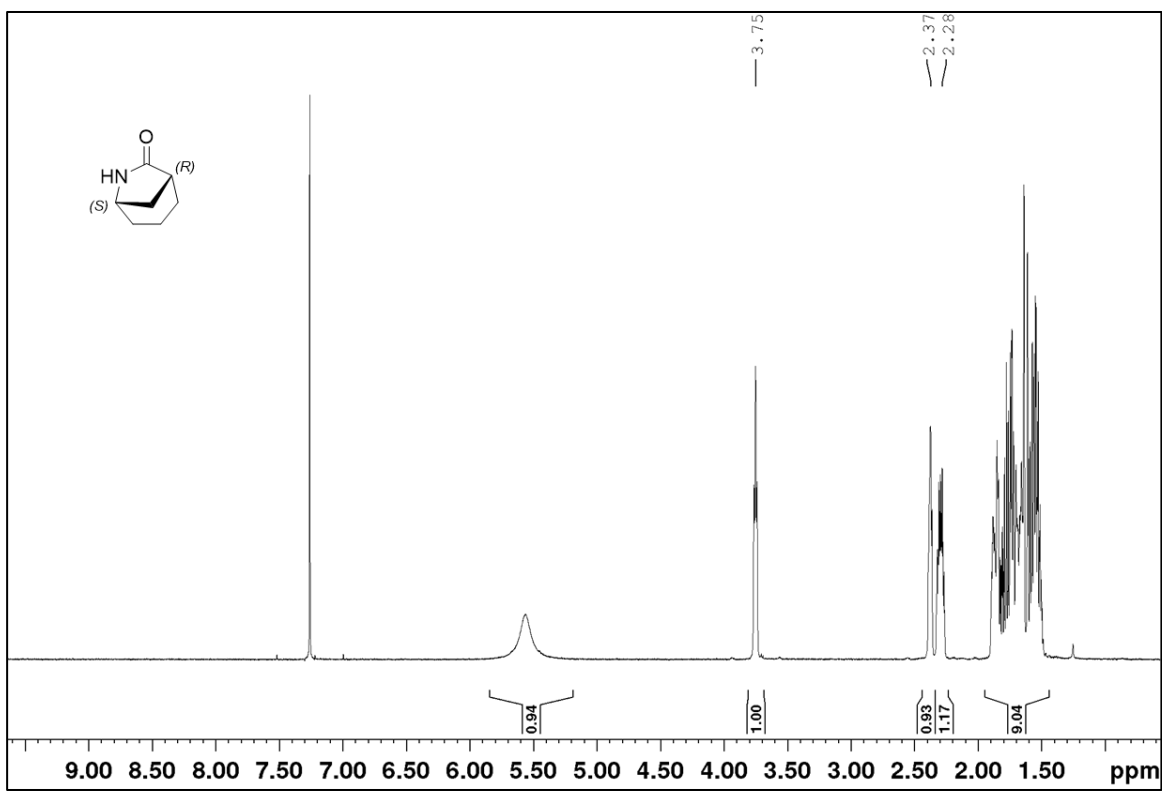


Figure S5.5. ^1H NMR (CDCl_3) of (-)-5/7-LM

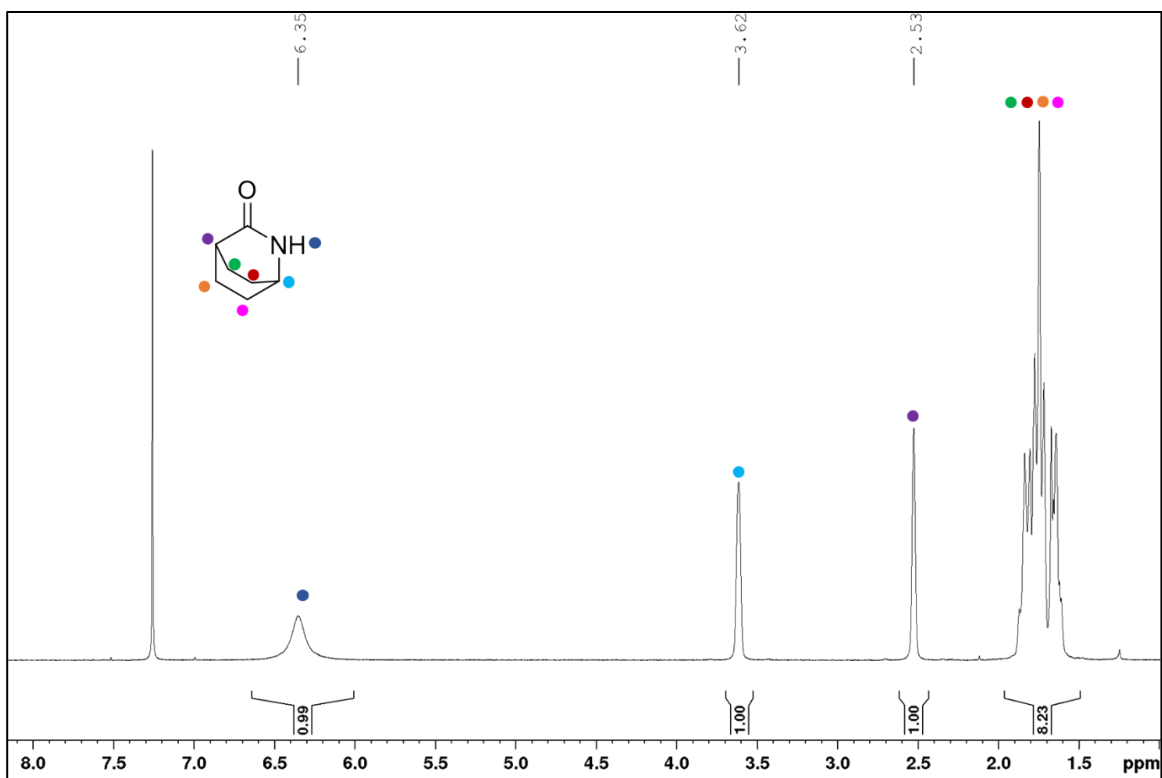


Figure S5.6. ^1H NMR (CDCl_3) of (\pm) -6/6-LM

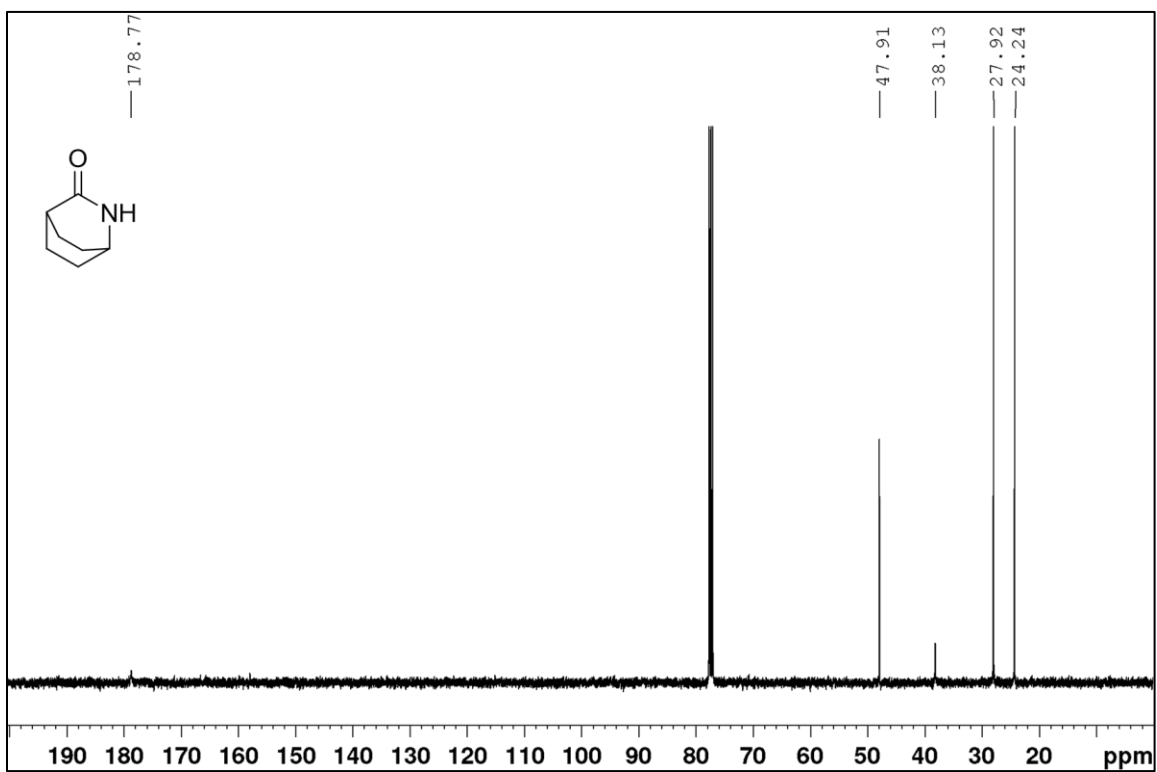


Figure S5.7. ^{13}C NMR (CDCl_3) of (\pm) -6/6-LM

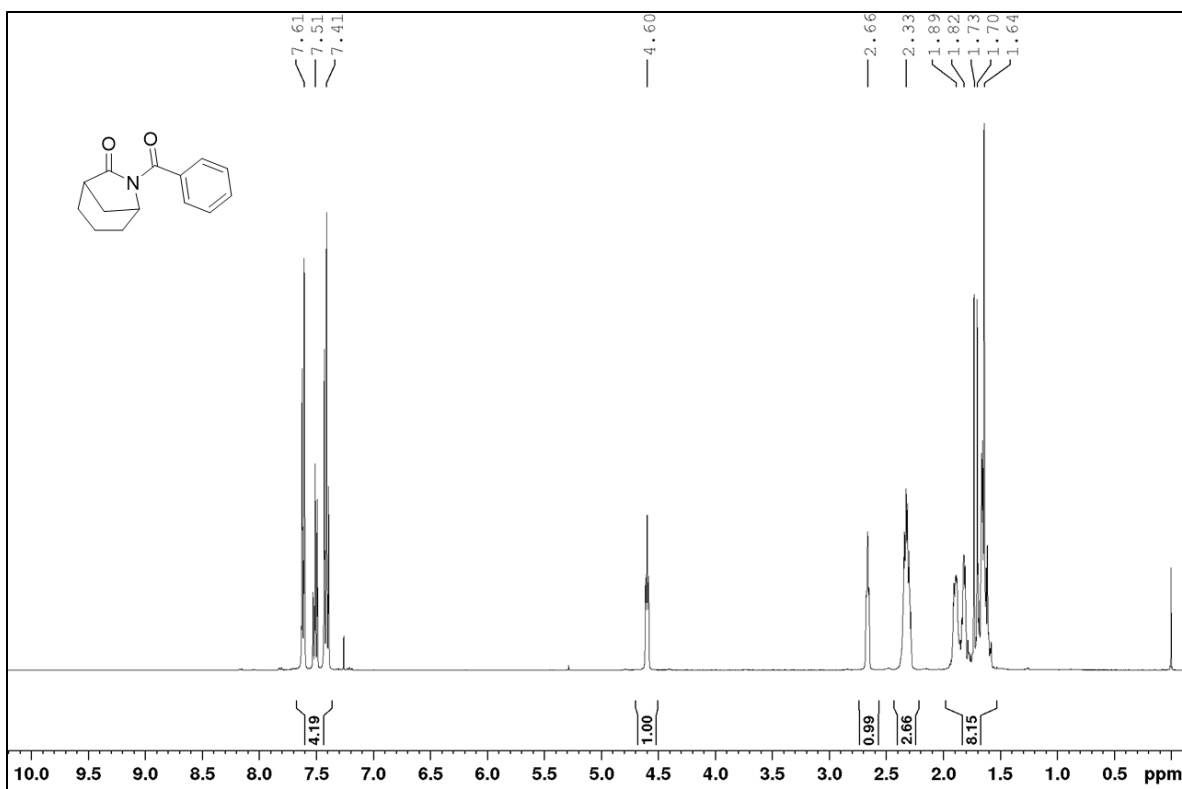


Figure S5.8. ^1H NMR (CDCl_3) of NBzM

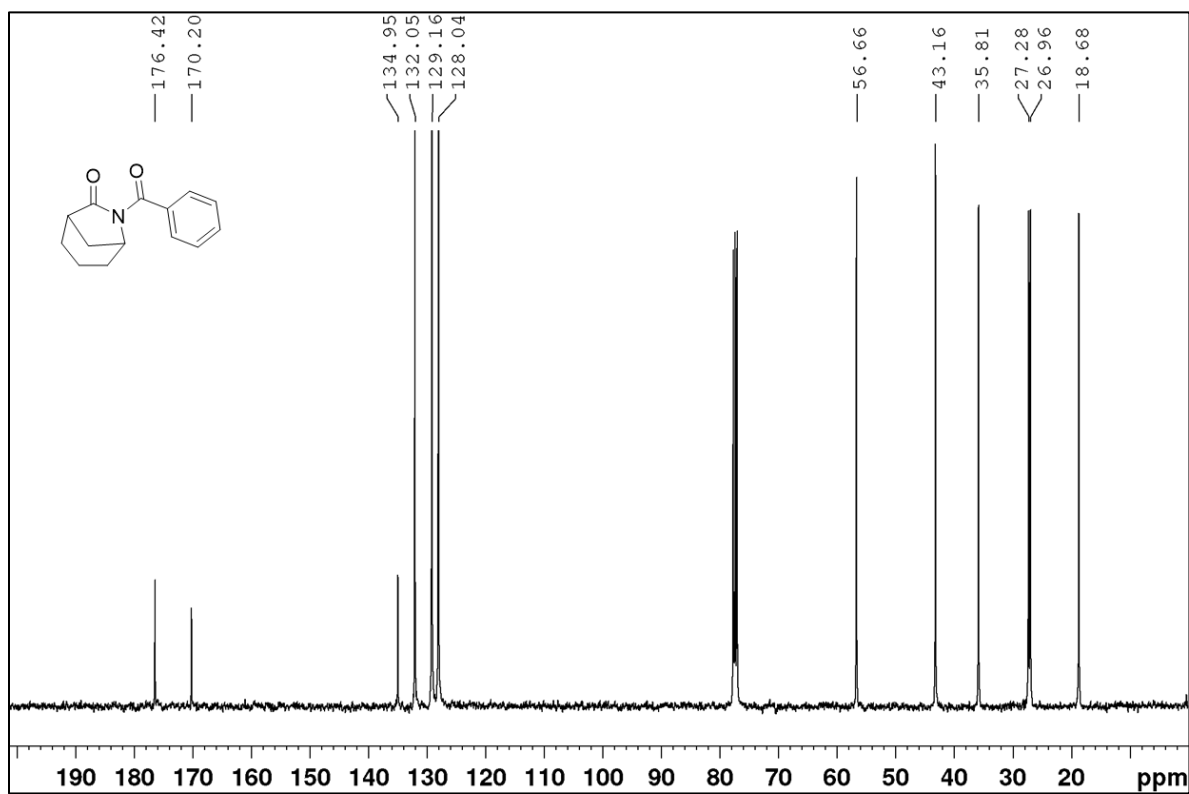


Figure S5.9. ^{13}C NMR (CDCl_3) of NBzM

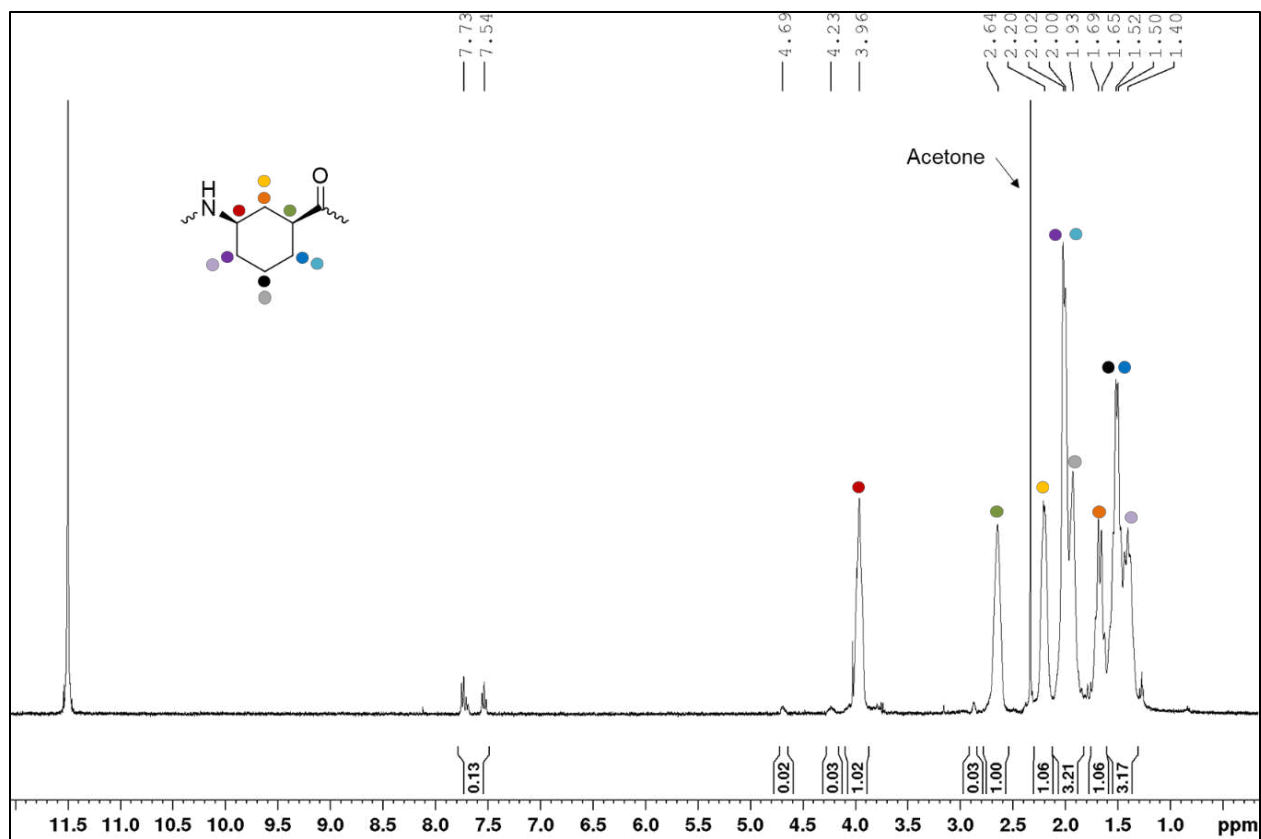


Figure S5.10. ^1H NMR ($\text{TFA-}d$) of representative nylon 4/6 produced by 50:1:1 [5/7-LM]:[$^t\text{Bu-P}_4$]:[NBzM] at 60 $^\circ\text{C}$ in NMP

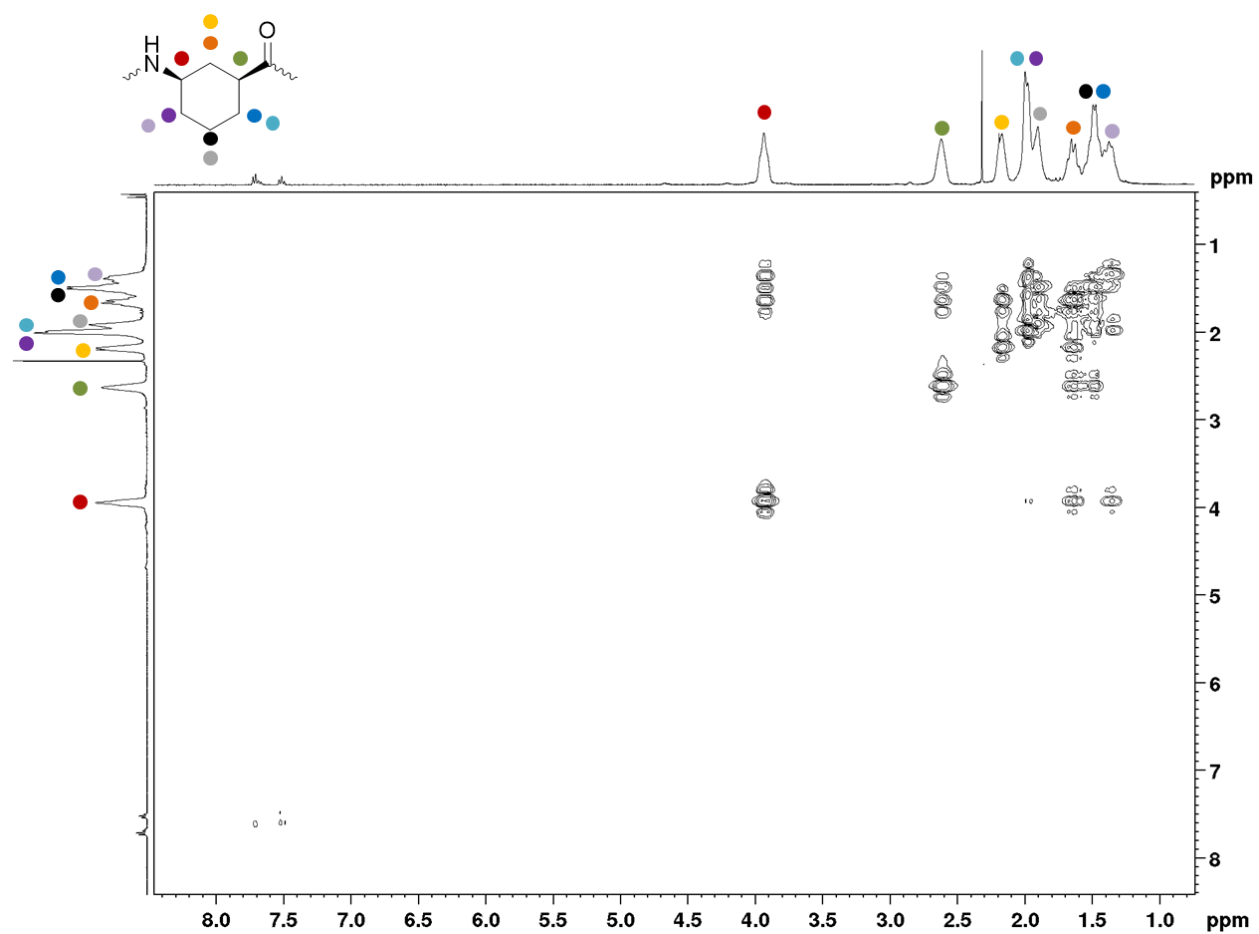


Figure S5.11. COSY NMR (TFA-*d*) of representative nylon 4/6 produced by 50:1:1 [5/7-LM]:[^tBu-P₄]:[NBzM] at 60 °C in NMP

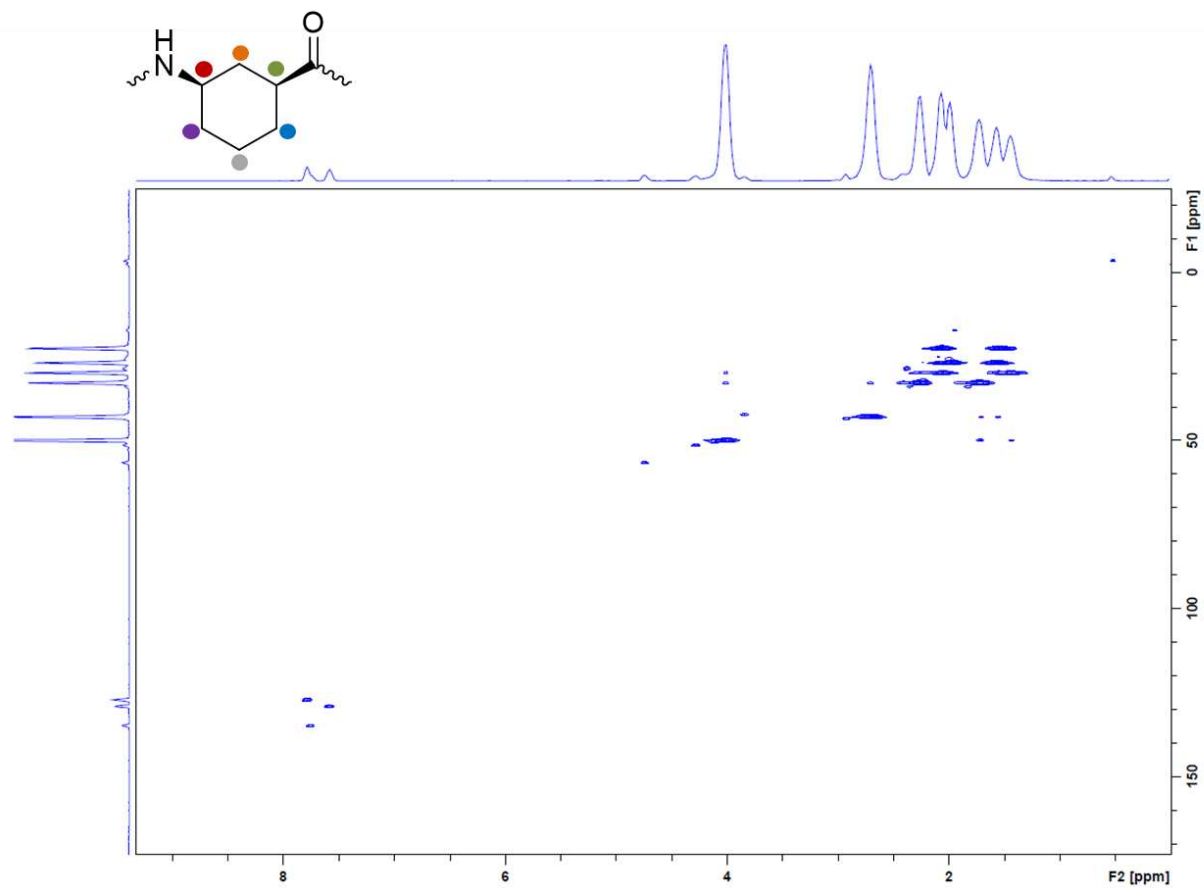


Figure S5.13. HSQC NMR (TFA-*d*) of representative nylon 4/6 produced by 50:1:1 [5/7-LM]:[^tBu-P₄]:[NBzM] at 60 °C in NMP

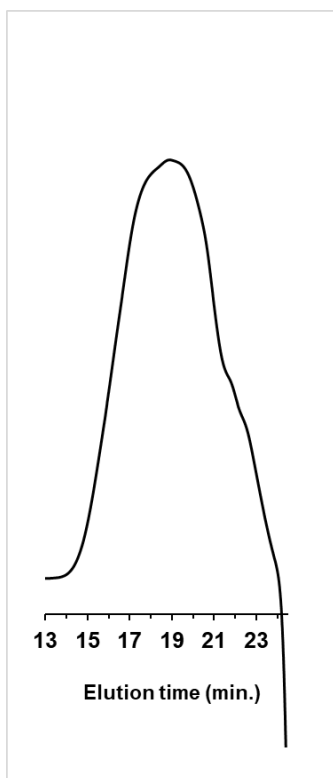


Figure S5.14. GPC trace (RI signal) of nylon 4/6 produced by 50:1:1 [5/7-LM]:[*t*-Bu-P₄]:[NBzM] at RT in NMP

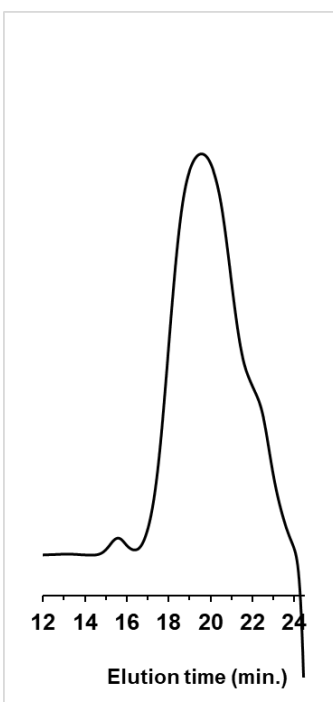


Figure S5.15. GPC trace (RI signal) of nylon 4/6 produced by 50:1:1 [5/7-LM]:[*t*-Bu-P₄]:[NBzM] at 60 °C in NMP

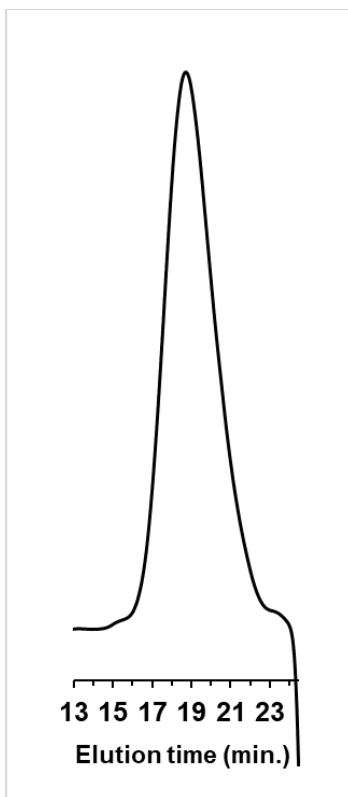


Figure S5.16. GPC trace (RI signal) of nylon 4/6 produced by 50:1:0. [5/7-LM]:[*t*-Bu-P₄]:[NBzM] at 120 °C in NMP

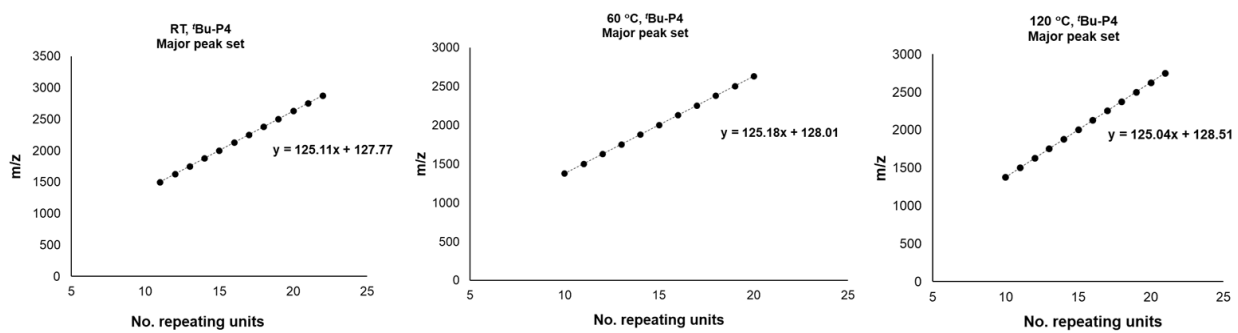


Figure S5.17. MALDI-TOF end-group analysis of *major* peak set for nylon 4/6 produced by 50:1:1 [5/7-LM]:[*t*-Bu-P₄]:[NBzM] at RT, 60, and 120 °C in NMP

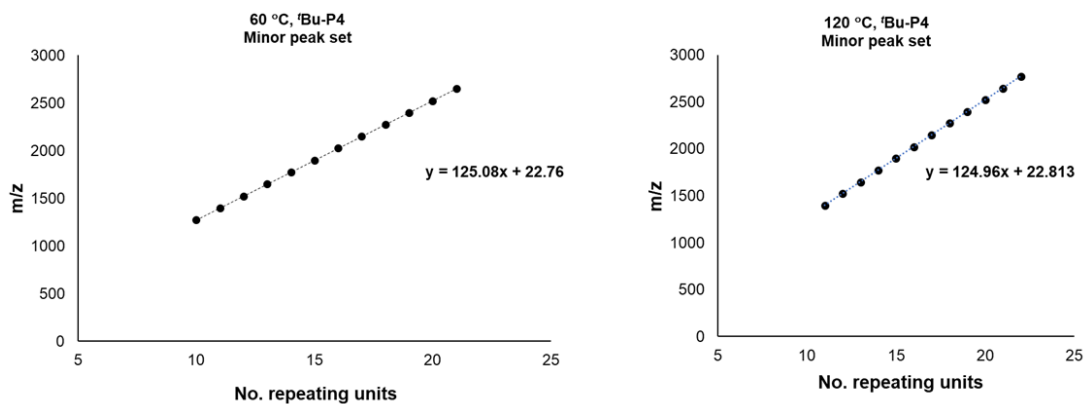


Figure S5.18. MALDI-TOF end-group analysis of *minor* peak sets for nylon 4/6 produced by 50:1:1 [5/7-LM]:['Bu-P₄]:[NBzM] at 60 and 120 °C in NMP

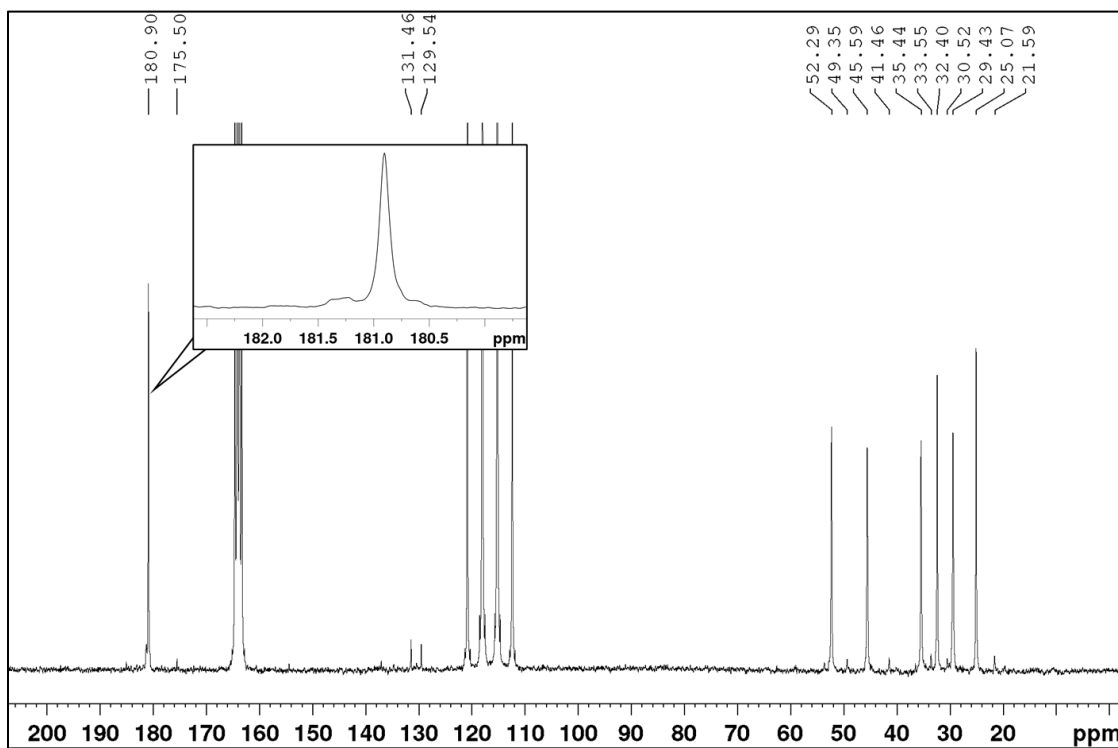


Figure S5.19. ¹³C NMR (TFA-*d*) of nylon 4/6 produced by 50:1:1 [5/7-LM]:['Bu-P₄]:[NBzM] at 120 °C in NMP

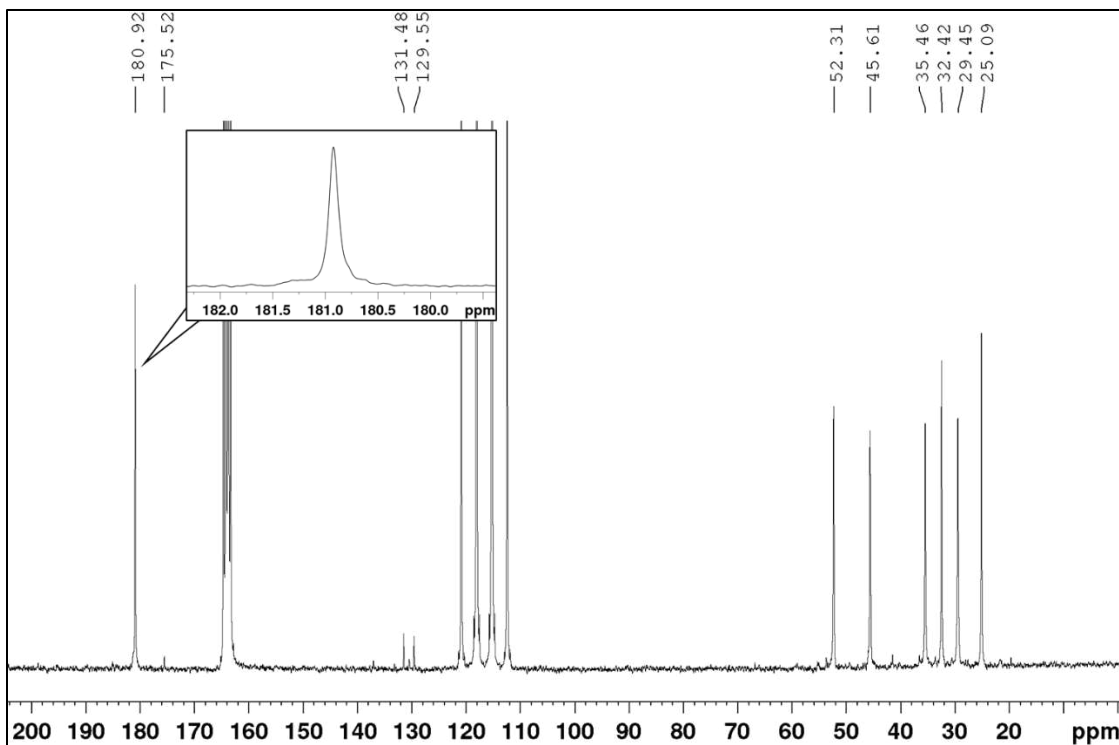


Figure S5.20. ^{13}C NMR (TFA-*d*) of nylon 4/6 produced by 50:1:1 [5/7-LM]:[NaM]:[NBzM] at 120 °C in NMP

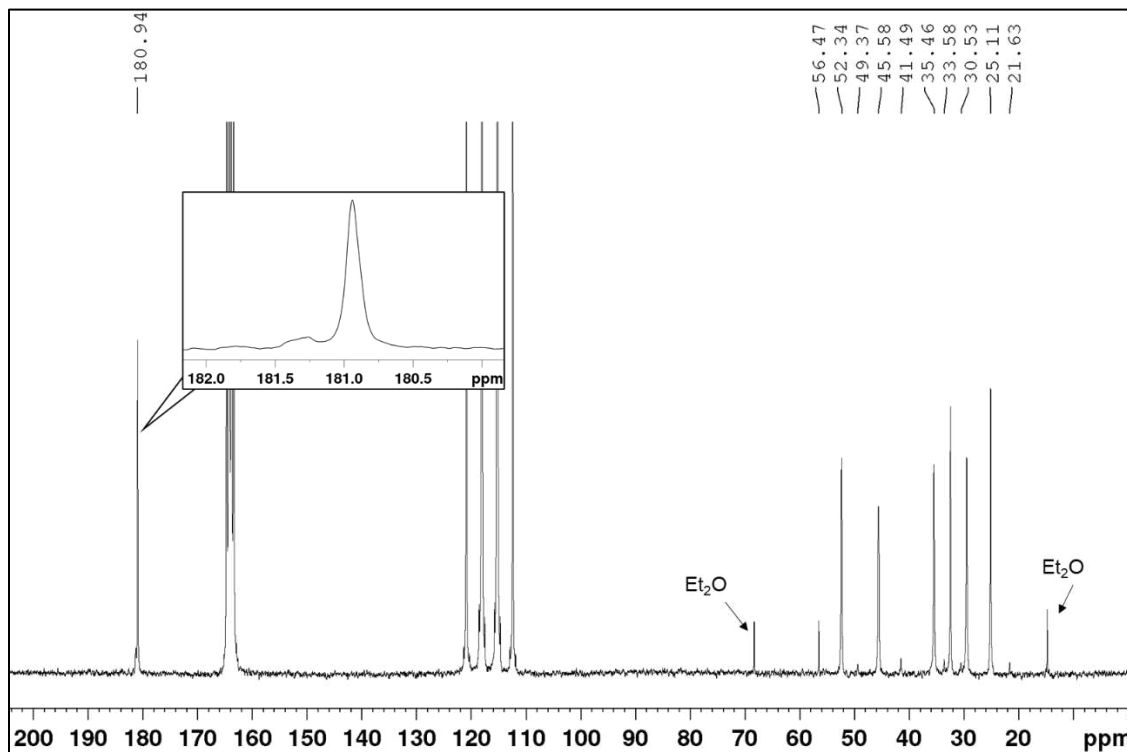


Figure S5.21. ^{13}C NMR (TFA-*d*) of nylon 4/6 produced by 50:1:0 [5/7-LM]:[*t*Bu-P₄]:[NBzM] at 120 °C in NMP

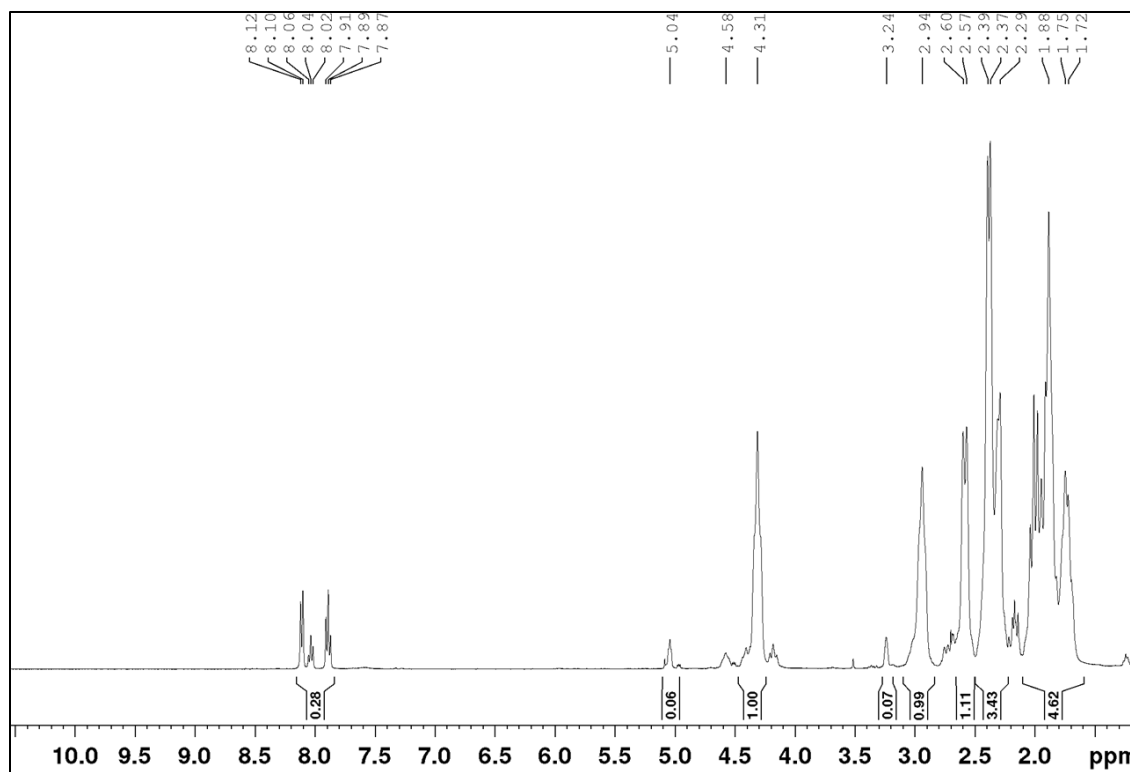


Figure S5.22. ^1H NMR (TFA-*d*, 55 °C) of chiral (-)-nylon 4/6 produced by 50:1:1 [(-)-5/7-LM]:[^tBu-P₄]:[NBzM] at RT in NMP

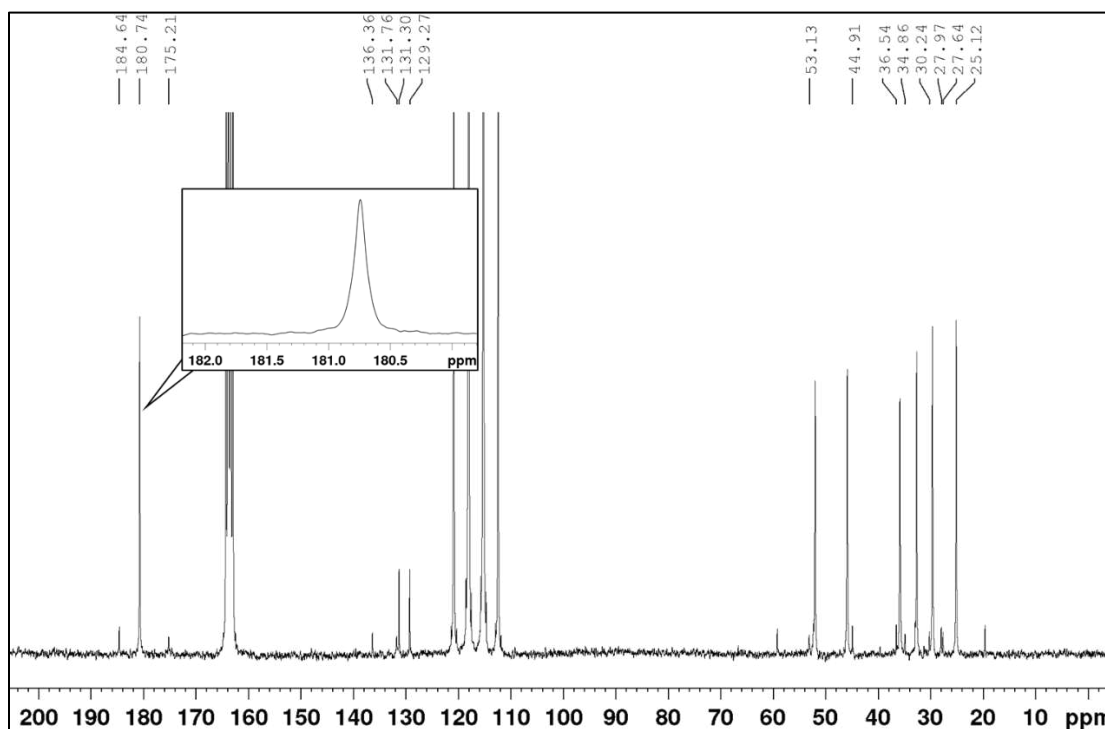


Figure S5.23. ^{13}C NMR (TFA-*d*, 55 °C) of chiral (-)-nylon 4/6 produced by 50:1:1 [(-)-5/7-LM]:[^tBu-P₄]:[NBzM] at RT in NMP

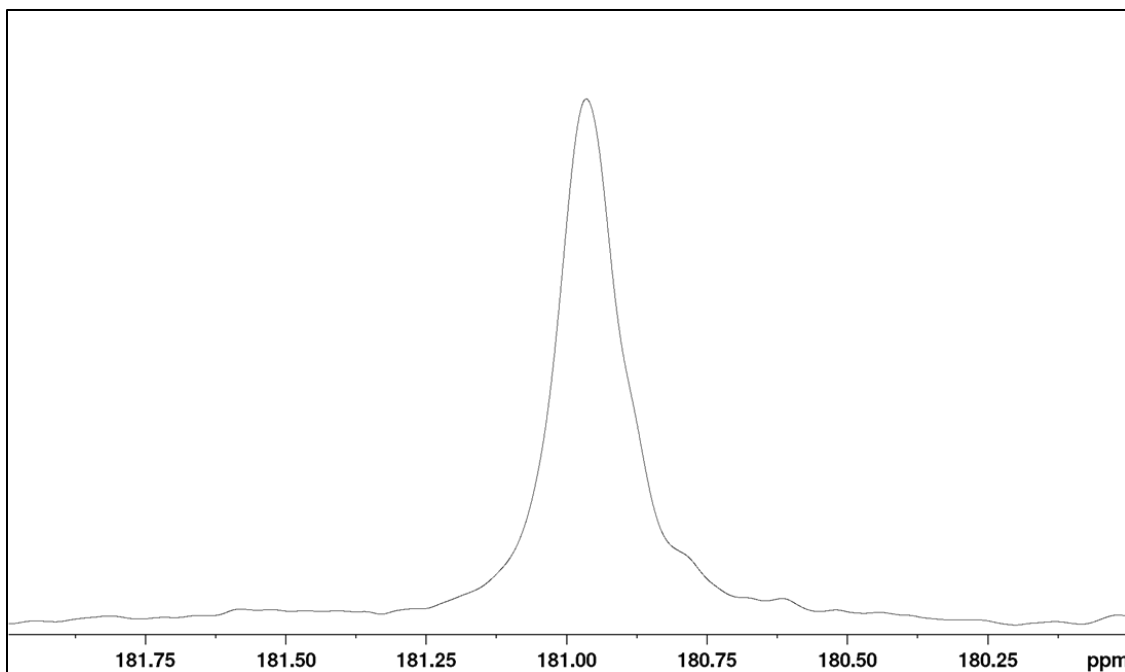


Figure S5.24. ^{13}C NMR (TFA-*d*), carbonyl region of nylon 4/6 produced by 50:1:1 [5/7-LM]:[^tBu-P₄]:[NBzM] at RT in NMP

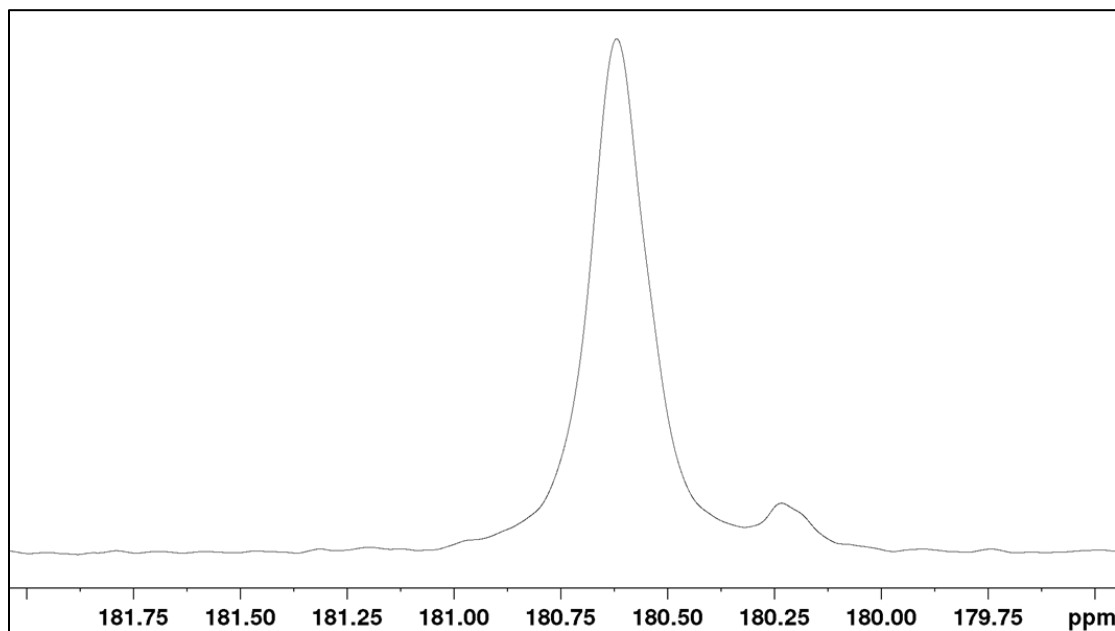


Figure S5.25. ^{13}C NMR (TFA-*d*), carbonyl region of nylon 4/6 produced by 50:1:1 [5/7-LM]:[^tBu-P₄]:[NBzM] at RT in THF

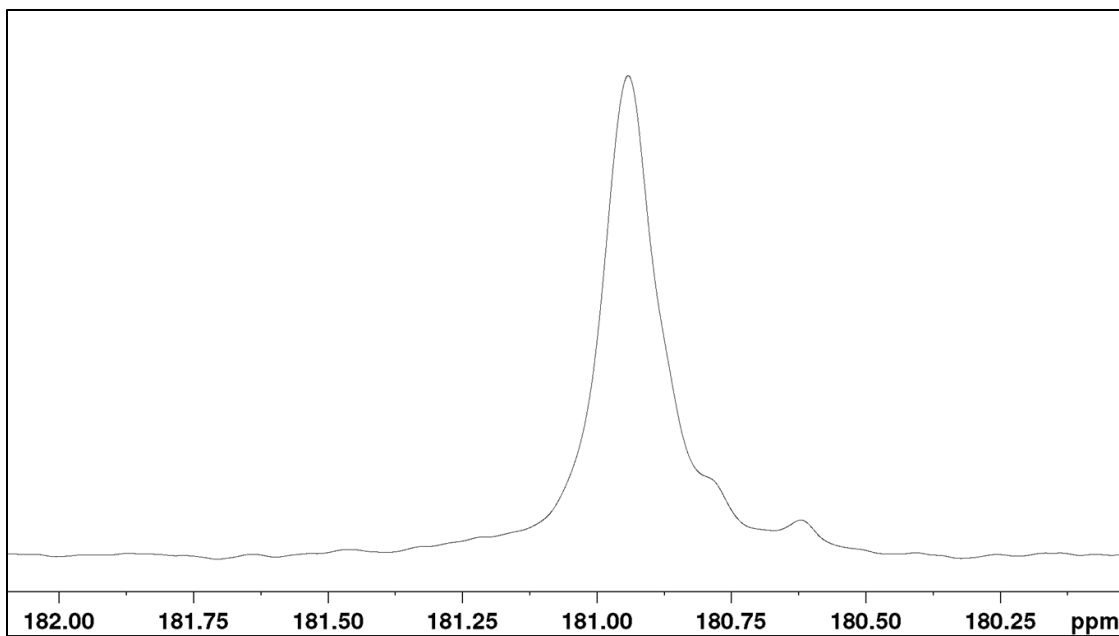


Figure S5.26. ¹³C NMR (TFA-*d*), carbonyl region of nylon 4/6 produced by 50:1:1 [5/7-LM]:[IMes]:[NBzM] at 60 °C in NMP

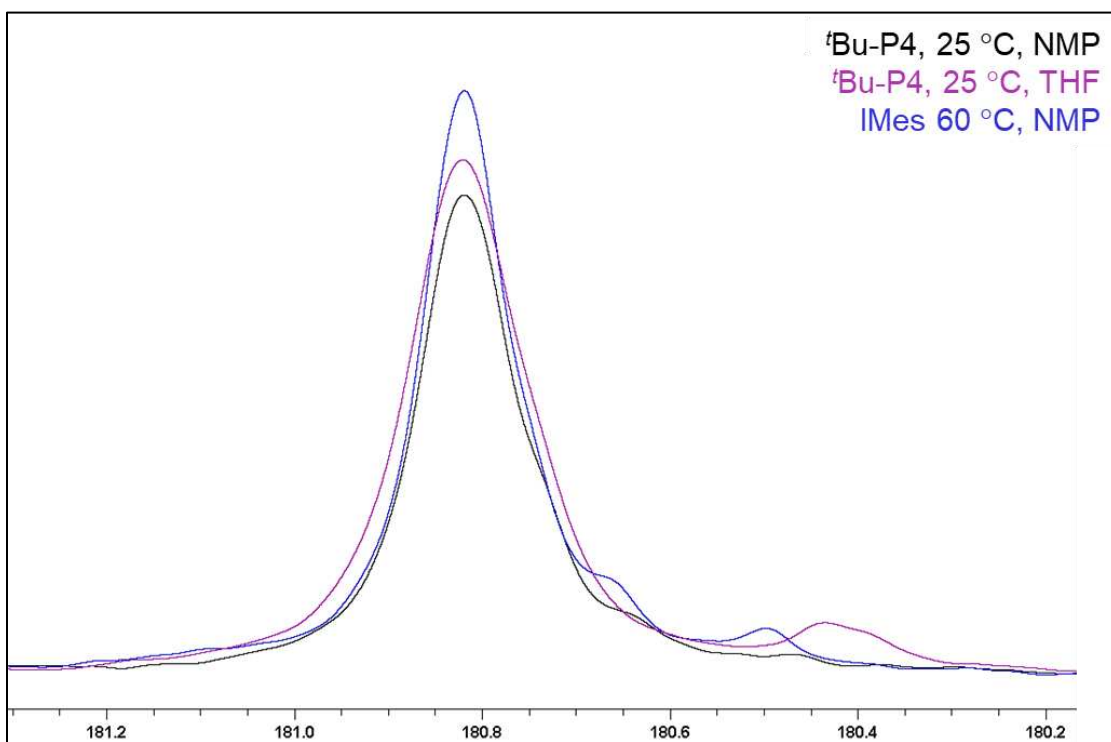


Figure S5.27. Overlay of carbonyl regions of Figures S5.22-24 highlighting tacticity differences

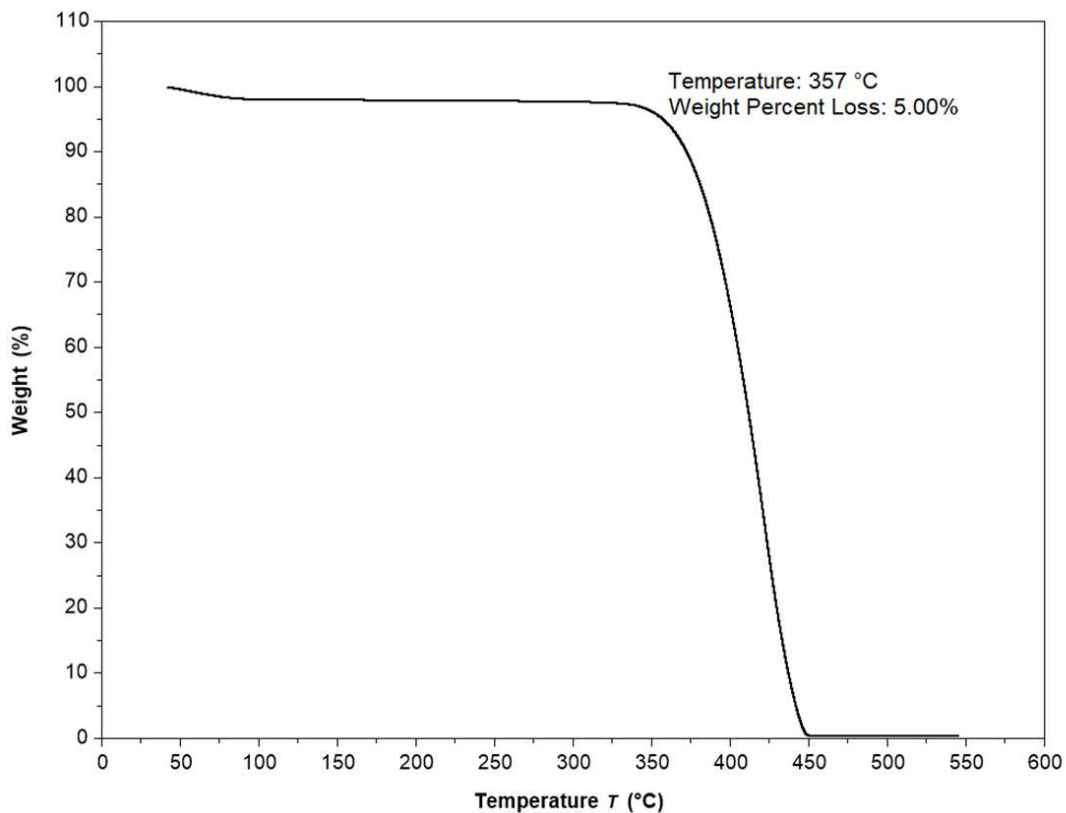


Figure S5.28. TGA Profile of nylon 4/6 produced by 50:1:1 [5/7-LM]:[*t*Bu-P₄]:[NBzM] at RT in NMP

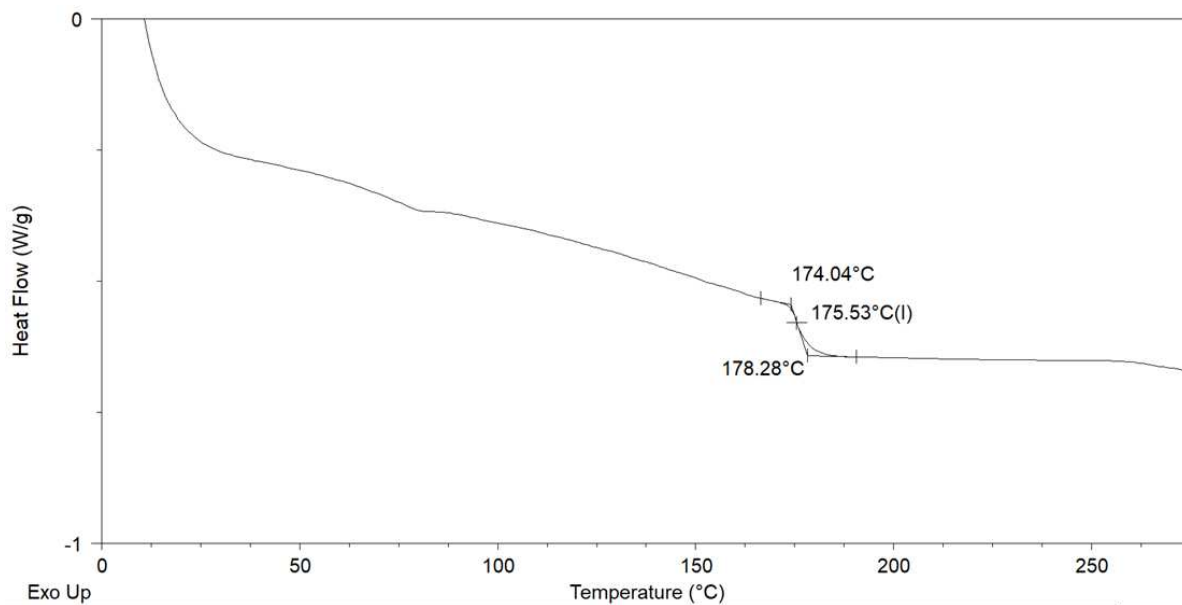


Figure S5.29. DSC of nylon 4/6 thin film ramped 40 °C/min, first scan

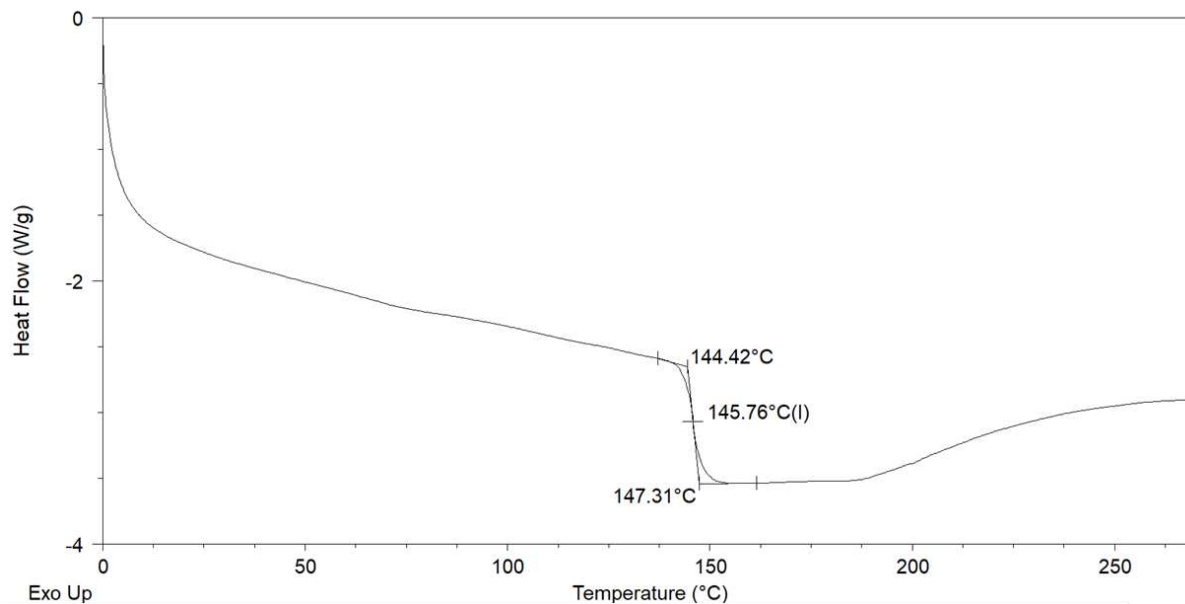


Figure S5.30. DSC of nylon 4/6 thin film ramped 40 °C/min, first scan

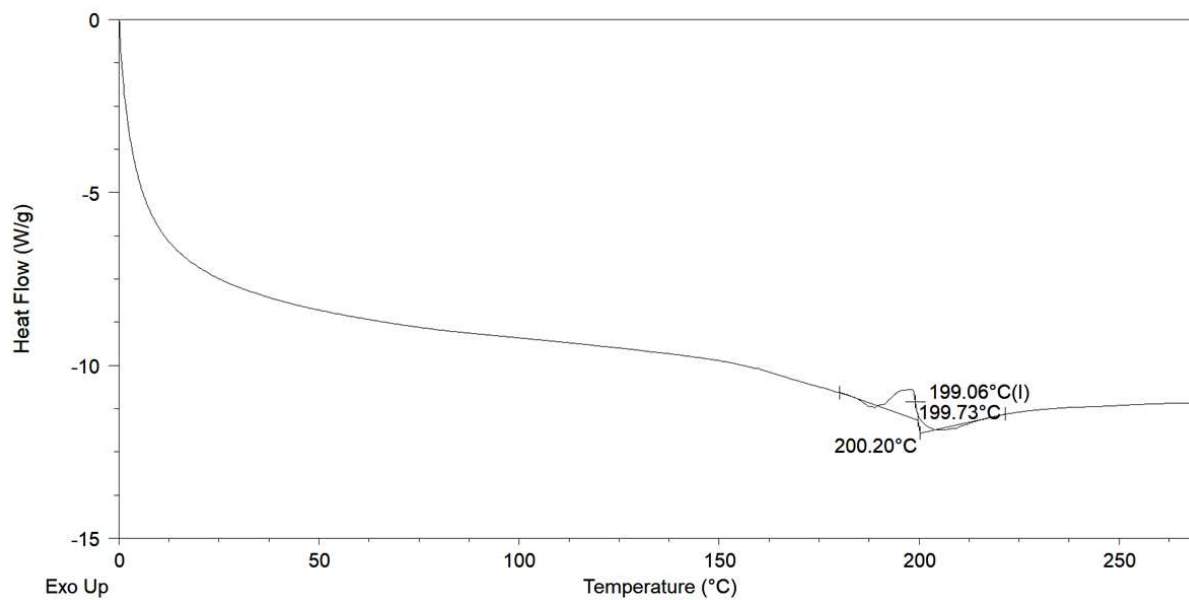


Figure S5.31. DSC of nylon 4/6 thin film ramped 40 °C/min, first scan

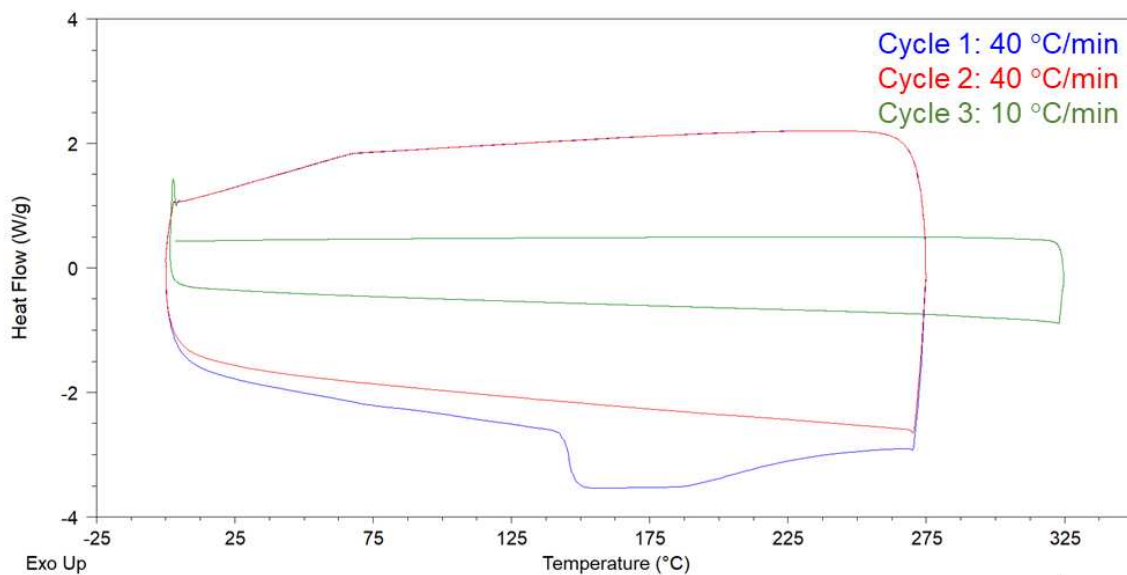


Figure S5.32. DSC of nylon 4/6 thin film, all cycles

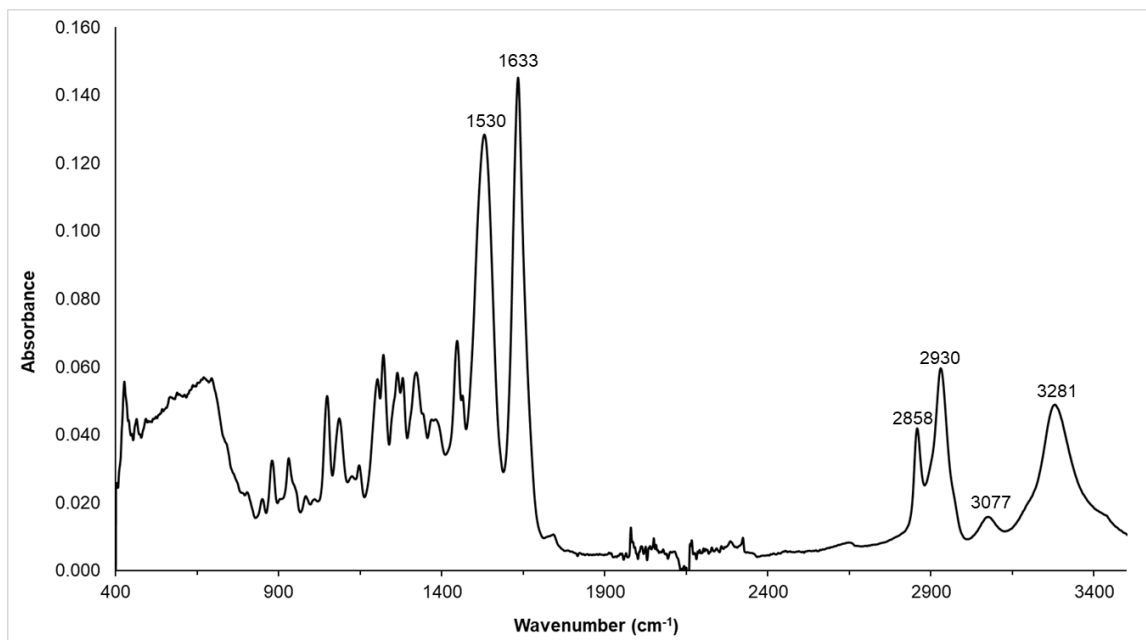


Figure S5.33. FTIR spectrum of nylon 4/6

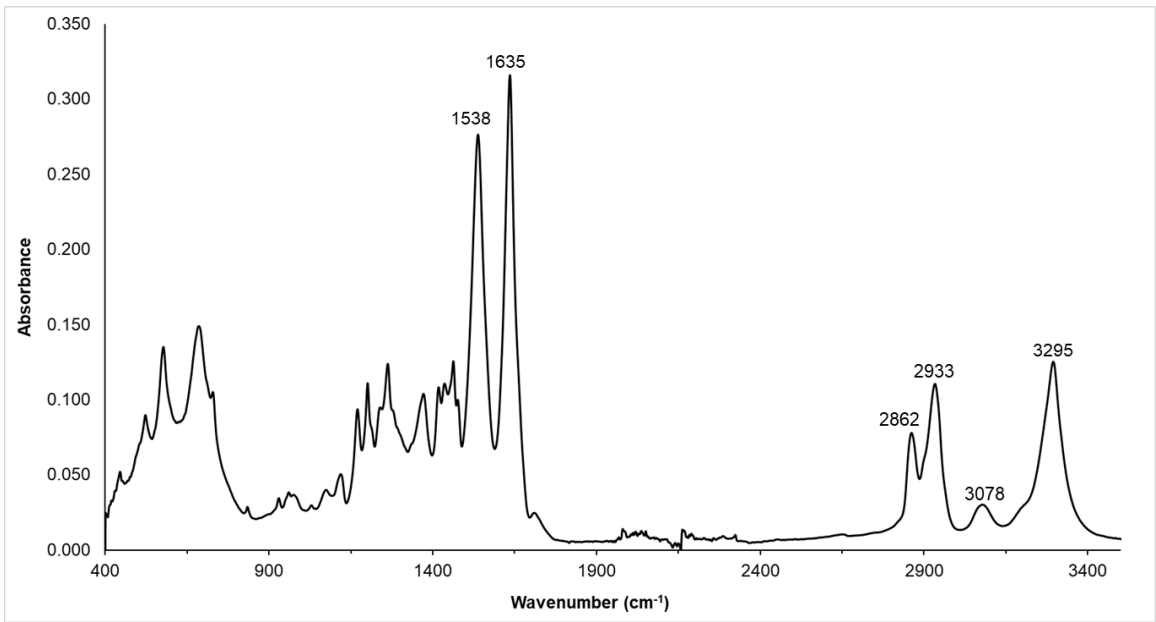


Figure S5.34. FTIR spectrum of nylon 6

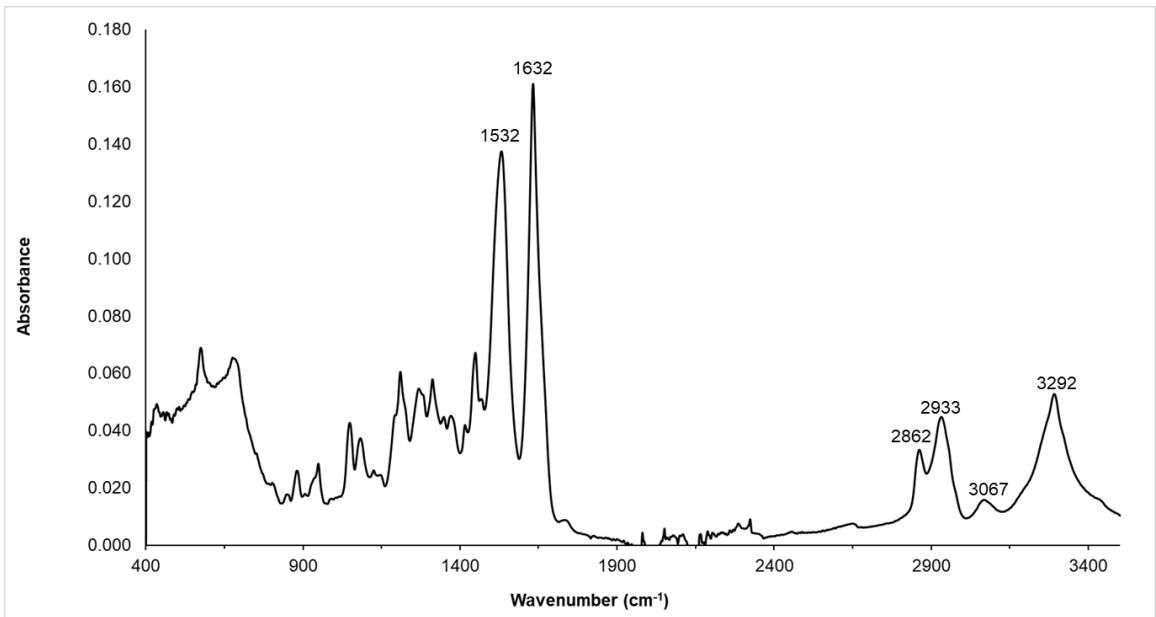
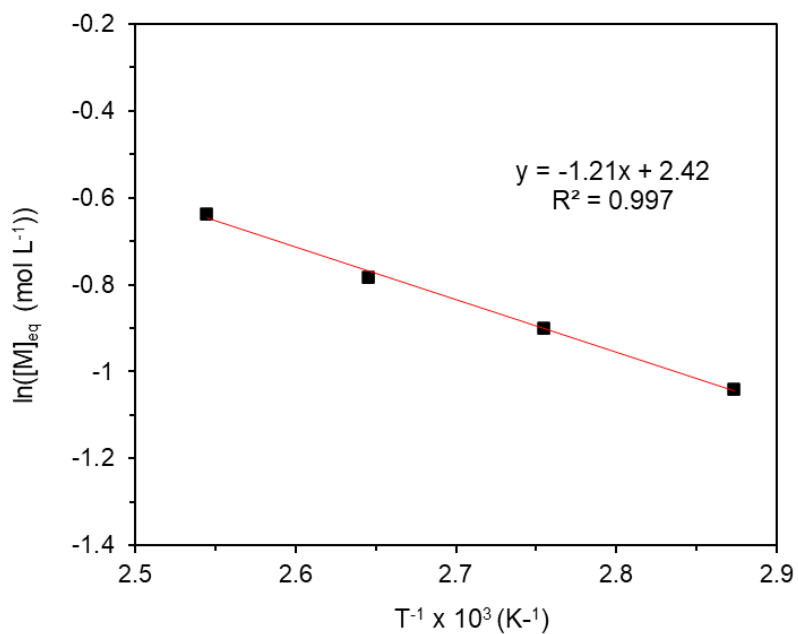


Figure S5.35. FTIR spectrum of nylon 4



$T, ^\circ\text{C}$	MS Concentration Values, $\mu\text{g/ml}$	Dilution Factors applied, g/L ($2.81 \times 15 \times 10$)	Mol/L ($[M]_{\text{eq}}$)	$\ln[M]_{\text{eq}}$
75	104.923	44.224	0.353	-1.0404
90	120.632	50.846	0.406	-0.90088
105	135.748	57.217	0.457	-0.78282
120	156.886	66.126	0.528	-0.63811

Figure S5.36. Van 't Hoff Plot and raw data for 5/7-LM polymerization at $[M]_0 = 0.96 \text{ M}$



Figure S5.37. Photos of nylon 4/6 (275 mg) before and after recycling by chemolysis with ZnCl_2 at $290 \text{ }^\circ\text{C}$ (external temperature), 18h.

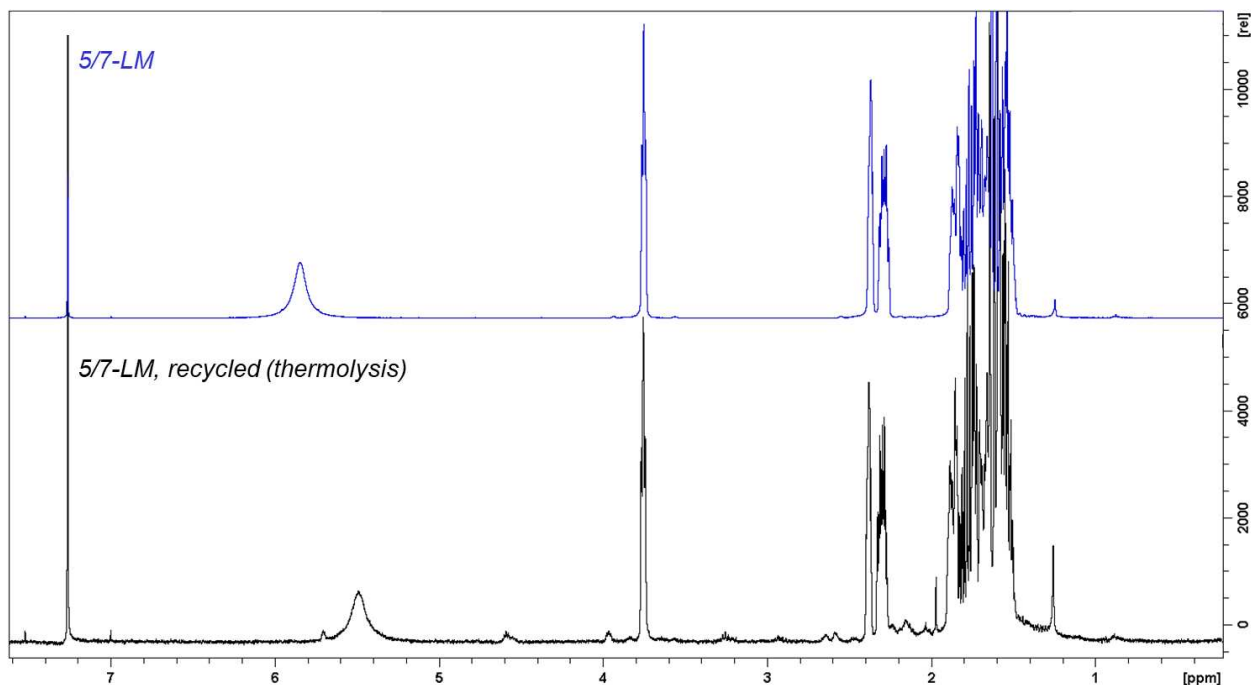


Figure S5.38. ^1H NMR (CDCl_3) of recycled monomer via thermolysis (100 mg nylon 4/6 decomposed at 400-475 $^\circ\text{C}$ (external temperature), 3.5h) compared to pure, starting monomer.

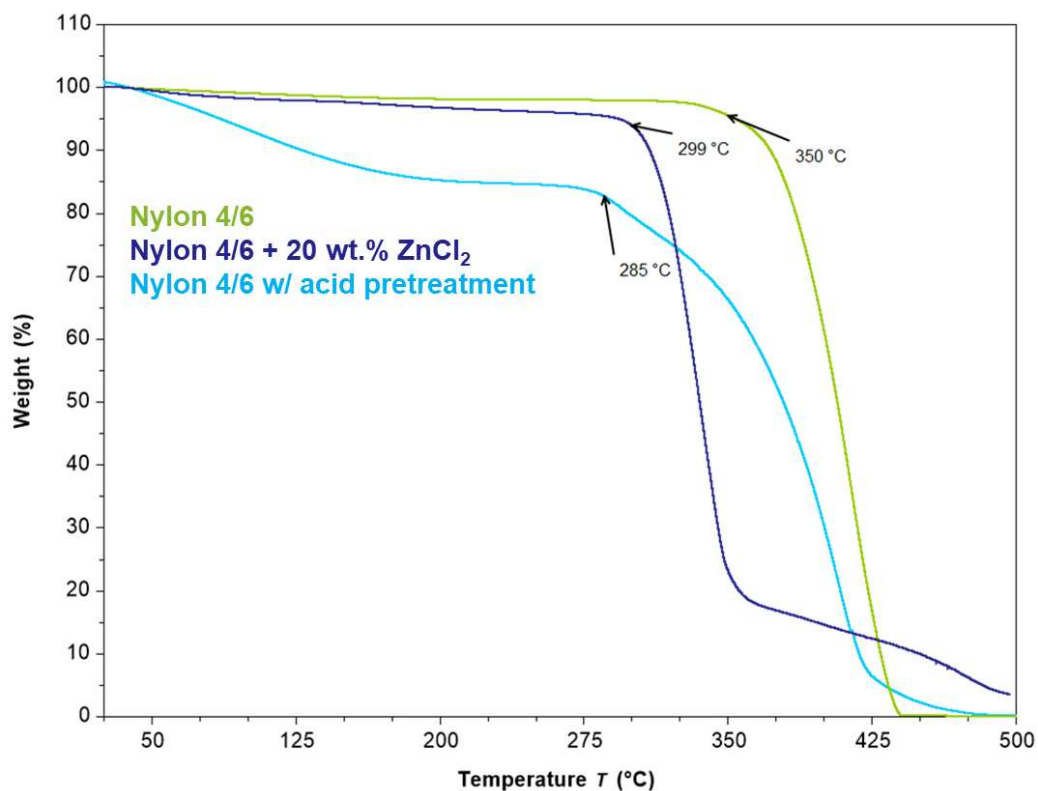


Figure S5.39. Effect of ZnCl_2 catalyst and HCl pretreatment on nylon 4/6 decomposition. Residue in ZnCl_2 profile (navy) after ~ 350 $^\circ\text{C}$ is degradation of the 20 wt.% catalyst.

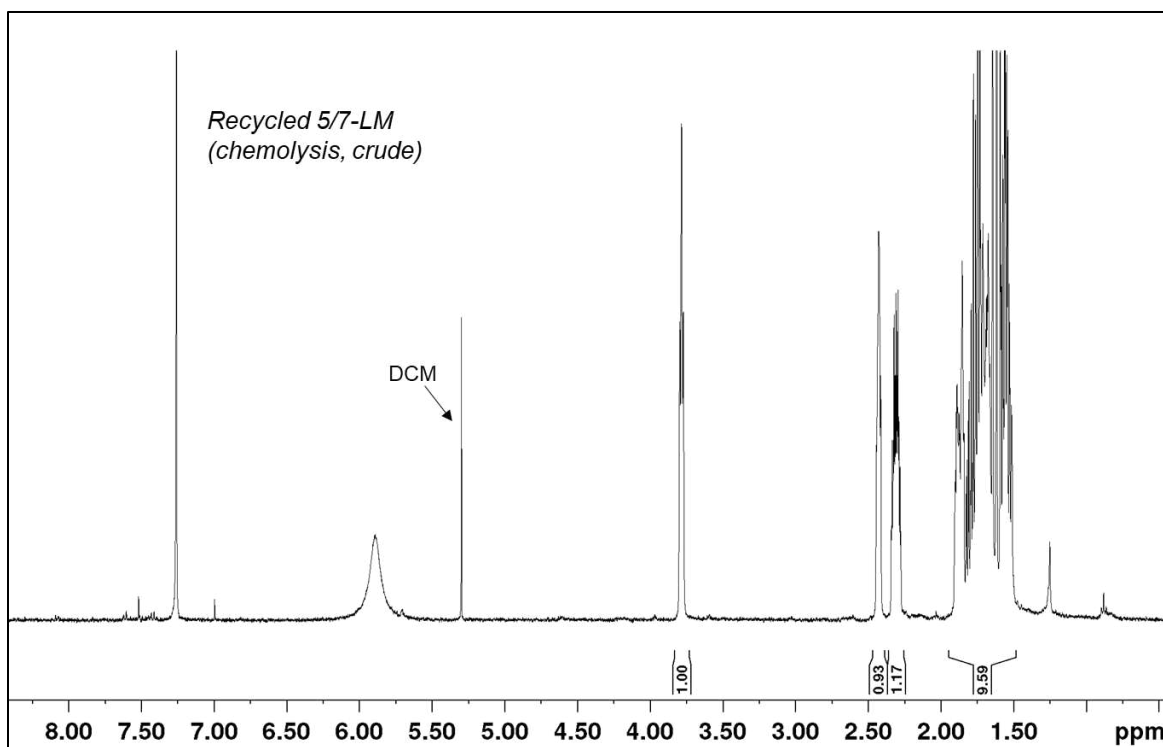


Figure S5.40. ^1H NMR (CDCl_3) of crude, recycled 5/7-LM after recycling 275 mg nylon 4/6 with 20 wt.% ZnCl_2 at 290 °C (external temperature) over 18h

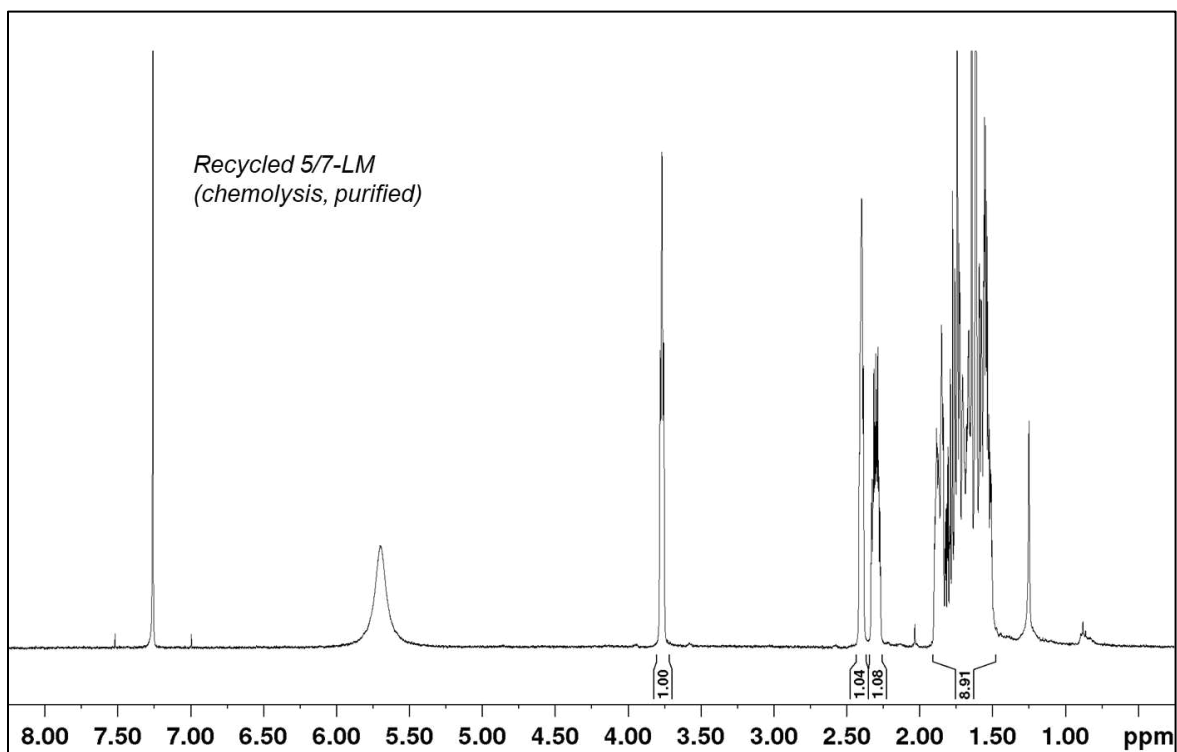


Figure S5.41. ^1H NMR (CDCl_3) of purified, recycled 5/7-LM

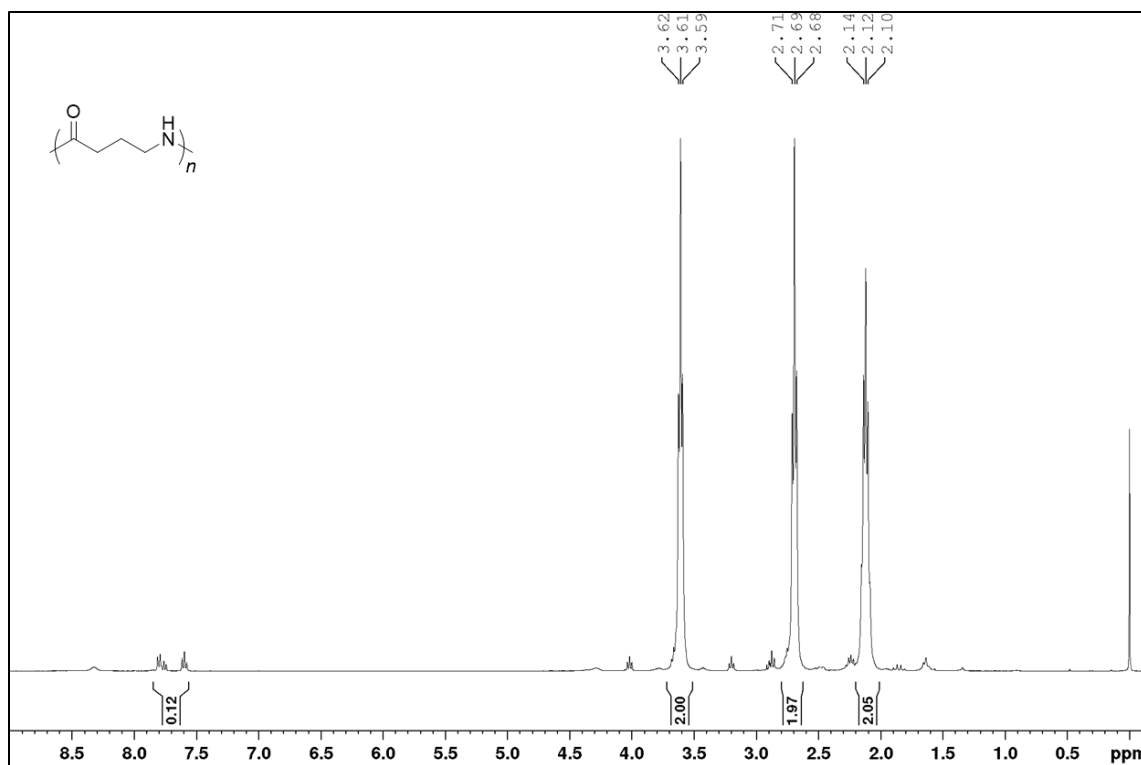


Figure S5.42. ^1H NMR ($\text{TFA-}d$) of nylon 4 produced by 50:1:1 [5-LM]:[$t\text{-Bu-P}_4$]:[NBzM]

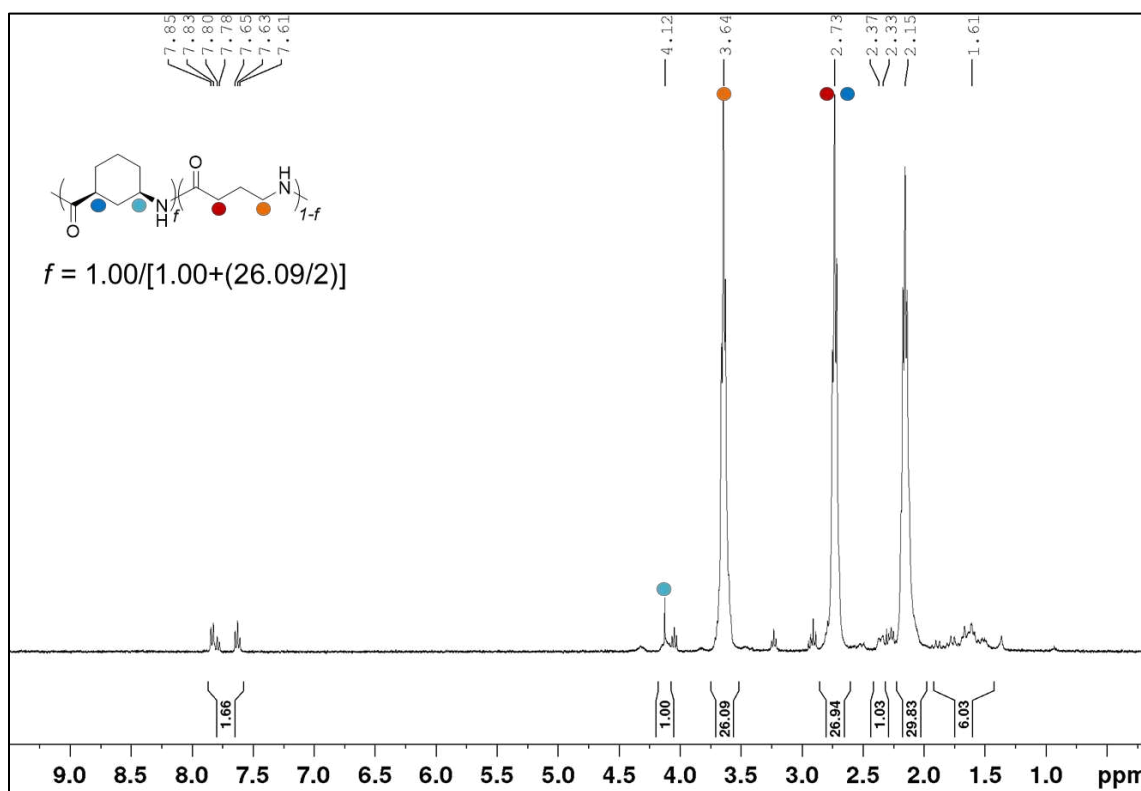


Figure S43. ^1H NMR ($\text{TFA-}d$) of nylon 4/6-co-nylon 4 produced with 5:95 monomer ratio and 50:1:1 [M_{tot}]:[$t\text{-Bu-P}_4$]:[NBzM]

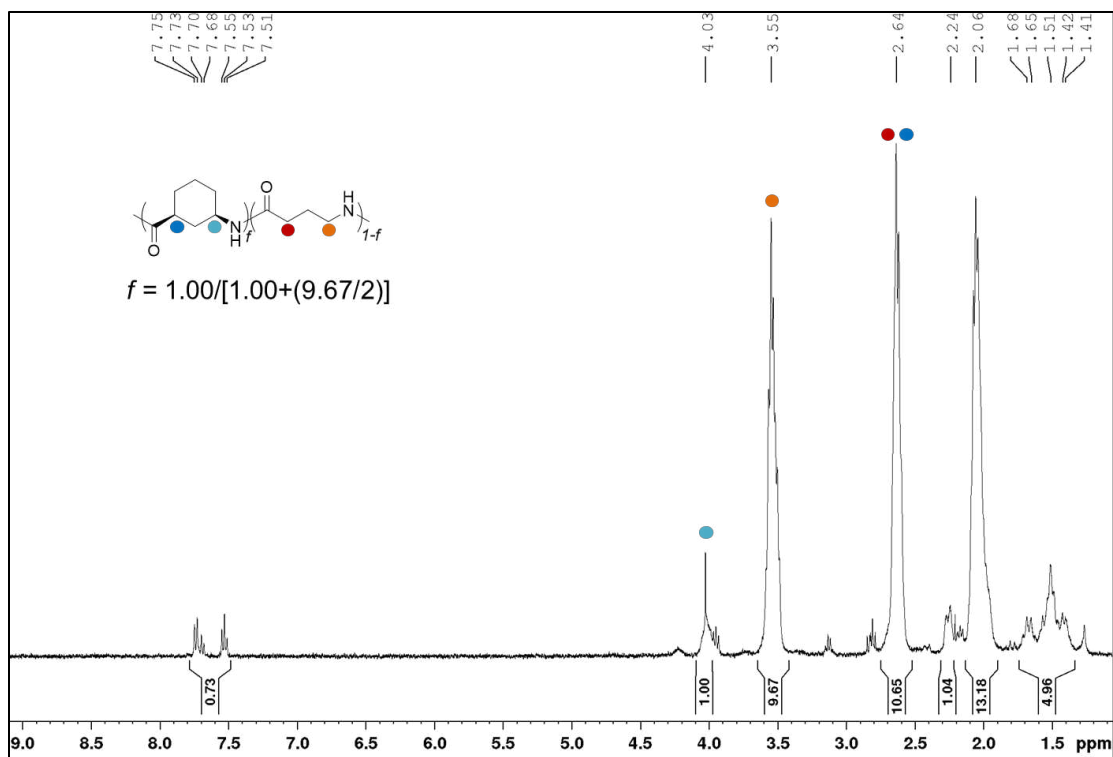


Figure S5.44. ^1H NMR (TFA-*d*) of nylon 4/6-*co*-nylon 4 produced with 15:85 monomer ratio and 50:1:1 $[\text{M}_{\text{tot}}]:[\text{Bu-P}_4]:[\text{NBzM}]$

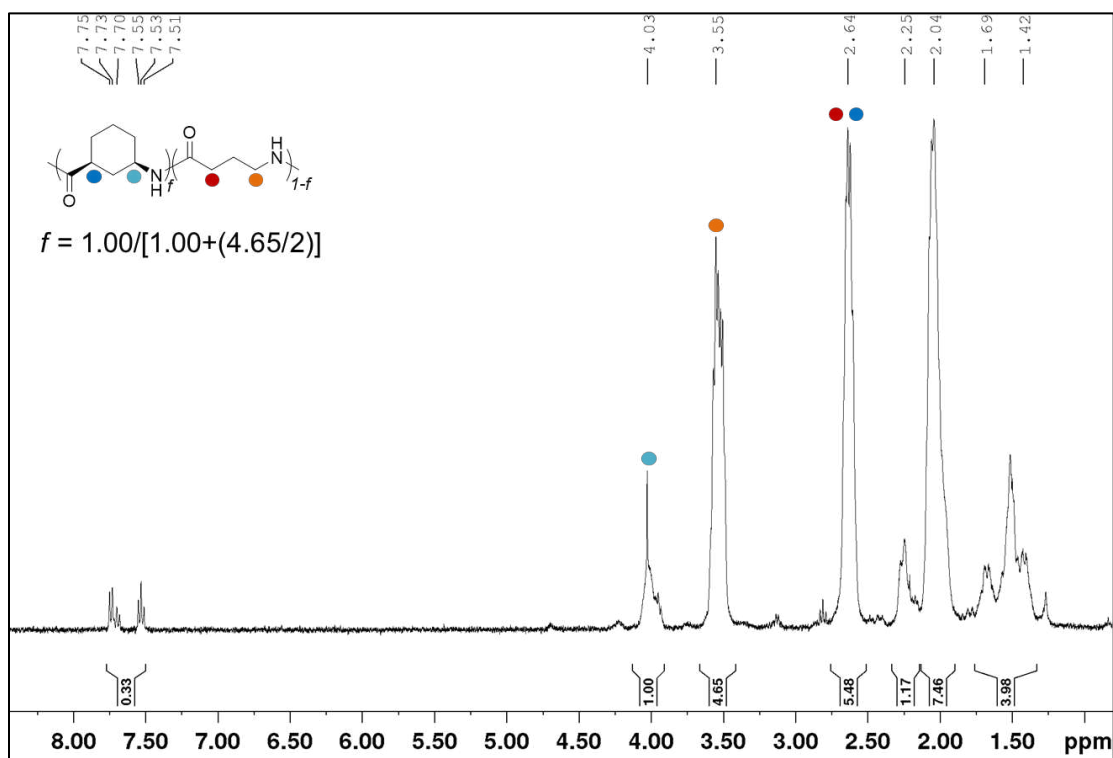


Figure S5.45. ^1H NMR (TFA-*d*) of nylon 4/6-*co*-nylon 4 produced with 25:75 monomer ratio and 50:1:1 $[\text{M}_{\text{tot}}]:[\text{Bu-P}_4]:[\text{NBzM}]$

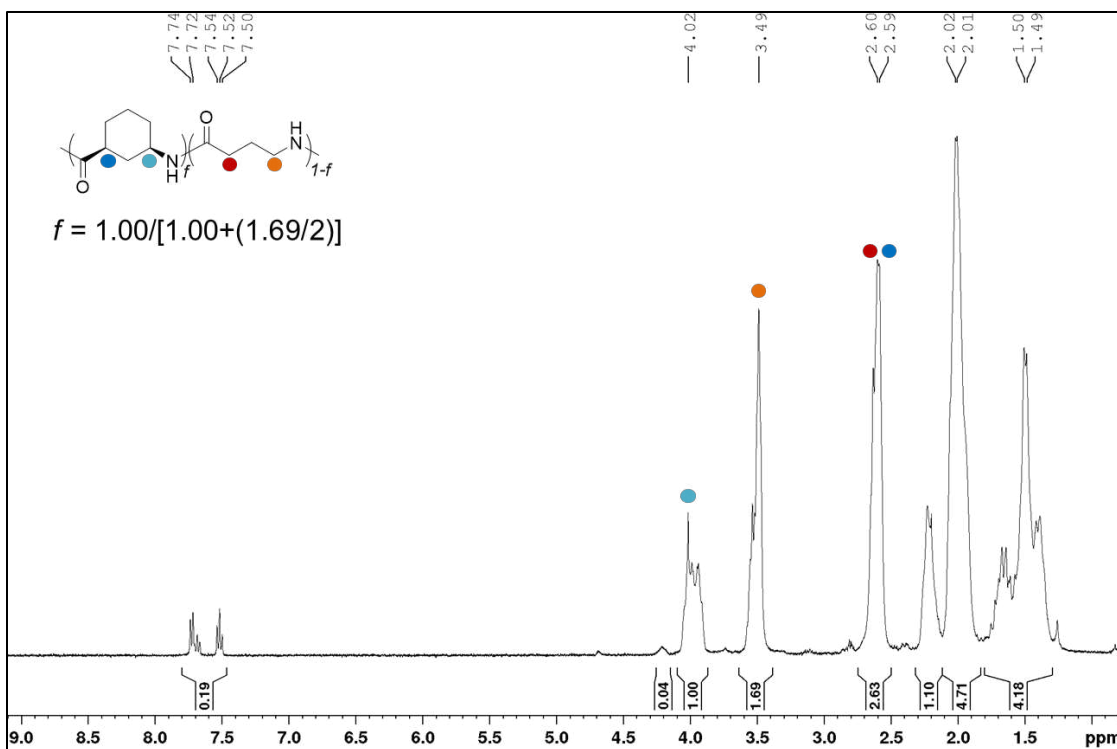


Figure S5.46. ^1H NMR (TFA-*d*) of nylon 4/6-*co*-nylon 4 produced with 50:50 monomer ratio and 50:1:1 $[\text{M}_{\text{tot}}]:[\text{Bu-P}_4]:[\text{NBzM}]$

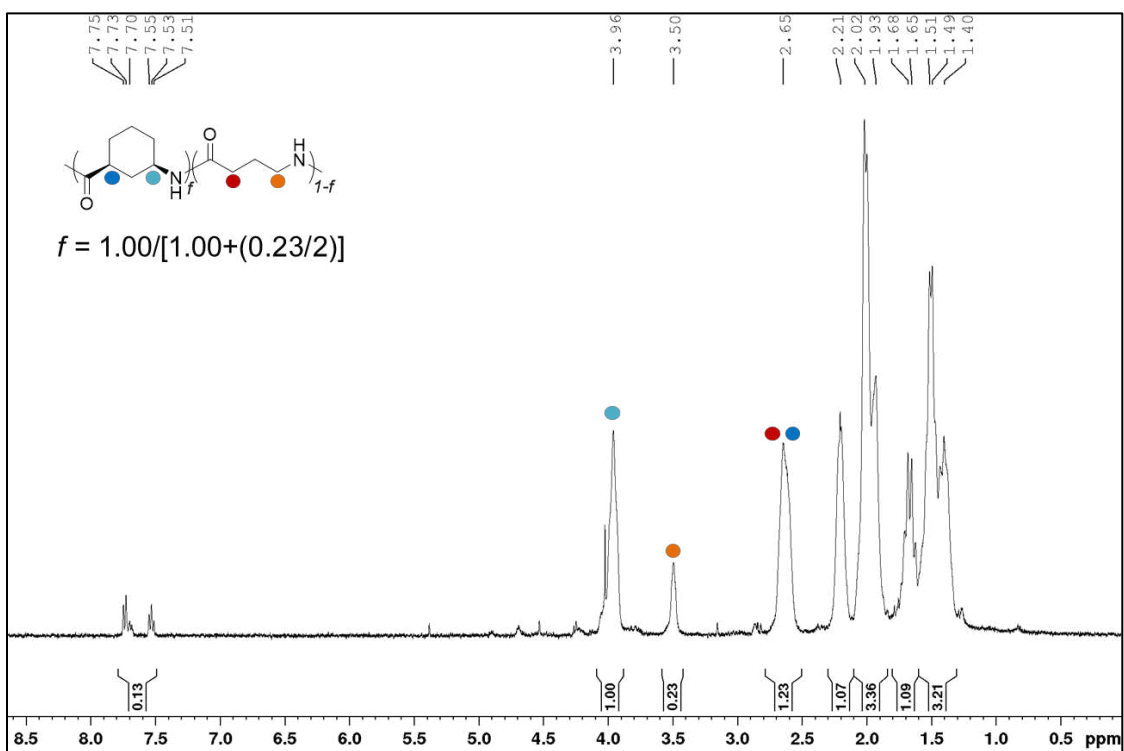


Figure S5.47. ^1H NMR (TFA-*d*) of nylon 4/6-*co*-nylon 4 produced with 85:15 monomer ratio and 50:1:1 $[\text{M}_{\text{tot}}]:[\text{Bu-P}_4]:[\text{NBzM}]$

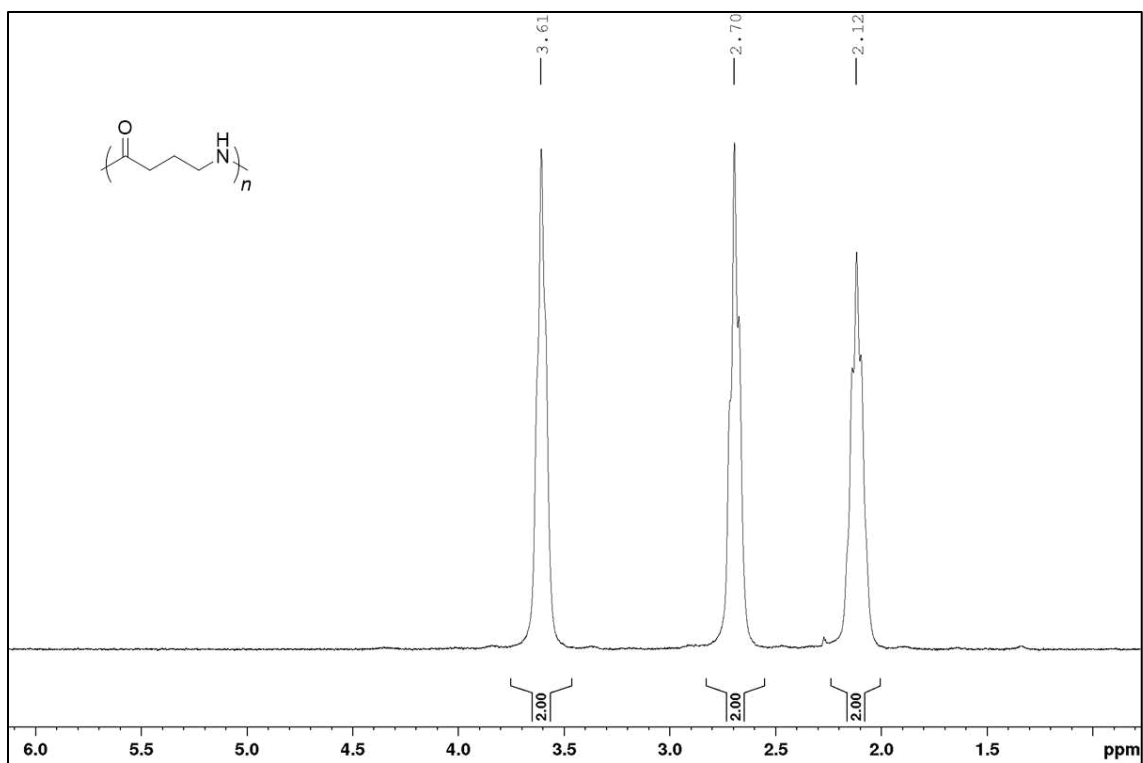


Figure S5.48. ^1H NMR ($\text{TFA-}d$) of nylon 4 produced by 250:1:1 [5-LM]:[Na5LM]:[NBzM]

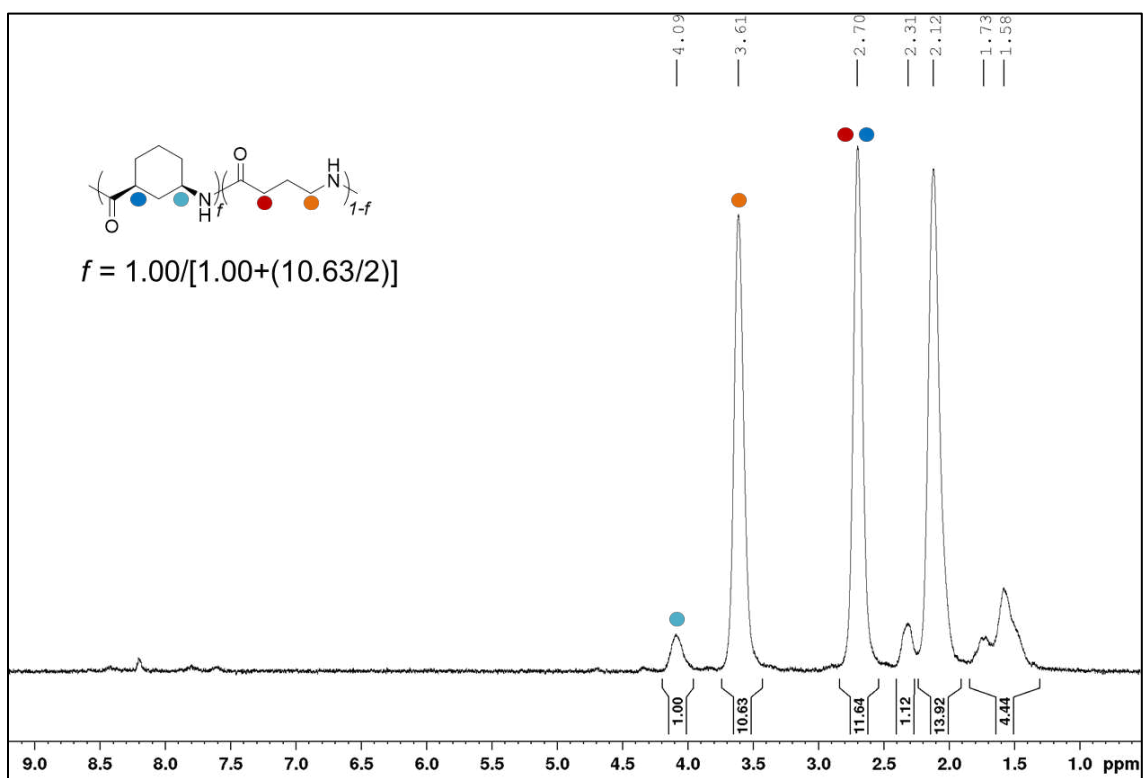


Figure S5.49. ^1H NMR ($\text{TFA-}d$) of nylon 4/6-co-nylon 4 produced with 15:85 monomer ratio and 250:5:1 [M_{tot}]:[Na5LM]:[NBzM]

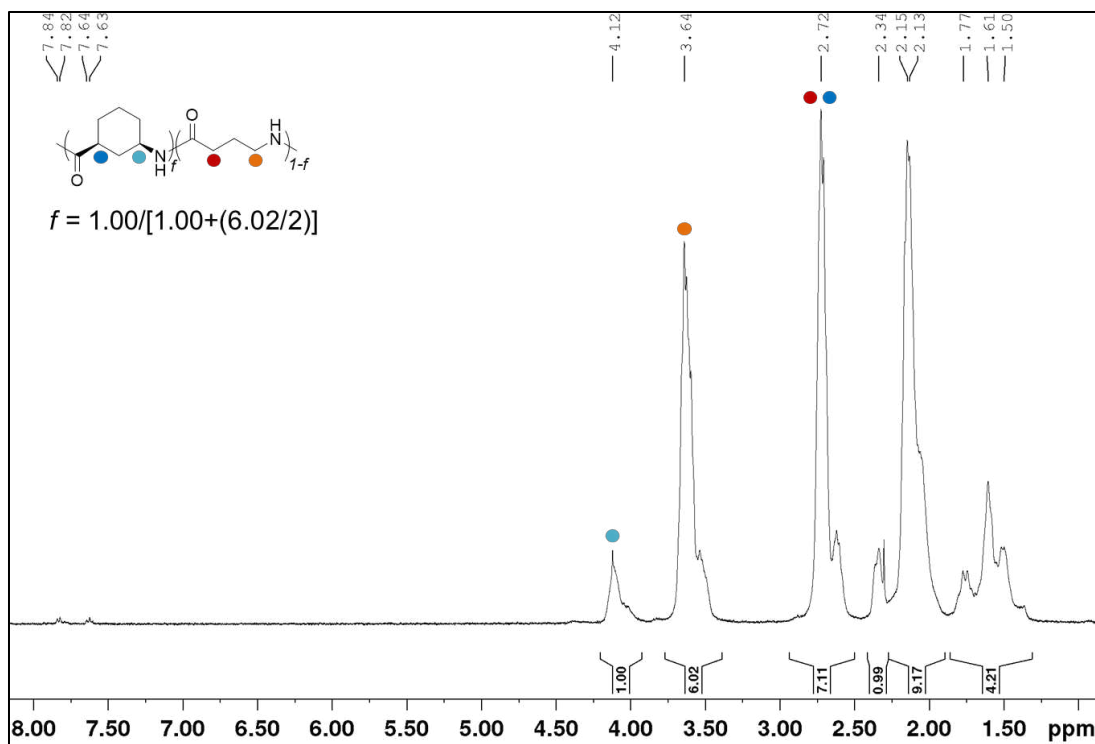


Figure S5.50. ^1H NMR (TFA-*d*) of nylon 4/6-*co*-nylon 4 produced with 25:75 monomer ratio and 250:5:1 $[\text{M}_{\text{tot}}]:[\text{Na5LM}]:[\text{NBzM}]$

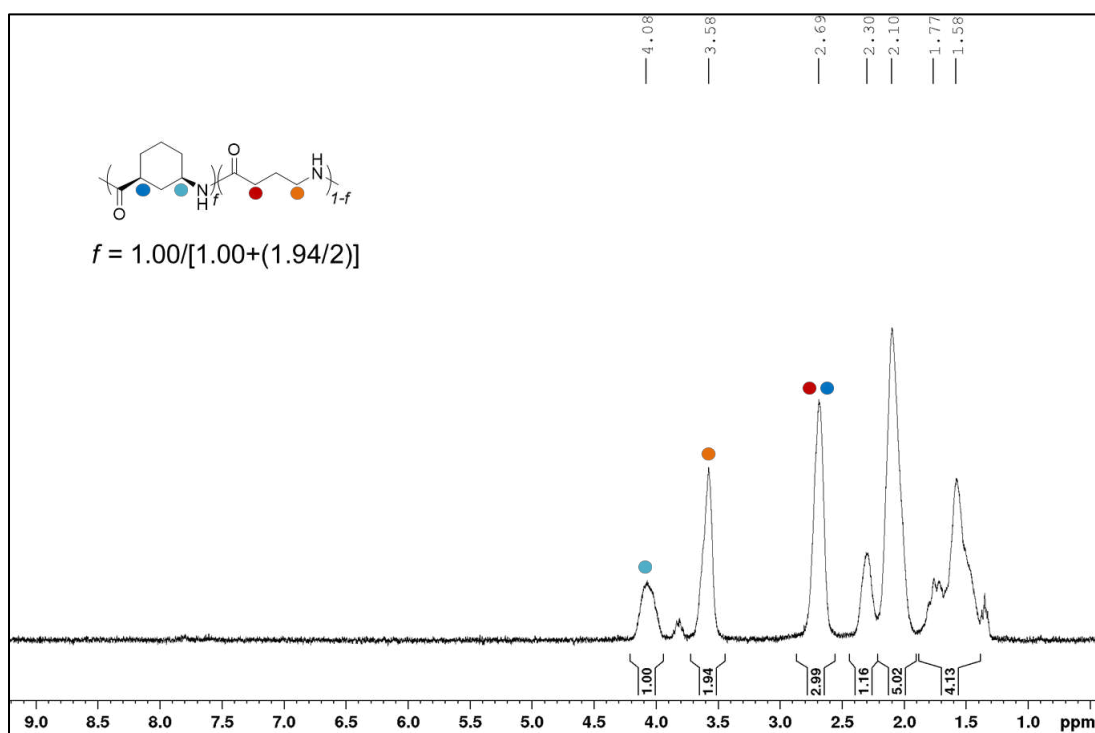


Figure S5.51. ^1H NMR (TFA-*d*) of nylon 4/6-*co*-nylon 4 produced with 50:50 monomer ratio and 250:5:1 $[\text{M}_{\text{tot}}]:[\text{Na5LM}]:[\text{NBzM}]$

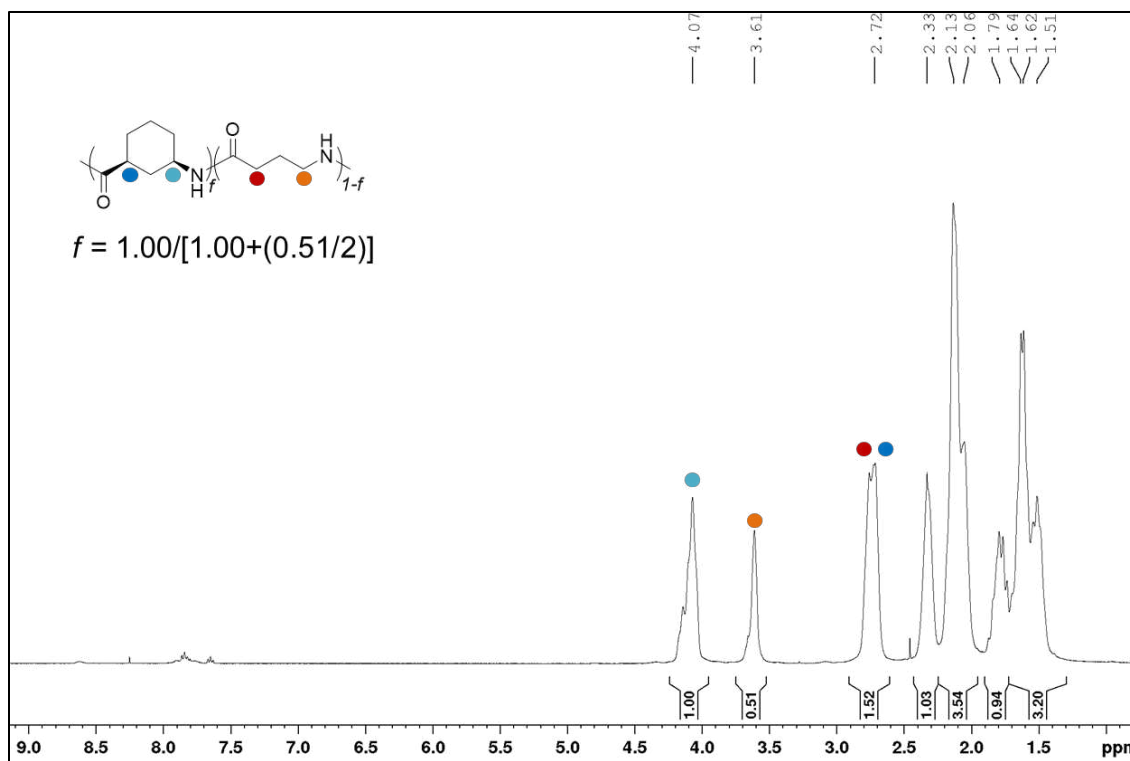


Figure S5.52. ^1H NMR (TFA-*d*) of nylon 4/6-*co*-nylon 4 produced with 85:15 monomer ratio and 250:5:1 $[\text{M}_{\text{tot}}]:[\text{Na5LM}]:[\text{NBzM}]$

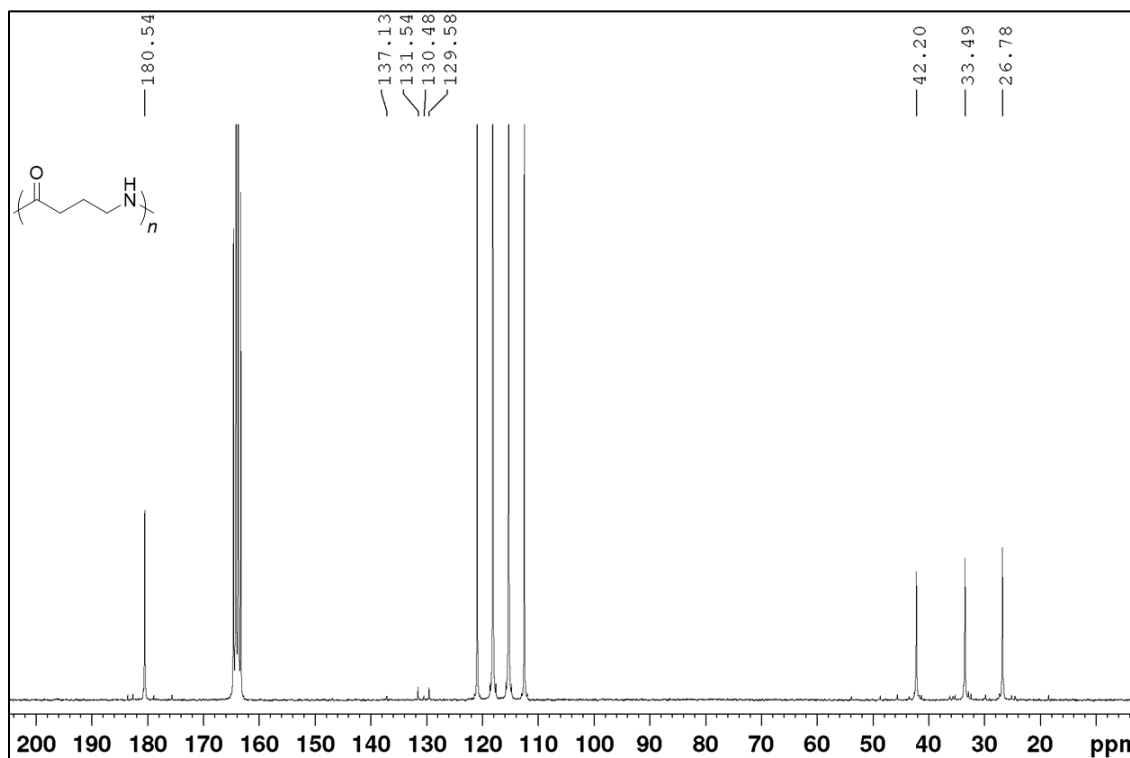


Figure S5.53. ^{13}C NMR (TFA-*d*) of nylon 4 produced by 50:1:1 [5-LM]:[t Bu-P₄]:[NBzM]

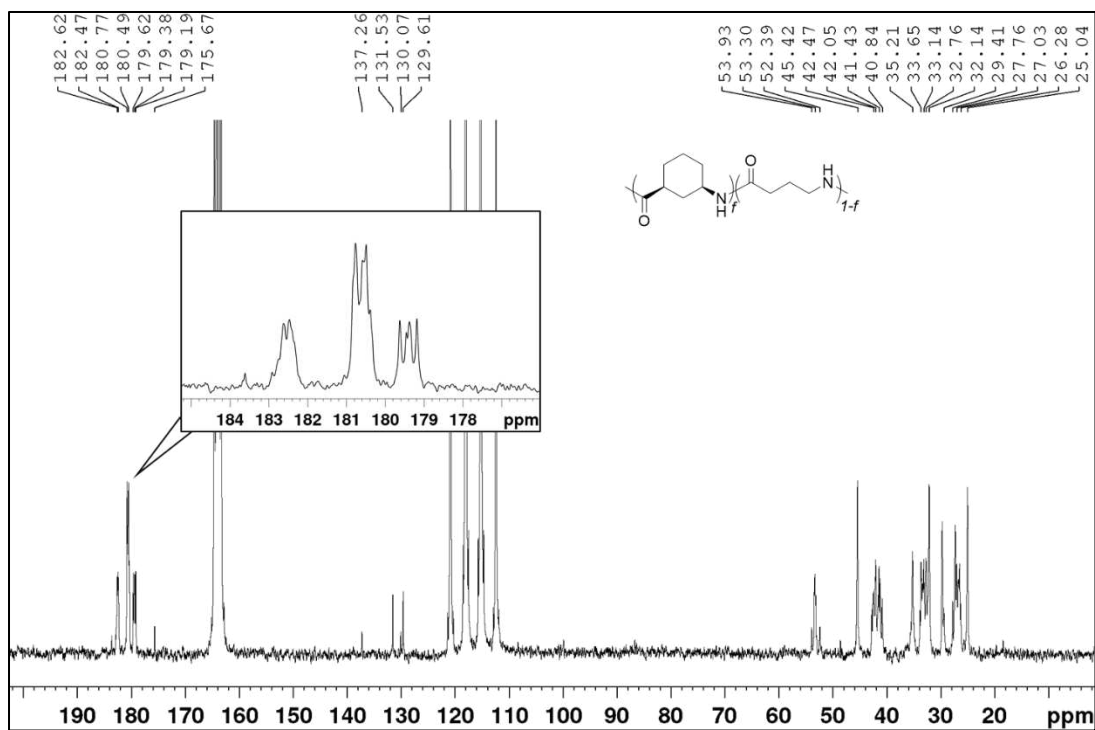


Figure S5.54. ^{13}C NMR (TFA-*d*) of nylon 4/6-*co*-nylon 4 produced with 15:85 monomer ratio and 50:1:1 $[\text{M}_{\text{tot}}]:[\text{'Bu-P}_4]:[\text{NBzM}]$

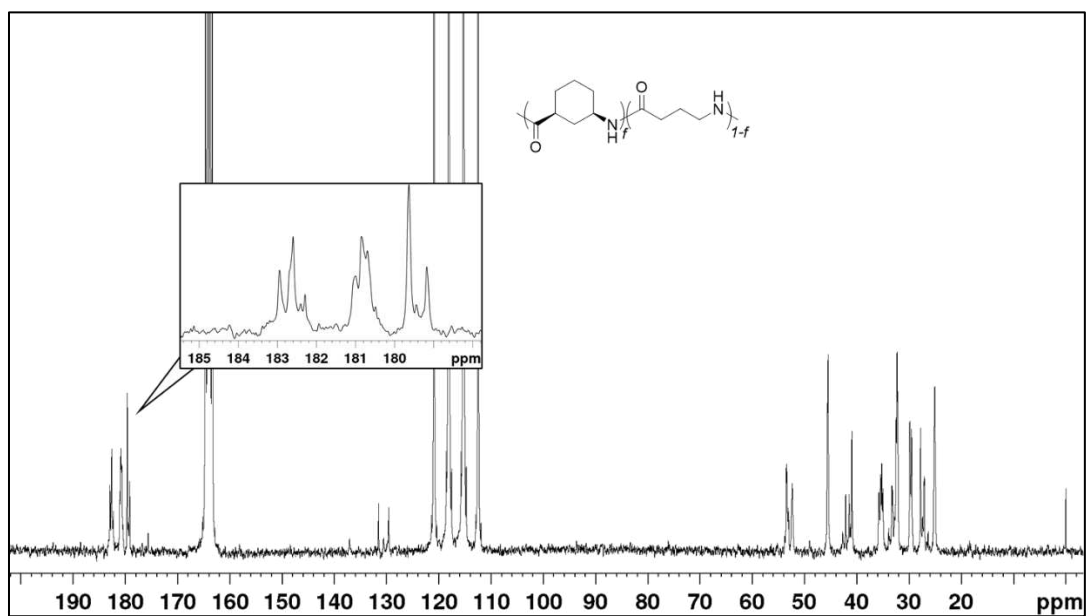


Figure S5.55. ^{13}C NMR (TFA-*d*) of nylon 4/6-*co*-nylon 4 produced with 50:50 monomer ratio and 50:1:1 $[\text{M}_{\text{tot}}]:[\text{'Bu-P}_4]:[\text{NBzM}]$

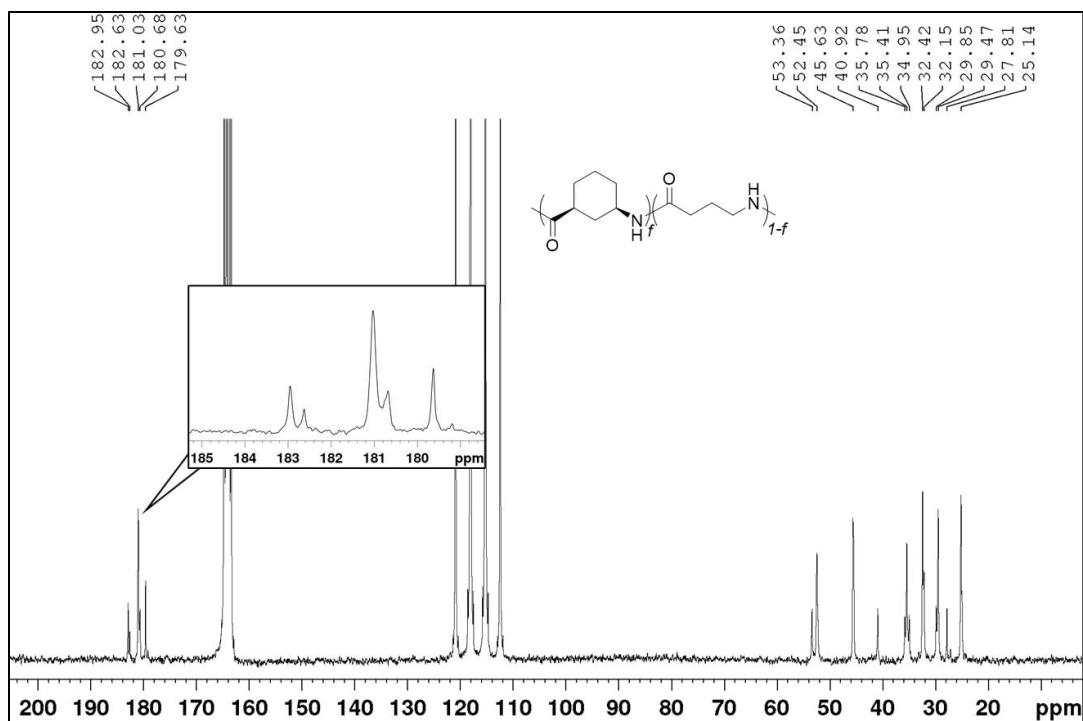


Figure S5.56. ^{13}C NMR (TFA-*d*) of nylon 4/6-*co*-nylon 4 produced with 85:15 monomer ratio and 250:5:1 $[\text{M}_{\text{tot}}]:[\text{Na5LM}]:[\text{NBzM}]$

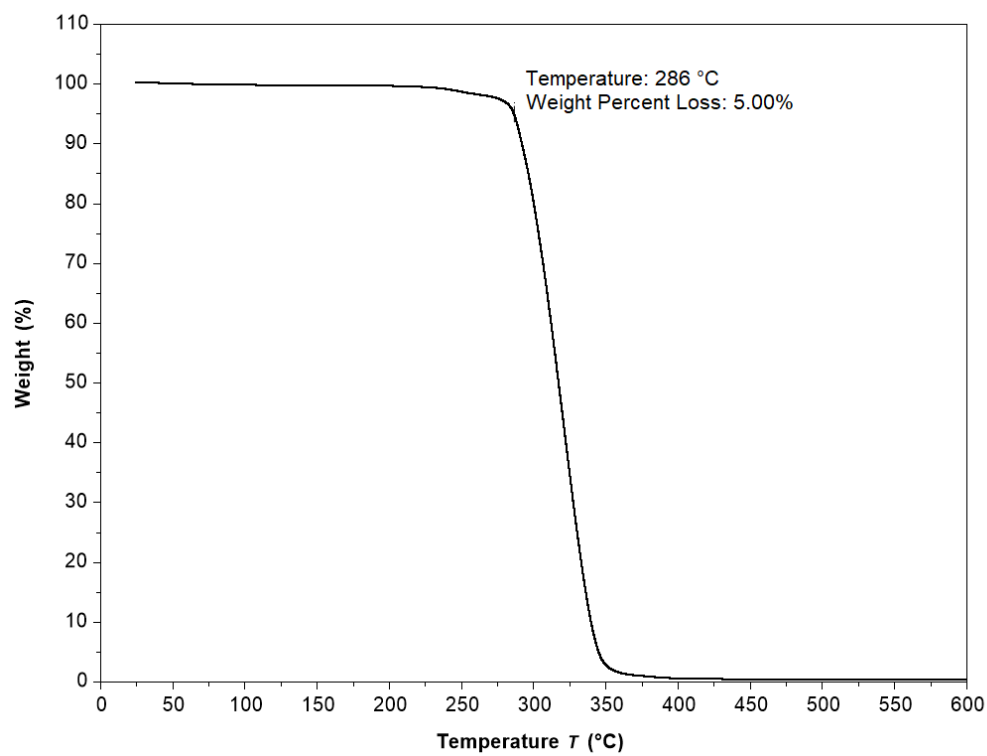


Figure S5.57. TGA profile of nylon 4 prepared with 50:1:1 $[\text{5-LM}]:[\text{tBu-P}_4]:[\text{NBzM}]$

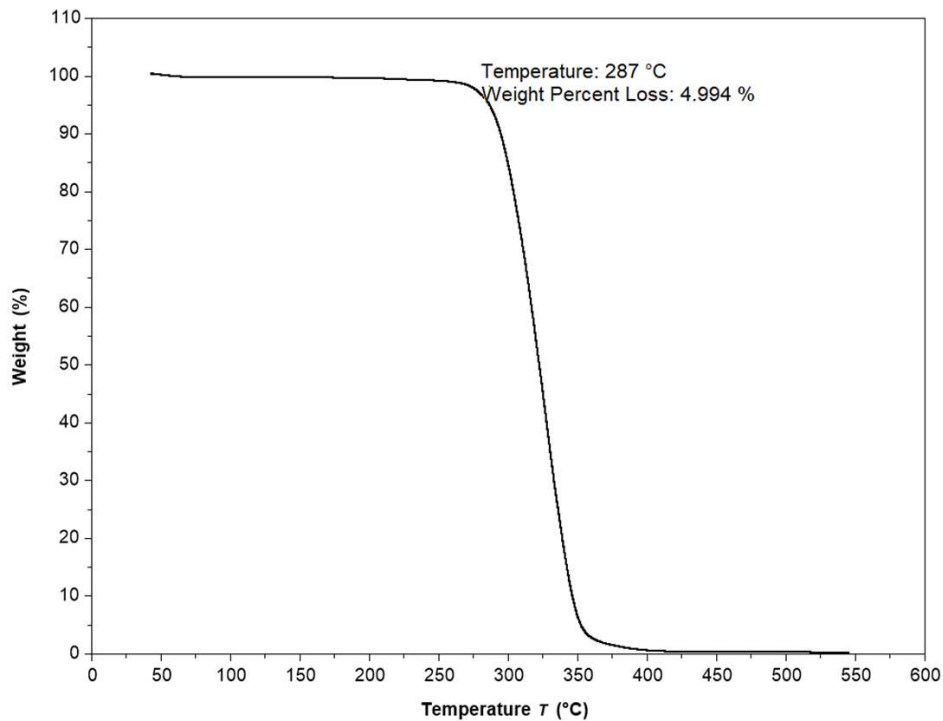


Figure S5.58. TGA profile of nylon 4/6-*co*-nylon 4 (7% 5/7-LM) prepared with 5:95 monomer ratio and 50:1:1 [M_{tot}]:[^tBu-P₄]:[NBzM]

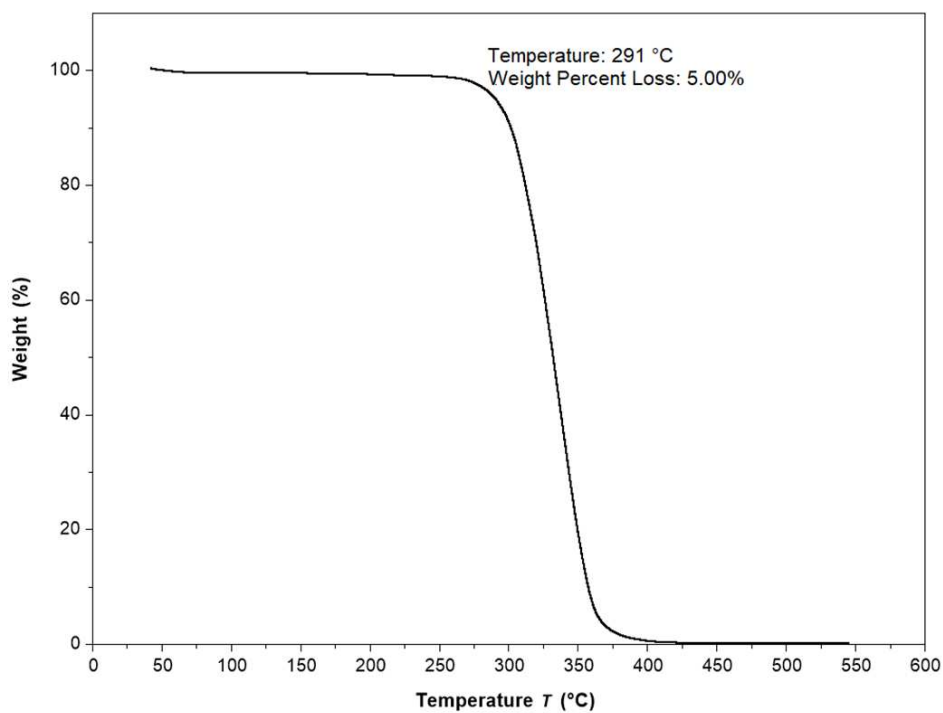


Figure S5.59. TGA profile of nylon 4/6-*co*-nylon 4 (17% 5/7-LM) prepared with 15:85 monomer ratio and 50:1:1 [M_{tot}]:[^tBu-P₄]:[NBzM]

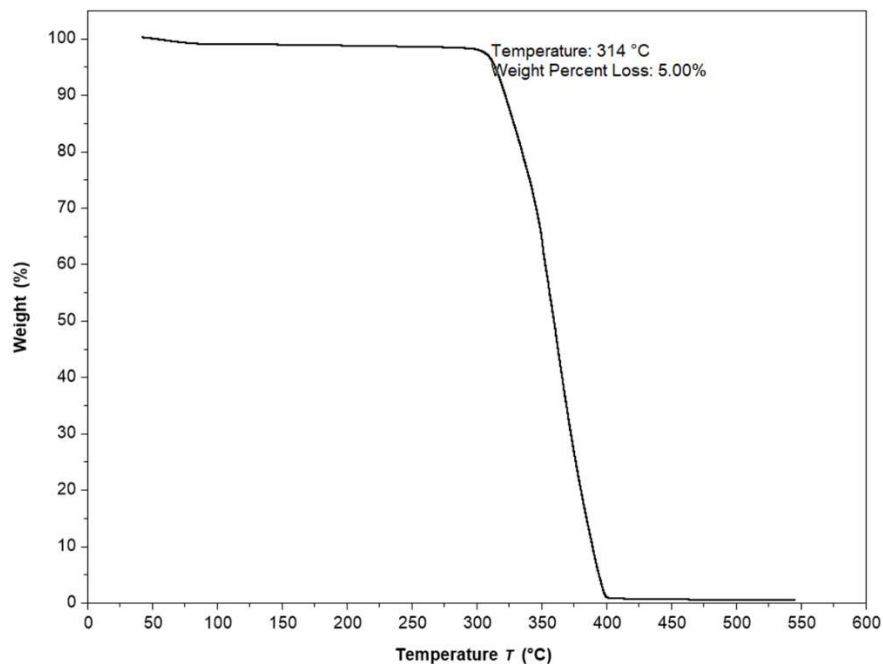


Figure S5.60. TGA profile of nylon 4/6-*co*-nylon 4 (54% 5/7-LM) prepared with 50:50 monomer ratio and 50:1:1 $[M_{\text{tot}}]:[t\text{Bu-P}_4]:[\text{NBzM}]$

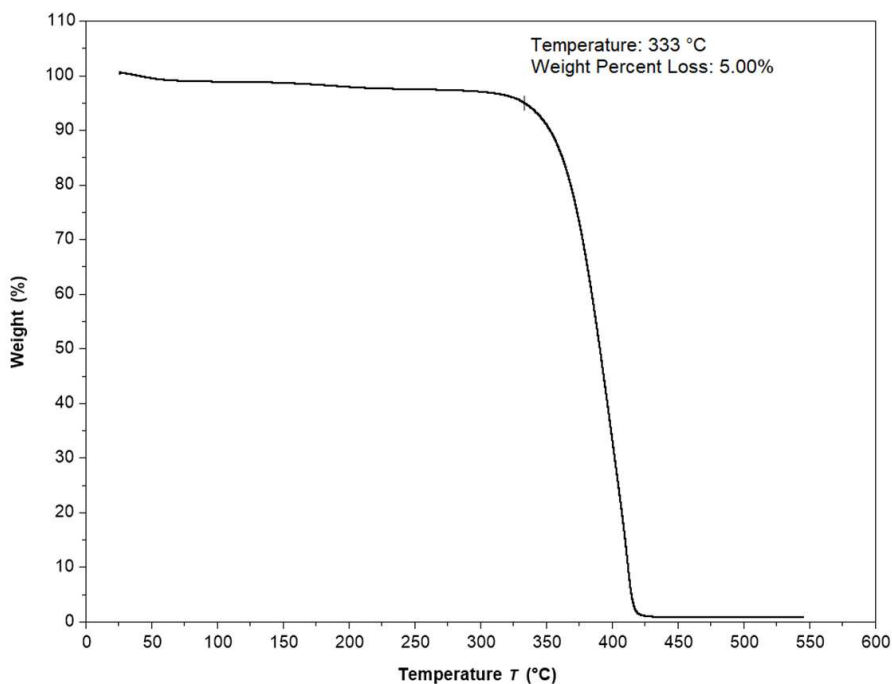


Figure S5.61. TGA profile of nylon 4/6-*co*-nylon 4 (90% 5/7-LM) prepared with 85:15 monomer ratio and 50:1:1 $[M_{\text{tot}}]:[t\text{Bu-P}_4]:[\text{NBzM}]$

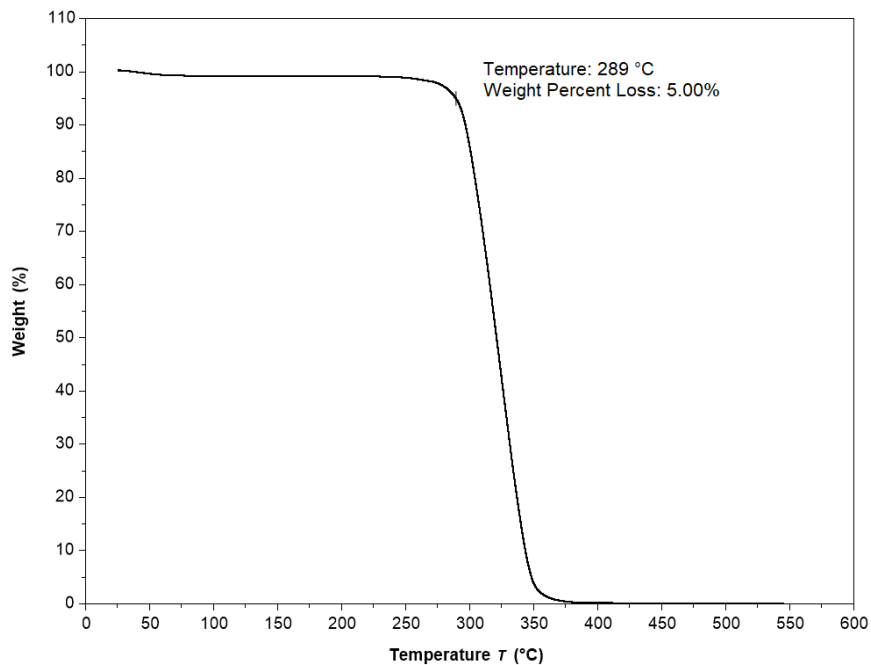


Figure S5.62. TGA profile of nylon 4 prepared with 250:5:1 [5-LM]:[Na5LM]:[NBzM]

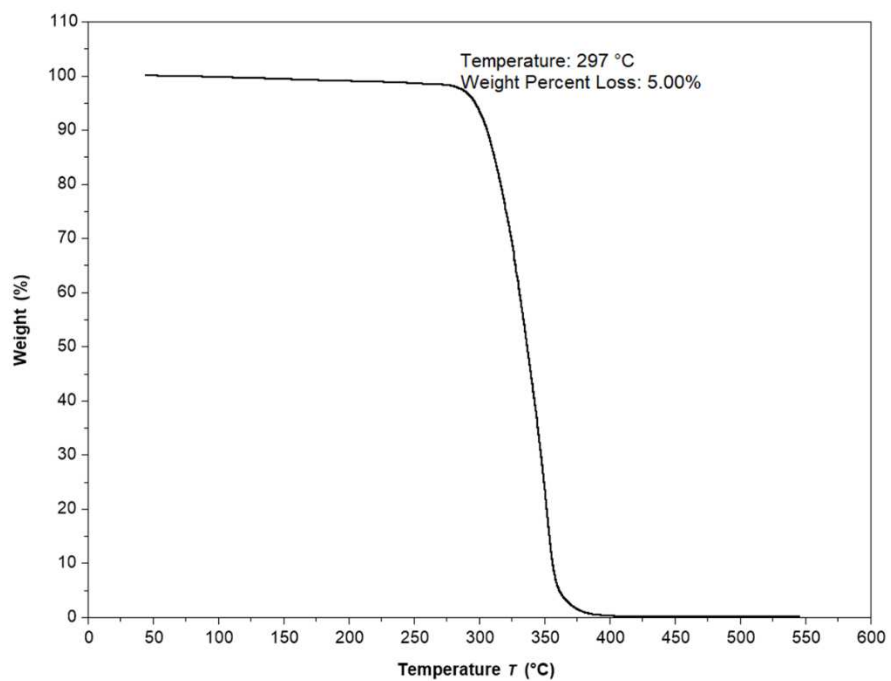


Figure S5.63. TGA profile of nylon 4/6-co-nylon 4 (15% 5/7-LM) prepared with 15:85 monomer ratio and 250:5:1 [M_{tot}]:[Na5LM]:[NBzM]

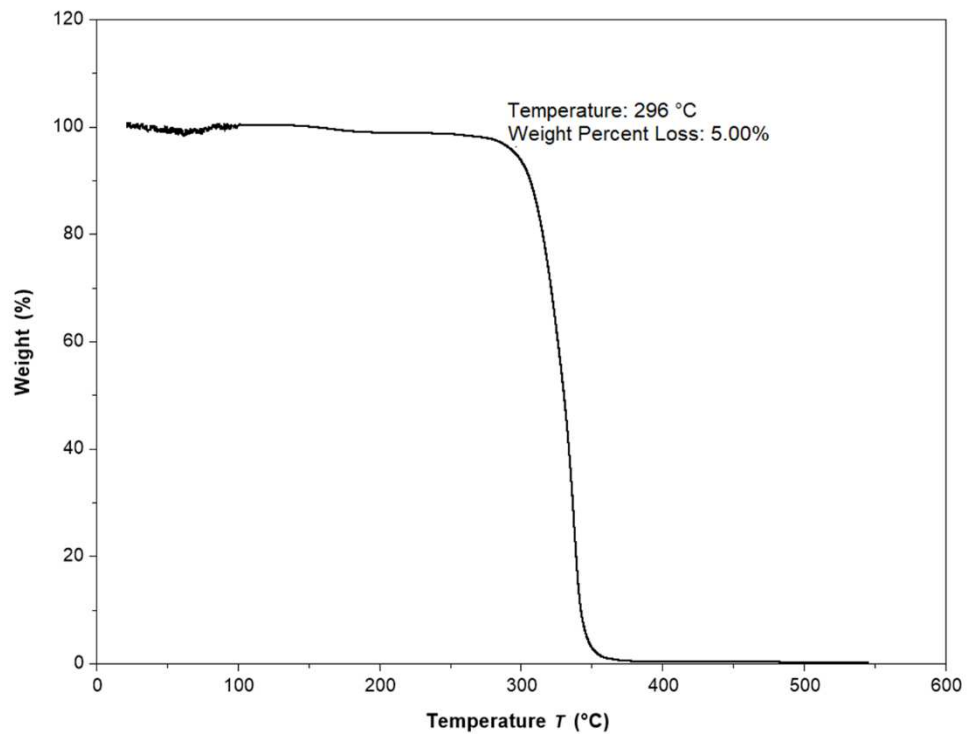


Figure S5.64. TGA profile of nylon 4/6-*co*-nylon 4 (25% 5/7-LM) prepared with 25:75 monomer ratio and 250:5:1 $[M_{\text{tot}}]:[\text{Na5LM}]:[\text{NBzM}]$

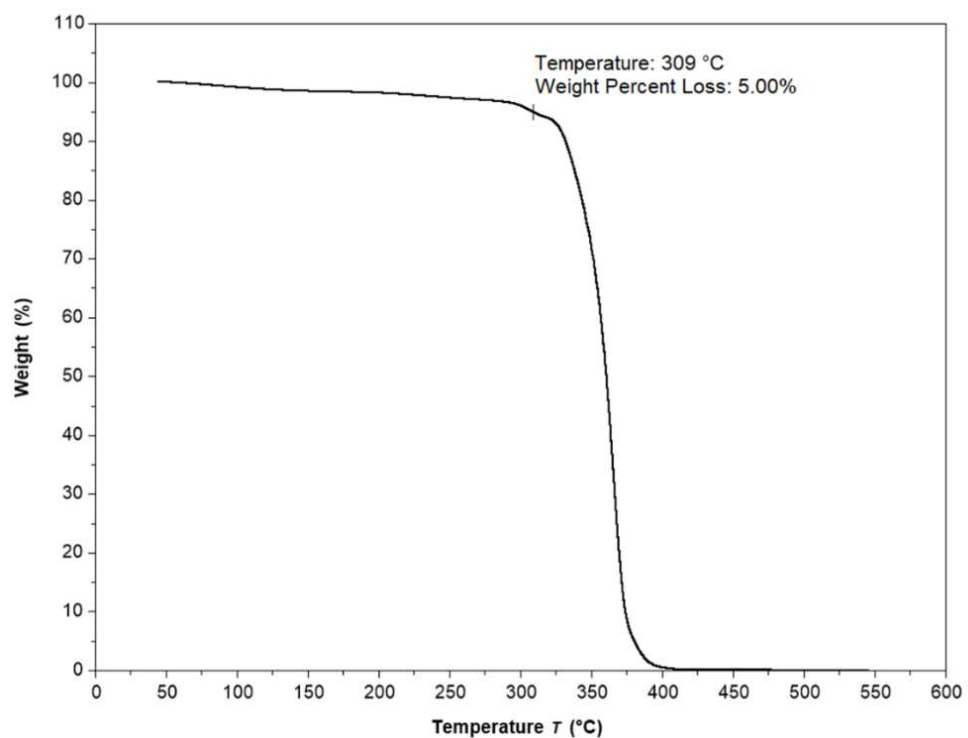


Figure S5.65. TGA profile of nylon 4/6-*co*-nylon 4 (48% 5/7-LM) prepared with 50:50 monomer ratio and 250:5:1 $[M_{\text{tot}}]:[\text{Na5LM}]:[\text{NBzM}]$

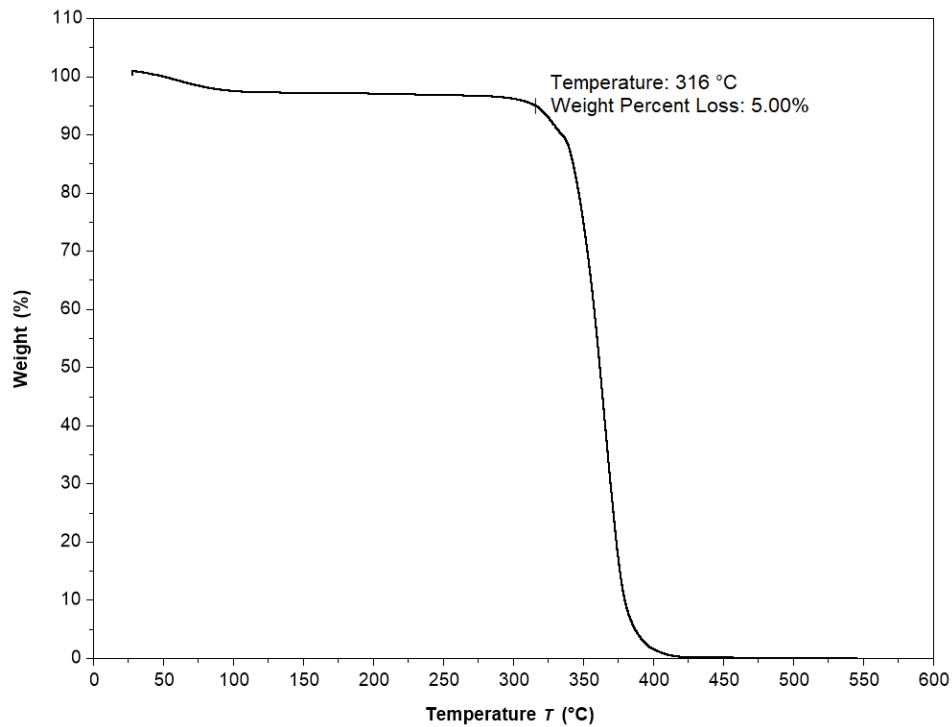


Figure S5.66. TGA profile of nylon 4/6-*co*-nylon 4 (51% 5/7-LM) prepared with 50:50 monomer ratio and 250:5:1 $[M_{\text{tot}}]:[\text{Na5LM}]:[\text{NBzM}]$ on 10 gram scale

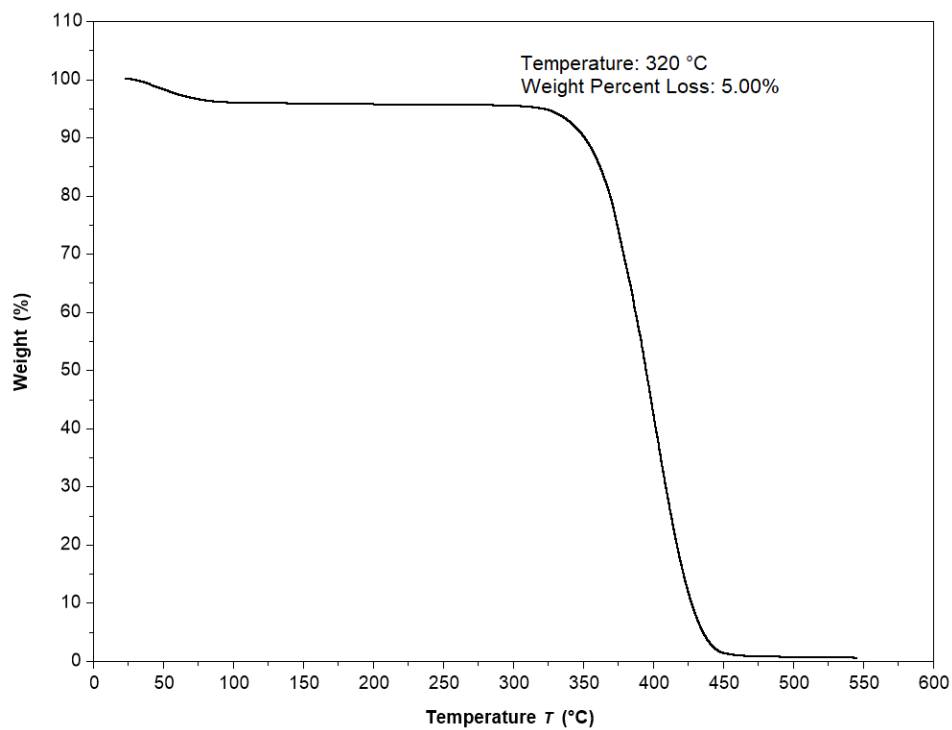


Figure S5.67. TGA profile of nylon 4/6-*co*-nylon 4 (80% 5/7-LM) prepared with 85:15 monomer ratio and 250:5:1 $[M_{\text{tot}}]:[\text{Na5LM}]:[\text{NBzM}]$

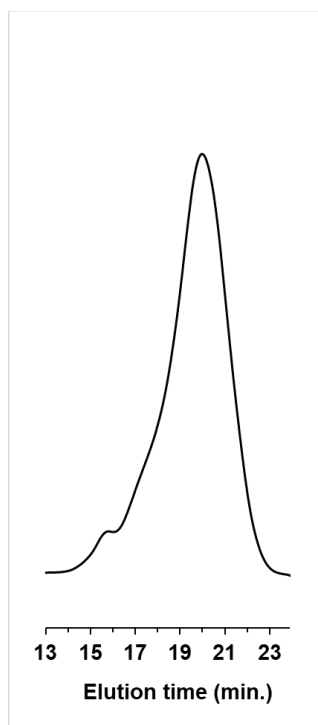


Figure S5.68. GPC trace (RI signal) of nylon 4 prepared with 50:1:1 [5-LM]:[*t*-Bu-P₄]:[NBzM]

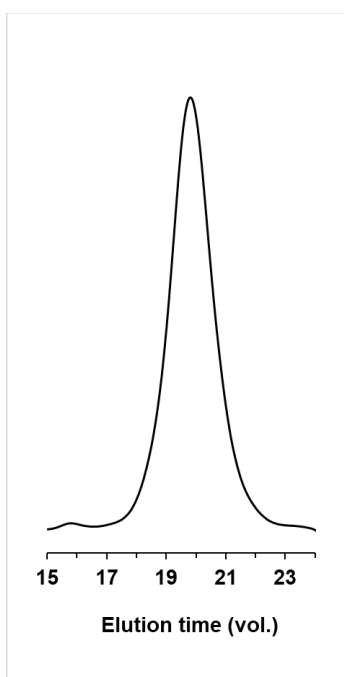


Figure S5.69. GPC trace (RI signal) of nylon 4/6-*co*-nylon 4 (54% 5/7-LM) prepared with 50:1:1 [M_{tot}]:[*t*-Bu-P₄]:[NBzM]

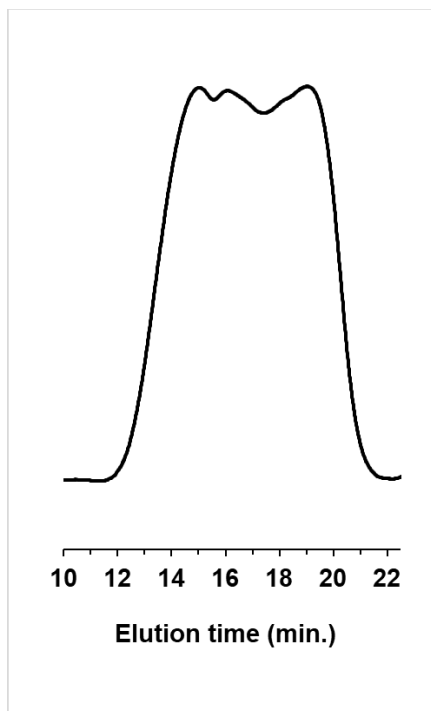


Figure S5.70. GPC trace (RI signal) of nylon 4 prepared with 250:5:1 [5-LM]:[Na5LM]:[NBzM]

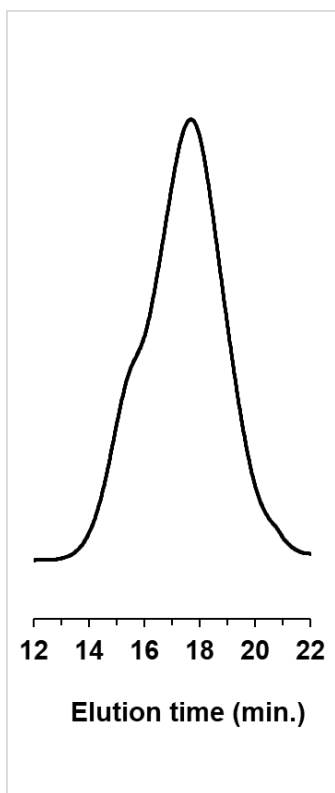


Figure S5.71. GPC trace (RI signal) of nylon 4/6-co-nylon 4 (15% 5/7-LM) prepared with 85:15 monomer ratio and 250:5:1 [M_{tot}]:[Na5LM]:[NBzM]

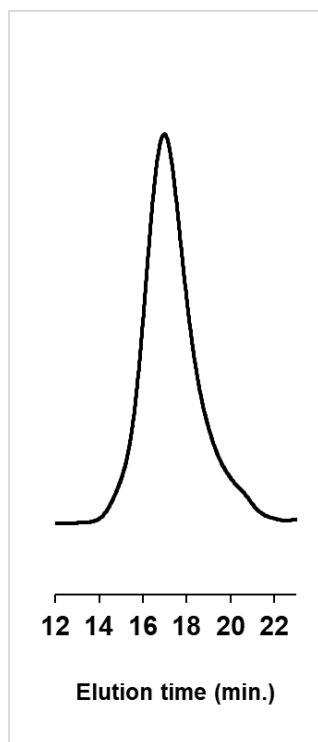


Figure S5.72. GPC trace (RI signal) of nylon 4/6-*co*-nylon 4 (48% 5/7-LM) prepared with 50:50 monomer ratio and 250:5:1 $[M_{\text{tot}}]:[\text{Na5LM}]:[\text{NBzM}]$

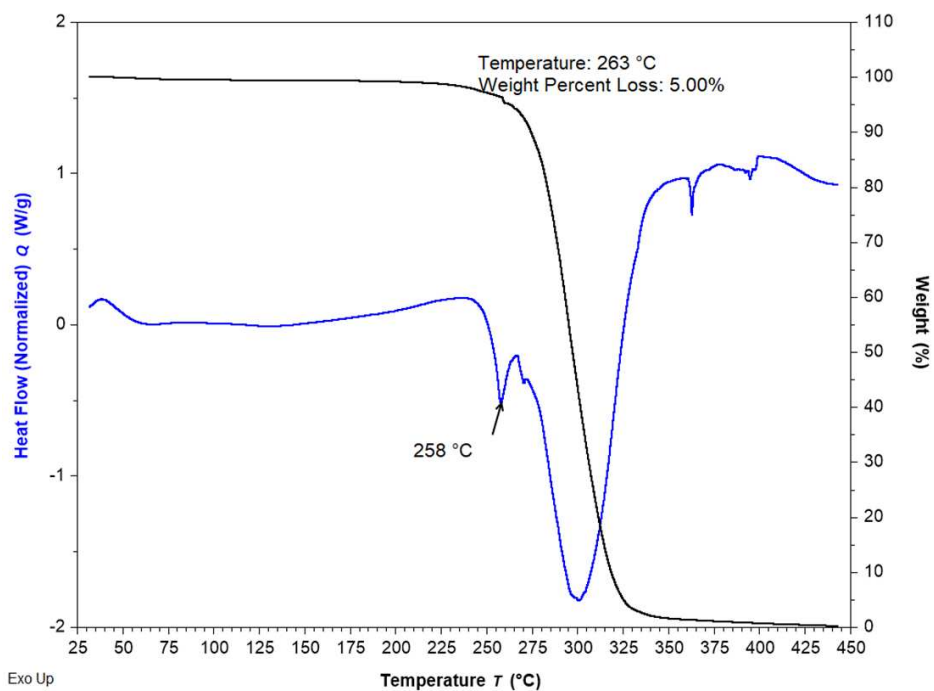


Figure S5.73. Heat flow and weight loss profiles of nylon 4 prepared with 50:1:1 $[5\text{-LM}]:[\text{Bu-P}_4]:[\text{NBzM}]$, measured by SDT

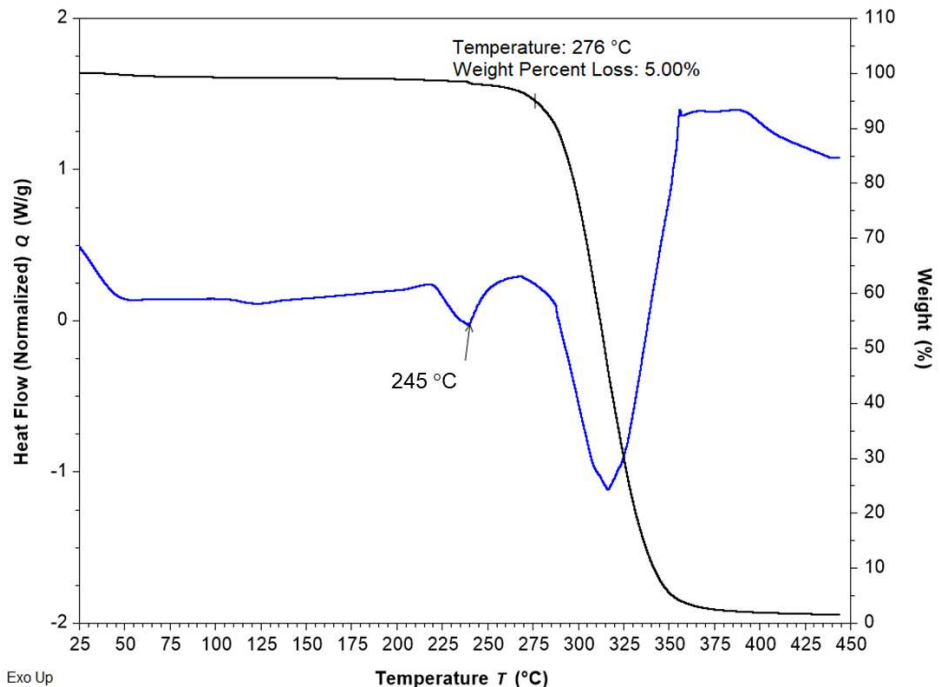


Figure S5.74. Heat flow and weight loss profiles of nylon 4/6-*co*-nylon 4 (17% 5/7-LM) prepared with 15:85 monomer ratio and 50:1:1 $[M_{\text{tot}}]:[{}^t\text{Bu-P}_4]:[\text{NBzM}]$, measured by SDT

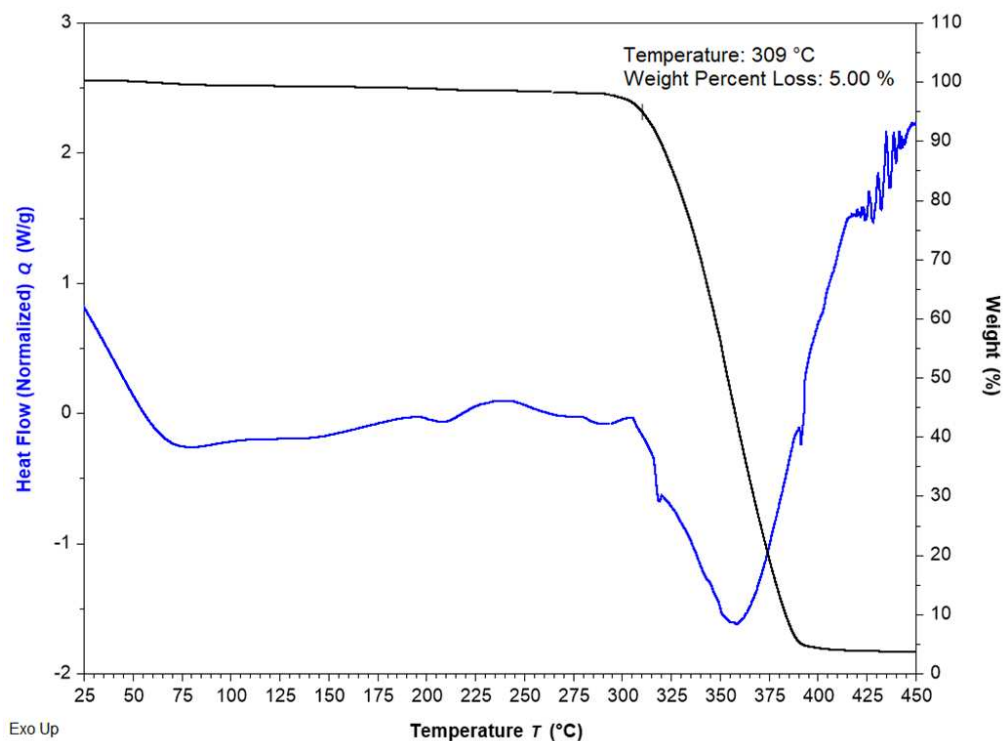


Figure S5.75. Heat flow and weight loss profiles of nylon 4/6-*co*-nylon 4 (54% 5/7-LM) prepared with 50:50 monomer ratio and 50:1:1 $[M_{\text{tot}}]:[{}^t\text{Bu-P}_4]:[\text{NBzM}]$, measured by SDT

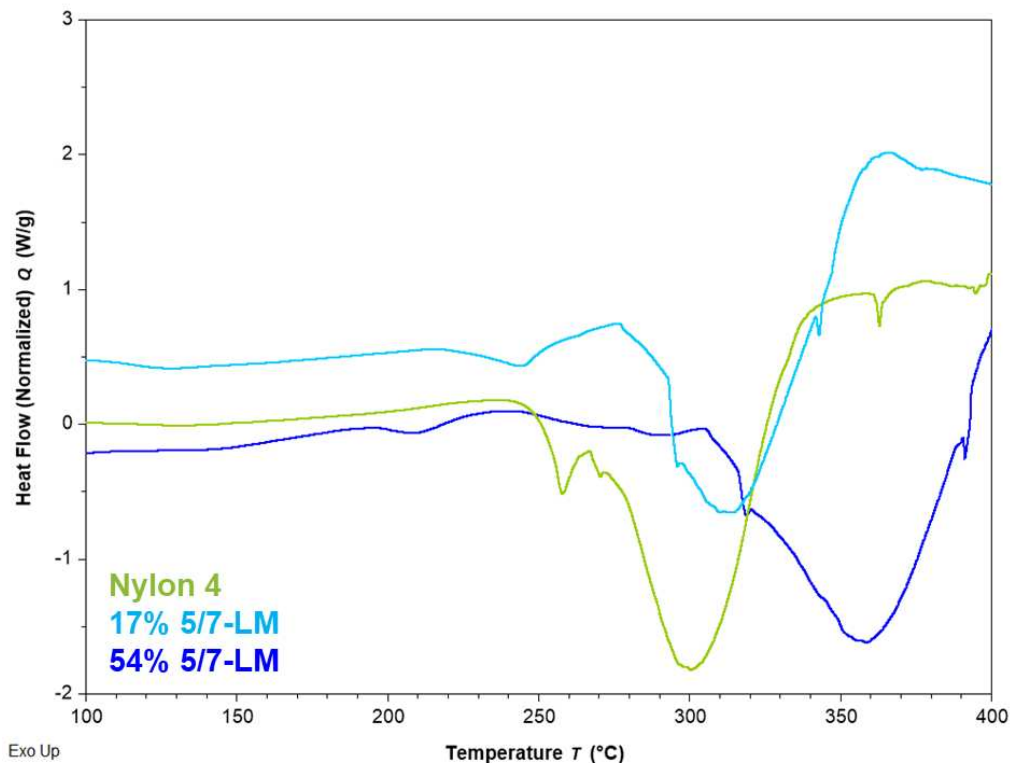


Figure S5.76. Overlay of SDT thermograms shown in Fig. S70-72.

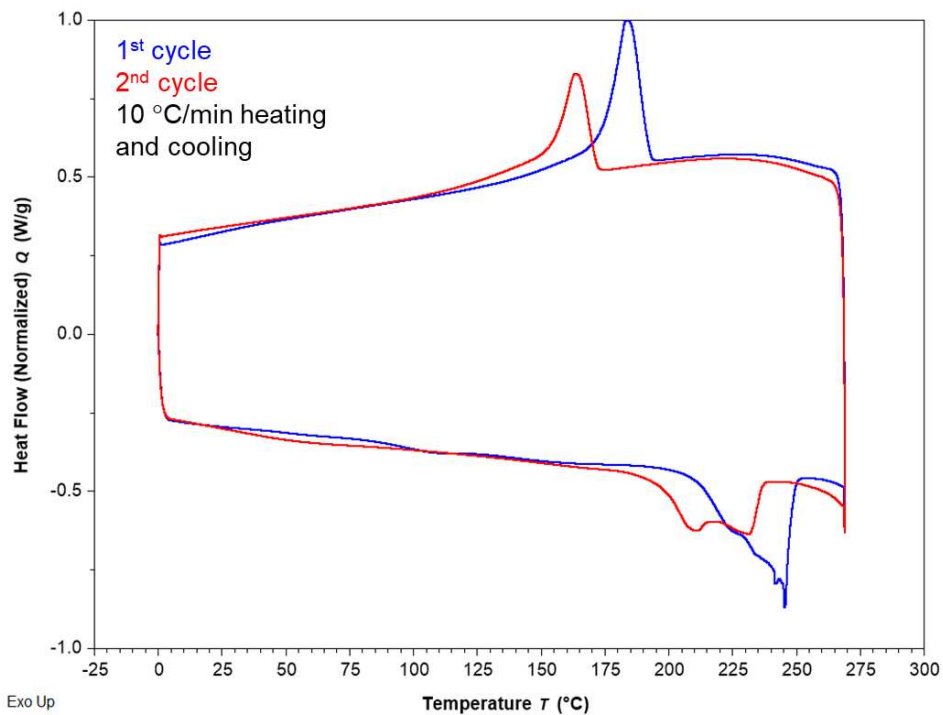


Figure S5.77. DSC curves for nylon 4/6-*co*-nylon 4 (17% 5/7-LM) prepared with 15:85 monomer ratio and 50:1:1 [M_{tot}]:[^tBu-P₄]:[NBz/M]

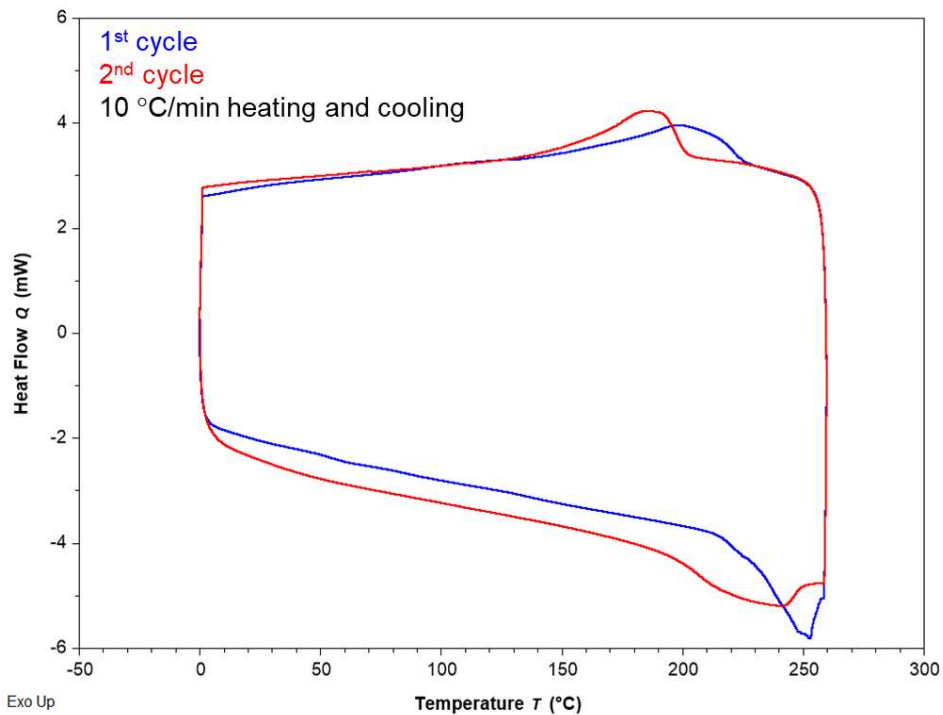


Figure S5.78. DSC curves for nylon 4/6-*co*-nylon 4 (15% 5/7-LM) prepared with 15:85 monomer ratio and 250:5:1 $[M_{\text{tot}}]:[\text{Na5LM}]:[\text{NBzM}]$

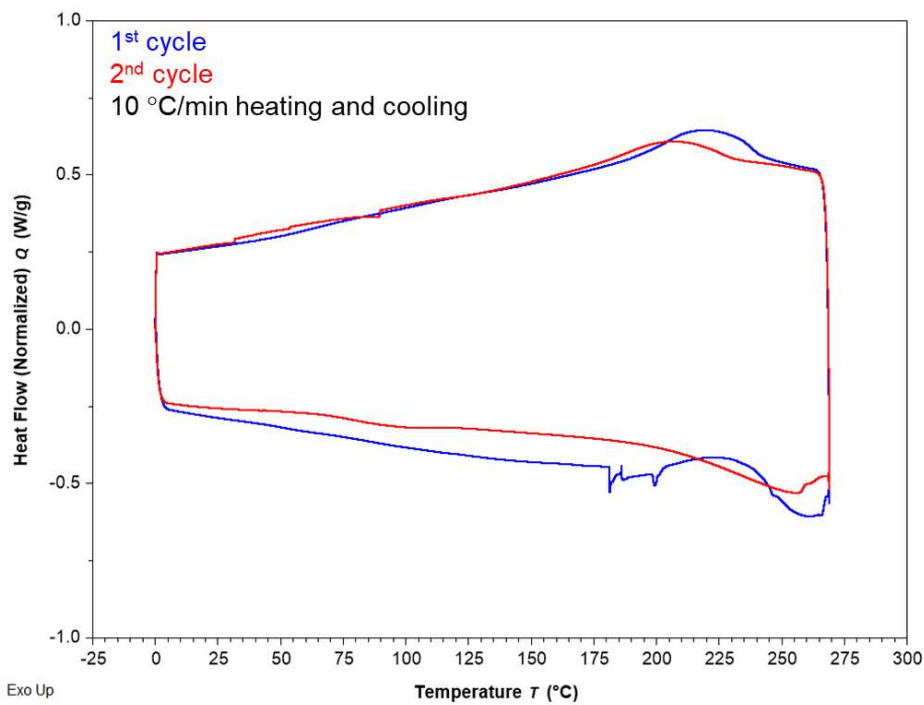


Figure S5.79. DSC curves nylon 4/6-*co*-nylon 4 (25% 5/7-LM) prepared with 25:75 monomer ratio and 250:5:1 $[M_{\text{tot}}]:[\text{Na5LM}]:[\text{NBzM}]$

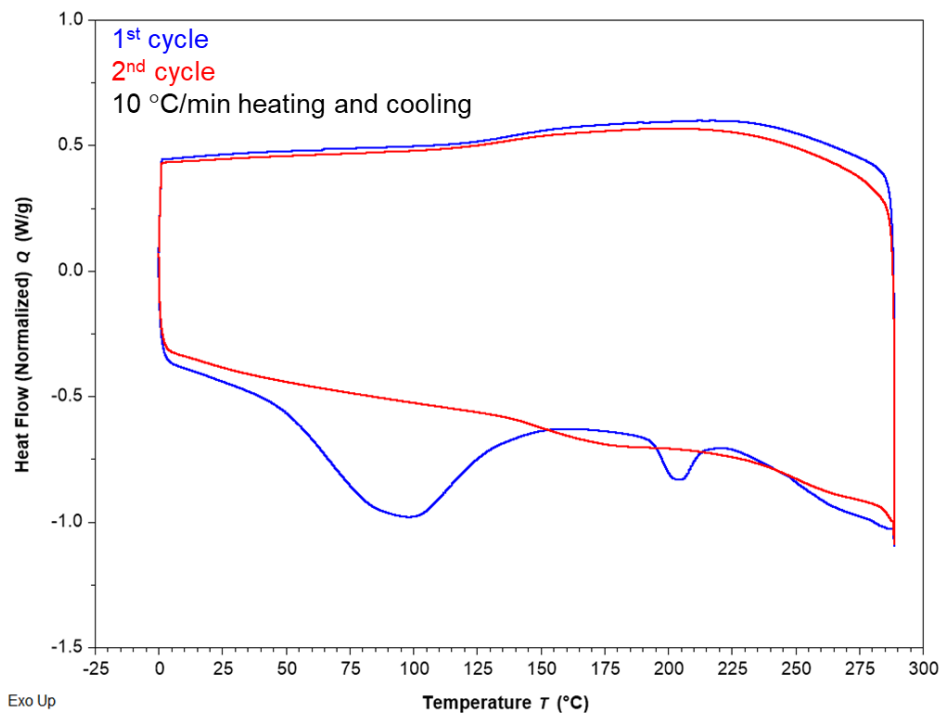


Figure S5.80. DSC curves for nylon 4/6-*co*-nylon 4 (54% 5/7-LM) prepared with 50:50 monomer ratio and 50:1:1 $[M_{\text{tot}}]:[t\text{Bu-P}_4]:[\text{NBzM}]$

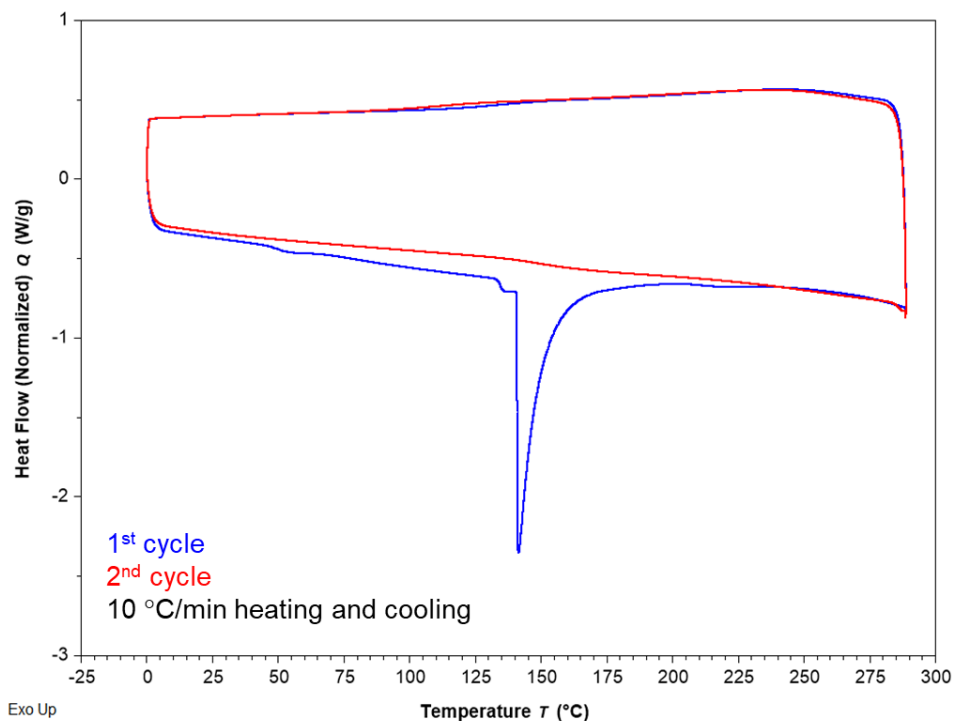


Figure S81. DSC curves for nylon 4/6-*co*-nylon 4 (48% 5/7-LM) prepared with 50:50 monomer ratio and 250:5:1 $[M_{\text{tot}}]:[\text{Na5LM}]:[\text{NBzM}]$

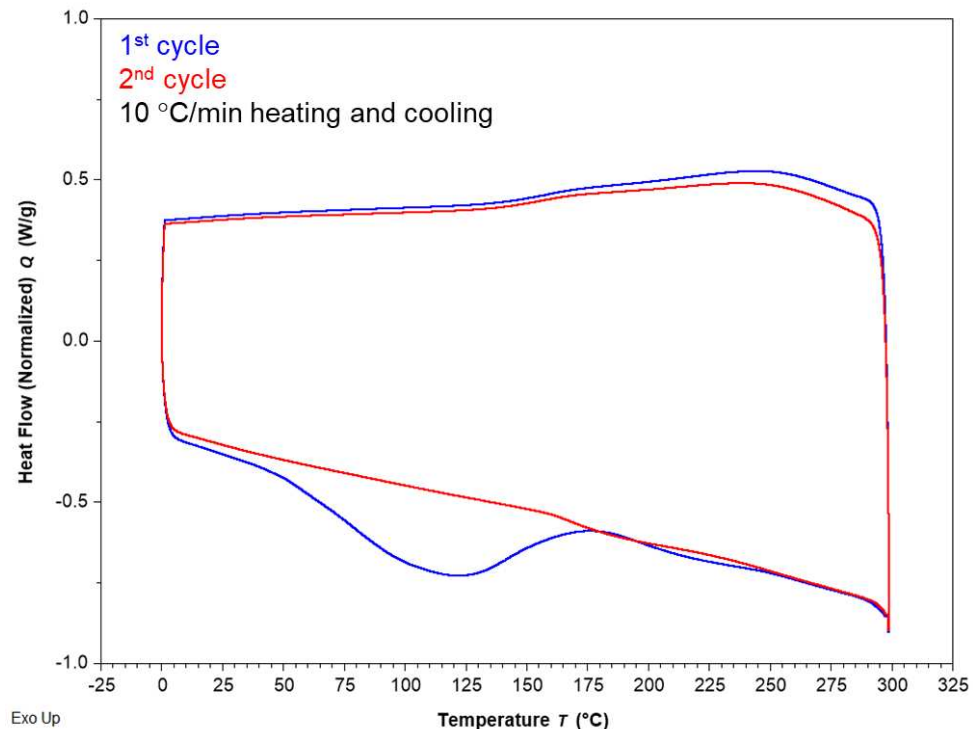


Figure S5.82. DSC curves for nylon 4/6-*co*-nylon 4 (51% 5/7-LM) prepared with 50:50 monomer ratio and 250:5:1 $[M_{\text{tot}}]:[\text{Na5LM}]:[\text{NBzM}]$ on a 10g scale

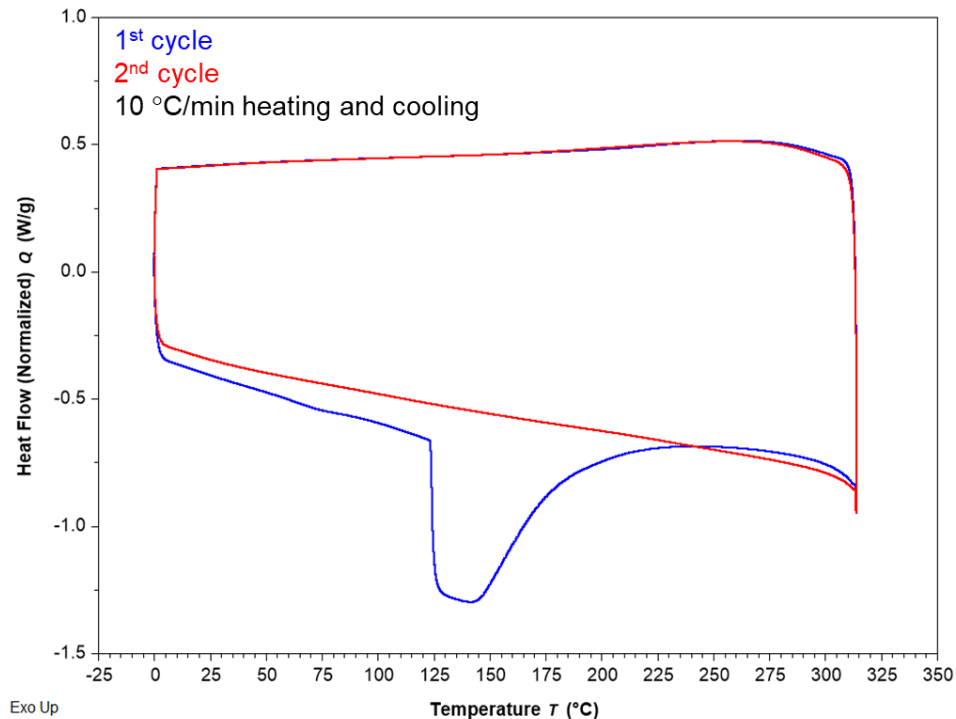


Figure S5.83. DSC curves for nylon 4/6-*co*-nylon 4 (90% 5/7-LM) prepared with 85:15 monomer ratio and 50:1:1 $[M_{\text{tot}}]:[\text{tBu-P}_4]:[\text{NBzM}]$

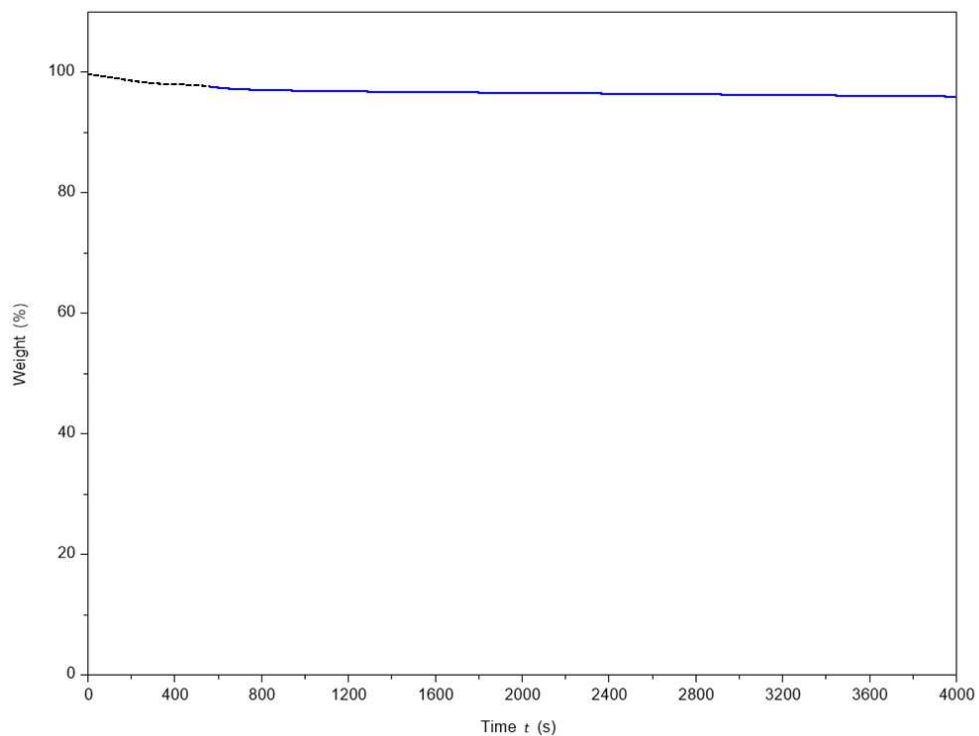


Figure S5.84. Isothermal hold at 230 °C for nylon 4/6-*co*-nylon 4 (48% 5/7-LM) prepared with 250:5:1 [M_{tot}]:[^tBu-P₄]:[NBzM]

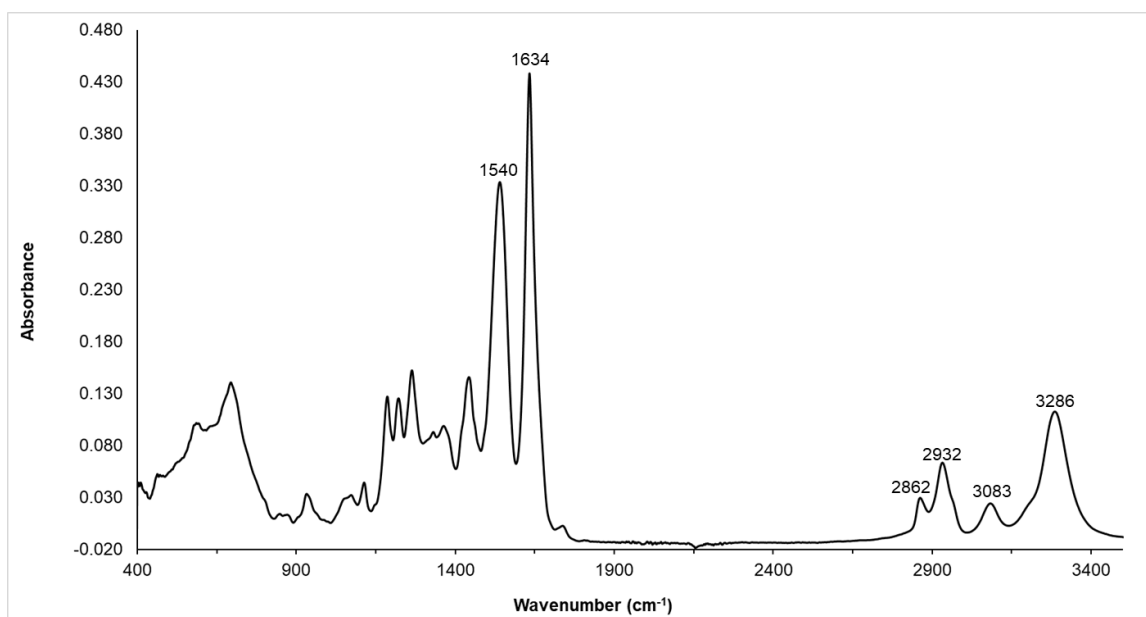


Figure S5.85. FTIR spectrum of nylon 4/6-*co*-nylon 4 (17% 5/7-LM)

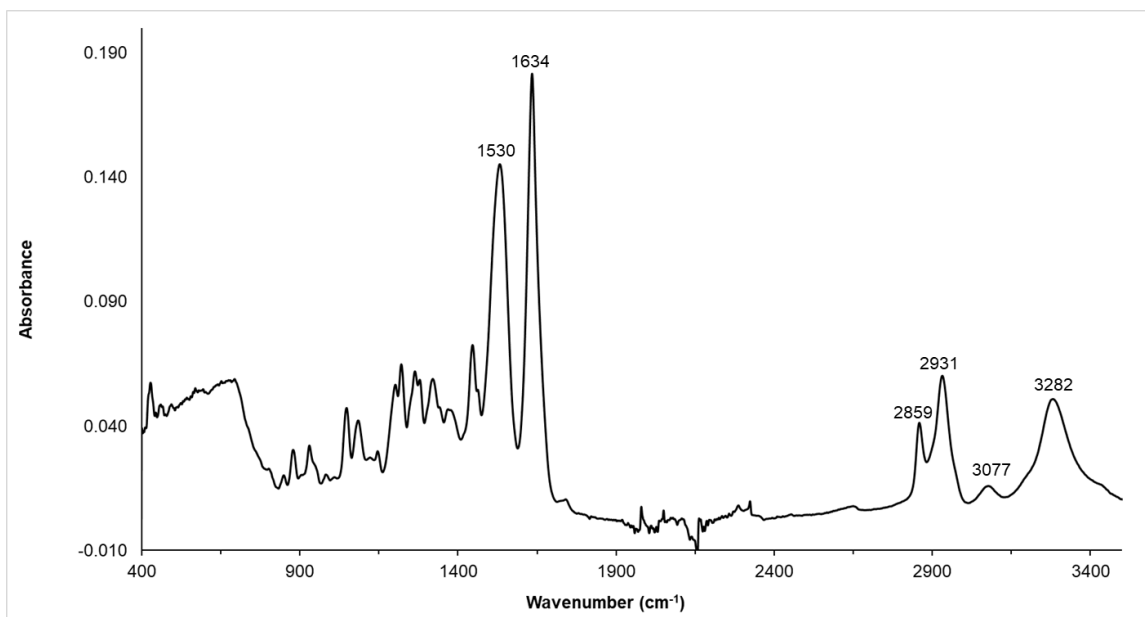


Figure S5.86. FTIR spectrum of nylon 4/6-co-nylon 4 (54% 5/7-LM)

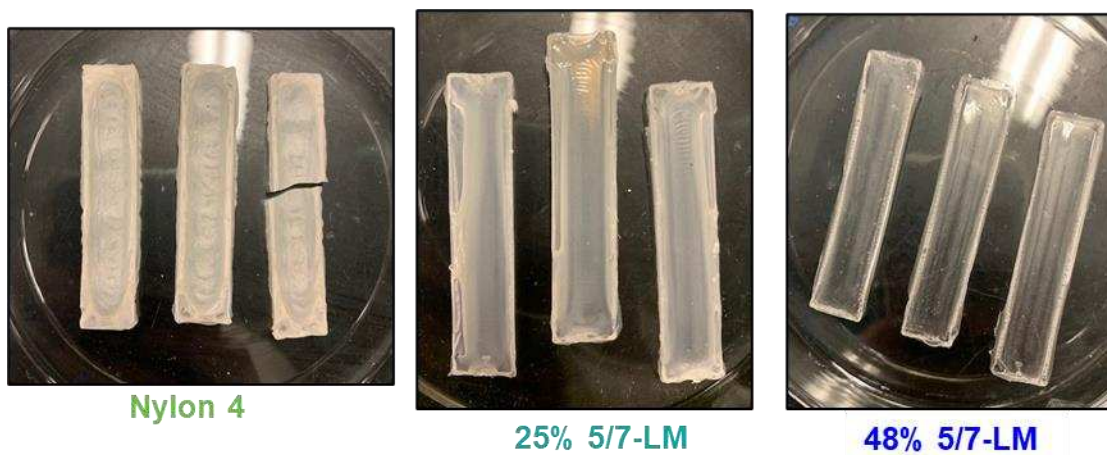


Figure S5.87. Photographs of nylon 4 and copolymer thin films

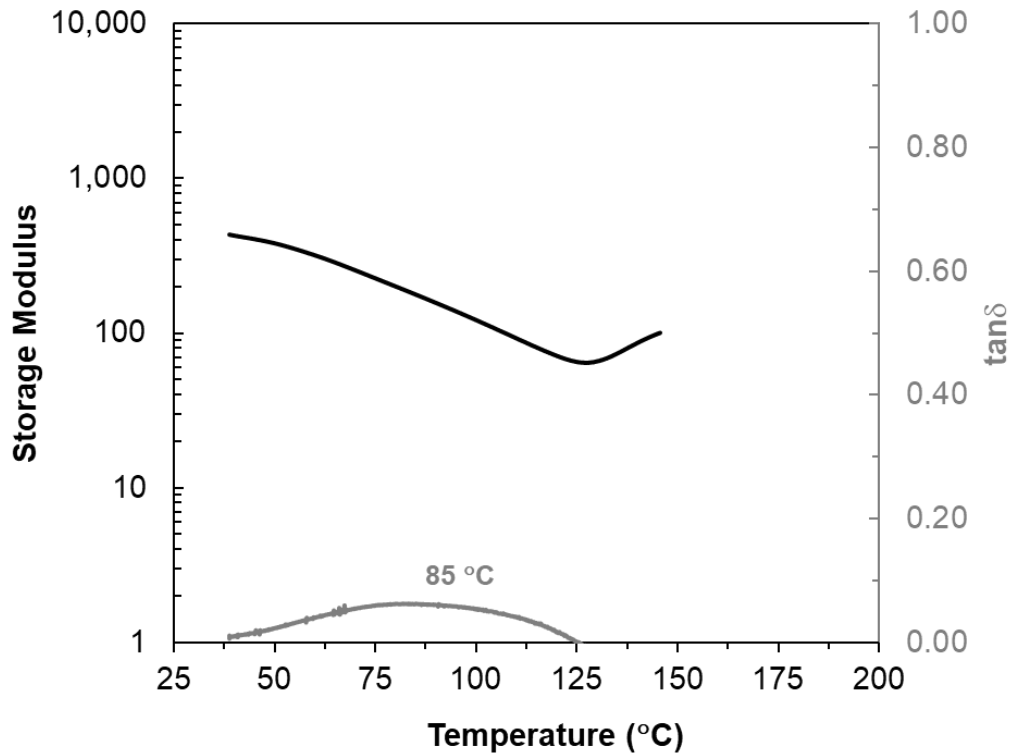


Figure S5.88. First heating scan of DMA for nylon 4/6-co-nylon 4 (25% 5/7-LM)

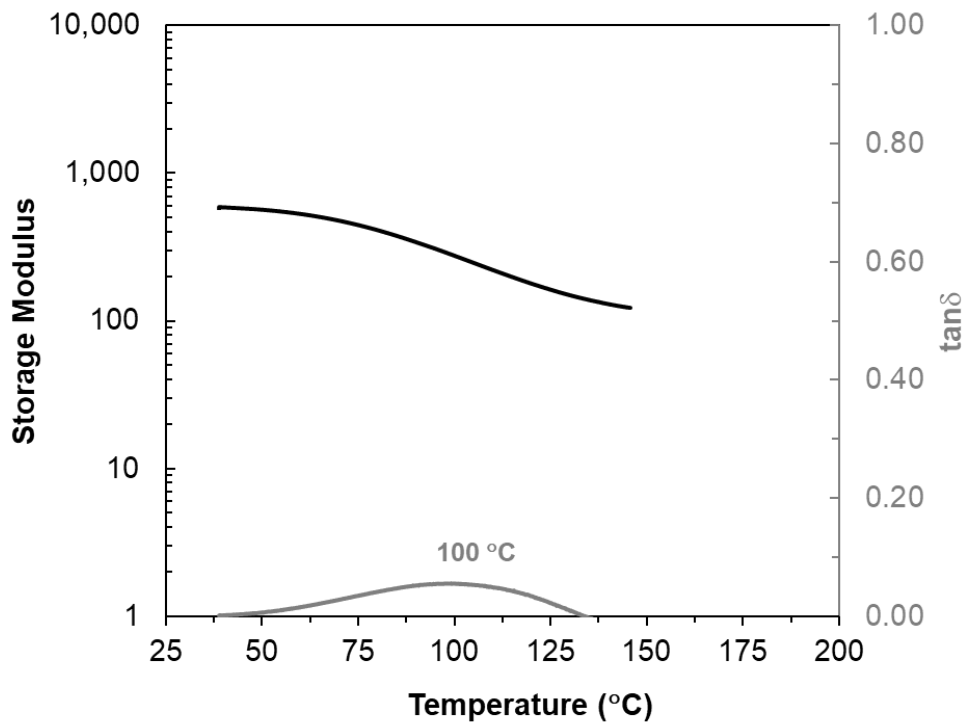


Figure S5.89. Second heating scan of DMA for nylon 4/6-co-nylon 4 (25% 5/7-LM)

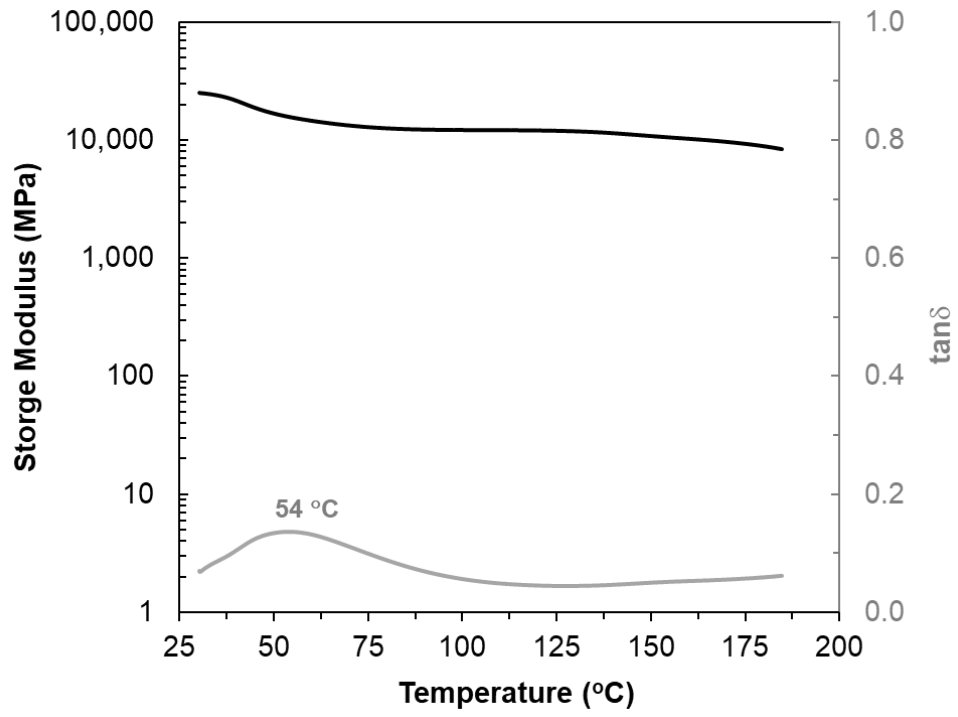


Figure S5.90. First heating scan of DMA for nylon 6

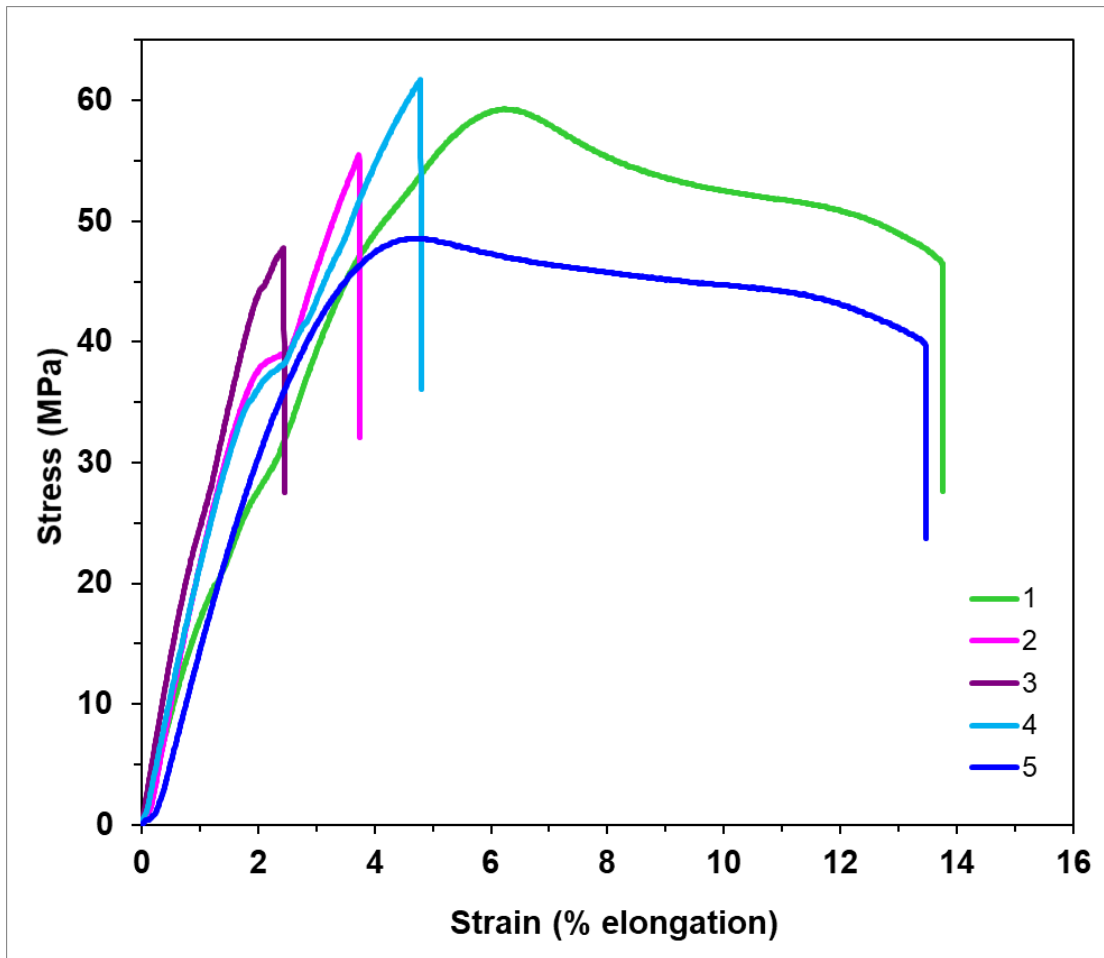


Figure S5.91. Overlay of stress-strain curves obtained for 5 x nylon 4/6-co-nylon 4 (51% 5/7-LM) thin film samples

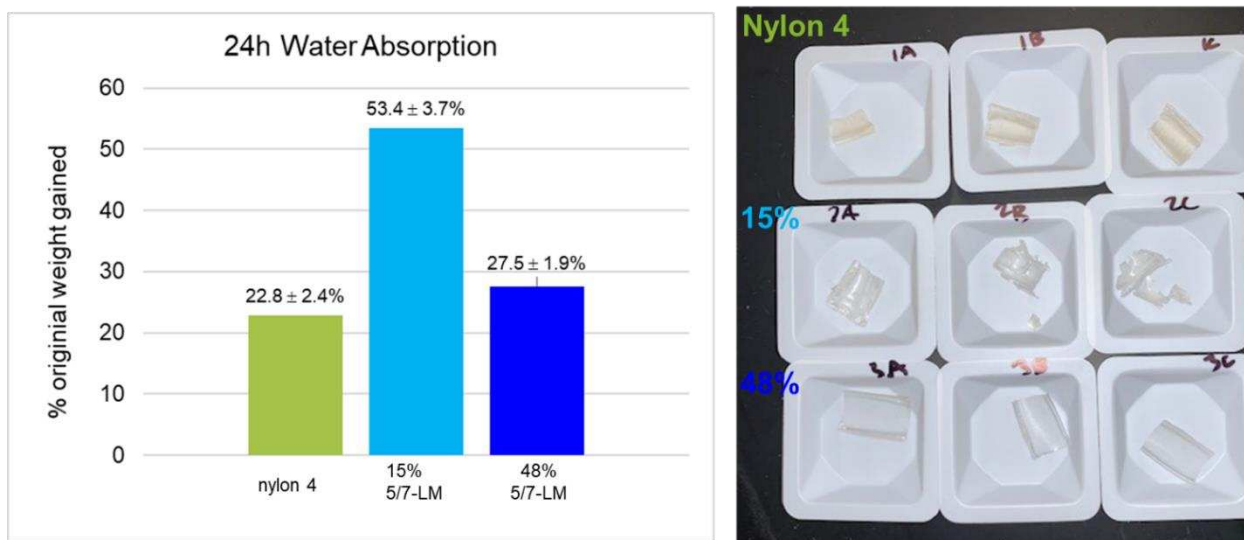


Figure S5.92. Water absorption after 24 hours of immersion

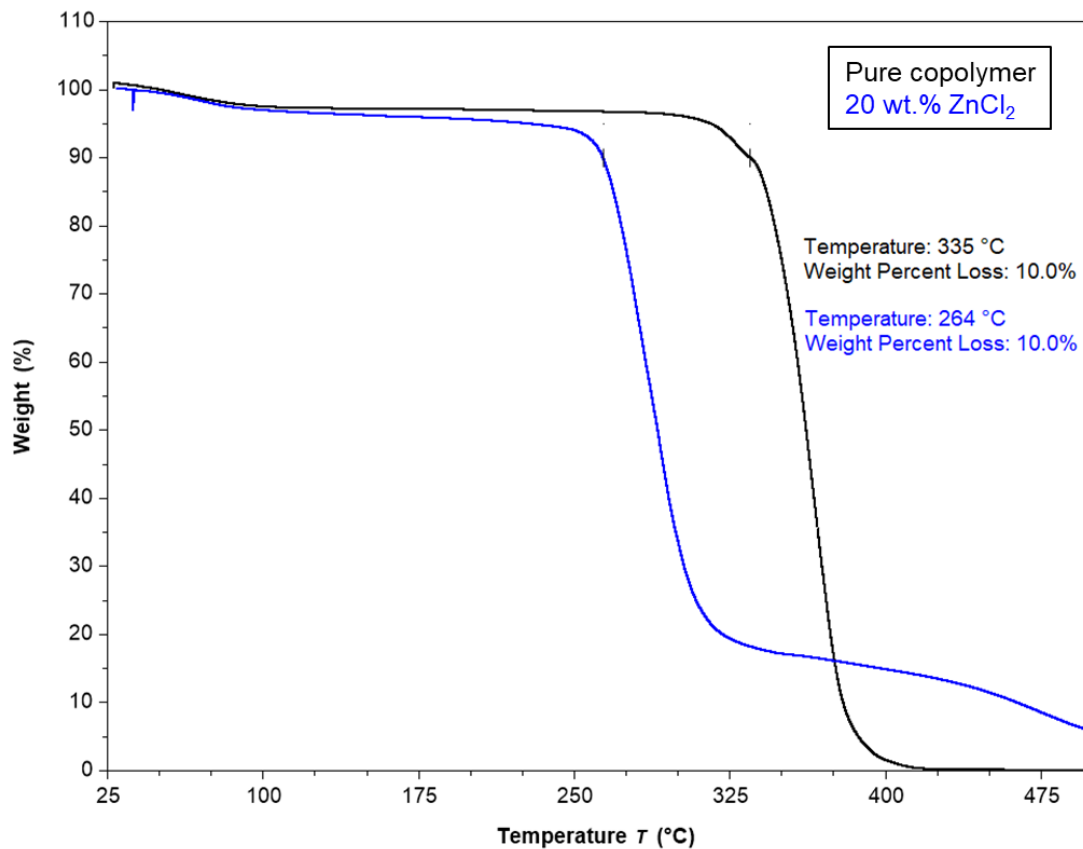


Figure S5.93. Effect of ZnCl₂ catalyst on nylon 4/6-co-nylon 4 (51% 5/7-LM) decomposition

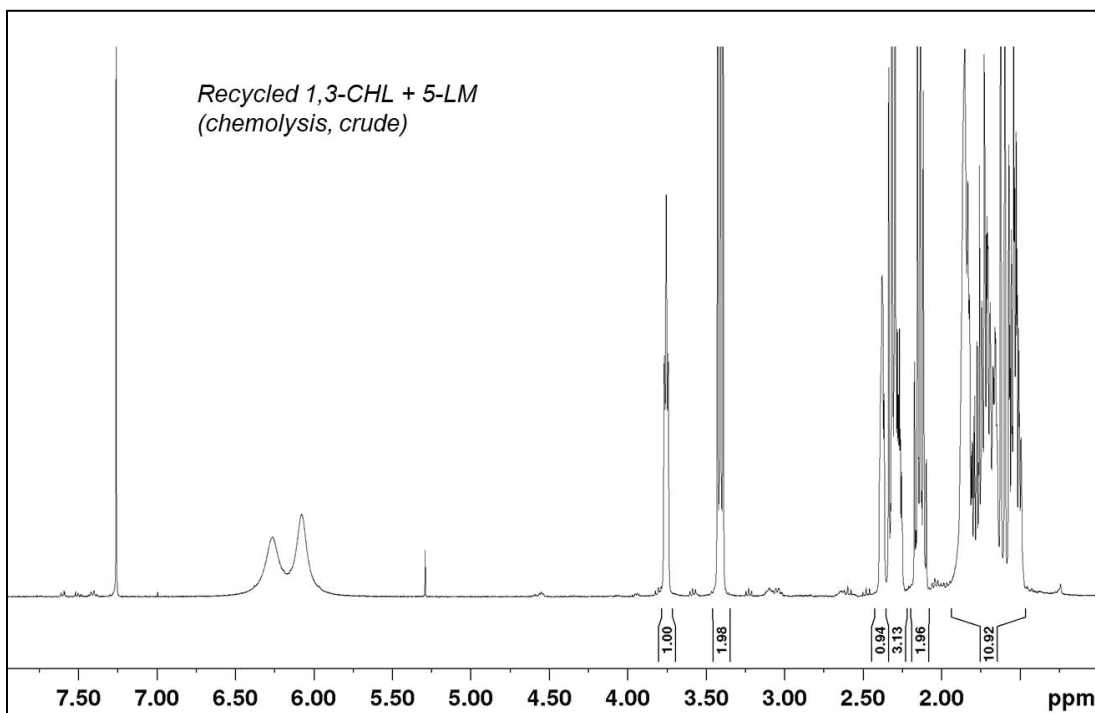


Figure S5.94. ^1H NMR (CDCl_3) of crude monomers after recycling 275 mg nylon 4/6-*co*-nylon 4, produced by 250:5:1 $[\text{M}_{\text{tot}}]:[\text{Na5LM}]:[\text{NBzM}]$ (51% 5/7-LM) with 10 wt.% ZnCl_2 at 300 °C (external temperature), 3h.

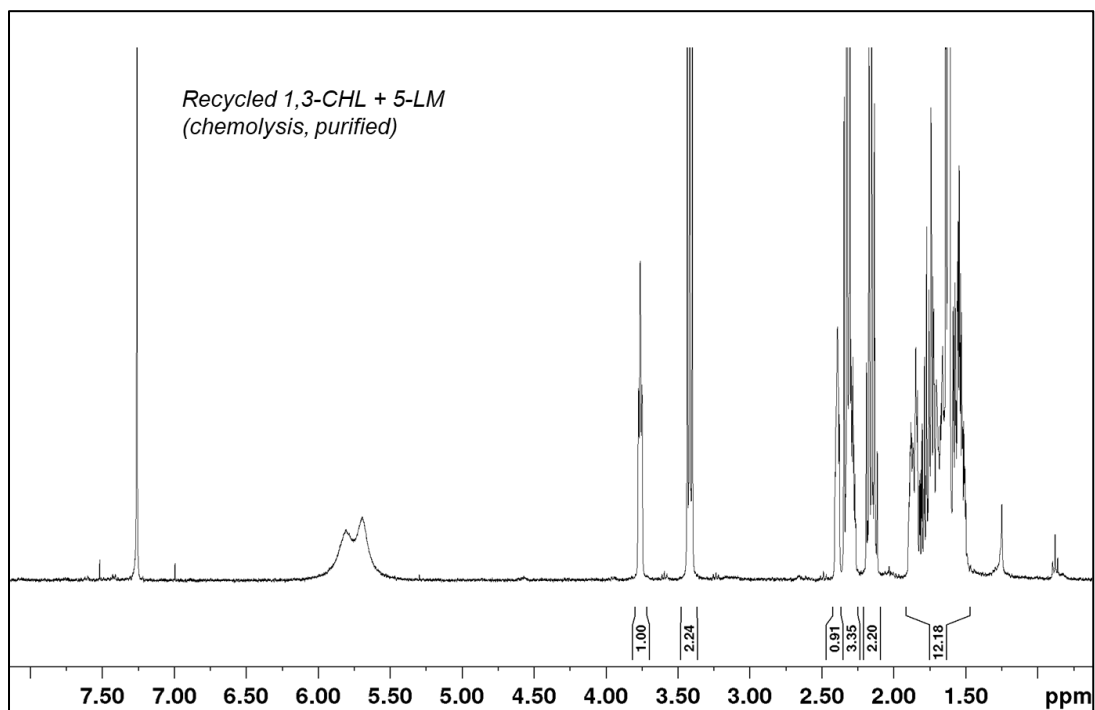


Figure S5.95. ^1H NMR (CDCl_3) of crude, recycled monomers after crystallization under layer of cold pentane.

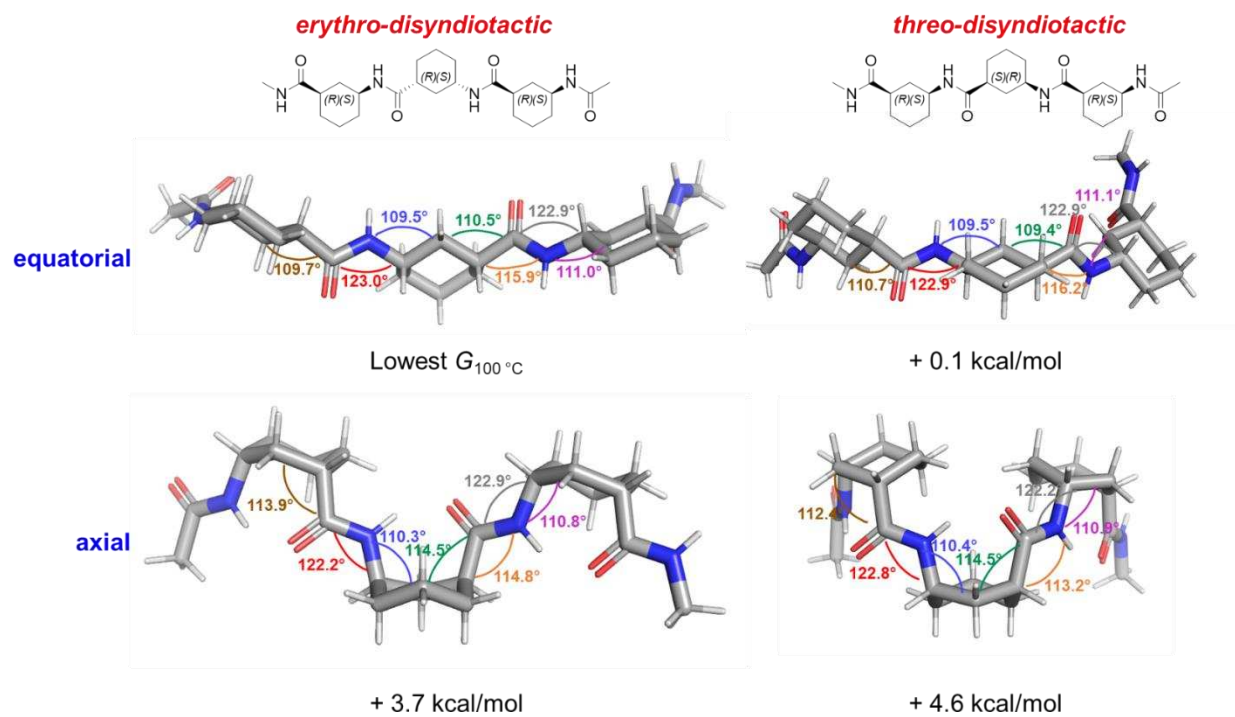


Figure S5.96. Bond angles of model trimer chains in lowest energy state as optimized by DFT at the M06-2X2/Def2TZVP level of theory in implicit nitrobenzene.

Table S5.1. AROP Activity of 5/7-LM

Entry	[M]/[B]/[A]	Base	Solvent	Temp. (°C)	Time (h)	Yield (%)
1	50/1/0	^t BuP ₄	THF (1M)	RT	4	<1
2	50/1/0	^t BuP ₄	THF (1M)	60	4	5
3	50/1/0	^t BuP ₄	NMP (3M)	120	4	63
4	50/1/1	^t BuP ₄	THF (1M)	RT	3	82
5	50/1/1	^t BuP ₄	NMP (3M)	RT	3	95
6 ^a	50/1/1	^t BuP ₄	NMP (3M)	RT	3	80
7	50/1/1	^t BuP ₄	NMP (3M)	60	1.5	90
8	50/1/1	^t BuP ₄	NMP (3M)	120	1	73
9 ^b	50/1/1	^t BuP ₄	NMP (3M)	RT	3	23
10 ^b	50/1/1	^t BuP ₄	THF (1M)	RT	3	32
11	50/1/1	NaM	THF (1M)	RT	24	20
12	50/1/1	NaM	NMP (3M)	RT	3	29
13	50/1/1	NaM	NMP (3M)	RT	24	76
14	50/1/1	NaM	NMP (3M)	60	24	74
15 ^b	50/1/1	NaM	NMP (3M)	60	24	54
16	50/1/1	NaM	NMP (3M)	120	1	68
17	50/1/1	IMes	NMP (3M)	60	3	40
18 ^a	50/1/0.5	^t BuP ₄	NMP (3M)	60	1	80
19	50/1/0.5	^t BuP ₄	NMP (3M)	120	1	75
20 ^a	250/5/1	^t BuP ₄	NMP (3M)	RT	24	42

[M]/[B]/[A] = [Monomer]:[Base]:[Activator]. All runs performed with approx. 200 mg 5/7-LM and A = NBzM, unless otherwise noted. NaM = sodium adduct of 5/7-LM. ^a1.50 g 5/7-LM used. ^b(-)-5/7-LM (75 mg) used. RT = room temperature (~22-23 °C)

Table S5.2. GPC molecular weight data for select nylon 4/6 homopolymer samples

Table S1 Entry No.	Base	[M]/[B]/[A]	Solvent	Temp. (°C)	Time (h)	Yield (%)	M_n , Theor. ^a	M_n , NMR (kDa)	M_n , GPC (kDa)	\bar{D}
5	^t Bu-P ₄	50/1/1	NMP (3M)	RT	3	95	5.95	6.6	12.7	2.04
7	^t Bu-P ₄	50/1/1	NMP (3M)	60	1.5	90	5.63	4.8	6.02	1.71
8	^t Bu-P ₄	50/1/1	NMP (3M)	120	1	73	4.57	6.06	6.05	1.45
16	NaM	50/1/1	NMP (3M)	120	1	68	4.26	4.5	5.22	1.35
19	^t Bu-P ₄	50/1/0.5	NMP (3M)	120	1	75	9.39	9.89	11.6	1.48
20 ^b	^t Bu-P ₄	250/5/1	NMP (3M)	RT	24	42	13.1	14.5	12.9	4.15

^aEstimated by (isolated yield)*([M]/[A])*(125.17 g/mol) ^b1.50g 5/7-LM used

Table S5.3. Results of stereoselectivity analysis by DFT. Results shown at the M06-2X/Def2TZVP level of theory in implicit nitrobenzene, as described in the Materials and Methods.

Selectivity	Stereochemistry			Enthalpy and Gibbs Free Energy differences (kcal/mol)											
	Penultimate	Chain end (bicyclic)	Attacking anion	25 °C				100 °C				120 °C			
				ΔH^\ddagger	ΔG^\ddagger	ΔH_{rxn}	ΔG_{rxn}	ΔH^\ddagger	ΔG^\ddagger	ΔH_{rxn}	ΔG_{rxn}	ΔH^\ddagger	ΔG^\ddagger	ΔH_{rxn}	ΔG_{rxn}
<i>Erythro</i>	RS	RS	RS	-0.4	12.7	-9.6	-1.1	-0.3	15.9	-9.3	0.8	-0.3	16.7	-9.2	1.3
<i>Threo</i>	RS	SR	RS	-5.6	7.3	-11.2	-1.8	-5.5	10.3	-11.0	0.3	-5.4	11.1	-10.9	0.9

Table S5.4. Amide A band peaks for homo- and co-polyamide samples

Amide A Band, Peak (cm ⁻¹)	
Nylon 6	3295
Nylon 4	3292
17% 5/7-LM	3286
54% 5/7-LM	3282
Nylon 4/6	3281

Table S5.5. Tensile stress-strain data for nylon 4/6-co-nylon 4 (51% 5/7-LM) thin film samples

Sample	Ultimate Stress (MPa)	Elongation at Ultimate Stress	Elongation at Break (%)	Young's Modulus
1	59.31	6.23	13.76	1872.43
2	55.48	3.74	3.74	2502.62
3	47.77	2.44	2.44	2826.39
4	60.94	4.68	4.68	2360.63
5	48.58	4.73	13.46	1828.53
Average	54.42	4.36	7.62	2278.12
Standard deviation	5.40	1.25	4.95	380.66

C.3.

DFT Cartesian Coordinates

All species were optimized as singlets. Charged species are noted; the remaining are neutral.

Model trimers (Figures 5.11 and S5.94)

erythro-disyndiotactic, equatorial

N	-4.726944	4.242632	1.936027
H	-3.760738	4.055555	2.153242
C	-5.146429	5.629405	1.813849
C	-4.283028	6.514319	2.704318
C	-5.090967	6.095059	0.359231
H	-6.183377	5.676036	2.157105
C	-4.695903	7.978225	2.578619
H	-3.235383	6.404140	2.401310
H	-4.361046	6.178604	3.740095
C	-5.520327	7.559230	0.235787
H	-4.065331	5.995525	-0.007522
H	-5.729769	5.453476	-0.251404
C	-4.647428	8.447848	1.127610
H	-4.046207	8.601380	3.194681
H	-5.712584	8.099540	2.965338
H	-6.561044	7.649559	0.562814
H	-4.975611	9.486801	1.052864
H	-3.619909	8.401997	0.756378
C	-5.409422	8.004452	-1.210390
O	-4.337204	7.983741	-1.805503
N	-6.547655	8.432701	-1.788366
H	-7.405552	8.381530	-1.261297
C	-6.619574	8.858041	-3.177331
C	-6.772640	7.666800	-4.122035
C	-7.768145	9.845228	-3.347783
H	-5.674456	9.360174	-3.400330
C	-6.875991	8.133111	-5.570931
H	-7.679808	7.119986	-3.843699
H	-5.926187	6.991477	-3.987032
C	-7.874459	10.314585	-4.797985
H	-8.709382	9.361985	-3.068182
H	-7.624321	10.698663	-2.681280
C	-8.028085	9.117681	-5.747068
H	-7.012046	7.276392	-6.232485
H	-5.938622	8.616275	-5.864625
H	-6.958229	10.850969	-5.063805
H	-8.078785	9.469422	-6.779818

H	-8.976525	8.620167	-5.523297
C	-9.062571	11.242721	-4.971213
O	-10.166199	10.967743	-4.513079
N	-8.833733	12.365337	-5.679003
H	-7.913979	12.514116	-6.064826
C	-9.884340	13.308217	-6.027817
C	-9.288956	14.692494	-6.252057
C	-10.658601	12.836500	-7.258196
H	-10.568335	13.344282	-5.175868
C	-10.374546	15.693944	-6.636510
H	-8.547666	14.631848	-7.057204
H	-8.766175	15.016399	-5.350202
C	-11.755680	13.836007	-7.631923
H	-9.966489	12.740568	-8.099748
H	-11.085679	11.850693	-7.061544
C	-11.153960	15.226564	-7.862134
H	-9.927845	16.670468	-6.828314
H	-11.062969	15.819091	-5.794896
H	-12.472912	13.896623	-6.807252
H	-11.945464	15.939055	-8.104034
H	-10.487360	15.172215	-8.727383
C	-12.472626	13.370521	-8.884363
O	-11.873008	13.180467	-9.937770
N	-13.799558	13.186809	-8.782408
H	-14.250245	13.351108	-7.898593
C	-14.593973	12.754451	-9.914193
H	-15.633088	12.685237	-9.605639
H	-14.509826	13.465858	-10.735811
H	-14.259405	11.779481	-10.269238
C	-5.548539	3.205151	1.686682
C	-4.947975	1.828356	1.826540
H	-5.041478	1.312706	0.871453
H	-3.902559	1.845423	2.126111
H	-5.526353	1.272831	2.563714
O	-6.723414	3.359710	1.370938

erythro-disyndiotactic, axial

N	-20.366242	15.317797	9.670432
C	-17.467241	16.182478	9.023036
C	-16.719604	14.858500	8.905140
C	-18.195046	16.260184	10.360893

H	-18.188543	16.275508	8.203112	O	-22.397473	-6.730945	-10.456142
C	-17.687610	13.666388	8.980770	C	-20.811730	-6.925370	-8.615011
H	-16.013150	14.774403	9.736165	C	-20.000386	-5.745948	-9.174168
H	-16.130772	14.820392	7.987820	C	-19.966629	-8.212652	-8.571103
H	-18.721367	17.208492	10.473776	H	-21.082968	-6.671679	-7.586819
H	-17.462914	16.193684	11.171713	C	-19.145358	-6.025299	-10.415786
C	-18.558895	13.754216	10.241680	H	-19.309092	-5.443439	-8.384682
H	-17.089488	12.753410	9.060941	H	-20.655444	-4.894259	-9.365867
H	-19.331015	12.983688	10.221454	C	-19.297302	-8.492985	-9.912188
H	-17.907225	13.533427	11.090045	H	-19.192384	-8.081166	-7.810057
C	-18.486249	13.494610	7.686973	H	-20.582038	-9.056493	-8.256004
O	-19.721317	13.494089	7.650359	C	-18.372146	-7.341023	-10.287459
N	-17.746672	13.316206	6.589703	H	-18.432032	-5.207189	-10.526079
H	-16.731386	13.325896	6.639438	H	-18.734375	-9.426189	-9.859188
C	-18.327944	13.138353	5.265182	H	-20.057303	-8.625684	-10.690987
C	-18.844065	11.709021	5.074819	H	-17.861011	-7.535800	-11.231525
C	-17.313314	13.523835	4.181892	H	-17.604151	-7.225933	-9.516341
H	-19.173959	13.824802	5.200557	N	-19.967141	-6.038525	-11.619272
C	-17.699483	10.714196	4.912462	H	-20.957706	-6.219093	-11.485918
H	-19.470186	11.684183	4.177600	C	-19.442912	-5.911955	-12.840014
H	-19.479240	11.450135	5.922728	O	-18.239063	-5.686747	-13.010074
C	-16.226205	12.484190	3.874395	C	-20.430158	-6.024054	-14.003765
H	-17.878979	13.668634	3.258805	C	-21.323949	-7.267869	-13.888812
H	-16.859204	14.483575	4.433254	C	-19.749827	-5.981450	-15.379612
C	-16.844175	11.086275	3.705926	H	-21.063883	-5.135293	-13.922371
H	-18.094580	9.704244	4.794691	C	-20.521969	-8.533670	-14.172204
H	-17.081621	10.707926	5.817818	H	-22.124838	-7.179436	-14.628726
H	-15.766929	12.765160	2.921769	H	-21.807580	-7.320730	-12.913109
H	-16.067035	10.341248	3.531249	C	-19.069874	-7.281899	-15.825617
H	-17.475754	11.099781	2.812897	H	-20.529779	-5.765888	-16.112980
C	-15.070800	12.475290	4.876973	H	-19.032965	-5.160624	-15.422321
O	-15.054031	13.173807	5.897108	C	-19.969159	-8.500846	-15.592970
N	-14.060547	11.663470	4.558317	H	-21.146826	-9.417161	-14.033651
H	-14.077741	11.121177	3.697946	H	-19.696604	-8.615568	-13.453514
C	-12.865623	11.526859	5.378975	H	-18.855189	-7.207442	-16.893326
C	-11.873545	12.657674	5.094491	H	-19.401166	-9.404371	-15.818560
C	-12.223148	10.148006	5.180459	H	-20.802675	-8.454150	-16.300461
H	-13.193505	11.599547	6.416614	N	-17.789762	-7.447832	-15.143789
C	-11.216357	12.486554	3.729189	H	-17.628350	-6.863807	-14.330833
H	-11.101738	12.649536	5.870228	C	-16.848240	-8.528173	-15.591789
H	-12.398783	13.611023	5.166071	O	-17.004514	-8.944586	-16.623086
C	-11.369056	9.956703	3.916577	C	-15.543367	-8.338151	-14.791042
H	-11.554682	9.993085	6.030279	C	-14.689098	-9.562829	-15.149369
H	-12.992977	9.376216	5.237494	C	-15.744818	-8.265230	-13.271979
C	-10.449209	11.169741	3.675875	H	-14.990823	-7.448142	-15.110610
H	-10.537817	13.317360	3.531200	C	-15.174207	-10.885002	-14.545358
H	-11.980623	12.507716	2.945101	H	-13.685269	-9.381525	-14.759670
H	-10.729886	9.087261	4.089052	H	-14.604278	-9.661140	-16.231690
H	-9.925898	11.057651	2.724838	C	-16.363342	-9.555787	-12.741961
H	-9.687468	11.172987	4.460574	H	-14.761963	-8.127277	-12.811495
C	-12.169171	9.640601	2.660908	H	-16.338366	-7.396067	-12.984905
O	-13.349510	9.955303	2.495220	C	-15.457679	-10.744978	-13.046411
H	-16.770632	17.016354	8.925597	H	-14.389981	-11.633882	-14.678114
C	-19.202221	15.117645	10.522924	H	-17.347642	-9.708495	-13.200627
H	-19.563305	15.117892	11.553332	H	-15.890680	-11.676444	-12.681798
H	-20.434554	14.730520	8.845463	H	-14.501479	-10.605783	-12.532506
N	-11.493507	8.994031	1.701531	N	-16.348340	-11.366219	-15.266107
H	-10.536983	8.730304	1.869636	H	-16.784151	-10.730799	-15.923203
C	-21.339060	16.187815	9.973057	H	-16.527061	-9.482429	-11.665262
O	-21.318498	16.891761	10.981866	N	-23.019045	-7.917273	-8.666021
C	-22.489337	16.259179	8.997034	H	-22.789801	-8.237975	-7.739937
H	-22.573873	17.282748	8.633380	C	-24.307893	-8.261991	-9.232759
H	-22.369021	15.584392	8.151953	H	-24.844405	-8.884771	-8.523030
H	-23.410461	16.016553	9.526079	H	-24.891241	-7.363948	-9.436024
C	-12.101035	8.670213	0.425901	H	-24.180562	-8.808908	-10.166782
H	-11.365909	8.160839	-0.190203	C	-16.758680	-12.642553	-15.204796
H	-12.964370	8.020003	0.566712	C	-17.959822	-12.991772	-16.050871
H	-12.431028	9.576052	-0.082457	H	-18.758171	-13.335902	-15.393743
				H	-18.319117	-12.152846	-16.643679
				H	-17.693569	-13.815975	-16.711495
				O	-16.205345	-13.488755	-14.506204
threo-disyndiotactic, axial							
C	-22.131448	-7.169992	-9.335668				

threo-disyndiotactic, equatorial

C	-13.943732	-9.547065	-0.386169
C	-13.028855	-8.539714	-1.077355
C	-11.576565	-8.995631	-1.014530
C	-11.413322	-10.390548	-1.617220
C	-12.319387	-11.400238	-0.907458
C	-13.780313	-10.944766	-0.976409
H	-13.322587	-8.442658	-2.128904
H	-13.123859	-7.553780	-0.618451
H	-13.706482	-9.574204	0.681936
H	-14.982273	-9.224630	-0.471925
H	-11.684117	-10.354775	-2.676460
H	-10.367186	-10.695316	-1.547161
H	-12.020579	-11.461430	0.143843
H	-14.089912	-10.943540	-2.025141
H	-14.418099	-11.657084	-0.448722
H	-11.253863	-9.026810	0.029791
N	-10.723742	-8.029898	-1.689621
H	-11.124567	-7.474449	-2.429318
C	-9.409015	-7.907307	-1.428054
C	-12.165991	-12.765278	-1.549655
O	-12.443812	-12.958726	-2.729003
O	-8.843558	-8.581955	-0.574134
C	-8.655876	-6.874567	-2.246285
C	-8.037880	-5.820310	-1.322605
C	-7.572949	-7.573323	-3.073781
H	-9.351204	-6.377358	-2.929465
C	-7.215726	-4.811341	-2.118886
H	-7.397301	-6.331767	-0.599030
H	-8.826149	-5.314810	-0.760646
C	-6.752735	-6.560716	-3.863852
H	-6.915173	-8.121559	-2.391439
H	-8.023845	-8.298164	-3.755731
C	-6.136836	-5.511933	-2.939270
H	-6.761334	-4.084107	-1.444509
H	-7.875959	-4.252818	-2.790164
H	-7.401092	-6.053745	-4.583453
H	-5.571459	-4.795417	-3.537437
H	-5.430784	-6.014614	-2.269716
N	-5.735429	-7.256159	-4.636577
H	-5.349939	-8.108298	-4.259260
C	-5.187568	-6.741430	-5.754254
O	-5.563819	-5.682023	-6.243253
C	-4.043933	-7.537135	-6.356584
C	-4.181110	-7.611689	-7.876143
C	-2.714053	-6.878629	-5.961816
H	-4.060398	-8.552914	-5.949117
C	-2.998529	-8.347287	-8.495438
H	-4.224650	-6.592426	-8.272077
H	-5.112707	-8.111994	-8.149974
C	-1.534764	-7.618704	-6.585486
H	-2.725615	-5.841824	-6.311511
H	-2.621687	-6.856045	-4.873771
C	-1.675742	-7.690794	-8.102840
H	-2.991293	-9.382346	-8.143846
H	-0.599666	-7.124544	-6.317966
H	-1.487000	-8.633078	-6.176664
H	-0.851452	-8.251928	-8.545866
H	-1.653066	-6.680461	-8.524909
N	-3.162643	-8.399923	-9.939536
H	-3.641986	-7.637332	-10.391878
N	-11.710221	-13.751230	-0.758912
H	-11.495733	-13.548204	0.202350
C	-2.620233	-9.367460	-10.703309
O	-1.979790	-10.298844	-10.227685
C	-2.849896	-9.252285	-12.189971
H	-3.327278	-10.167542	-12.537414
H	-3.464261	-8.397632	-12.463754
H	-1.881676	-9.172981	-12.683243
C	-11.520602	-15.097923	-1.258286

H	-10.811863	-15.103569	-2.086488
H	-11.135483	-15.717742	-0.453787
H	-12.464279	-15.514010	-1.611632

Species used in calculating changes in energy along reaction coordinates (Figure 5.4)**bicyclic lactam monomer**

C	-2.164878	1.109711	-0.010622
C	-0.694807	1.279031	-0.434010
C	-0.020323	2.561609	0.083249
C	-2.417645	1.590758	1.443813
C	-0.510811	2.940834	1.492995
H	-2.827901	1.653868	-0.687144
H	-0.132860	0.424696	-0.053686
H	-0.209487	3.403277	-0.585938
H	-2.434098	0.056841	-0.095488
H	-0.618480	1.228204	-1.520327
H	1.059893	2.408370	0.101734
H	-3.182475	0.997288	1.937907
H	0.262476	3.449325	2.064438
C	-1.091578	1.710048	2.203677
H	-1.263325	1.925054	3.257932
H	-0.454066	0.832655	2.119526
N	-1.711649	3.780704	1.428197
H	-1.691641	4.755224	1.168186
C	-2.844346	3.049833	1.350966
O	-3.974465	3.476991	1.179537

bicyclic lactamate anion (-1 charge)

C	-2.159464	1.078026	-0.012318
C	-0.689798	1.245656	-0.441657
C	-0.016562	2.534741	0.064213
C	-2.407312	1.607272	1.420121
C	-0.536822	2.956938	1.457206
H	-2.825858	1.604814	-0.700662
H	-0.128159	0.396179	-0.047290
H	-0.197824	3.364900	-0.621968
H	-2.419785	0.019350	-0.080794
H	-0.609592	1.175110	-1.528144
H	1.064503	2.371118	0.090307
H	-3.192656	1.604369	1.922586
H	0.262209	3.452785	2.013454
C	-1.090129	1.717604	2.184280
H	-1.271634	1.944382	3.236357
H	-0.445773	0.838617	2.121892
N	-1.696572	3.850391	1.331109
C	-2.774058	3.100254	1.305583
O	-3.969118	3.471401	1.151189

Model erythro-disyndiotactic propagation reactant: RS(equatorial polymer segment)-RS(bicyclic end group)

C	-0.827111	0.363910	-0.755492
O	-0.796881	1.300352	-1.526541
C	0.420592	-0.248472	-0.166764
C	0.690290	-1.610121	-0.830043
C	1.615459	0.683239	-0.342136
H	0.245363	-0.424826	0.896001
C	1.952231	-2.240045	-0.248604
H	0.818275	-1.454290	-1.406576
H	-0.164282	-2.271194	-0.688650
C	2.871123	0.048589	0.244986
H	1.423397	1.643881	0.139229
H	1.771463	0.878147	-1.407555
C	3.151996	-1.309551	-0.396707
H	2.153557	-3.193007	-0.739966

H	1.785730	-2.455804	0.811776	C	-7.563190	-1.692670	2.345300
H	2.734556	-0.095533	1.319964	H	-7.009743	-1.075602	3.049839
H	4.042885	-1.744684	0.058963	C	-8.979919	-1.138853	2.107164
H	3.367529	-1.150757	-1.458670	H	-8.928386	-0.078665	1.852640
N	3.994686	0.958221	0.087329	H	-9.533883	-1.222032	3.046262
H	4.004175	1.569790	-0.713712	C	-9.715198	-1.896754	0.990517
C	5.061407	0.952372	0.909343	H	-9.330340	-1.549257	0.028718
O	5.143422	0.200083	1.874248	H	-10.777789	-1.649948	1.007825
C	6.159572	1.934554	0.584642	C	-9.521610	-3.417263	1.066162
H	5.927291	2.570258	-0.266756	H	-10.141137	-3.848089	1.857540
H	7.072149	1.375929	0.378956	H	-9.827056	-3.878169	0.124642
H	6.338568	2.554821	1.461810	C	-2.054282	-2.670756	0.790921
N	-2.055793	-0.208439	-0.441639	C	-2.107652	-1.162454	0.486317
C	-2.374213	-1.116913	0.572412	C	-3.422037	-0.468886	0.890852
O	-1.600057	-1.680623	1.307624	C	-2.764485	-3.021311	2.119822
C	-3.295814	0.326915	-1.050481	C	-4.051119	-1.097814	2.154346
H	-3.107430	0.558396	-2.094638	H	-2.522316	-3.244789	-0.014133
C	-4.253020	-0.843498	-0.832139	H	-1.289774	-0.684340	1.029414
H	-4.033661	-1.658209	-1.522359	H	-4.162134	-0.513835	0.091923
H	-5.294862	-0.548281	-0.943515	H	-1.007764	-2.980772	0.823795
C	-3.889705	-1.211670	0.603905	H	-1.899183	-0.989514	-0.571962
H	-4.198144	-2.203838	0.924098	H	-3.211717	0.589636	1.067662
C	-4.422798	-0.121020	1.556055	H	-2.290394	-3.867100	2.616239
H	-5.509680	-0.100974	1.450207	H	-4.604681	-0.338162	2.711589
H	-4.199368	-0.386758	2.590101	C	-2.943467	-1.772074	2.983500
C	-3.828790	1.257491	1.232732	H	-3.315714	-2.037507	3.974303
H	-2.811261	1.304427	1.630515	H	-2.045949	-1.162031	3.096390
H	-4.391726	2.033999	1.750380	N	-4.937905	-2.214434	1.819055
C	-3.783025	1.553139	-0.272180	C	-4.234377	-3.327923	1.778769
H	-3.130106	2.404448	-0.466513	O	-4.626732	-4.474715	1.464933
H	-4.776992	1.809546	-0.645641				

Model erythro-disyndiotactic propagation transition state structure: RS(equatorial polymer segment)-RS(bicyclic end group), RS monomer addition (-1 charge)

C	-6.665656	-3.632266	-0.653191
O	-7.095376	-4.719637	-1.027232
C	-5.585054	-2.909014	-1.426458
C	-4.579051	-3.887931	-2.028149
C	-6.238985	-2.062581	-2.525788
H	-5.062769	-2.242432	-0.739349
C	-3.518158	-3.131923	-2.824500
H	-5.103033	-4.587738	-2.684393
H	-4.124484	-4.469330	-1.223318
C	-5.176511	-1.309598	-3.315748
H	-6.791430	-2.724584	-3.203964
H	-6.941859	-1.357192	-2.081033
C	-4.153845	-2.273679	-3.914831
H	-2.805139	-3.830773	-3.265807
H	-2.949734	-2.484207	-2.147830
H	-4.656669	-0.621348	-2.642164
H	-3.398014	-1.704876	-4.459090
H	-4.669863	-2.915208	-4.637443
N	-5.812348	-0.497493	-4.342788
H	-6.702677	-0.800277	-4.704866
C	-5.233759	0.592385	-4.879013
O	-4.136228	1.002168	-4.514535
C	-6.013181	1.299738	-5.960482
H	-6.981855	0.845931	-6.157396
H	-5.419430	1.292013	-6.873995
H	-6.153537	2.337983	-5.662601
N	-7.164489	-3.030137	0.455292
C	-6.832224	-1.736686	1.002542
O	-6.605277	-0.753014	0.308014
C	-8.057701	-3.756130	1.369520
H	-7.866587	-4.822406	1.281852
C	-7.662883	-3.164122	2.722966
H	-8.416179	-3.359815	3.486309
H	-6.696980	-3.552767	3.038068

Model erythro-disyndiotactic propagation intermediate charged product: RS(equatorial polymer segment)-RS(polymer segment)-RS(bicyclic end group) (-1 charge)

C	0.339467	1.633347	1.251879
O	0.634478	2.668048	1.866017
C	0.884145	1.396521	-0.143444
C	1.003257	2.687931	-0.948535
C	2.246706	0.705080	-0.055049
H	0.215147	0.714287	-0.667743
C	1.560526	2.400554	-2.343054
H	1.662820	3.380481	-0.419956
H	0.024330	3.167734	-1.024658
C	2.730614	0.367272	-1.462359
H	2.974018	1.370499	0.424078
H	2.148993	-0.203071	0.538011
C	2.884817	1.638108	-2.289361
H	1.691686	3.331785	-2.896853
H	0.835585	1.799641	-2.903496
H	1.972264	-0.256083	-1.944752
H	3.655758	2.266589	-1.829021
H	3.224680	1.387038	-3.296266
N	3.972530	-0.391528	-1.446728
H	4.840844	0.125752	-1.411482
C	4.085999	-1.720734	-1.238816
O	5.184581	-2.253800	-1.107233
C	2.806756	-2.522858	-1.215524
H	2.056262	-2.096429	-0.545086
H	3.047679	-3.537924	-0.913385
H	2.374372	-2.545386	-2.218525
N	-0.432838	0.683727	1.789643
C	-0.844779	-0.650952	1.168648
O	0.114487	-1.393880	0.718807
C	-1.086895	0.903447	3.079432
H	-1.321382	1.960511	3.191511
C	-2.323546	0.012538	2.964950
H	-3.060239	0.469078	2.304167
H	-2.782586	-0.176779	3.936479
C	-1.700302	-1.228968	2.340755

H	-2.433451	-1.928067	1.933593	C	0.508723	-3.139537	3.978628
C	-0.819592	-1.928541	3.380896	H	-0.306365	-3.744573	4.374975
H	-1.466854	-2.261179	4.199328	H	1.105698	-3.774835	3.315648
H	-0.366318	-2.818438	2.942469	C	1.382293	-2.619381	5.116006
C	0.287177	-1.016633	3.928895	H	1.800141	-3.456280	5.677145
H	0.731573	-1.460632	4.822179	H	0.758393	-2.047753	5.810269
H	1.072338	-0.954188	3.174129	C	2.507050	-1.728750	4.596216
C	-0.202585	0.404204	4.228049	H	3.182653	-2.324419	3.971460
H	0.649531	1.073530	4.362993	H	3.095412	-1.327474	5.423382
H	-0.789497	0.430934	5.151115	C	-5.111532	-2.295816	2.690679
C	-2.175384	0.853901	-2.762556	C	-5.111254	-2.227979	1.156272
C	-1.431340	-0.416061	-3.212594	C	-3.745551	-2.525052	0.518516
C	-1.074961	-1.389278	-2.074410	C	-4.263450	-3.484461	3.227378
C	-3.186341	0.570327	-1.622456	C	-2.988549	-3.627168	1.280193
C	-2.120741	-1.373960	-0.944485	H	-4.736636	-1.362983	3.118251
H	-1.469434	1.617815	-2.422377	H	-5.833531	-2.954547	0.781446
H	-2.068223	-0.939185	-3.928423	H	-3.893524	-2.838730	-0.515560
H	-1.008662	-2.399579	-2.485964	H	-6.136883	-2.405813	3.042299
H	-2.695754	1.278218	-3.622166	H	-5.470546	-1.251080	0.832859
H	-0.530597	-0.138006	-3.764036	H	-3.120037	-1.631541	0.490393
H	-0.108929	-1.167903	-1.624704	H	-4.699729	-3.914288	4.124847
H	-4.064460	1.207926	-1.697336	H	-2.343241	-4.200133	0.621849
H	-2.148006	-2.333492	-0.431824	C	-3.954118	-4.478534	2.106522
C	-3.474341	-0.926278	-1.503533	H	-4.828594	-4.789161	1.539797
H	-3.727329	-1.411334	-2.445487	H	-3.452017	-5.364068	2.495362
H	-4.271841	-1.111066	-0.782751	N	-2.154683	-3.032095	2.350788
N	-1.844548	-0.313922	0.041467	C	-2.880510	-2.947601	3.537861
C	-2.457120	0.832123	-0.305298	O	-2.500187	-2.496150	4.591362
O	-2.427544	1.928187	0.251237	H	3.921286	-0.203210	3.064795

Model erythro-disyndiotactic propagation
neutral product: RS(equatorial polymer
segment)-RS(equatorial polymer segment)-
RS(bicyclic end group)

C	2.892074	1.546590	2.960958
O	1.834121	2.144496	3.126489
C	4.120641	2.248829	2.414002
C	3.824704	2.822071	1.024872
C	4.546063	3.365685	3.371201
H	4.940460	1.528537	2.329393
C	5.029414	3.584623	0.481595
H	2.966355	3.494238	1.107716
H	3.544006	2.017401	0.341816
C	5.756373	4.121772	2.823982
H	3.713674	4.065166	3.491283
H	4.787991	2.958405	4.355103
C	5.467427	4.689049	1.439759
H	4.792020	4.012017	-0.493548
H	5.860989	2.889376	0.329902
H	6.600879	3.430368	2.760516
H	4.669295	5.435688	1.523869
H	6.354630	5.199814	1.060839
N	6.157512	5.189997	3.725144
H	5.790972	6.114283	3.560520
C	6.916246	4.978137	4.817488
O	7.354794	3.870047	5.106734
C	7.208516	6.185913	5.672675
H	6.794668	7.106783	5.268203
H	8.288461	6.286352	5.771715
H	6.796951	6.011884	6.666428
N	3.037943	0.241799	3.260053
C	-0.908904	-2.499637	2.036049
O	-0.537811	-2.524769	0.880759
C	1.949771	-0.582637	3.760687
H	1.336187	0.061163	4.396174
C	1.085856	-1.107530	2.613904
H	1.710859	-1.703668	1.943671
H	0.694875	-0.267253	2.037675
C	-0.051748	-1.965656	3.157236
H	-0.683266	-1.368108	3.817147

Model threo-disyndiotactic propagation
reactant: RS(equatorial polymer segment)-
SR(bicyclic end group)

C	0.471530	-0.167403	1.616044
O	1.290020	-0.833066	2.216135
C	0.866131	0.842936	0.566263
C	0.928108	2.236616	1.216534
C	2.214096	0.480611	-0.051815
H	0.100375	0.865846	-0.209174
C	1.338680	3.282066	0.184378
H	1.663290	2.208201	2.027725
H	-0.038915	2.491139	1.650690
C	2.621020	1.526881	-1.083053
H	2.972279	0.431724	0.735199
H	2.165857	-0.504176	-0.520892
C	2.673112	2.921854	-0.461079
H	1.401691	4.264880	0.653630
H	0.563971	3.344812	-0.586621
H	1.892026	1.535249	-1.897711
H	2.944380	3.646752	-1.230042
H	3.463987	2.931487	0.296399
N	3.898666	1.156892	-1.671060
H	4.554101	0.644337	-1.102324
C	4.280321	1.555427	-2.899510
O	3.556168	2.226675	-3.626669
C	5.654584	1.121533	-3.345717
H	6.172480	0.513037	-2.607882
H	6.245351	2.012006	-3.557775
H	5.554730	0.558873	-4.273045
N	-0.874733	-0.314384	1.928542
C	-1.980180	0.411055	1.472780
O	-1.977485	1.292799	0.648324
C	-1.287110	-1.245064	3.004879
H	-0.656066	-2.127899	2.973081
C	-2.743660	-1.504599	2.624932
H	-3.314237	-1.926634	3.450371
H	-2.807015	-2.171601	1.765077
C	-3.175595	-0.085340	2.267091
H	-4.081786	-0.008538	1.671312
C	-3.278323	0.752119	3.558886

H	-3.615967	1.762125	3.322857
H	-4.043826	0.288932	4.185272
C	-1.939395	0.813376	4.308840
H	-1.289272	1.537955	3.810485
H	-2.097506	1.194057	5.317734
C	-1.216540	-0.539578	4.362309
H	-1.678303	-1.196006	5.103239
H	-0.176049	-0.395477	4.656190

**Model threo-disyndiotactic propagation
transition state structure: RS(equatorial
polymer segment)-SR(bicyclic end group), RS
monomer addition (-1 charge)**

C	-9.137677	-9.017112	-0.183650
O	-8.499190	-9.373910	0.804421
C	-8.432771	-8.434725	-1.391194
C	-8.110791	-6.957370	-1.131410
C	-7.160483	-9.224661	-1.694882
H	-9.102165	-8.486776	-2.248425
C	-7.370567	-6.355634	-2.322180
H	-7.487425	-6.883330	-0.233987
H	-9.038865	-6.415752	-0.941342
C	-6.418174	-8.614761	-2.877516
H	-6.509440	-9.212829	-0.814993
H	-7.415785	-10.265674	-1.907215
C	-6.098806	-7.141100	-2.629856
H	-7.127755	-5.309286	-2.128714
H	-8.028564	-6.373418	-3.197941
H	-7.039373	-8.688166	-3.774143
H	-5.585314	-6.732517	-3.502015
H	-5.410596	-7.076180	-1.780048
N	-5.213404	-9.386225	-3.145014
H	-4.770558	-9.857147	-2.371852
C	-4.629853	-9.441332	-4.355900
O	-5.090425	-8.864822	-5.336346
C	-3.367564	-10.262671	-4.452916
H	-3.101456	-10.751651	-3.518466
H	-2.553130	-9.607945	-4.761554
H	-3.503351	-11.014696	-5.228985
N	-10.487146	-9.109162	-0.213965
C	-11.397294	-8.682215	-1.258723
O	-11.219788	-7.657768	-1.914920
C	-11.221366	-9.814496	0.845605
H	-10.580462	-10.578949	1.277111
C	-12.420380	-10.371297	0.076044
H	-13.227235	-10.670313	0.745398
H	-12.113804	-11.210611	-0.545079
C	-12.769057	-9.160809	-0.777890
H	-13.404628	-9.374846	-1.634667
C	-13.383773	-8.072234	0.119225
H	-13.653786	-7.201929	-0.481843
H	-14.307634	-8.472655	0.545949
C	-12.427885	-7.639641	1.242263
H	-11.673721	-6.974847	0.814258
H	-12.968192	-7.057425	1.990282
C	-11.706901	-8.820129	1.906589
H	-12.377132	-9.350531	2.588637
H	-10.862466	-8.455816	2.495035
C	-10.395758	-12.452930	-4.649353
C	-11.900025	-12.191477	-4.464550
C	-12.288729	-10.721646	-4.681664
C	-9.549065	-11.341527	-4.002954
C	-11.266219	-9.789445	-4.008259
H	-10.140815	-13.424358	-4.219582
H	-12.476921	-12.841103	-5.125574
H	-13.286427	-10.544363	-4.272109
H	-10.149092	-12.497414	-5.714326
H	-12.171314	-12.466238	-3.442689
H	-12.331868	-10.488972	-5.750281
H	-8.489251	-11.599503	-3.997783

H	-11.596730	-8.749954	-4.048647
C	-9.898443	-10.016642	-4.670736
H	-9.201165	-9.226654	-4.384571
H	-9.943631	-10.070999	-5.760427
N	-11.051708	-10.185121	-2.618466
C	-10.076651	-11.081549	-2.575160
O	-9.643896	-11.691243	-1.575229

**Model threo-disyndiotactic propagation
intermediate charged product: RS(equatorial
polymer segment)-SR(polymer segment)-
RS(bicyclic end group) (-1 charge)**

C	0.258498	0.545415	1.924305
O	0.869047	0.330532	2.982142
C	0.995461	1.193465	0.761752
C	1.491527	2.582795	1.177593
C	2.170914	0.310375	0.336791
H	0.311317	1.313854	-0.076828
C	2.293319	3.236477	0.055831
H	2.118326	2.480830	2.068065
H	0.638063	3.208478	1.450029
C	2.965138	0.968828	-0.784425
H	2.828116	0.149206	1.198298
H	1.811432	-0.669008	0.010058
C	3.462383	2.351576	-0.367251
H	2.659410	4.214899	0.372197
H	1.639280	3.405596	-0.806098
H	2.324679	1.085454	-1.663036
H	4.016920	2.799880	-1.193641
H	4.157372	2.230161	0.470723
N	4.061825	0.098297	-1.181107
H	4.464325	-0.505138	-0.481277
C	4.606087	0.114240	-2.411531
O	4.194273	0.847499	-3.304999
C	5.758475	-0.831675	-2.645031
H	5.996090	-1.440361	-1.775546
H	6.633595	-0.246223	-2.925159
H	5.508790	-1.480378	-3.483668
N	-1.029105	0.239233	1.770427
C	-1.887970	0.430877	0.519493
O	-1.911616	1.622083	0.019360
C	-1.762753	-0.471669	2.822316
H	-1.082860	-1.131297	3.357979
C	-2.843263	-1.213636	2.033487
H	-3.666078	-1.529207	2.677062
H	-2.423317	-2.083915	1.534289
C	-3.247862	-0.127101	1.047166
H	-3.835528	-0.497332	0.206015
C	-4.024831	0.956502	1.803518
H	-4.327858	1.746930	1.116337
H	-4.937561	0.497567	2.197804
C	-3.212730	1.573613	2.952232
H	-2.496756	2.270602	2.514669
H	-3.868498	2.151989	3.606412
C	-2.431784	0.534866	3.766268
H	-3.094383	-0.014463	4.441537
H	-1.678277	1.032512	4.380488
C	-1.447387	-3.164257	-2.191241
C	-2.809758	-2.477731	-2.001659
C	-2.799996	-1.008435	-2.441567
C	-0.287199	-2.255062	-1.744572
C	-1.529482	-0.304992	-1.940076
H	-1.427838	-4.101342	-1.631392
H	-3.583853	-3.030548	-2.535626
H	-3.690795	-0.499741	-2.067536
H	-1.293988	-3.413068	-3.244735
H	-3.075368	-2.519059	-0.941493
H	-2.823549	-0.933246	-3.532216
H	0.659624	-2.793170	-1.739301
H	-1.577581	0.768647	-2.090526

C	-0.308119	-0.975210	-2.570983
H	0.588612	-0.376730	-2.396562
H	-0.423209	-1.148294	-3.641190
N	-1.307064	-0.570883	-0.509741
C	-0.602401	-1.710741	-0.347555
O	-0.272948	-2.278650	0.692162

**Model threo-disyndiotactic propagation
neutral product: RS(equatorial polymer
segment)-SR(equatorial polymer segment)-
RS(bicyclic end group)**

C	2.077731	-1.175243	-1.333456
O	1.554496	-2.148440	-0.798767
C	3.585883	-0.985897	-1.276684
C	4.174156	0.084718	-2.193679
C	3.987041	-0.722629	0.181242
H	3.998092	-1.957681	-1.570232
C	5.695456	0.119692	-2.060693
H	3.891099	-0.102877	-3.231676
H	3.783145	1.069550	-1.913393
C	5.508704	-0.661718	0.317225
H	3.593400	-1.513186	0.821019
H	3.559062	0.227304	0.510553
C	6.116344	0.383566	-0.617503
H	6.106308	-0.838667	-2.394191
H	6.109240	0.887836	-2.715239
H	5.905595	-1.638999	0.028804
H	7.203698	0.360696	-0.523443
H	5.776393	1.373256	-0.306573
N	5.924225	-0.476788	1.705976
H	6.460539	-1.215019	2.129502
C	5.641907	0.599852	2.465618
O	4.992708	1.557174	2.059359
C	6.179536	0.570031	3.876987
H	6.717313	-0.344442	4.116333
H	5.343729	0.688215	4.565388
H	6.843622	1.423530	4.009293
N	1.355609	-0.236871	-1.971579

C	-2.873549	0.720290	0.435532
O	-2.258083	1.358366	1.263737
C	-0.097213	-0.272665	-2.038126
H	-0.382709	-1.320817	-2.161367
C	-0.719692	0.255422	-0.745743
H	-0.391321	1.286512	-0.589659
H	-0.361816	-0.335036	0.098844
C	-2.241172	0.206251	-0.834588
H	-2.569919	-0.823927	-0.985191
C	-2.732909	1.036375	-2.032607
H	-3.819492	0.995163	-2.101124
H	-2.447412	2.081555	-1.872623
C	-2.103249	0.522939	-3.323909
H	-2.431285	1.133199	-4.166436
H	-2.456199	-0.496281	-3.510137
C	-0.579268	0.524436	-3.243952
H	-0.222028	1.556452	-3.149529
H	-0.144945	0.110239	-4.155806
C	-6.314099	-1.460342	1.834844
C	-5.025246	-1.338406	2.660697
C	-4.686901	0.110842	3.034413
C	-6.398449	-0.374629	0.742100
C	-4.901786	1.043988	1.838677
H	-7.189715	-1.343086	2.477082
H	-4.195651	-1.754046	2.082085
H	-5.328394	0.459772	3.846831
H	-6.370568	-2.450972	1.381783
H	-5.102172	-1.949108	3.560106
H	-3.655060	0.176549	3.380480
H	-7.235544	-0.551037	0.071053
H	-4.524017	2.043563	2.032431
C	-6.364595	1.001998	1.400500
H	-7.048657	1.086076	2.243092
H	-6.577500	1.794681	0.683144
N	-4.233414	0.498570	0.634238
C	-5.092916	-0.377624	-0.034272
O	-4.835096	-1.040609	-1.009996
H	1.827012	0.559385	-2.369794

References

1. Frisch, M. J.; Trucks, G. W.; Schlegel, H. B.; Scuseria, G. E.; Robb, M. A.; Cheeseman, J. R.; Scalmani, G.; Barone, V.; Petersson, G. A.; Nakatsuji, H.; Li, X.; Caricato, M.; Marenich, A. V.; Bloino, J.; Janesko, B. G.; Gomperts, R.; Mennucci, B.; Hratchian, H. P.; Ortiz, J. V.; Izmaylov, A. F.; Sonnenberg, J. L.; Williams-Young, D.; Ding, F.; Lipparini, F.; Egidi, F.; Goings, J.; Peng, B.; Petrone, A.; Henderson, T.; Ranasinghe, D.; Zakrzewski, V. G.; Gao, J.; Rega, N.; Zheng, G.; Liang, W.; Hada, M.; Ehara, M.; Toyota, K.; Fukuda, R.; Hasegawa, J.; Ishida, M.; Nakajima, T.; Honda, Y.; Kitao, O.; Nakai, H.; Vreven, T.; Throssell, K.; Montgomery, J. J. A.; Peralta, J. E.; Ogliaro, F.; Bearpark, M. J.; Heyd, J. J.; Brothers, E. N.; Kudin, K. N.; Staroverov, V. N.; Keith, T. A.; Kobayashi, R.; Normand, J.; Raghavachari, K.; Rendell, A. P.; Burant, J. C.; Iyengar, S. S.; Tomasi, J.; Cossi, M.; Millam, J. M.; Klene, M.; Adamo, C.; Cammi, R.; Ochterski, J. W.; Martin, R. L.; Morokuma, K.; Farkas, O.; Foresman, J. B.; Fox, D. J. *Gaussian 16, Revision C.01*, Gaussian, Inc.: Wallingford CT, 2016.
2. Zhao, Y.; Truhlar, D. G., The M06 suite of density functionals for main group thermochemistry, thermochemical kinetics, noncovalent interactions, excited states, and transition elements: two new functionals and systematic testing of four M06-class functionals and 12 other function. *Theor. Chem. Acc.* **2008**, *120*, 215-241.
3. Weigend, F.; Ahlrichs, R., Balanced basis sets of split valence, triple zeta valence and quadruple zeta valence quality for H to Rn: Design and assessment of accuracy. *Phys. Chem. Chem. Phys.* **2005**, *7*, 3297-3305.
4. Weigend, F., Accurate Coulomb-fitting basis sets for H to Rn. *Phys. Chem. Chem. Phys.* **2006**, *8*, 1057-1065.

5. Scalmani, G.; Frisch, M. J., Continuous surface charge polarizable continuum models of solvation. I. General formalism. *J. Chem. Phys.* **2010**, *132*.
6. Tomasi, J.; Mennucci, B.; Cammi, R., Quantum mechanical continuum solvation models. *Chem. Rev.* **2005**, *105*, 2999-3093.
7. Fukui, K., The path of chemical reactions - the IRC approach. *Acct. Chem. Res.* **1981**, *14*, 363-368.
8. Tiesinga, E.; Mohr, P. J.; Newell, D. B.; Taylor, B. N. The NIST Reference on Constants, Units, and Uncertainty. <https://physics.nist.gov/cuu/Constants/index.html>.
9. Kesharwani, M. K.; Brauer, B.; Martin, J. M. L., Frequency and Zero-Point Vibrational Energy Scale Factors for Double-Hybrid Density Functionals (and Other Selected Methods): Can Anharmonic Force Fields Be Avoided? *J. Phys. Chem. A.* **2015**, *119*, 1701-1714.
10. Chung, J. Y.-L.; H, G.-J., An Improved Preparation of 2-Azabicyclo[2.2.2]octane. *Synth. Comm.* **2002**, *32*, 1985-1995.
11. Lamas, A.; Guerra, A.; Amorín, M.; Granja, J. R., New self-assembling peptide nanotubes of large diameter using δ -amino acids. *Chem. Sci.* **2018**, *9*, 8228-8233.
12. Amorín, M.; Castedo, L.; Granja, J. R., Self-Assembled Peptide Tubelets with 7 Å Pores. *Chem. Eur. J.* **2005**, *11*, 6543-6551.
13. Stockmann, P. N.; Van Opdenbosch, D.; Poethig, A.; Pastoetter, D. L.; Hoehenberger, M.; Lessig, S.; Raab, J.; Woelbing, M.; Falcke, C.; Winnacker, M.; Zollfrank, C.; Strittmatter, H.; Sieber, V., Biobased chiral semi-crystalline or amorphous high-performance polyamides and their scalable stereoselective synthesis. *Nat. Comm.* **2020**, *11*, 509.